QUARTZ VEIN STYLES AND GOLD MINERALIZATION IN THE PENJOM GOLD MINE, PAHANG, PENINSULAR MALAYSIA

ZAKARIA BIN ENDUT

THESIS SUBMITTED IN FULFILLMENT OF THE REQUIREMENTS FOR THE DEGREE OF DOCTOR OF PHILOSOPHY

**FACULTY OF SCIENCE
UNIVERSITY OF MALAYA
KUALA LUMPUR**

2016

UNIVERSITY OF MALAYA

ORIGINAL LITERARY WORK DECLARATION

Name : **ZAKARIA BIN ENDUT** (I.C/Passport No.:)

Registration / Matric No.: **SHC100082**

Name of Degree: **DOCTOR OF PHILOSOPHY**

Title of Project Paper/Research Report/Thesis ("this Work")

Quartz Vein Styles and Gold Mineralization in the Penjom Gold Mine, Pahang, Peninsular Malaysia.

I do solemnly and sincerely declare that:

(1) I am the sole author/writer of this Work;
(2) This Work is original;
(3) Any use of any work in which copyright exists was done by way of fair dealing and for permitted purposes and any excerpt or extract from, or reference to or reproduction of any copyright work has been disclosed expressly and sufficiently and the title of the Work and its authorship have been acknowledged in this Work;
(4) I do not have any actual knowledge nor do I ought reasonably to know that the making of this work constitutes an infringement of any copyright work;
(5) I hereby assign all and every rights in the copyright to this Work to the University of Malaya ("UM"), who henceforth shall be owner of the copyright in this Work and that any reproduction or use in any form or by any means whatsoever is prohibited without the written consent of UM having been first had and obtained;
(6) I am fully aware that if in the course of making this Work I have infringed any copyright whether intentionally or otherwise, I may be subject to legal action or any other action as may be determined by UM.

Candidate's Signature Date:

Subscribed and solemnly declared before,

Witness's Signature Date:

Name:

Designation:

ABSTRACT

The study area (Penjom Gold Deposit, Pahang, Malaysia) lies 30 km east of the major terrane boundary Bentong-Raub Suture within the central belt of Peninsular Malaysia along the NNE trending splay from the Suture line. Host rock is comprised of turbiditic sequence of Early to Late Permian ranging from well bedded siltstone, calcareous shale, carbonaceous shale, tuffaceous sandstone and conglomerate. These sequences were intruded by fine grained and porphyritic medium grained felsite intrusives (222.4 +/- 1.8 Ma). Quartz veins found here are categorized into two main types, namely shear veins and extension veins. Shear veins are ribbon to laminated veins developed only in carbonaceous units and are either thick or very thin units, parallel to bedding or shearing. This vein type is interpreted as formed during folding and thrusting events involving repeated opening of bedding and shearing planes. Associated with shear veins are several types of extensional veins including sub-vertical extensional vein arrays, hydrothermal quartz breccias and stockwork in felsite rocks. NE to NNE thrust-parallel reverse to dextral faults overprinted the earlier D2 event and generated extensional veins of similar morphology, mostly at intersections of sediment-intrusive contact or as shallowly dipping veins within the intrusive bodies. Local NNW fault controls significant mineralization at the west wall of Jalis Corridor in the form of shear vein, massive to sheeted extension vein. Several north-south trending sinistral faults, intercept at the footwall folded sequence initiated mainly after the main veining event interpreted as during D4. Normal sense of movement of the same fault crosscut and displace the vein is occurring during D5 event, are not associated with the above style of veins but locally host barren quartz calcite-veins and are in certain areas associated with the late stage galena. Common alteration minerals based on XRD analysis are fine grain muscovite, chlorite and illite, which is typically characterized the phyllic alteration. Fluid inclusions were analyzed using eleven doubly polished sections of veins including

two calcite veins and one quartz sample from hanging wall. No measureable fluid inclusions were found in calcite and hanging wall vein. Fluid inclusions fall in two populations. Population 1 is made up of H_2O-NaCl were having $T_h$final between 145^oC and 265^oC while population 2 is consist of H_2O-NaCl-CO_2 fluid inclusions with higher $T_h$final from 200^oC to 375^oC. Sulphides are comprised of pyrite, arsenopyrite, galena, sphalerite and chalcopyrite. Gold is commonly found with galena but also can be found together with early sulphide. Galena samples from two groups (6 from the mineralised zone and 3 from the non mineralised area) have been sampled and analyzed for trace element geochemistry and lead isotopes. The lead isotope ratios for both groups plot around the bulk crustal growth curve of the plumbotectonic model indicating Pb derived from mixed crustal and magmatic sources. Based on the Cumming and Richards (1975) growth curves, two groups of lead can be interpreted as having formed at 250 Ma and 160 Ma. The Penjom gold deposit shows many similarities with other orogenic gold deposits formed in a terrain subjected to compressional to transpressional event. Gold and other metal could be derived from mix metamorphic-magmatic sources migrated from deeper sources and deposited at mid crustal level during the late stages of an orogenic event.

ABSTRAK

Kawasan kajian (Lombong Emas Penjom) terletak 30km timur daripada sempadan terrain utama, Bentong-Raub Suture di dalam jalur tengah semenanjung Malaysia di lineament berarah NNE iaitu cabang daripada jalur suture. Unit batuan utama adalah jujukan turbidit yang berusia Permian awal hingga Lewat yang terdiri daripada perlapisan batu lodak, shale berkapur, shale berkarbon, batu pasir bertuf dan conglomerate. Jujukan ini di terobosi oleh batuan felsic (222.4 +/- 1.8 Ma) yang bersize halus dan berporfir. Telerang kuarzayang terdapat di sini diklasifikasikan kepada dua jenis iaitu telerang ricih dan telerang ekstensi. Telerang ricih adalah berbentuk ribbon dan berlaminasi yang terbentuk di dalam unit berkarbon sama ada tebal atau nipis, selari dengan satah perlapisan dan ricih. Telerang jenis ini ditafsirkan sabagai terbentuk semasa proses perlipatan dan sesar sungkup yang melibatkan proses pembukaan dan penutupan ruang perlapisan atau zon ricih. Berkait dengan telerang ricih adalah beberapa telerang ekstensi termasuk telerang hampir menegak, hidroterma quartz breksia dan stockwork di dalam batuan felsik. Sesar sungkup berarah NNE dan sesar yang selari dengannya bersifat songsang dan dextral bertindan terhadap peristiwa yang awal dan menghasilkan telerang kuarza dengan ciri yang sama, terutamanya di kawasan sentuhan intrusive dan batuan sedimen. Sesar NNW mengawal pemineralan yang penting di barat koridor Jalis dalam bentuk telerang ricih dan ekstensi. Beberapa sesar berarah utara-selatan dengan ciri sinistral memotong jujukan yang terlipat yang terbentuk selepas pembentukan telerang utama iaitu semasa D4. Pergerakan normal pada sesar yang sama memotong dan mengalihkan vein semasa D5 berkait dengan telerang calcite yang tidak berkait dengan emas dan di beberapa kawasan berkait dengan mineral galena fasa lewat. Mineral ubahan batuan yang biasa berdasarkan kajian XRD adalah muskovit, klorit, illit yang mencirikan perubahan batuan jenis phyllic. Kajian inklusi terkandung terdiri dari sebelas sampel kilatan telerang termasuk dua telerang

kalsit dan satu sampel kuarza di bahagian atas daripada Sesar Penjom. Tiada inklusi terkandung di dalam kalsit dan vein di atas Sesar Penjom. Populasi inklusi terkandung boleh dibahagikan kepada dua populasi. Populasi 1 terdiri dari pada sistem H_2O-NaCl yang mempunyai suhu $T_h$final diantara 145^oC to 265^oC manakala populasi 2 terdiri dari H_2O-NaCl-CO_2 dengan bacaan Thfinal dari 200^oC to 375^oC. Mineral sulfida utama terdiri dari pirit, arsenopirit, galena, sphalerite dan chalcopirit. Emas selalu berada bersama galena tetapi juga selalu bersama sulfida yang awal. Galena dari dua kumpulan (6 dari zone bermineralisasi dan 3 dari zon yang tidak bermineralisasi) telah di sampel dan di analisi untuk mineral surih dan Pb isotop. Nisbah isotop Pb di plotkan dan berada pada lengkungan pertumbuhan model plumbotectonic yang menunjukkan kedudukannya pada campuran kerak bumi dan sumber magmatic. Berdasarkan pada lengkungan pertumbuhan Cumming dan Richards (1975), dua kumpulan Pb boleh di tafsirkan sebagai terbentuk pada usia 250 Ma dan 160 Ma. Lombong Emas Penjom menunjukkan persamaan dengan jenis Orogenic Gold yang terletak di terrain yang mengalami tegasan compressive dan transpressive. Emas dan base metal mungkin berpunca dari gabungan sumber metamorphic-magmatic yang bergerak dari sumber yang dalam dan termendap di kerak pertengahan semasa fasa orogenic lewat.

ACKNOWLEDGMENTS

I would like to express my gratitude to Assoc Prof Dr. Ng Tham Fatt, Dr. Jasmi Hafiz Abdul Aziz and Prof Dr. Teh Guan Hoe for being my supervisors and for their invaluable encouragement, support and guidance in completing this thesis. I would also like to acknowledge the supports from other lecturers and staffs at Geology Department, University Malaya. They are Dr. Iskandar Taib (XRD and Micro-XRF analysis), Prof. Wan Hasiah Abdullah (carbon analyzer), En Zamrud (thin section), En Zaharuddin (XRD analysis) and other staffs at Geology Department. I am most grateful to Head of Deparment Prof. Dr Azman Abdul Ghani and Prof. Dr Ismail Yusof for the support. Great thanks extended to Assoc. Prof. Zhaoshan Chang from University of James Cook, Australia for the fluid inclusion study and Dr Sebastien Meffre and Charles Makoundi from University of Tasmania, Australia for the LA ICP MS analyses.

My deepest appreciation goes to all geologists and management at Penjom Gold Mine including general managers and managers at Specific Resources Sdn. Bhd. and management at Avocet Gold (UK) and JResources, Jakarta.

I would like to extend my appreciation to my lovely wife Suziati Mustaffa for the support, patient and understanding throughout my study and also to my three lovely daughter and sons (Farah, Farhan and Fahmi) for their encouragement and inspiration.

Thank you also to my mother Khatijah Setapa and other family members for the supports and prayer for my success. Finally, to my late father Endut Bin Musa who is always in my heart and my prayers. Thank you Allah Almighty for giving me a wonderful life, opportunities and energy to complete this study and for everything.

TABLE OF CONTENTS

TITLE PAGE		i
DECLARATION		ii
ABSTRACT		iii
ABSTRAK		v
ACKNOWLEDGMENT		vii
TABLE OF CONTENTS		viii
LIST OF FIGURES		xix
LIST OF TABLES		xxxi
LIST OF APPENDICES		xxxiii
CHAPTER 1 INTRODUCTION		
1.0	Introduction	1
1.1	Location	2
1.2	Objective	2
1.3	Scope of study	2
1.4	Method of mapping	6
	1.4.1 Introduction	6
	1.4.2 Geological mapping and methodology	7
	1.4.2.1 Pit wall mapping	8
	1.4.2.2 Temporary bench face mapping	8
	1.4.2.3 Mapping during the ore excavation	10
	1.4.2.4 Floor mapping	11
	1.4.2.5 Mapping from blast hole sample logging	11
	1.4.2.6 Core samples	12
1.5	Geological observation	12

1.6	Previous study	13
1.7	Conclusion	14

CHAPTER 2 GOLD DEPOSIT CLASSIFICATION

2.1	Introduction	16
2.2	Ore forming process	18
	2.2.1 Igneous/magmatic process	18
	2.2.2 Hydrothermal process	19
	2.2.3 Sedimentary and surficial process	19
2.3	Several class of gold deposit	20
	2.3.1 Orogenic gold deposit	22
	2.3.1.1 Geology of the host terrains	22
	2.3.2 Intrusion Related Gold Deposit	23
	2.3.2.1 Geology of the host terranes	24
	2.3.3 Porphyry (copper) and gold deposit	24
	2.3.3.1 Geology of the host terranes	25
	2.3.4 Epithermal gold deposit	25
	2.3.4.1 Geology of the host terranes	25
2.4	Other subclass of gold deposit	26
	2.4.1 Disseminated sedimentary hosted/Carlin type	26
	2.4.2 Volcanogenic massive sulphide	26
2.5	Gold deposits related to vein textures	27
2.6	Tectonic setting and gold deposit: Mainland South East Asia (SEA)	28

CHAPTER 3 HOST ROCK OF THE PENJOM GOLD DEPOSIT

3.1	Regional geology	33
3.2	District geology and stratigraphy	34
3.3	Stratigraphy setting of PGM	35
	3.3.1 Introduction	35
	3.3.2 Mine stratigraphy	36
3.4	Detail description of sedimentary rock units	37
	3.4.1 Upper well-bedded laminated siltstone and shale (UMS 1)	37
	3.4.2 Sandstone with minor thinly bedded shale and siltstone (UMS 2)	37
	3.4.3 Lower well bedded laminated siltstone (UMS 3)	38
	3.4.4 Greenish grey tuffaceous laminated siltstone (UMS 4)	40
	3.4.5 Calcareous shale/siltstone (UMS 5)	40
	3.4.6 Carbonaceous dominant unit (MMS 1)	40
	3.4.7 Interbedded sandstone, carbonaceous shale and thin conglomerate (MMS 2)	42
	3.4.8 Greenish/reddish tuffaceous siltstone, sandstone and conglomerate (LMS 1)	42
3.5	Stratigraphy Sequences	45
	3.5.1 Upper Mine Sequence (UMS)	47
	3.5.2 Middle Mine Sequence (MMS)	47
	3.5.3 Lower Mine Sequence (LMS)	48
3.6	Stratigraphy and mineralisation	49
3.7	Stratigraphy Repetition	52
3.8	Stratigraphy Break	52
3.9	Igneous rock	53
	3.9.1 Introduction	53
	3.9.2 Intrusive rock	53

3.9.2.1 Field occurrence 53

3.9.2.2 Petrography 54

3.9.3 Volcanic rock 57

3.9.3.1 Field occurrence 57

3.9.2.2 Petrography 57

3.10 Discussion and conclusion 59

CHAPTER 4 CARBONACEOUS ORE BODY

4.1 Introduction 62

4.2 Various type and origin of carbonaceous matter 62

4.2.1 Sedimentary origin 63

4.2.2 Carbon from metamorphic or hydrothermal origin carbon 64

4.3 Origin of carbonaceous material in Penjom 65

4.4 Carbonaceous matters and the genesis of gold mineralization 66

4.4.1 Physical control 66

4.4.2 Chemical control 67

4.5 Chemical analysis 67

4.5.1 Chromatography 67

4.6 Field classification of carbonaceous zone 68

4.6.1 Highly carbonaceous zone 69

4.6.2 Moderately carbonaceous zone 71

4.6.3 Low carbonaceous zone 72

4.6.4 Distribution of high carbon ore in geological setting 73

4.7 Carbonaceous break 75

4.7.1 Structural break 75

4.7.2 Natural break 77

4.8 Remobilisation of carbon 77

4.9 Mineralisation break 77

4.9.1 Structural break 78

4.9.2 Natural break 79

4.10 Different types of carbonaceous shale and percentage of carbon. 80

4.11 Other organic matter (meta-anthracite) 82

4.12 Conclusion 82

CHAPTER 5 STRUCTURAL GEOLOGY AND VEINS SYSTEM

5.1 Introduction 85

5.2 Regional structural geology 85

5.3 Previous studies 87

5.3.1 Geological modeling 1 (1997-1999) 87

5.3.2 Geological modeling 2 (2000-2001) 88

5.3.3 This study 89

5.4 Folding 91

5.4.1 Introduction 91

5.4.2 Bedding 94

5.4.2.1 Bedding analysis 94

5.4.2.2 Stratigraphy correlation and style of the fold 96

5.4.3 Cleavage development 100

5.5 Fault 102

5.5.1 Introduction 102

5.5.2 Fold related fault 103

5.5.3 Compression fault 103

5.5.4 Strike slip regime 105

5.5.4.1 Dextral fault 105

5.5.4.2 Sinistral fault 105

5.5.5 Extensional regime 105

5.5.6 Summary of the new structural framework 108

5.6 Quartz-carbonate vein system 109

5.6.1 Introduction 109

5.6.2 Different style of quartz veining 110

5.6.3 Thrust and fold (D2) related vein 111

5.6.3.1 Penjom Thrust shear vein 112

5.6.3.2 Bedding-parallel shear veins 114

5.6.3.3 Sheeted extension veins 117

5.6.3.4 Quartz breccias 120

5.6.3.5 Quartz stockworks 120

5.6.4 Fault (D3) related vein 120

5.6.4.1 Sheeted extension vein 121

5.6.4.2 Quartz breccias 122

5.6.4.3 Quartz stockwork 124

5.6.5 Structural explanation of vein formation 125

5.6.5.1 Fold- and thrust-related veins (D2) 126

5.6.5.2 Fault-related veins (D3) 127

5.6.6 Role of competence contrast 130

5.7 Relative roles of fold and fault on quartz veining 132

5.8 Conclusions 134

CHAPTER 6 MINERALOGY, TEXTURE, SULPHIDE AND GOLD MINERALIZATION

6.1 Vein mineralogy 136

6.1.1 Quartz veins 136

6.1.2 Quartz carbonate veins 137

6.1.3 Carbonate veins 138

6.1.4 Late calcite veins (gold barren) 139

6.2 Veins texture 141

6.2.1 Introduction 141

6.2.2 Textural classification 142

6.2.2.1 Buck texture 143

6.2.2.2 Comb texture 143

6.2.2.3 Lamination texture (vein septa) 145

6.2.2.4 Ribbon texture 145

6.2.2.5 Stylolite texture 147

6.2.2.6 Breccias texture 147

6.2.2.7 Minor veinlet texture 148

6.3 Application of quartz textures 149

6.4 Ore mineralogy 152

6.4.1 Introduction 152

6.4.2 Previous study 154

6.4.3 Sulphide mineral 155

6.4.3.1 Pyrite 155

6.4.3.1.1 Field observation 155

6.4.3.1.2 Microscopic study 156

6.4.3.2 Arsenopyrite 158

6.4.3.2.1 Field observation 158

6.4.3.2.2 Microscopic study 159

6.4.3.3 Sphalerite 162

6.4.3.3.1 Field observation 162

6.4.3.3.2 Microscopic study 162

6.4.3.4 Chalcopyrite 164

6.4.3.4.1 Field observation 164

6.4.3.4.2 Microscopic study 164

6.4.3.5 Galena 165

6.4.3.5.1 Field observation 165

6.4.3.5.2 Microscopic study 166

6.4.4 Gold 167

6.4.4.1 Field observation 167

6.4.4.2 Microscopic study 168

6.5 Vein and mineral paragenesis 170

6.5.1 Sulphide-gold paragenesis 170

6.5.2.1 Disseminated early syn-sedimentary and diagenetic pyrite 170

6.5.2.2 Quartz +/- carbonate-early sulphide gold (Fe, As, S)- Assemblage A 170

6.5.2.2 Quartz carbonate-pyrite, minor arsenopyrite, base metal-gold (Fe, As, Pb, Cu, Zn) Assemblage B 171

6.5.2.3 Calcite galena vein 173

CHAPTER 7 GEOCHEMISTRY OF VEIN AND ORE

7.1 Introduction 176

7.2 Fluid inclusion 176

7.2.1 Introduction 176

7.2.2 Previous fluid inclusion studies 177

7.2.3 Samples selection 177

7.2.4 Fluid inclusion petrography 179

7.2.4.1 SEM- CL imaging and crystal growth 179

7.2.4.2 Microscopic observation 180

7.2.5 Distribution of fluid inclusions 181

7.2.5.1 Shear vein (stage 1) 181

7.2.5.2 Extension vein (Stage 1) 184

7.2.5.3 Extension vein (Stage 2) 185

7.2.6 Thermometric measurement and results 185

7.2.6.1 Freezing and heating experiments 188

7.2.7 Discussion 190

7.2.7.1 Fluid composition 190

7.2.7.2 Temperature and pressure condition 192

7.3 Geochemistry of carbonate minerals in veins 194

7.3.1 Introduction 194

7.3.2 Quartz carbonate vein 194

7.3.3 Samples for analysis 195

7.4 Alteration of wall rocks 199

7.4.1 Introduction 199

7.4.2 Difficulties in studying alteration in Penjom 199

7.4.3 Wall rock alteration 200

7.4.3.1 Pyritization 201

7.4.3.2 Arsenification 202

7.4.3.3 Phyllic alteration 202

7.4.3.4 De-silicification 203

7.4.5 Discussion 203

7.5 Major, REE and trace element analysis 209

7.5.1 Introduction 209

7.5.2 Methods of study 209

7.5.3 Results 210

7.5.4 Discussion 213

CHAPTER 8 GALENA GEOCHEMISTRY AND LEAD ISOTOPE

8.0 Introduction 215

8.1 Methodology and purpose 215

8.1.1 Trace elements 218

8.1.2 Lead isotope 218

8.2 Results 219

8.2.1 LA ICP MS: Trace elements 219

8.2.2 Pb isotopes 224

8.2.2.1 Group 1 224

8.2.2.2 Group 2 225

8.3 Discussion 227

8.4 Conclusion 229

CHAPTER 9 DISCUSSION AND CONCLUSION

9.0	Introduction	231
9.1	Gold deposit classification	231
9.2	Summary of structural deformation	232
9.3	Veins, sulphides and gold	234
9.4	Geochemistry and wall rock alteration	236
9.5	Implication for regional tectonic setting	237
9.6	Conclusion	239

LIST OF FIGURES

Figure 1.1: Geological map of Malaysia Peninsular and location of Penjom Gold Mine in central belt. 3

Figure 1.2: Location of Penjom Gold Mine, Kuala lipis. BRS: Bentong-Raub Suture, PS: Penjom Splay, KKL: Kelau Karak Lineament 4

Figure 1.3: Flow chart of mapping activity and compilation into geological map. 7

Figure 1.4: Example of pit wall map of southern wall across the ore zone. Scale 1:1000. 9

Figure 1.5: Geological observation during ore excavation has been plot on grade control mining plan. 10

Figure 2.1: Tectonic settings of gold-rich epigenetic mineral deposits. Vertical scale is exaggerated to allow schematic depths of formation of various deposit styles to be shown (Groves et al., 1998). 20

Figure 2.2: Idealised cross section of gold deposit in different tectonic regime (after Groves, 1999). 21

Figure 2.3: Conceptual model for styles of magmatic arc epithermal Au-Ag and porphyry Au-Cu mineralization (Corbett, 1997) 21

Figure 2.4: Gold deposit environment used by Morrison (2007) for vein texture classification 28

Figure 2.5: Location of primary gold deposit in Malaysia Peninsular (after Yeap, 1999). Gold deposit in between purple and blue line lineament in inset figure hosted within vein system. 30

Figure 2.6: Gold deposits along Central Belt (Malaysia Peninsula)-Sukhotai Fold Belt and South East Asia granite provinces (after Cobbing et al., 1986; Ng et al., 2015) 31

Figure 2.7: Hydrothermal ore deposit and its location in geological setting of magmatic bodies and major shear/ fault system (Stephens, 2004). a: Orogenic gold, b: Intrusion related, c: Porphyry gold. 32

Figure 3.1: (Left) Well bedded sandstone of upper mine sequence. (Right) Photomicrograph of sandstone with poorly sorted quartz fragment (Q) dominant and minor lithic (L) fragment with sericite and patch of carbonate (UMS2). 38

Figure 3.2: (Left) Flaser bedding at upper part of sandstone bed. (Right) Pebbles of carbonaceous mudstone occasionally found in sandstone unit. 38

Figure 3.3: (Left) Parallel lamination in lower well bedded siltstone, (Right) cross lamination in the same unit. 39

Figure 3.4: Rock samples locations for greenish grey tuffaceous siltstone UMS4 (looking south). 39

Figure 3.5: (Left): Photomicrograph of light grey shale (UMS4) with minor quartz grain in matrix of fine grain lithic dominant and minor quartz. Sericite and patch of carbonate (yellowish) aligned parallel to foliation (S_0) or bedding. (Right): Photomicrograph of calcareous shale comprised of recrystallized calcite grain size is less than 0.2mm. Aligned dark opaque streak is carbon parallel to bedding (S_o). 39

Figure 3.6: Figure 3.6: Carbon result (%) from grade control ore block 924mRL Grey dot is 0.2 to 0.5 %C. Ore mark-out string comprised of ore grade above 0.8 g/t, red string ore block is above 6 g/t. Continuation of the high carbon ore zones along the Penjom thrust and NS corridor (western limb). High carbon content in the western limb is originated from carbonaceous shale. 41

Figure 3.7: Photomicrograph of sandstone in MMS comprised of dominant altered lithic (L) and quartz (Q) in sericitised matrix (location Western Limb 834mRL) 43

Figure 3.8: (Left) Light grey conglomerate of middle mine sequence underlying sandstone (SST) unit (location Western Limb 834mRL). (Right) Greenish grey conglomerate of lower mine sequence 43

Figure 3.9: Sedimentary rock of unit 8 (tuffaceous siltstone to conglomerate). A (Jalis corridor), B (Kalampong East fold axis), C (west wall). Looking to the north (photo May 2008) 44

Figure 3.10: Purple/reddish granule size of pebbly sandstone graded to conglomerate usually forming up to 5 to 10m thick. This unit is part of lower mine sequences. 44

Figure 3.11: General stratigraphy profiles for the west wall and east wall of Kalampong East pit (not to scale) and not included the west wall of Jalis. (SST-sedimentary sandstone, SSH- sedimentary shale, SSL-sedimentary siltstone, tufSSL-tuffaceous sedimentary siltstone, calSSH-calcareous sedimentary shale, cbnSSH-carbonaceous sedimentary shale, SCG-sedimentary conglomerate 45

Figure 3.12: Stratigraphy distribution in Kalampong pit (2007) 46

Figure 3.13: General stratigraphy sequences for eastern limb and western limb and the location of bedding parallel shear veins. Western limb shows stratigraphy repetition due to the E-W trending Blue Line Fault. 50

Figure 3.14: Looking southeast - Bottom of the pit, stratigraphy repetition as a result of displacement by Blue Line Structure (photo July 2008, bottom RL-792). 51

Figure 3.15: Looking south – Southwest wall of KE pit: Stratigraphy repetition indicated by lower mine sequence (LMS) comprised of massive conglomerate above carbonaceous dominance of MMS as a result of displacement by Jalis NNE reverse to dextral fault 51

Figure 3.16: Stratigraphy from RC samples logging shows three sequences of lithology. UMS-upper mine sequences, MMS- middle mine sequences, LMS-lower mine sequences 55

Figure 3.17: Felsite cross cut the host rock sequences. Blue line represent approximate boundary between middle and upper mine sequences. Green line represent the boundary of middle and upper mine sequences 55

Figure 3.18: (Left) Photomicrograph of medium grained felsites (ITN-1) with plagioclase (P) and quartz (Q) and minor alkali feldspar (F). (Right) Photomicrograph of fine grained felsite (ITN-2) comprised of quartz grain with some plagioclase. . Thin section view in transmitted light. 56

Figure 3.19: (Left) Photomicrograph of fine grained microdiorite comprised of quartz and plagioclase with carbonate vein. (Right) Hand specimen of medium (ITN-1) and fine grain felsites (ITN-2). Thin section view in transmitted light. 56

Figure 3.20: Photomicrograph of rhyolite to dacite porphyry comprised of quartz (Q) dominance with minor plagioclase. Thin section view in transmitted light. 58

Figure 3.21: Photomicrograph of volcanic rock (Andesit) made up by fine grained of plagioclase and quartz. Stringer of carbonate vein cross cut the lithology. Thin section view in transmitted light. 58

Figure 3.22: Lower sequences sedimentary rock is not hosted significant ore bodies based on grade control assay data. (The blue and reddish dot represents the ore grade above 0.5 g/t). Ore dominantly within the Middle sequences (example from the main KE pit) 60

Figure 3.23: KE geological map. Mineralised outline (>0.5 g/t) dominantly hosted in grey middle mines sequences. Some (in black circle) are hosted in felsite intrusive within the Lower Mine Sequence host rock 61

Figure 4.1: Different process of sedimentary origin of carbonaceous material (after Robb, 2008 and Bierlein, 2001). 65

Figure 4.2: Looking north. West dipping mineralized carbonaceous unit of the western limb at contact with felsites. 70

Figure 4.3: Looking north view of the western limb thick carbonaceous host rock. 70

Figure 4.4: Close up view of the sampling in sheared carbonaceous shale and carbonaceous siltstone. 70

Figure 4.5: Kalampong North, Penjom Thrust reactivates along carbonaceous unit of the east limb of anticline. 71

Figure 4.6: Overall picture of Figure 4.5 and location Figure 4.2, 4.3 and 4.5. 71

Figure 4.7: Interbedded of sheared carbonaceous shale with small unit of low carbon sandstone (pen in circle as a scale) will produce a moderate carbon content during ore mining. 72

Figure 4.8: Overall view of photo A at south of KE, near the Penjom Thrust zone. 72

Figure 4.9: Cross section at 50 000 show distribution of the main highly carbonaceous unit (>1.5% C). High carbon along thrust is made up by western limb carbonaceous sequences. The ore zone along the thrust (area A) is also considered as part of western limb sequences (part of NS corridor of previous interpretation and can be correlated with area c, usually separated by fold related fault). Area A also comprised of low carbon ore. Area B is eastern limb sequences. 74

Figure 4.10: Distribution of the mineralized zone (>0.5 g/t) for high carbonaceous zone (green, >0.5%C) and low carbonaceous zone, <0.5%C (blue) from Kalampong East pit. Data is from 945 to 960mRL. 76

Figure 4.11: (A) Natural break (area N) of carbonaceous unit due to the massive tonalite, Hill 7 and Hill 2 (west wall). (B) Structural break of carbonaceous and mineralization (east wall) due to fault displacement. 76

Figure 4.12: (A) Close up view of area Y (east wall), carbonaceous and mineralization break by the structure, (B) Overview of area X and Y, Penjom fault (dash line) responsible for area X and Hill 6 NS fault (dot line) reactivate/diffract along main fault responsible for area Y. 76

Figure 4.13: The main structural event affected the carbonaceous unit. 78

Figure 4.14: Grade control ore block (above 0.8g/t). NS corridor (Jewel Box/Area C) is also high carbon content. 80

Figure 4.15: Various types of carbonaceous shale. See explanations in text. 81

Figure 4.16: Reflectance scale of 4.5 to 5 indicates organic carbon is meta-anthracite. 83

Figure 4.17: (Left) Anthracite cemented by quartz vein infilled dominantly parallel to rock fabric in silicified carbonaceous shale. (Right) Polish section image of meta-anthracite (A) in carbonaceous shale and framboidal pyrite under reflected light. 84

Figure 4.18: (Left). The occurrence of framboidal pyrite (FP) (bright reflectance) associated with anthracite under reflected light. (Right). Meta-anthracite is observed with vesicles indicative of thermally altered. Framboidal pyrite can also be observed. 84

Figure 5.1: Tectonic-magmatic event involving the collision of Sibumasu-Indochina terrane (Metcalfe, 2013). 87

Figure 5.2: Geological map of Kalampong pit (2008), inset photo shows bird eye view of Kalampong and Manik pit. 90

Figure 5.3: North wall as current pit slope (2009). Area for bedding analysis plotted in stereonet. Bedding at area 1, 2 and 3 are dipping east and area 4 is dipping west. 92

Figure 5.4: North wall before cutback shows the same style of folding. 92

Figure 5.5: South wall during third cutback. Hill 6 NS fault intercepted along the eastern limb 93

Figure 5.6: South wall of Kalampong pit before 2009 cutback shows recumbent fold of tight inclined fold 93

Figure 5.7: Hanging wall, Area 1 - Hill 6: Mean Orientation = 44/126 (Dip/dip direction). Area 2 – Hill 5: Mean Orientation = 46/147 (Dip/dip direction). Foot wall, area 3 (zone B) - Eastern Limb near fold axis: Mean Orientation = 38/157. Area 4 (zone C) – West wall North: Mean Orientation = 64/277 95

Figure 5.8: Jalis-Manik corridor. Stereonet plot of bedding at Jalis west wall shows mild cross fold of the east dipping bedding: Mean Orientation = 30/094 95

Figure 5.9: Cross-section at 49700. 97

Figure 5.10: Cross-section at 49 900. 97

Figure 5.11: Cross-section at 50 100. 98

Figure 5.12: Cross-section at 50200. 98

Figure 5.13: The stereonet plot of fault orientation in several zones. Number of data in bracket 99

Figure 5.14: (Left) Undeformed shear vein with fracture cleavage S1 below the vein (western limb). (Right) S2 fold axis cleavage also affected the shear vein (refolded western limb) 100

Figure 5.15: (Left) Shearing at contact of felsites intrusive as indicate by shear vein V1, intrusive is undeformed. (Right) Shearing as a result of reactivation of the fold at contact with intrusive produced parallel fracture in narrow sill (refolded of the western limb) 101

Figure 5.16: (Left) S12develop in refolded fold below incline fold. (Right) Close up view of northerly strike parallel fracture cleavage. Dash line is bedding outline. 101

Figure 5.17: Structural classification for Kalampong East (KE) Pit shows three main structural events. 103

Figure 5.18: (Left) R1F and R2F displace felsite body, looking south (852mRL). (Right) R1F as expose on the wall 104

Figure 5.19: (Left) R4F (NNE fault) displace felsite rock in incline fold zone, base level 834mRL (looking south) after cutback. (Right) Close up view, intense quartz below R4F at contact with felsites intrusive. 104

Figure 5.20: Slickenline striation on Hill 6 NS fault plane shows slightly oblique normal fault 106

Figure 5.21: At the southern most part of the Kalampong pit, a steeply dipping N-S normal fault (DMF) (right side of the picture) cuts the gently dipping NNE-SSW reverse fault and high carbon zone. Other normal fault (NS Jalis) at left side reactivates along Penjom Thrust. 106

Figure 5.22: NNW fault developed as a Riedel fault in between NS indicating normal sense of movement 107

Figure 5.23: Fault striation indicates normal sense of small scale NS fault cross cut quartz-carbonate shear vein. 107

Figure 5.24: (Left) Normal north south fault displace flat dipping high grade laminated vein (looking south, 834mRL). (Right) Close up view of normal NS fault displace bedding parallel vein 107

Figure 5.25: (a) Penjom Thrust ore zone trending NNE and subparallel to bedding. (b) Close up of area ‘A’ shows laminated to ribbon quartz. (c) Another bedding parallel vein below the thrust ore zone (after further digging of area ‘B’ in photo ‘a’. (d) Ore zone comprised of shear veins (black line), cross cutting through intrusive rock (ITN). (e) Q2W shear veins as shown by slivers of host rock in sheared intrusive. Blocky intrusive on the right side lack quartz veining. 113

Figure 5.26: Looking mine north (35^{o} from true north), cross section at 50100 at the center of Kalampong Pit, shows structural framework of shear veins (Q1W, Q2W and Q3W) in the fold setting of the Kalampong Anticline. Inset figure is an evolution of the folding. 114

Figure 5.27: (a) Roughly laminated veins in carbonaceous shale unit with more planar laminations inside the veins. This shear vein type 2 in Table 1 was formed through shear induced lamination. (b) E-W extension vein array type 2 or planar sheeted vein developed at θ equals to 90^{o} below the main shear vein (red dash line), looking south and at level 840mRL. (c) A series of E-W striking sheeted veins (extension vein array type 2) exposed after the excavation of the main shear veins (looking east, at level 834mRL). (d) Equal area, lower-hemisphere stereographic projection showing the average dip and dip-direction and pole to vein. 118

Figure 5.28: (a) Dominant low angle extension veins Type 3 in felsites dyke perpendicular to contact, bedding and fault. Location: north of KE pit; Spacing: from 5 to 50cm; Thickness: from 1 to10cm. (b) Dominant vertical E-W extension veins Type 1 across the bedding and felsite intrusive at Jalis West Wall. Spacing: from 5 to 50cm; Thickness: from 1 to 20cm. Vein intensity increases in intrusive. (c) Dash line represent west dipping shear plan across felsite. 1-vein stockwork near shear plane (D2 deformation), 2-vein infilling parallel fracture resulted to low angle vein array, 3-less vein away from the shearing. (d) Vein across the lithology contact. 123

Figure 5.29: (a) Stockwork (ST) veins (extension vein Type 4) in intrusive rock below North-South trending West dipping shear veins (red line) and hydrothermal breccias (HB) in between two shear veins in intrusive and siltstone. (b) Fractures cleavage (S3) locally developed below NNE D3 fault affected the D2 shear vein. (c) Normal D5 fault (green line) displaces flat dipping along synform axis D2 shear vein. 124

Figure 5.30: (a) Lower hemisphere equal-area of sheeted vein orientation (poles plot of dip direction and dip) shows dominant steeply north dipping extension veins discordant to bedding from three areas. (b) Overall lower hemisphere equal-area of bedding orientation (poles plot of dip direction and dip, n = 1187), (c) Vein (poles plot of dip direction and dip, n = 797), 0.5% interval. 129

Figure 5.31: (Left) Stress field diagram shows relationship of extensional fractures perpendicular to maximum compressive stress. (Right) Dominance E-W sheeted extension vein Type 2 in felsite unit at fault intercept. Looking east at east wall. 129

Figure 5.32: (a) Crenulated extension veins as a result of ongoing deformation that also produced the cleavage at high angle to veins. (b) Late vein stringers across gold network within brecciated calcite vein. (c) Ribbon quartz from side view with gold along vein margin. (d) Laminated veins with sign of fault striations affecting the gold itself on the vein margin. 131

Figure 5.33: Location of Jalis NNW Fault Zone sub-parallel to carbonaceous shale (looking north). Red line is outline of the shear vein within and outside the fault zone. Economic mineralization (ore body) localised at intercept with dominant felsic host rock. 132

Figure 6.1: (Left) Late stage of white quartz infill along lamination but also cross cut lamination of gray quartz and carbonate vein (CO3). (Right) Milky quartz and micro-fault truncated stylolite, a band of grey quartz and carbonate (CO3) veins. 137

Figure 6.2: Intergrowth of prismatic carbonate (calcite dominance based on XRD analysis) and quartz in quartz carbonate veins. (Left) Ribbon to laminated vein comprised of carbonate (calcite) at the bottom and quartz on top. (Right) E-W sheeted carbonate veins cross cut the brecciated quartz within the vein but not continuous outside the brecciated quartz vein body. 137

Figure 6.3: (Left) Ankerite appears as red after expose to oxidation for certain period. (Right) Calcite extension vein parallel to the bedding with fibrous of veins growth perpendicular to vein wall 140

Figure 6.4: Quartz-carbonate veins, ribbon quartz on top and carbonate bottom 140

Figure 6.5: (Left) Ankerite appears as red after expose to oxidation for a certain period. (Right) Calcite extension vein parallel to the bedding with fibrous of the veins growth perpendicular to veins wall 140

Figure 6.6: Late calcite veins at different phase with sheeted quartz carbonate vein. Reverse sense of movement were evidence in both photo. 141

Figure 6.7: A. Ribbon quartz and massive inside the vein. B. Coarse grains quartz inside the vein made up the passive grain. C. Fine grain along the laminated veins represents the active plane. D. Anhedral to euhedral quartz grain close to carbonate veins along ribbon. 144

Figure 6.8: Medium comb with crystal growth perpendicular to vein margin, (Right) Coarse comb but the with a more random crystal growth texture.. 144

Figure 6.9: Parallel veins in siltstone with multiple veins to form lamination or septa. Vein crystals align parallel to the wall and with no fibre or comb quartz are indicative of veins forming in the confined space. 145

Figure 6.10: (Left) Reactivated shear on ribbon (in box) which produced the cataclasite quartz grain and massive anhedral buck below the ribbon. (Right) Photomicrograph of fine abrasive quartz represents the mill grain and anhedral buck quartz below the shear. 146

Figure 6.11: (Left): Bedding parallel shear vein with parallel wavy style stylolite. (Right) Shear vein with fractured fill stylolite or infill breccias texture. 148

Figure 6.12: (Left) Fractured stylolite or infill breccias texture. (Right) Superimposes features of aggregate breccias in shear vein can be originated from recrystallized fractured stylolite or infilled texture (sample half core HQ). 149

Figure 6.13: Quartz carbonate vein near to fold axis and Penjom Thrust has a network of thin veinlets overprint the earlier ribbon texture. 150

Figure 6.14: Gold infilling the local breccias texture in reactivated shear vein as in circle 1, 5, 6 and along stylolite in circle 2 and 4. Discordant vein (black line 7) as a late stage veins cross cut the massive brecciated veins and gold. 151

Figure 6.15: Discordant quartz veinlet as a late stage event cross cut the stylolite and gold. Stylolite made up of soluble carbon and sulphide. 151

Figure 6.16: Pyrite py1 hosted along the host rock remnants in vein and along mineralogy boundary. (Right) Pyrite Py1 is more randomly distributed in carbonate (CO3) vein. 156

Figure 6.17: (left) Deformed pyrite as indicated by shining yellowish surface as a result of fault (KE, Q2W shear vein). (Right) Late stage quartz vein (v1b) cross cut lamination and pyrite py1 aggregate. 157

Figure 6.18: Mild refolded of shear vein (V1) (Q3W shear vein) hosts to pyrite (Py1) and galena (ga1b), Calcite crystal growth (V2b) on the shear plain during the later stage not associated with any sulphide mineral. 157

Figure 6.19: (Left) Extension vein-Gold (Au) and galena (Ga) infilling fracture in pyrite (sample q3w879- Q3W near to fold axis). (Right) sample q3wb gold and chalcopyrite infilling crack and fracture in pyrite. 158

Figure 6.20: (Left) Disseminated subhedral to anhedral arsenopyrite around thin network of quartz veinlet in tuffaceous shale. (Right) Thinly bedding parallel veins has been buckled-up as a result of ongoing deformation (sample FQ1) and also affects sulphide mineral. 160

Figure 6.21: (Left) Aggregates of arsenopyrite in extension vein. (Right) Band of cataclasite arsenopyrite at lower contact of shear vein along slivers of carbonaceous shale (sample MNQ2A). 160

Figure 6.22: (Left). Photomicrograph of gold occurs as inclusion in arsenopyrite. (Right) Photomicrograph of the shear vein FQ1-Arsenopyrite intergrowth with pyrite and also in corroded pyrite. Reflected light. 161

Figure 6.23: Photomicrograph of sample MNQ2A in Manik (left) and FQ1 (right) in eastern limb of the fold (KE) shows cataclastic features of arsenopyrite along the active shear plane. Reflected light. 161

Figure 6.24: Photomicrograph of Q3WA shows galena (ga) at a margin and infilling fractured arsenopyrite (apy) in Q3W quartz carbonate-early sulphide and base metal. Reflected light. 162

Figure 6.25: (Left) Laminated vein Q3W shear vein with galena (black) and sphalerite (honey red) occupy along the lamination. (Right) Visible gold (yellow), sphalerite and galena along the lamination. 163

Figure 6.26: (Left) Small pieces of sphalerite in quartz carbonate vein in circle have been prepared for the polish sample. (Right) Photomicrograph of chalcopyrite diseases occur in sphalerite as a fine bleb. Fine particles of galena surrounding the fracture sphalerite. Reflected light. 163

Figure 6.27: (Left) Occurrence of galena and chalcopyrite in extensional veins within intrusive rock. No association with carbonate vein. (Right) Spot of pyrite and chalcopyrite in fill the fracture in quartz. 164

Figure 6.28: (Left) Band of dendritic galena infilling local breccias in a milky quartz vein. (Right) Coarse grain galena associated with calcite but not associated with gold. 166

Figure 6.29: Left. Photomicrograph of galena (ga1b) in Janik area near the fold hinge is observed as fractured (reflected light). (Right) Sample Q3WL: Galena in thicker segment of vein and absent in ribbon quartz. 167

Figure 6.30: (Left) Photomicrograph of gold and galena infilling fractures in arsenopyrite. (Right) Photomicrograph of gold and galena infilling pyrite. 167

Figure 6.31: (Left) Gold in quartz carbonate shear vein forming a layer parallel to vein margin. (Right) Gold infilling fractures in vein which part of shear vein. 169

Figure 6.32: (Left) Gold along the lamination has faulted/sheared effect indicating gold synchronously deposited during repeated opening and shearing of the bedding. (Right) Gold associated with pyrite within wall rock inclusion and late quartz cross cutting the early quartz. 169

Figure 6.33: Summary of several phase of structure, veins and sulphides mineral paragenesis. Py-pyrite, Apy-arsenopyrite, Ga-galena, Sph-sphalerite, Cpy-chalcopyrite. 175

Figure 7.1: Fractures zone in shear vein shown by low angle string outline and overlapped with zone of trail inclusion. Vertical fractures are less coincided with zones of trail. (A) SEM CL image. (B) Under reflected light. 182

Figure 7.2: (A) Sample (Z2N), extension vein-Stage 1: Several trails (T) of inclusion and cluster (CL) within the grain. Trail mainly L-V of Type 1 inclusion and cluster made up of L-V of Type 1, 2 and 4. (B) Extension vein, stage 1: Occurrence of both Type 1 L-V and Type 2 L-V inclusion along trail. (C) Similar sample: Type 1, L-V homogenized at 189oC and Type 2, L-V still preserve the inclusion. (D) Shear vein, stage 1: Cluster of Type 2 and Type 3 L-V inclusion. (E) Close up view of photo D: Coexistence of Type 3 L-V with double-bubble of CO2 inclusion and Type 2 L–V with dark rim. (F) Shear vein, Stage 1: Overall view of photo G and H containing inclusion forming as a cluster. (G) Close up of photo F. Top two inclusions are vapor rich of Type 5 and bottom two are Type 3 V-L. (H) Inclusion at 15oC showing the formation of CO2 liquid and vapor in all inclusions. 183

Figure 7.3: Thermometric experiment is using LINKAM MDS600C with Olympus camera attached. 186

Figure 7.4: Temperatures of final homogenization (T_h) obtained from all samples (85 data). 192

Figure 7.5: Final melting temperatures of Ice and Clath (T_m) plotted against temperatures of final homogenization (T_h) (85 data). 193

Figure 7.6: Final homogenization temperatures (T_h) plotted against salinity. 193

Figure 7.7: Calcite vein with gold. Gold infilling brecciated portion of the vein (sample Q1jn) 196

Figure 7.8: XRD analysis of sample Q1jn with higher calcite peak 196

Figure 7.9: Extension quartz carbonate vein with reddish color after expose to oxidation at the edge of the vein (inset photo) confirmed from XRD analysis as ankerite. Sericite alteration detected as indicated by occurrence of muscovite. 197

Figure 7.10: Deformed shear vein from Penjom Thrust zone at Janik hosted in high carbon zone have quartz carbonate vein of ankerite and calcite. 198

Figure 7.11: (A) Sulphides in vein comprised of mainly pyrite and a black shining galena and disseminated pyrite in altered wall rock zone. B: Altered wall rock and disseminated pyrite 204

Figure 7.12: Disseminated pyrite in felsite intrusive within the bleached altered host rock around the vein. 205

Figure 7.13: XRD analysis of samples along Penjom Thrust hosted vein comprised of quartz, calcite and illite. 206

Figure 7.14: XRD analysis of Penjom Thrust wall rock comprised of quartz, muscovite, pyrite and calcite. 207

Figure 7.15: XRD analysis of altered wall rock at southern pit extension vein comprised of quartz, muscovite and chlorite. 208

Figure 7.16: Location of samples for XRF analysis. Hanging wall samples are HW-R and HW-NSF 211

Figure 7.17: Plot of Au, As and Pb in the ore (11 samples, refer to Table 7.6), hanging wall rock (HW-R and HW-NSF) and waste rock outside the mine site (KLGM and KLB). 213

Figure 8.1: Location of galena sample for geochemistry study 216

Figure 8.2: Galena samples for the analysis. A. Close up view of sample Q3WA, B. Sample ZNNW, C. JNNE: Galena infilling brecciated calcite along fault plane, D. Hanging wall galena (HW S2). Broad correlation of all elements in galena (in log scale) except Cd, Se, Ag, Te and Bi which is very low in hanging wall galena. 217

Figure 8.3: Broad correlation of all element in galena (in log scale) except Cd, Se, Ag, Te and Bi, which is very low in hanging wall galena. Refer to Table 8.1 for galena stages. 220

Figure 8.4: Plot of trace element in galena hosted in bedding parallel shear vein (sample Q2WL), dendritic galena (Q2WA) and galena along lamination. All show broad correlation especially the first two samples. 221

Figure 8.5: Plot of Cd, Te, Se, Ag, Bi of galena in Penjom, Tanah Merah (near Ulu Sokor) and other places (MI-Mount Isa, BH-Broken Hill, MM-Mt Murchison, BM-Baja Mare, TY-Tynagh, OD-Olimpic Dam). 221

Figure 8.6: Summary plot of lead-isotope ratio 206Pb/204Pb vs207Pb/204Pb. SRABCG- Subduction-related and bulk crustal growth, SK-Stacey and Kramers (1975), CR- Cumming and Richards (1975). 226

Figure 8.7: Summary plot of lead-isotope ratio 206Pb/204Pb vs208Pb/204Pb. SRABCG- Subduction-related and bulk crustal growth, SK-Stacey and Kramers 227

(1975), CR- Cumming and Richards (1975).

Figure 9.1: Summary of the geological elements studied and a possible correlation with a deformation event. 240

Figure 9.2: Cross section at Bukit Koman (Raub) underground gold mine showing vein parallel to compression fault and bedding. 241

TABLES

Tables 1.1: The main geological aspects focused in this study include rock unit, vein, geological structures and sulphide minerals 13

Tables 1.2: Previous geological study conducted by geologists in Penjom mainly for resources estimation 15

Tables 2.1: Summary of the Lindgren gold classification (after Lindgren, 1922) 16

Tables 2.2: Summary of gold deposit classification based on fluid source and crustal depth. Depth is only relative in two groups and superimposes may occur due to the uplift and reactivation. 17

Tables 2.3: Several type of gold deposit in mainland of South East Asia 29

Tables 3.1: Group of rock units in stratigraphy sequences 36

Tables 4.1: Different types of carbonaceous preg-robbing ore 63

Tables 4.2: Chromatography analysis of carbon in Penjom by SKM Consultant (2002) not detected any total hydrocarbon petroleum. 68

Tables 4.3: Carbon contains in different fold related shear vein ore zone. 69

Tables 4.4: Various type of carbonaceous shale and result of carbon content and sulfur (as analyzed at Penjom Lab) 81

Tables 5.1: Summary of deformation events in Peninsula Malaysia (Shuib, 2009) 86

Tables 5.2: Summary of structural event in PGM indicates two main structural events. D2 to D3 involving compression to transpressional and D4-5 extensional period. 108

Tables 5.3: Classification of vein type, host rock and superimposed reactivation by later fault 135

Tables 6.1: Quartz texture types for different deposits environment (Dowling and Morrison, 1989). Blank-absent, 1-rare, 2-present, 3-common, 4-abundant, 5-predominant. 152

Tables 6.2: List of the polish section samples. 154

Tables 6.3: Structural phases, description of veins, gold content of ore zones and the occurrence of sulphides. Ore grade – low: 0.5 to 1 g/t; medium: 1 to 3 g/t; high: 3 to 6 g/t; very high: >6 g/t). Py: pyrite; Apy: arsenopyrite 174

Table 7.1: Sample for fluid inclusion represents different vein type and sulphide assemblage. Stage 1 vein is controlled by D2 deformation, Stage 2 vein by D3 deformation. Vein type based on Table 5.03. Sulphide assemblage as described in Chapter 6.5. Py-pyrite, Apy-arsenopyrite, Ga-galena, Sph-sphalerite. 178

Tables 7.2: Summary of micro-thermometry results 187

Tables 7.3: Results from XRD analysis. Some of the vein samples are the same with Table 7.2. 195

Tables 7.4: Total carbon percentage in vein sample reflected the inorganic carbon from quartz carbonate vein in various ore zone (analysis at Penjom Lab). 196

Tables 7.5: Summary of XRD analysis of vein and wall rock alteration mineral of several main ore bodies which is typical of phyllic alteration. 201

Tables 7.6: Geochemical results of trace elements analysis in three types of rock. Fe, Mn, Cr, in %: Au in ppb, others in ppm 212

Tables 8.1: List of galena samples (n=9) from Penjom from several stages. 217

Tables 8.2: Results (in ppm) of the trace elements in galena for samples (Q2WL, Q2WA, JL2, ZX3, JNNE, ZNNW, HW-S2, G1a HW-S, HW-E. Three analyses were undertaken for each sample. Other samples are from University of Tasmania collection: MT Isa-Mount Isa, B Hill-Broken Hill, MT M-Mount Murchison, B Mare-Baja Mare, Tynagh, SW-Sweet Water and O Dam-Olympic Dam. 222

Tables 8.3: Lead isotope ratio of various stages of galena in Penjom. 225

Tables 9.1: Tectonic setting, structural episodes and timing of veins formation for several major gold deposits and comparison to Penjom gold deposit. 242

LIST OF PUBLICATION AND PAPER PRESENTED 244

LIST OF APPENDICES

Appendix A: Fluid inclusion data 245

Appendix B: XRF geochemistry data 248

CHAPTER 1 INTRODUCTION

1.0 Introduction

Penjom Gold Mine (PGM) is the biggest gold mine in Malaysia and has produced more than 45 tonnes (1.4 Moz) of gold since 1997. As in 2014, Penjom still has resources of 21 Mt @ 1.63 g/t or 1.1Moz (J Resources website 2014, Endut et al., 2014) and resource drilling is still on-going to extend mine life. PGM is operated by Specific Resources Sdn. Bhd. which is owned by Indonesia based PT J Resources Nusantara. Prior to June 2011, Penjom was under Avocet Gold (UK).

Geological aspects of PGM have been studied by several researchers during the exploration stage and mine development. During the exploration stage, studies are based on core samples and soil focusing on geochemistry and gold-sulphide paragenesis (Gunn et al., 1993; Ariffin, 1995). During mine development, pit exposure allowed more structural aspects incorporated into the geological understanding.

This study focuses more on the pit observation based on wall mapping and ore mining supervision for the last 17 years of mine operation, combining all aspects of geology through systematic geological mapping. Several aspects of geology related to mineralisation are (in order of importance) the gold itself, vein (type and texture), sulphide minerals, structural deformation (fold and fault), hydrothermal alteration, host rock (sedimentary rock and felsite intrusive) and geochemistry. Other researchers carried out some aspects of geochemistry such as sulphur isotope and EPMA analysis (Abdul Aziz, 2007 and Makoundi, 2012).

1.1 Location

The Penjom gold deposit is situated in northwest Pahang in Kuala Lipis district, which is about 180km northeast of Kuala Lumpur. Penjom lies in the Central Belt, 30 km east of Bentong-Raub Suture that is a major terrane boundary separating Western and Central belts of the Malaysia Peninsular (Figures 1.1 and 1.2). Penjom is located about 2 km west of the main road, which is about 15 km from Kuala Lipis town.

1.2 Objectives

The objectives of the study were to understand the style and episode of vein formation, mineralogy, sulphide, gold mineralisation mineralization and structural deformation in the PGM. Correlation of the structural events and vein paragenesis will be established and correlated to regional geological processes. Geochemistry analysis of sulphide minerals, micro-thermometry analysis of veins and lead isotope study will provide a better understanding of gold mineralization in the PGM.

1.3 Scope of study

The scope of study covering various aspects of geology and gold mineralization is presented in 9 Chapters as follows:

a) Chapter 1: The purpose of the study, methodology and mapping method for data collection.

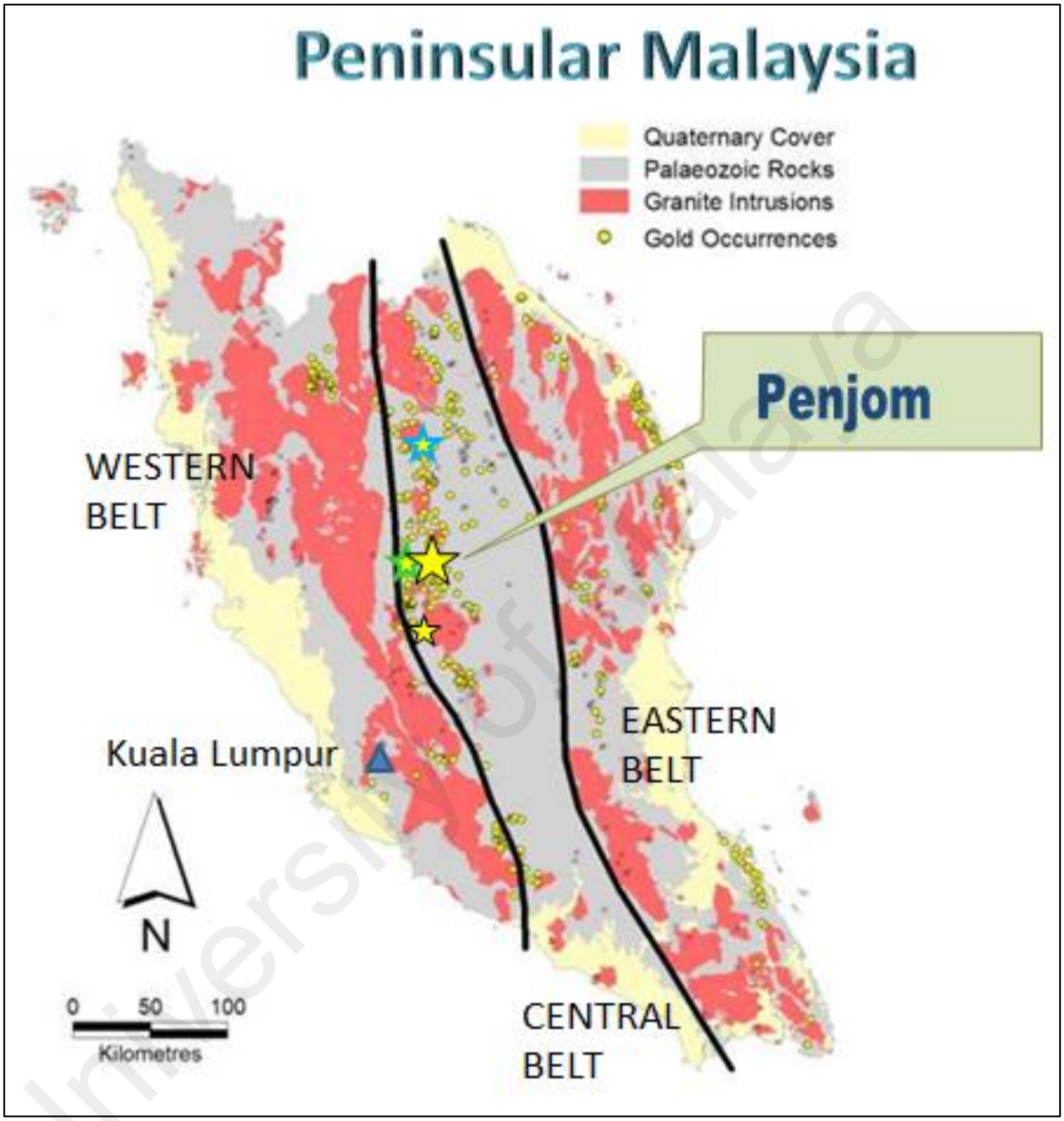

Figure 1.1: Simplified geological map of Malaysia Peninsular showing the location of Penjom gold deposit in the Central Belt.

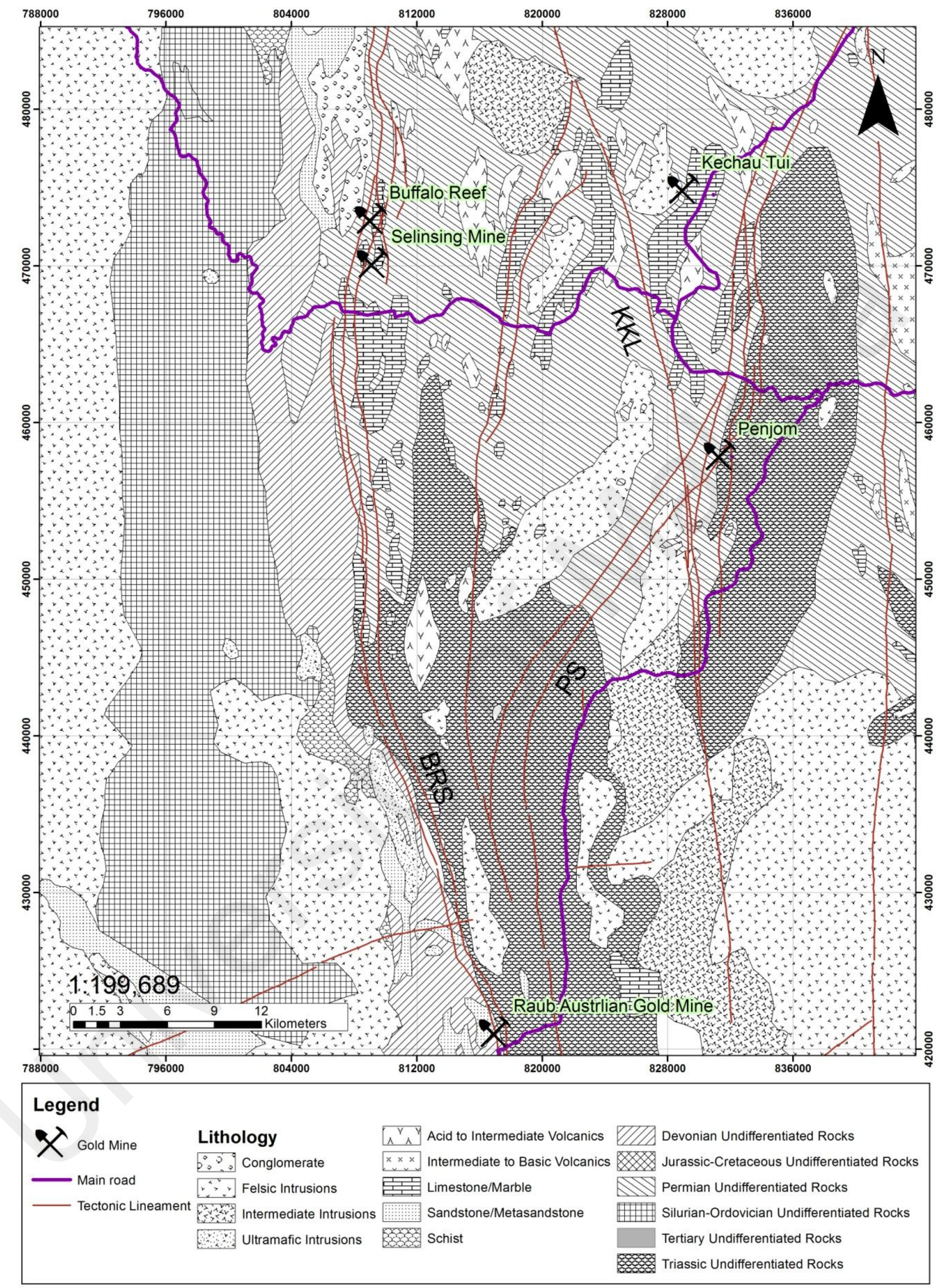

Figure 1.2: Location of Penjom gold mine, Kuala Lipis. BRS: Bentong-Raub Suture, PS: Penjom Splay, KKL: Kelau-Karak fault/lineament.

a) Chapter 2: Gold deposit classification: This aims to provide a systematic characteristic of the gold deposit and its relationship to structural setting and geochemistry.

b) Chapter 3: Host rock including sedimentary and intrusive rock. Sequences of host rocks have been divided into several sequences and their spatial relationship to veining system is shown in several cross-sections. The importance of physical properties of host rock such as felsite intrusive and other brittle rocks is also explained especially for the late stage mineralisation. Approximately eighty per-cents of ore are hosted in sedimentary rock, especially higher grade veins.

c) Chapter 4: Explaining the aspect of carbonaceous shale that hosts the mineralised veins and its influence on structural deformation by providing weak planes and geochemical contrast for the mineralised fluid. Several types of carbonaceous material and analysis of the carbon content will be documented.

d) Chapter 5: This chapter outlines the structural episodes and structural classification of veins as an important aspect to understanding geological control of episodes of vein emplacement. The role of folding and faulting in controlling vein emplacement and associated mineralisation is presented. Late structural deformation that is responsible for the displacement and deformation of vein is documented.

e) Chapter 6: This chapter outlines vein textures at various scales from hand specimen to microscopic aspects in thin sections. In addition this chapter presented the distribution and paragenesis of sulphide assemblages and their relationship to textural and structural deformation.

f) Chapters 7 and 8: The focuses here is on mineralogy of vein and clay minerals using X-ray diffraction (XRD), fluid inclusions, X-ray fluorescence study of major and trace elements of ore and hanging wall rock, trace element and lead isotope of galena by LA ICP MS.

g) Chapter 9: Conclusions on the process of structural deformation from regional to local settings. The vein system as a product of structural episode and its relationship to gold-sulphides mineralisation will be discussed. The formation of quartz veins, plus deposition of sulphides and gold, occurred within a single, major, deformation-fluid flow event is summarised in one table that comprises all elements discussed in each chapter. Geological control of the mineralisation event in PGM will also be compared to other regions such as at Bendigo Gold field, Victoria, Australia and Meguma Terrane, Canada.

1.4 Method of mapping

1.4.1 Introduction

Pit development started in late1996 and since then several phases of cut-back has taken place mainly to the south along the Penjom thrust for shallow ore bodies, east and west expansion to mine the deeper-ore bodies. The Jalis ore body was earlier mined in a separate pit, later combined with Kalampong East as the Kalampong pit. The Manik pit was first developed for an oxide ore as a separate pit. Fresh and less weathered ore from this area contributes to higher gold locking in sulphide compared to other areas.

At least four cut-backs to the south, two major push back to the north, three cutbacks to the east and three cut-backs to the west have taken place. Pit mapping of the pit wall for every cut-back were carried out to gain knowledge of the structural and geological styles including stratigraphy, fold, intrusive body, fault, as well as mineralogy of vein and distribution of sulphide minerals.

1.4.2 Geological mapping and methodology

Geological mapping involved pit wall mapping, temporary bench face mapping, mapping during the ore mining supervision and floor mapping. Pit wall mapping used 1:500 scale because it covers a wide area while geological mapping during the ore excavation and face mapping used 1:250 scale for the grade control plan and covers a small area. The flow chart of mapping methods and map compilation into plans and cross sections are shown in Figure 1.3.

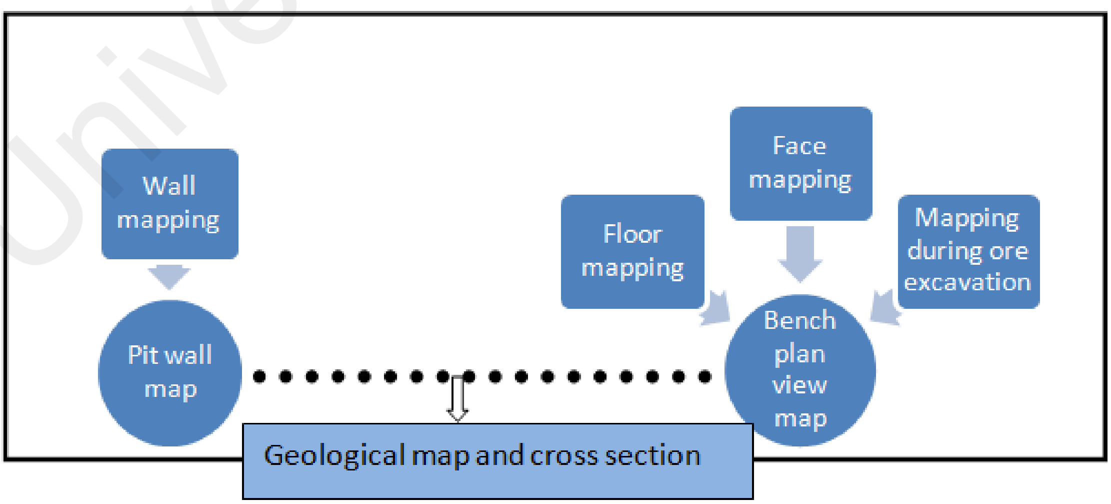

Figure 1.3: Flow chart of mapping activity and compilation into geological map.

1.4.2.1 Pit wall mapping

Pit walls were mapped as part of pit development. As the pit changed with each new cutback every one or two years depending on the resources model, geological mapping for every pit design was undertaken before a new cutback took place.

Pit wall mapping was conducted after the slope was trimmed so it represents the permanent pit wall map. Otherwise, it is just categorized as a temporary face mapping. Reference points were marked on the toe and crest of the cut. Reference points are marked on the geological features to be recorded instead of on the interval line. The points can also be transferred directly to the datamine/surpac/Arc view software.

Sketch of mapping and features of geology will be carried out and then marked with paint on the ground with their point ID. All the points will be picked-up by the surveyor. Geological assistant helps to mark the 1m interval between reference points if detailed geological mapping is to be carried out. Because the face exposure is good, the type of sulphides can be studied and recorded. This is important to correlate the vein genesis and sulphide mineralisation.

All the points were downloaded into the computer program and the base map with pit outline that shows the location of the reference point is produced. Now geological mapping for the whole face of the wall can begin. All the data will be plotted in datamine as a point and string for better visualization and structural continuity analysis. The wall mapping gave a good picture of the broad style of geological structure. Example of pit wall map is as shown in Figure 1.4.

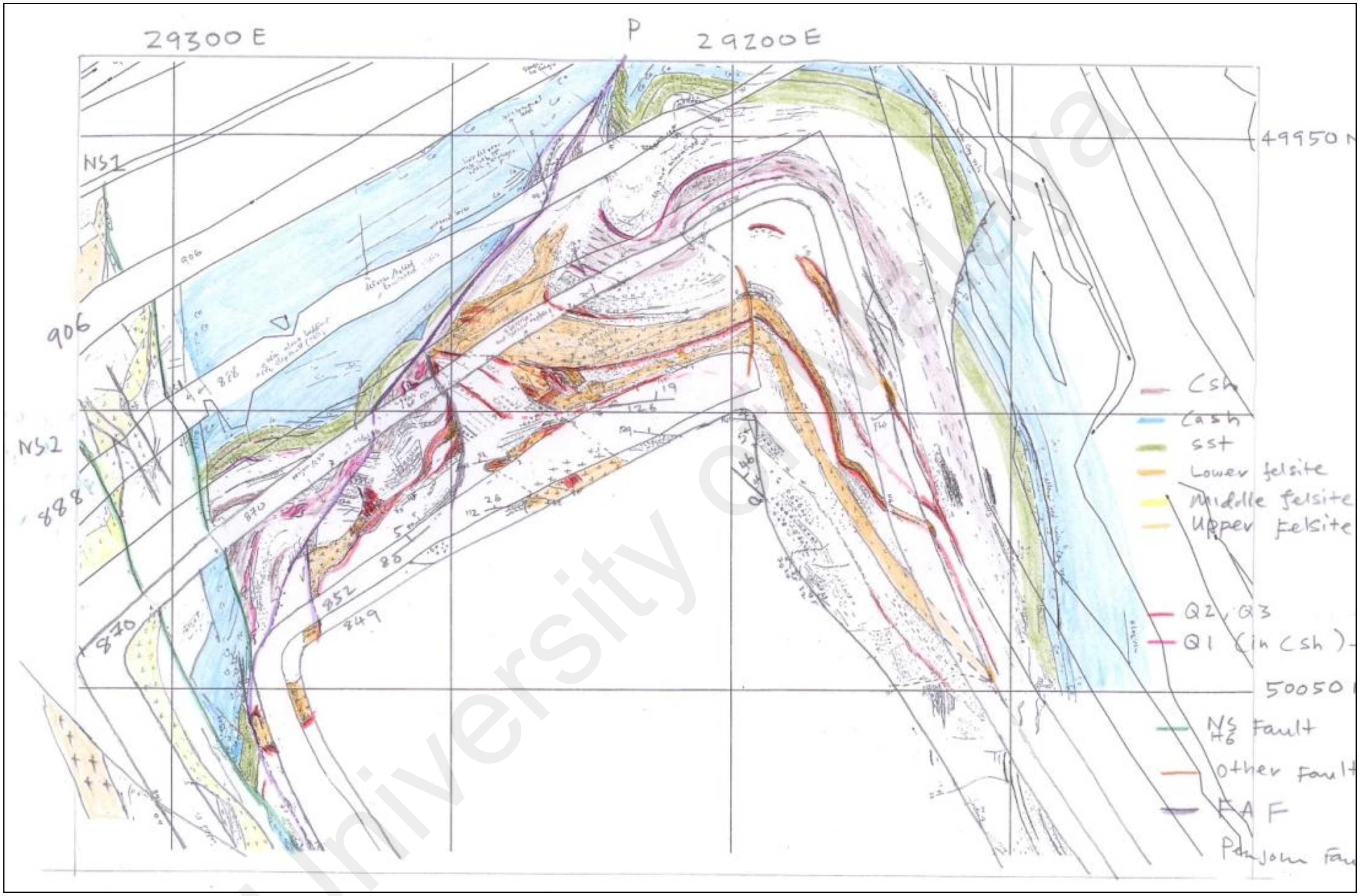

Figure 1.4: Example of pit wall map of the southern wall across the ore zone. Scale 1:1000.

1.4.2.2 Temporary bench face mapping

The purpose of this mapping is to collect geological features in the pit in active mining area and to know the extension of the structures from the pit wall in area where no ore mark out can be used for references. The close up view of the face and detailed observation can be done as addition to the mapping during the ore excavation.

Temporary bench face mapping was usually carried out on a notebook and later transferred into the grade control plan or datamine as an actual point location based on the survey location. Face mapping can also cover the ore zone area together with face/grab sampling to check the grade of the ore block. For latter exercise, the location of the sampling will be picked-up by the surveyor. The location of lithological boundary and structures of temporary bench face will be picked-up by the surveyor either on the toe or crest.

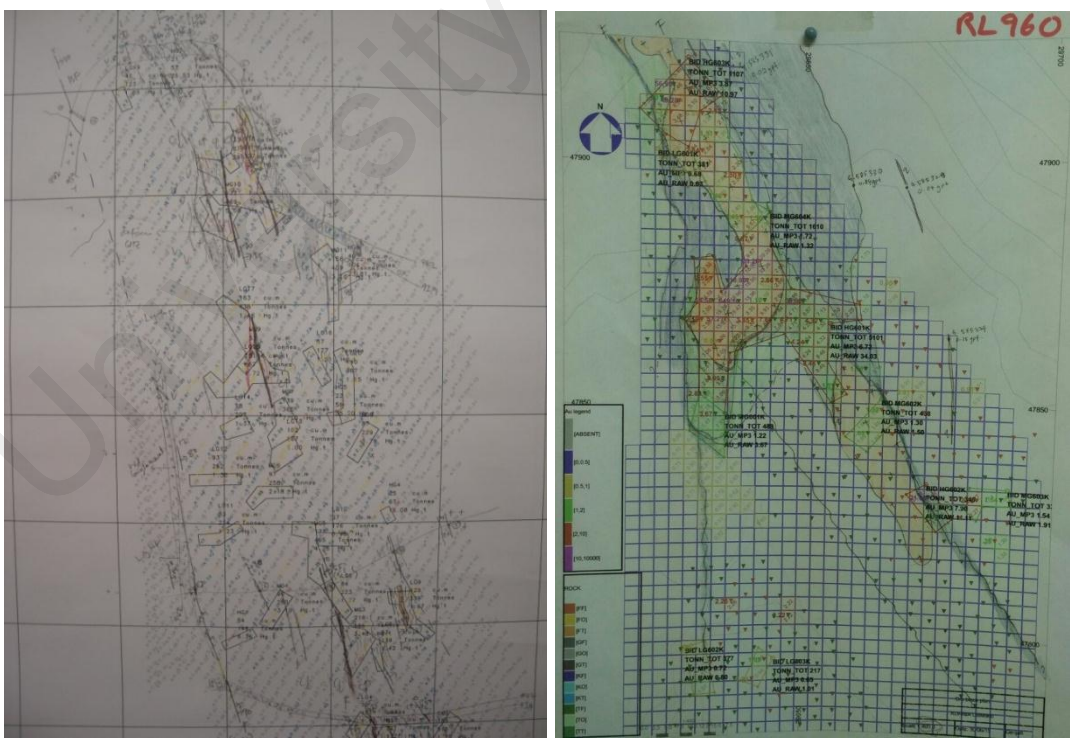

Figure 1.5: Example of geological observations during ore excavation plotted on grade control mining plan.

1.4.2.3 Mapping during the ore excavation

The inspection during ore excavation is a very important geological observation directly on the ore body and the geologist can observe the style of the quartz veining, continuation of the structures and other geological control of ore within the ore zone.

The mine scale structure, bedding plane outline, felsite boundary and the boundary of sedimentary rock sequences can be marked on the grade control plan (Figure 1.5) together with the geological map from the bench mapping. All mapping will also be plotted as a vertical section for every100m to understand vertical continuity of orebody. Five cross sections in Kalampong Pit have been constructed based on pit wall mapping and mapping during ore excavation as in Chapter 5.

1.4.2.4 Floor mapping

This mapping is carried out on the pit floor especially for structures such as mine scale fault; shear vein and intrusive contact prior to the ore mining or during site preparation for grade control drilling. Reference points were marked on the floor and then were located by the surveyor. All points were transferred into the grade control plan and maps were refined. After blasting, the refined maps were used as a guide during ore mark-up.

Floor mapping was very useful especially in active mining area where face mapping and mapping during ore excavation could not provide as much information.

1.4.2.5 Mapping from blast holes sample logging

Grade control sample logging data is also useful not only for the specific gravity determination but also for mapping of lithology. Currently, blast hole sample logging is good at showing the distribution of the felsite body and another rock types such as carbonaceous shale. However, at the contact, or for a small scale felsite bodies, the sample could be mixed up with other rock types so it still needs information from other mapping.

1.4.2.6 Core samples

There is few diamond drill cores drilled during 2008–2009 for underground project evaluation and the author has an opportunity to study the geological elements of core samples especially the distribution of sulphide minerals. However, the activity is under exploration project and no detailed data will be used in this study.

1.5 Geological observation

During geological mapping, several aspects of geology related to mineralisation were recorded in detail, such as fault direction and sense of movement, stratigraphy correlation and bedding to determine style of the folding, vein type and sulphide mineralogy. Among the important faults is the Penjom Thrust, NNE to NE faults and fold related faults such as fold axis faults, NNW and NS faults. Only mine scale fault will be plotted and other small scale faults are only used to determine the sense of movement and cross-cutting relationship. The important geological element in Penjom is outlined in Table 1.1.

Micro-structural aspects of the veins and host rock deformation were also recorded and have been studied under microscope to support field observation. Alteration minerals even though not always visible on outcrop scale, were also tested with XRD analysis to determine the clay minerals that may be related to alteration and mineralisation.

Table 1.1: The main geological aspects focused in this study include rock unit, vein, geological structures and sulphide minerals.

Geology	Stratigraphy	Intrusive rock	Vein	Fault	Sulphide minerals
	Upper sandstone	Medium grain intrusive	Shear vein Q1E, Q1W, Q2E, Q2W, Q3W	NNE fault	Various forms of pyrite
	Calcareous siltstone	Fine grain intrusive	Sheeted extension vein	Blue line fault (E-W)	Two forms of arsenopyrite
	Light grey shale	Micro-diorite	Quartz stockwork	Fold axis fault	Sphalerite
Element	Calcareous shale	Rhyodacite	Quartz breccia	Penjom Thrust,	Chalcopyrite
	Carbonaceous shale	Volcanic rock		NNW fault	Galena-quartz
	Sandstone			E-W fault,	Galena-calcite
	Massive siltstone			Penjom splay fault,	
	Conglomerate			NS fault, other fault	

1.6 Previous study

Table 1.2 shows previous geological study by different geologists during mine development mainly for the purpose of resource modelling. The overview by Corbett (1999) on sulphide paragenesis very much followed the porphyry-epithermal systems; hence is regarded as not applicable for further discussion. Bogie (2004) and Groves (2005) had pit visit and added further academic presentation of gold deposit classification by introducing the concept of Orogenic Gold deposits and their comparison to intrusion related gold deposit. Davis (2006) added structural paragenesis and clarified two phases of structural deformation where gold mineralisation is in its early stage.

Other studies are from local universities such as sulphides and geochemistry by Gunn (1993) and Ariffin (1994) during the preliminary exploration stages, wall rock alteration by Purwanto (2002), a stratigraphy and fossil study by Leman et al. (2004), an EPMA study by Abdul Aziz (2007) and the characteristic of fluid inclusions (Makoundi, 2012).

1.7 Conclusions

The comprehensive mapping and geological observation has led to a better understanding of ore formation. Performing all the technique of mapping practised in PGM is very important in understanding the geological aspects of mineralisation. All available geological data and understanding were compiled for this study. Three aspects are important in understanding gold mineralisation especially related to orogenic gold deposit: (1) sources of metal, (2) enrichment and deposition of metal to economic level commonly associated with the vein system, and (3) modification, remobilisation and displacement of the vein or metal. This study focuses in detail about the second and third aspects but only limited geochemical analysis for the first aspect especially involving invisible gold.

Table 1.2: Previous geological study conducted by geologists in Penjom mainly for resources estimation.

Year	Geologist	Downstream geological study	Upstream geological study
1997 1999	Greg Corbett and Exploration geologists	Pit visit. Limited diamond core logging. Ore deposit classification	
2000	Phil Fillis and exploration geologists	Pit mapping Optimized existing drill holes logging Ore structural setting	Resources modeling Generating ore target
2002	Menzies Consultant	Pit wall mapping Drill holes logging	Review geology and resources
2003	Penjom and Avocet geologists	Review the existing mapping Review existing drill holes logging. Ore structural setting	Produce cross section Resources modeling Generating ore target
2004	Ian Bogie	Petrography, age dating, ore deposit classification	
2005	David I Groves	Pit visit Ore deposit classification	
2006	Exploration geologists and Boyet Bautista	Pit wall mapping. Structural and deformation paragenesis	
2013	Brett Davis (Orefind)	Pit mapping and geology domaining	3D fold outline, modeling for resources domaining

CHAPTER 2.0 GOLD DEPOSIT CLASSIFICATION

2.1 Introduction

Understanding ore deposit models is essential because it can provide a set of basic characteristics in a concise and comprehensible manner for the overall understanding and targeting the extension of an orebody. Ore deposits are complex due to a wide range of genetic factors. Important factors include tectonic setting, host rock, structure, source and fluid composition and post-depositional modification.

Table 2.1: Summary of the Lindgren gold classification (after Lindgren, 1933)

Deposit	Temperature and pressure
1- Hypothermal deposit	High temperature and high pressure
2- Mesothermal deposit	Low temperature (200-300^{o}C) and moderate depth (1200-4500m)
3- Epithermal deposit	Low temperature (50-200^{o}C) Near surface (0-1500m)
4- Lepothermal deposit	Temperature and pressure in between epithermal and mesothermal
5- Telethermal deposit	Low temperature and pressure but away from sources
6- Xenothermal deposit	Broad range of P-T condition

Fluid sources, tectonic environments and timing relative to an orogenic event or tectonic activity has become popular in defining gold deposit classification, as described by Groves et al. (1999), rather than simple classification by depth of ore formation, as described by Lindgren (Table 2.1). In addition, vein styles are not the same in different structural environment and stress control, as described by Stephens et al. (2004, Figure 2.7). Different styles of vein texture provide the simplest way for classifying a gold deposit, especially low-sulphidation epithermal and orogenic gold (slate belt), as described by Dowling and Morrison (1998). Furthermore, recent developments in analytical methods has encouraged in depth study in every field to characterize different criteria such as by isotope and microprobe analysis on veins and sulphides. Some problems may occur if spatial relationship between magmatisms and ore deposit exist, especially when intrusive rock is the host to gold deposit.

Some of the essential gold deposit classification model include the Witwatersrand type, porphyry, epithermal (low and high sulphidation), orogenic, intrusion related, Carlin type and skarn gold deposit. Table 2.2 shows the comparison of three main groups such as orogenic, intrusion related and porphyry-epithermal systems (magmatic arc gold deposit).

Table 2.2: Summary of gold deposits classification based on fluid sources and crustal depth. Depth is only relative in two groups and superimposes may occur due to the uplift and reactivation.

	Depth	**Orogenic lode gold**	**Intrusion related gold**	**Porphyry system (Magmatic arc/intrusion sources) (Corbett,1997)**
Tectonic environment		Orogenic/ metamorphic belt/accreted terrane	Orogenic /metamorphic belt/accreted terrane	Magmatic arc, rift system
Metal association and sub-class	Shallow	Epizonal Au–Sb (Depth < 6km).	Epizonal Intrusion Related gold	Epithermal low or high sulphidation (Depth < 2 km)
	Moderate	Mesozonal Au-As-Te (Depth 6-12km) (Carbonate base metal and quartz sulphide gold only as mineral assemblage)	Mesozonal Intrusion Related gold	Carbonate base metal gold Quartz sulphide gold +copper (Depth: 2-5 km)
	Deep	Hypozonal Au-As (Depth >12 km) (May have skarn like assemblage, fluid salinities differ from the skarn)		Porphyry copper-gold Skarn gold (Depth 2-5 km)

2.2 Ore forming process

More than one mechanism may be responsible for the formation of ore bodies. Secondary processes can involve the modification of earlier ore body or superimposed by another style of mineralisation. This results in a complex style of ore occurrence. Ore deposit classification requires an understanding involving sources, transportation and association of metal and the physico-chemical environment of mineralisation. The processes are also related to the stress condition and tectonic environment including igneous activity and remobilisation. Gold is economically formed through certain process and as trace elements (not economic) in other different ore forming processes.

These processes can be divided into three major categories:

a) Igneous/magmatic process
b) Hydrothermal process
c) Sedimentary and surficial process

2.2.1 Igneous/magmatic process

Precious metals that are spatially and temporally related to igneous rocks are classified as occurring through igneous process involving the in-situ crystallization of magma and contain the economic concentration of metals. The in-situ ore is located within the igneous body itself. Magmatic segregation involves two processes: (i) fractional crystallization that forms an alternate layer of ore and silicate (eg. chromite–magnetite Bushveld igneous complexes) and (ii) immiscible liquid where different metal density will be settled out separately (iron sulphide, nickel, copper and platinum Sudbury, Canada). These processes are not common for gold, but new research shows gold can be found as inclusions in quartz grains in igneous rock (Zhaoshan Chang, pers. Comm., 2013).

2.2.2 Hydrothermal process

Hydrothermal fluid originated from intrusive body or metamorphic fluid formed the major part of ore deposits. The fluid is forming the vein system infiltrated into the wall rock or solidified portion of intrusive itself. The hot hydrothermal fluid moves upward and is capable of scavenging, remobilizing, concentrating and depositing the metals into a structural trap. The sources of gold in the case of sedimentary-hosted gold deposits are from the sedimentary rock (carbonaceous shale) itself.

2.2.3 Sedimentary and surficial process

Sedimentary processes involve gold particulates within sulphides, in particular pyrite in a sedimentary basin involving carbonaceous shale sedimentation in an anoxic environment. Gold could be extracted from seawater, or introduced by a river into the basin as microscopic or colloidal gold (Large et al., 2011, Makoundi et al., 2013, Makoundi 2012). Later, diagenesis and concentration by the hydrothermal fluids are required to form the economic deposit as a two-stage process.

Surficial process involves chemical weathering processes such as supergene enrichment. The alluvial gold deposit as a result of erosion of bedrock that containing gold and re-deposited on the valley or basin. These processes form small gold deposits and are viable for small-scale gold extraction.

2.3 Several classes of gold deposits

Figures 2.1 show the regional tectonic setting for formation of gold deposit. The main gold deposits mentioned in this discussion are vein-hosted gold deposits, which include orogenic, intrusion-related, low-sulphidation epithermal and porphyry gold deposits. Previously, the first two types of deposit were known as mesothermal gold deposit. As shown in Figures 2.2 and 2.3, a significant proportion of porphyry deposits are from overlying subduction zones that are distal to the continental margins or within the continental margins but during the post-collisional extension (Groves, 2003). Many other epithermal deposits are associated with alkali-mantle-related rock that reflects extensional episodes in a convergent margin.

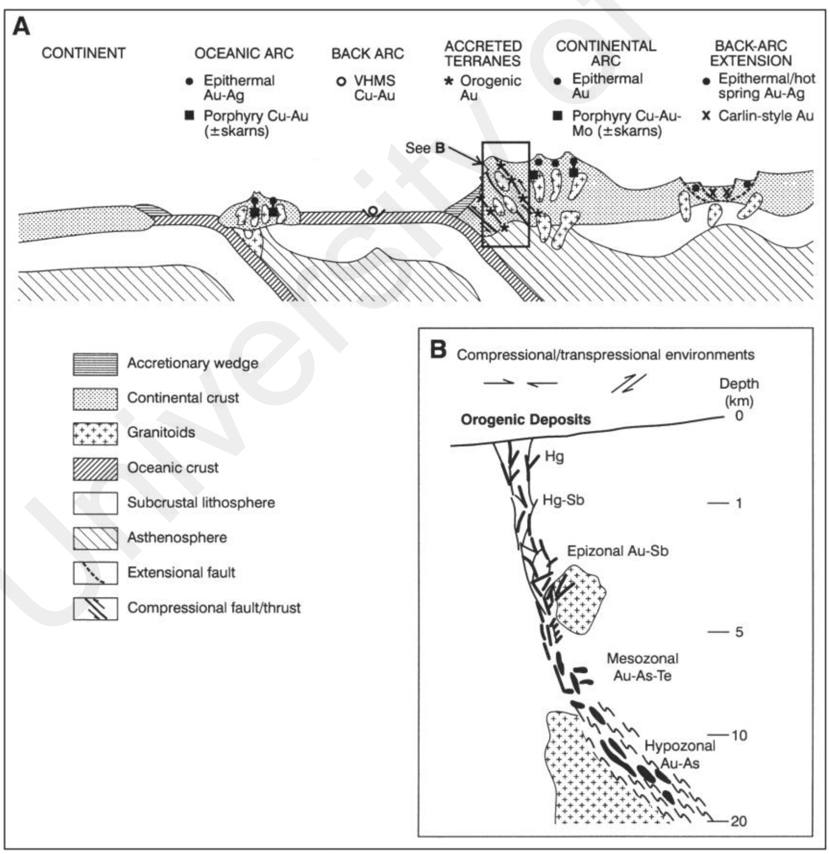

Figure 2.1: Tectonic settings of gold-rich epigenetic mineral deposits. Vertical scale is exaggerated to allow schematic depths of formation of various deposit styles (Groves et al., 1998).

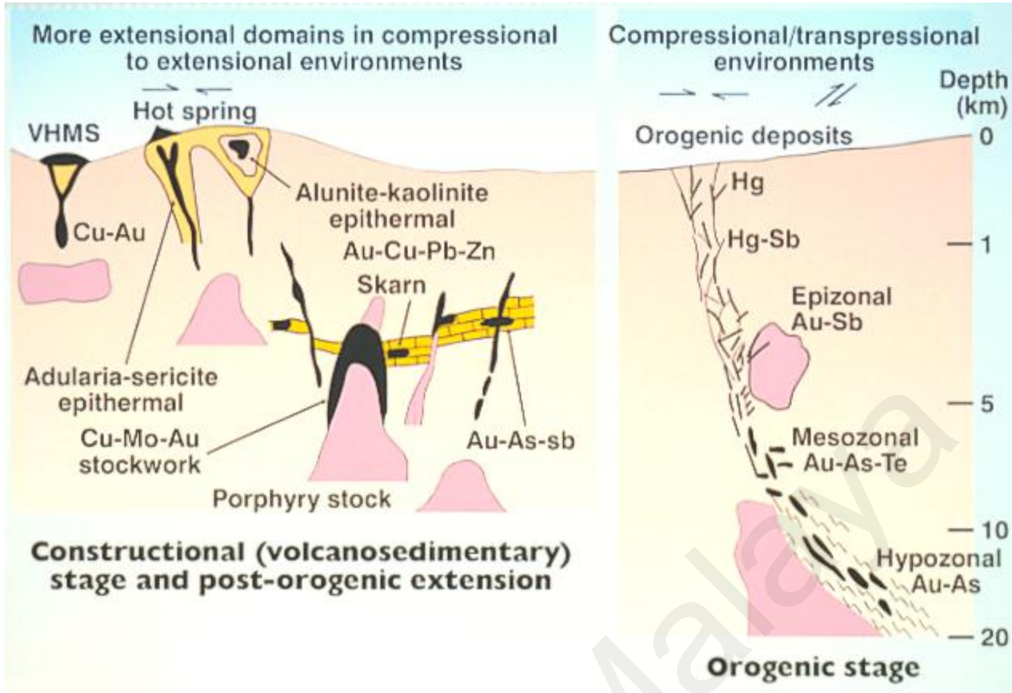

Figure 2.2: Idealised cross section of gold deposit in different tectonic regime (after Groves, 1999).

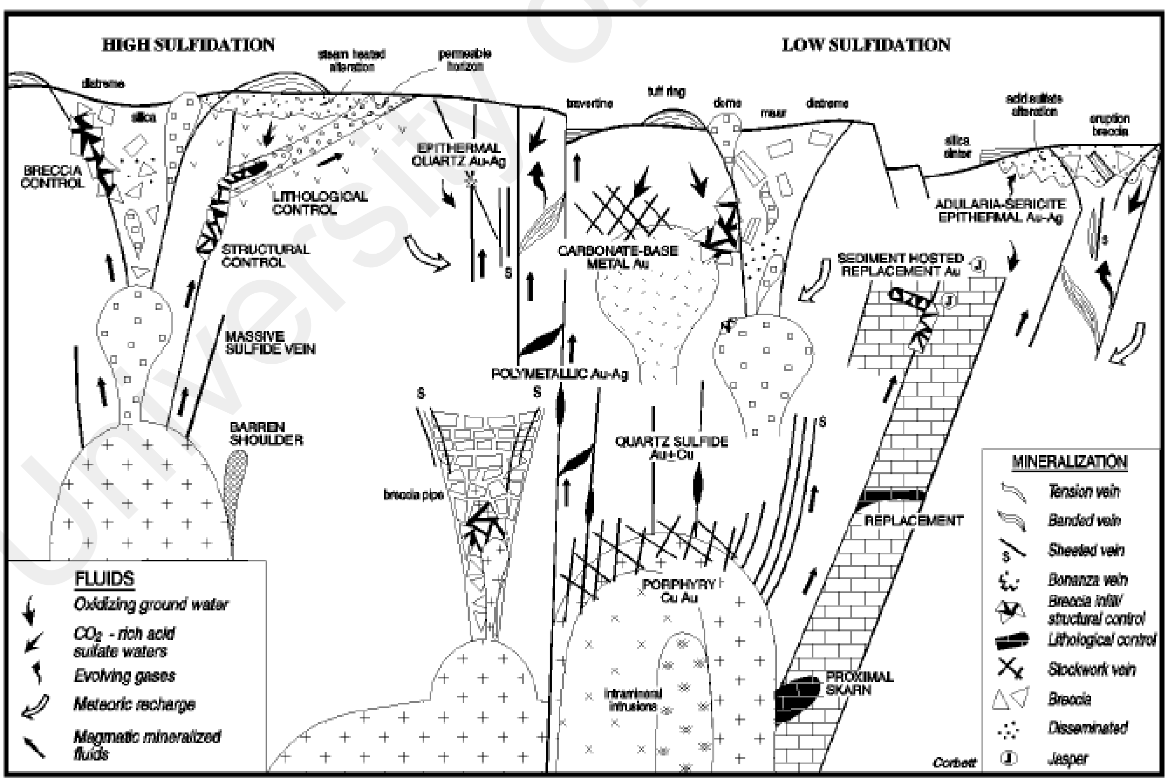

Figure 2.3: Conceptual model for styles of magmatic arc epithermal Au-Ag and porphyry Au-Cu mineralization (Corbett, 1997).

While most gold deposits are located along convergent plate margin (Groves, 2003), a few subclasses of epithermal deposits are located along spreading ocean ridges such as gold-rich volcanogenic massive sulphide deposits. Subclasses of gold deposits such as Carlin-style sediment hosted disseminated gold deposits associated with pyrite are located at the back arc extensional regime of a post-orogenic event. In Nevada (USA), this deposit is related to a continental rift setting. Post-rifting compressional event formed a favorable site for auriferous fluid into permeable and reactive calcareous host rocks (Cline et al., 2005).

2.3.1 Orogenic gold deposit

Grove et al. (1998) defined the term orogenic lode gold deposit to include those deposits widely referred to as mesothermal (Nesbitt et al., 1986). In the past 20 years, gold deposit terms are based on their ore associations (e.g. gold only), their host sequences (e.g. greenstone-hosted, slate-belt style or turbidite-hosted), their form (e.g. lode gold, quartz carbonate vein or disseminated deposits), age of host rock (Archean type) or even their specific location (e.g. Mother lode-style deposits).

Grove et al. (1998) further suggested the use of the terms epizonal, mesozonal and hypozonal to describe specific depth segments of the vertically extensive orogenic gold systems, with epizonal deposits <5 km, mesozonal deposits from 5 to 10 km and hypozonal deposits >12 km (Figure 2.2).

2.3.1.1 Geology of the host terrains

The deposit commonly occurs within deformed metamorphic terrain or orogeny belt of greenschist facies but certain ore deposit hosted within rocks with lower or higher degree of regional metamorphism. Majority of the deposit are located near the first-order major fault or crustal-scale fault zone, and vein ores commonly occur along the second or third-order fault.

Deposits formed within a dilational space because of deformation that occurs commonly at a fold-hinge, competency contrast unit, especially for deformation related to compressional or transpressional fault. Gold mineralisation timing is always structurally late, syn to post-peak metamorphic events. Veins are common hosts to gold and other sulphides, in addition to altered wall rocks. Stockworks and breccias are common in brittle or shallow units and ribbon to laminated deposits occur in more ductile processes, especially the fold involving repeated opening of the structure or bedding. Understanding the vein formation is essential to unravel the structural control of gold formation.

2.3.2 Intrusion-related gold deposit

The class evidently reflects many different types of gold deposits that are suggested to show a relatively local and spatial zonation within and surrounding causative pluton. With some exceptions (e.g. Muruntau, Charters Towers and Jiaodong), there is little debate that most of these gold deposits are genetically associated with a well-defined igneous body and are thus well-classified as intrusion-related deposits.

Intrusion-related deposit differs from gold deposit in magmatic arc where they are related to low primary oxidation state granitoid and relatively hosted within metamorphic terrane. They have many similarities to orogenic deposits in terms of metal associations, wall rock alteration assemblages, ore fluids and to a lesser extent structural controls. Hence, some deposits, especially those with close spatial relationships to granitoid intrusions, have been placed in orogenic as well as intrusion-related categories by different authors (Groves et al., 1998).

2.3.2.1 Geology of the host terranes

Intrusion-related deposits are located at the same tectonic setting with orogenic lode gold but occurring at more landward from the accreted terrain. What distinguishes them is they are related to intrusive with a stronger relationship than the intrusive just being the country rock. Ore body is commonly low grade and sources of fluid originated from reduced granitoids that emplaced into the country rock.

Sillitoe (2000) described intrusion-related gold deposits as being mainly restricted to accreted terranes in Phanerozoic convergent plate margins, spatially associated with porphyry Mo or Cu–Mo mineralisation, related to magnetite series I-type intrusions, characterised by an As–Bi–Te geochemical signature, and having formed from magmatic and/or meteoric fluids.

Mineralisation is approximately coeval with the host or associated intrusion. These intrusive hosted deposits can be differentiated from the ore hosted within the older intrusive and related to structural control and that the timing of gold is later than the intrusive. For the later deposit style, it falls into orogenic lode gold.

2.3.3 Porphyry (copper) and gold deposits

These deposits are commonly host to large tonnage, bulk mineable deposits related to porphyritic intrusions. The deposits are commonly associated to skarns and epithermal deposits. Cu, Au and Mo (molybdenum) are the main metals and can be used for classifying the porphyry deposit type to either as Cu–Au (e.g. Grasberg), Cu–Au–Mo (Bingham Canyon, US) or Cu–Mo (Rio Blanco, Chile). Two main porphyry intrusives associated with the deposits are alkali series with silica saturated to under-saturated basically associated with Cu–Au, and calc-alkalic series with a higher percentage of silica associated with Cu–Mo (Lang et al., 1995). Metal endowment, especially Cu–Au, also controlled by higher oxidation state, which is more associated with Cu–Au (Blevin, 2008).

2.3.3.1 Geology of the host terrains

Porphyry (copper) and gold deposits are formed at shallow crustal level (<3km) related to the multi-phase of magmatic hydrothermal activities within compressional arc setting with common relationship to subduction environment and magmatic belt. The deposits are formed around the intrusion emplaced at higher level when fluid pressure exceeds lithostatic load and rock tensile strength, producing the stockwork veins.

2.3.4 Epithermal gold deposit

Epithermal gold deposits are formed at shallower crustal level (usually less than 1km below the water table and at 170°C–280°C). The deposit is classified into high and low sulphidation based on the occurrences of gangue minerals and mineralogy. Intermediate-sulphidation deposits are much more similar to low sulphidation deposits. Not all epithermal deposits contain economic gold and some are rich in Ag, Zn, Pb, Cu or Sn. Some of the deposits may not be related to porphyry copper but are commonly related to igneous volcanic rock (White and Hedenquist, 1995).

2.3.4.1 Geology of the host terrains

Even though subduction-related volcanic arc is a common place, some epithermal deposits also occur at large igneous provinces, post-collisional setting or rift setting. Calc-alkaline to alkaline series volcanic arc are common than the tholeiitic series. Epithermal deposits that are currently explored and mined are commonly from younger environments, because deposits in such environments are well preserved compared with those in older terrains. The older one may have eroded or covered by sedimentary successions.

Low-sulphidation epithermal are mainly hosted within the vein and disseminated in wall rock or replacement is minor in contrast to high-sulphidation system which is dominant as disseminated and replacement ore.

2.4 Other subclass of gold deposits

2.4.1 Disseminated sedimentary hosted/Carlin type

These deposits are characterised by an association with high-angle extensional structures, impure carbonate host rocks and arsenian pyrite ores in which gold may be encapsulated and disseminated in the host rock, anomalous Hg and Sb and locally intrusive rocks. Cline et al., (2005) summarised the various model of ore formation including the meteoric water circulation, epizonal plutons that contributed heat and possibly fluids and metals and deep metamorphic fluids +/- magmatic fluid. Large et al., (2011) proposed the carbonaceous shale as a potential source for gold in Carlin-type and sediment-hosted orogenic gold deposits.

2.4.2 Volcanogenic massive sulphide

This is part of the high-sulphidation system interpreted to have formed in a sub-aerial environment by modifying hot acidic fluids produced from the absorption of magmatic-derived volatiles into circulating meteoric waters (Sillitoe, 2000). Corbett (1997) further defines this gold deposit as:

- Related to submarine intermediate to felsic intrusions
- Associated with advanced argillic alteration and capped by barite-rich zones
- Gold mineralisation in pyrite-rich zones

Sillitoe (2000) assumes that copper–gold high-sulphidation exhalative deposits are formed proximal to the intrusive source of magmatic fluid, where more classical Zn–Pb-Cu volcanic massive sulphide is equivalent to a low-sulphidation system and develops at a more distal setting.

2.5 Gold deposits related to vein textures

Morrison (1998) simplified gold deposits for vein texture study and their relationship to sources of fluid and interaction with ground water. Four gold deposit environments, namely slate belt (orogenic/mesothermal deposit), plutonic (intrusion related), porphyry and epithermal, as shown in Figure 2.4, are associated with vein structure as a dominant host for gold and having characterised by the different styles of vein texture.

Shear hosted zone or mesothermal/orogenic gold has more metamorphic fluid as a metal source than the magmatic source. Plutonic environment deposit has a spatial correlation with intrusive and occurring within the orogenic environment. Fluid sources are basically from deeper intrusive but have temporal relationship with the host intrusive. Porphyry and epithermal deposits are within the same system, where the fluid is basically from magmatic and interact with the ground water.

Different environment produce different vein style, and subsequent deformation and reactivation further modified the vein style. Vein structures and textures in Penjom are described in chapters 5 and 6. Type of veins and continuity of the structure can be correlated to ore deposit types such as porphyry, intrusion related and orogenic. Vein and structural deformation were described by Stephens et al. (2004) that are based on the Alaska gold deposits.

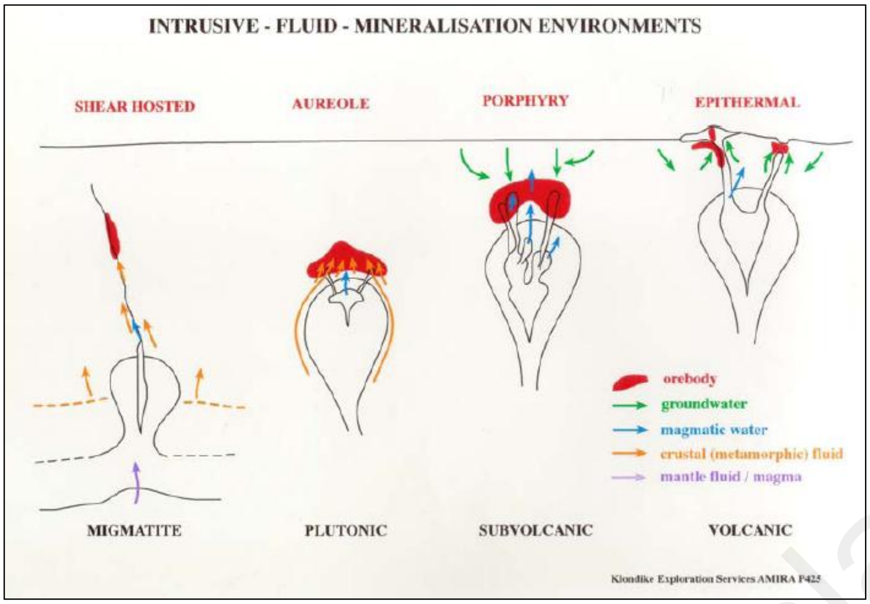

Figure 2.4: Gold deposit environment used by Morrison (2007) for vein texture classification

2.6. Tectonic setting and gold deposit: Mainland South East Asia (SEA)

The mainland region host many gold deposits of pre-Cenozoic age in Thailand–Malaysia and also of post-Cenozoic age such as in Myanmar. Major tectonic setting for the central belt of Malay Peninsula has been suggested as volcano–plutonic belt to accreted terrain (Hutchison, 2009; Tan, 1996) and strike slip transpressional corridor (Mustaffa Kamal, 2009) or aborted rift (Tan, 1996). Fold belt is not yet applied for the central and eastern belt of Malaysia but has been proposed for Thailand regions such as Sukhothai Fold Belt.

The Malay Peninsula hosts sediment-hosted/orogenic gold deposit, porphyry copper–iron gold skarn and volcanic exhalative massive sulphide gold deposit. Figure 2.5 shows the location of gold occurrences in Peninsular Malaysia. In Thailand–Myanmar–Laos, there are other types of deposit such as high-sulphidation copper–gold deposit (Zaw, 2014), disseminated sedimentary hosted gold and epithermal gold deposit. Table 2.3 shows the example of the type of gold deposits in central belt and mainland of South East Asia. The example of primary occurrences in the central belt of Malaysia Peninsular and Loei fold belt are shown in Figure 2.6.

Table 2.3: Several types of gold deposits in mainland of South East Asia

Deposit/sub-deposit type	Example	Reference
Orogenic lode gold/mesothermal	Penjom, Selinsing, Huai Kham On	Groves, 2003, Zaw, 2014
Porphyry-gold skarn	Mengapur (Pahang), Phukam (Loas)	Teh et al., 2008, Zaw, 2014
Low sulphidation epithermal	Chatree, Thailand	Zaw, 2014
Disseminated sedimentary hosted	Sepon, (Loas) Langu (Thailand)	Zaw, 2014
VHMS	Ulu Sokor, Tasik Chini, Badwin, Myammar	Yeap, 1998, Teh et al., 2008, Zaw, 2014.

.

On a regional scale, vein related gold deposits are always related to tectonic processes either subduction zone, major fault either compressional, transpressional or transtensional setting and associated with subsidiary structures such as fold, thrust/reverse and strike slip or extensional faults. Major first-order faults mainly provide the main conduit for fluid. Magmatic intrusives accompany these events and provides heat or fluid sources. For the orogenic gold, faulting and shear are dominant in controlling vein system especially in continental and accreted terrains. Structures provide the conduit and trap for the fluid. Regional structure is important in orogenic gold compare to the local fault which controls the conduit in intrusion related gold. The main stress controlling the direction of vein in porphyry system is related to the stress induced by the intrusion itself such as in Figure 2.7 as described by Stephen et al., (2004)

Gold mineralisation in the Central Belt requires more research to determine the tectonic environment, temporal relationship with intrusives by dating of both intrusive and mineralisation to constrain the geological processes that lead to gold mineralisation. The Central Belt hosts several orogenic mesozonal gold deposits in the inferred accreted terrain or structural deformation zone.

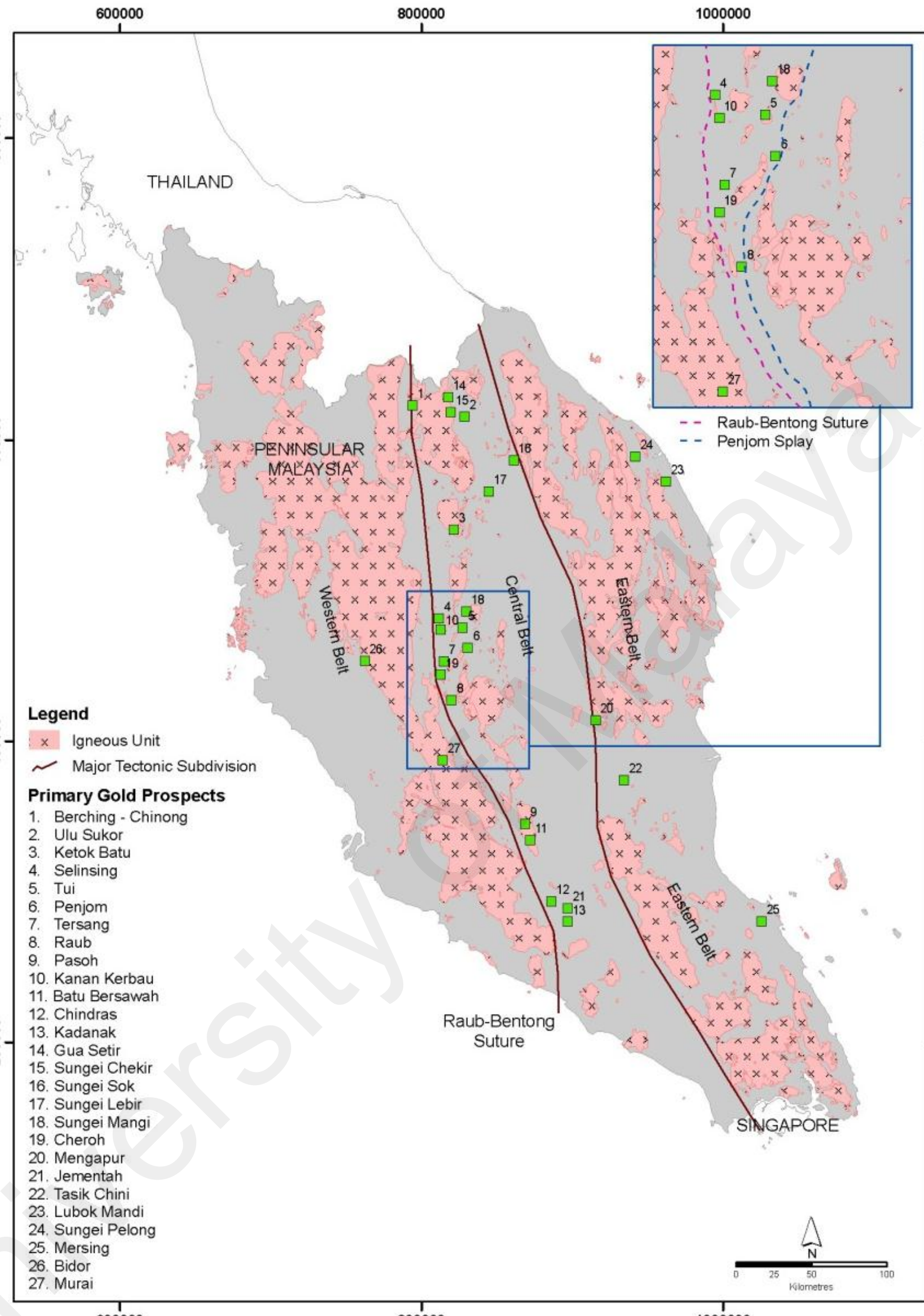

Figure 2.5: Location of primary gold deposit in Malaysia Peninsular (after Yeap, 1999). Gold deposit in between purple and blue line lineament in inset figure hosted within vein system.

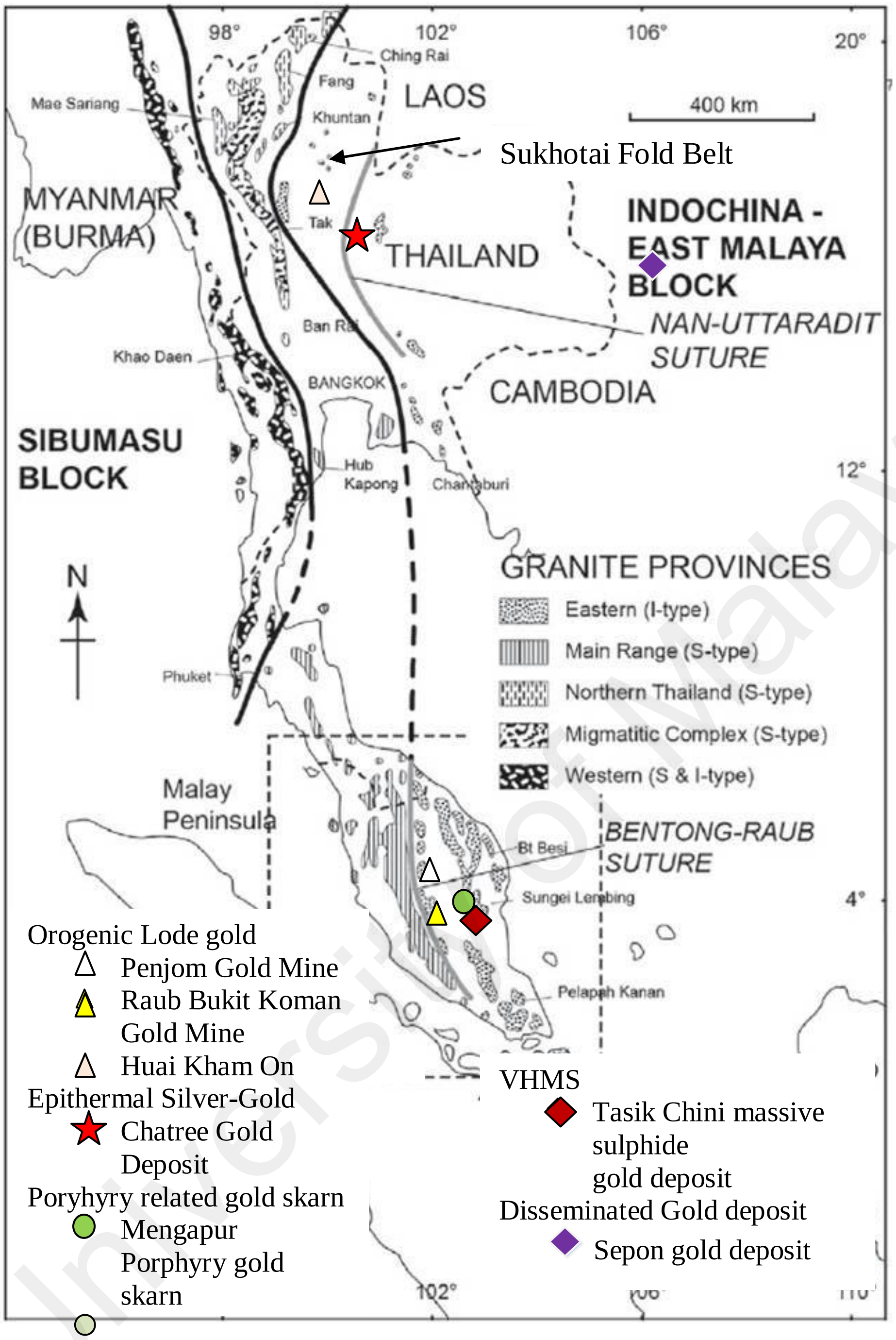

Figure 2.6: Gold deposits along Central Belt (Malaysia Peninsula)-Sukhotai Fold Belt and South East Asia granite provinces (after Cobbing et al., 1986; Ng et al., 2015)

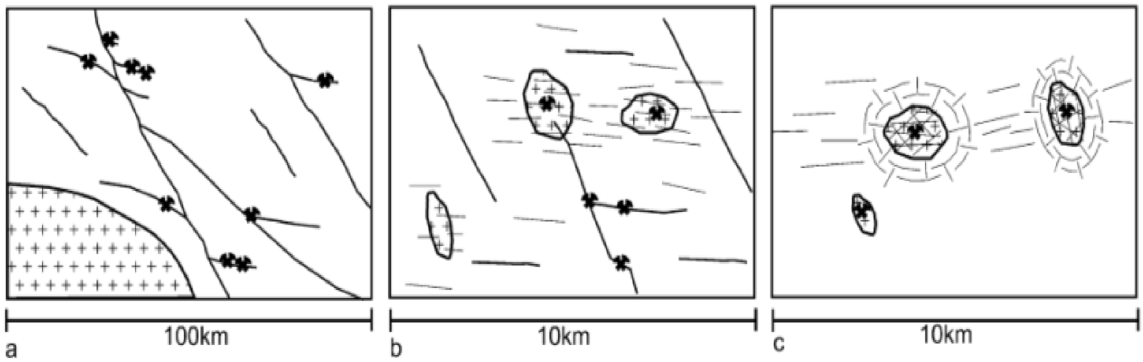

Figure 2.7: Hydrothermal ore deposit and its location in geological setting of magmatic bodies and major shear/ fault system (Stephens et al., 2004). a: Orogenic gold, b: Intrusion related, c: Porphyry gold.

CHAPTER 3 HOST ROCKS OF THE PENJOM GOLD DEPOSIT

3.1 Regional geology

The Malay Peninsula can be divided into three belts, namely the western, central and eastern belt (refer to Figure 1.1). The central belt of the Malay Peninsula is a part of the East Malaya or the Indochina block. This terrain and the Gondwana-affiliated Sibumasu terrain were joined together along the Bentong–Raub Suture at the end of the Permian (Metcalfe, 2000, 2013). According to Metcalfe (2002) an ocean was present between Sibumasu and Indochina in the early Permian and that suturing of this terrain occurred only in Triassic.

The central belt comprises Carboniferous to Cretaceous sedimentary sequences. The former is represented by the Raub Group, the Gua Musang Formation represents the Permian host rock and the Triassic (Early) is represented by the Semantan Formation. The youngest stratigraphic sequences are continental deposits of the Tembeling and the Gagau Group. The volcanic activities and related pyroclastic rocks and tuffaceous siliciclastics dominated during the Triassic times. Volcanic rocks such as the Pahang Volcanic Series can be found within the Gua Musang Formation and within the tuffaceous sediment in Semantan Formation.

Overall, the Central Belt granite forms narrow bodies parallel to Bentong-Raub Suture. The Western Belt granite famously related to tin deposits, is dominantly S-type, biotite granite intruded mainly during Mid-Triassic as a result of crustal thickening during the collisional of the Sibumasu and East Malaya (Indochina) block. The Eastern Belt is comprised of Permo-Triassic I-Type hornblende-biotite granitic bodies with subordinate S-Type plutons.

3.2 District geology and stratigraphy

Penjom Gold Mine (PGM) lies 30km east of a major terrain boundary, the Bentong-Raub suture within the Central Belt of the Malay Peninsula (refer to Figure 1.2). Regional structures, as seen on RADARSAT imagery shows that Penjom is situated along the NNE trending lineament splay from the main Bentong–Raub Suture as indicated by a lineament. The host rock sequence was previously classified as being part of the Padang Tengku Formation.

The sedimentary sequence at the vicinity of the mine has a fossil assemblage of Middle to Late Permian; this fact is based on the fossils in tuffaceous shale at Gua Sei, 5km from the mine site (Leman, 1993) and Gua Bama (4km from mine site, Nuraiteng, 2009). On the basis of fossil occurrences in the calcareous bed of upper mine sequence in the pit, Leman et al., (2004) had proposed the age of Penjom sedimentary sequences as Middle to Late Permian. Makoundi (2012) carried out U-Pb zircon dating and found and age of 260-265 Ma (Early Permian) in the tuffaceous siltstone and conglomerate unit.

The Padang Tengku Formation is part of the Permo–Carboniferous Raub Group which also comprises the Sungai Kenong and Sungai Sergis Formations, which overlie the older strata of the Bentong Group (Procter, 1972). A narrow strip of Triassic Arenaceous Series rocks of the Lipis Group lie just east of the study area. The regional strike of the Padang Tengku Formation and Lipis Group is approximately NNE with dips of 50^{o}–60^{o} towards the east (Gunn et al., 1993). Leman (1991) classified the entire Padang Tengku area, including Penjom, as being part of the Gua Musang Formation on the basis of the similarity with the rock sequence in Merapoh, near the Gua Musang area, 70km north of Penjom.

Two major Central Belt granitic masses intruded near the study area, the Bukit Lima granite to the west and the Gunung Benom Batholith to the south-west. The lithology of the former range from granodiorite to biotite granite in composition, and the latter from syenitic, monzonitic to gabbroic in composition (Procter, 1972). Dating has been performed on the Benom Complex and it has yielded an age of late Triassic 207Ma (Cobbing et al., 1986) close to the age of mineralization at Penjom, which is 197Ma (Bogie, 2002).

3.3 Stratigraphy setting of PGM

3.3.1 Introduction

The distribution of host rocks, especially sedimentary rocks, has been studied and is being utilized as a marker horizon for fold analysis, for the stratigraphic correlation of bedding parallel shear veins and to understand the displacement pattern of marker bed by faults. The end result is that stratigraphy is used as a structural approach in understanding the factors that control mineralization. Stratigraphy break and repetition complicates correlation in this study.

The relationship between stratigraphy and mineralization was correlated and established to make the stratigraphy study as the initial guide for targeting ore extension, both along the depth and strike of the mine area. The stratigraphy of the Penjom area during the early stage of the project was poorly documented, and most of the sedimentary rocks have been referred to as tuffaceous of pyroclastic origin. Continuous detailed mapping and structural analysis has led to a better understanding of the stratigraphy correlations in the pit area.

Representative rocks have been collected and prepared for petrography analysis of thin sections at the Geology Department, University Malaya. Altered and deformed host rocks are also studied under thin section for micro-structural analysis related to deformation.

3.3.2 Mine stratigraphy

A stratigraphic study has been conducted in the Kalampong East (KE), Jalis, Janik and Manik pits as the pits continue to develop and more fresh rocks were exposed to facilitate the study. Stratigraphy units in Penjom Gold Mine were grouped into three stratigraphic sequences: upper, middle and lower mine sequences (UMS, MMS and LMS). They comprise nine sedimentary rock facies or units. The stratigraphy successions are shown in Table 3.1.

Table 3.1: Group of rock units in the stratigraphy sequences.

Rock facies	Thickness (m)	Sample	Stratigraphic sequences
1. Upper well bedded calcareous siltstone 2. Sandstone with minor thinly bedded carbonaceous shale siltstone. 3. Lower well bedded calcareous siltstone 4. Greenish tuffaceous siltstone / reworked tuff 5. Calcareous shale	>100	UMS 1 UMS 2 UMS 3 UMS 4 UMS 5	**Upper Mine Sequence (UMS)**
6. Carbonaceous shale and siltstone 7. Greyish sandstone with thinly interbedded carbonaceous shale and conglomerate	Up to 80	MMS 1 MMS 1A MMS 1B MMS 2 MMS 3 MMS 4	**Middle Mine Sequence (MMS)**
8. Greenish/reddish grey tuffaceous massive siltstone to conglomerate 9. Well bedded siltstone with volcanic rock	>100	LMS 1 LMS 3 LMS 2	**Lower Mine sequence (LMS)**

In PGM, ores associated with shear veins are found to be hosted in the middle mine sequence and at the boundary between MMS and LMS sequence. Fault related veins in the form of an irregular vein network continue into the LMS, mainly at the felsite intrusive-fault contact such as in Jalis. Other veins in the LMS are in the form of a sheeted extension veins striking E–W. A few spots at the hanging wall within the UMS are host to some weakly mineralized sheeted and irregular veins but are not economically important. The trend of stratigraphy, as indicated by bedding, is along NNE and dips to the East, but below the Penjom Thrust, folding in the KE pit produced a local but a significant west dipping sequence, which hosts the main ore body including North–South Jewel Box.

3.4 Detail description of sedimentary rock units

The following detailed description of the sedimentary rock units is based on the field observation and petrographic study.

3.4.1 Upper well-bedded laminated siltstone and shale (UMS 1)

Well-bedded siltstone is the highest unit exposes in east wall of KE. It consists of mainly well-bedded siltstone (up to 30cm thick) with thinly interbedded carbonaceous shale and has a thickness up to 10cm. Two units (UMS 1 and 3) can be observed above and below the sandstone unit (UMS 2) with a total thickness of more than 50m. The rock is weathered in most parts of the pit and is slightly calcareous in some fresh parts.

3.4.2 Sandstone with minor thinly bedded shale and siltstone (UMS 2)

This sedimentary unit only is exposed on the east wall. It comprises light grey, thickly bedded to massive sandstone with minor thinly interbedded shale (Figure 3.1 Left). Quartz and minor lithic clasts made up the grain composition (Figure 3.1 right). No conglomerate was observed, but a few beds at the transition zone with siltstone have some pebbles of carbonaceous mudstone (Figure 3.2 right). The observed thickness of the individual sandstone bed was up to 1.5m. Lamination and flaser bedding (Figure 3.2 left) can be observed at the upper part of the sandstone unit, which comprises a dark thin layer of shale and siltstone.

Figure 3.1: (Left) Well bedded sandstone of upper mine sequence. (Right) Photomicrograph of sandstone with poorly sorted quartz fragment (Q) dominant and minor lithic (L) fragment with sericite and patch of carbonate (UMS2).

Figure 3.2: (Left) Flaser bedding at upper part of the sandstone bed. (Right) Pebbles of carbonaceous mudstone occasionally found in sandstone unit.

3.4.3 Lower well bedded laminated siltstone (UMS 3)

This third sedimentary unit is similar to the first unit but is becoming more calcareous at certain places. Parallel lamination (Figure 3.3 left) is a dominant sedimentary structure and at many places, cross lamination can be found (Figure 3.3 right). Lamination is made up of a finer grain particles interlayer with dominant siltstone.

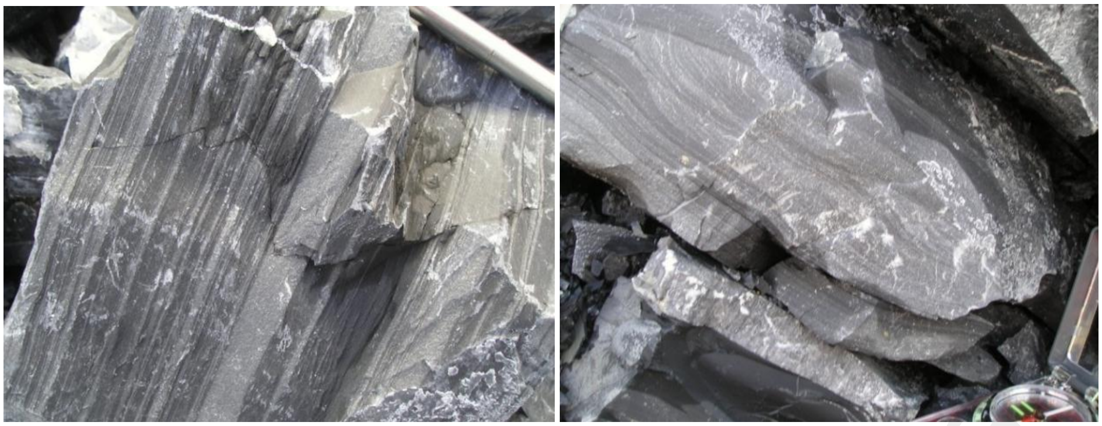

Figure 3.3: (Left) Parallel lamination in lower well bedded siltstone, (Right) cross-lamination in the same unit.

Figure 3.4: Rock samples locations for greenish grey tuffaceous siltstone UMS4 (looking south).

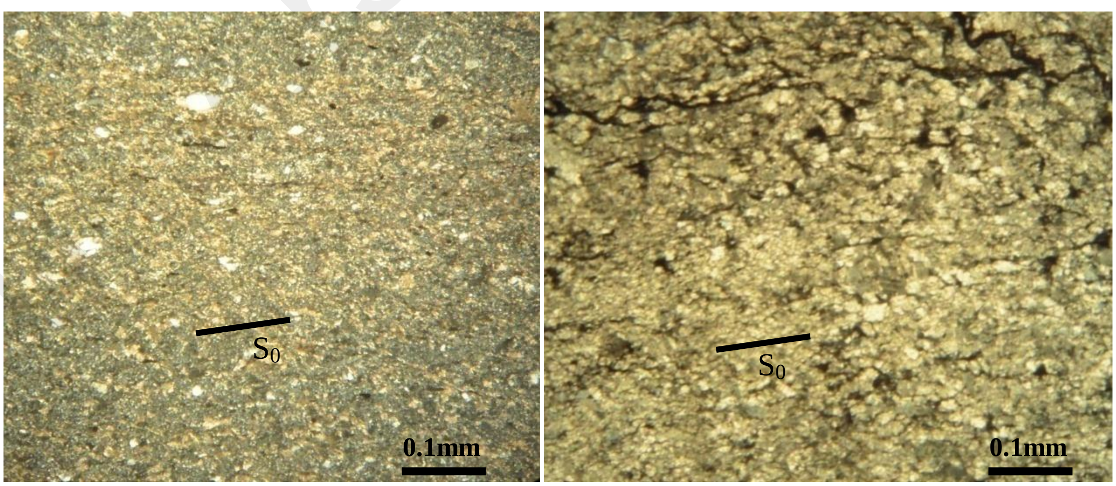

Figure 3.5 (Left): Photomicrograph of light grey shale (UMS4) with minor quartz grain in matrix of fine grain lithic dominant and minor quartz. Sericite and patch of carbonate (yellowish) aligned parallel to foliation (S_0) or bedding. (Right): Photomicrograph of calcareous shale comprised of recrystallized calcite grain size is less than 0.2mm. Aligned dark opaque streak is carbon parallel to bedding (S_o)

3.4.4 Greenish grey tuffaceous laminated siltstone (UMS 4)

This sedimentary unit is exposed on both east (figure 3.4) and south walls of the KE pit. On the west wall of Kalampong pit, only thin unit is exposed above the calcareous shale because the rest is already above the present topography. This unit is well bedded and comprises dominant siltstone interbedded with sandy silt and occasionally with sandstone. Colour is light grey to greenish, which is the main characteristic of this rock and contains no carbonaceous material.

The sample for petrography was fine grain light grey sediment with certain beds and has sandy silt and sandstone layers. The petrography study showed some coarse particles (>0.2mm) of quartz in the background sericite and possibly some patch of carbonate (figure 3.5 Left).

3.4.5 Calcareous shale/siltstone (UMS 5)

Calcareous shale (calSSH) is underlying the greenish grey tuffaceous siltstone/ reworked tuff and at certain places graded to carbonaceous limestone with an abundance of fossils such as foraminifera, sponge, brachiopod, etc. This unit is strong, blocky and mostly contains carbonates (figure 3.5 Right) especially calcite that has cemented carbonaceous material. This unit appears as black. This calcareous shale and all sedimentary units above it are grouped as the upper mine sequence.

Ramli (2004) records some sedimentary structures in this unit including flute cast and graded bedding. One sample (UMS5) of this unit was analysed for petrography description.

3.4.6 Carbonaceous dominant unit (MMS 1)

This unit is underlying the calcareous shale and is composed of carbonaceous shale with thinly interbedded fine-grained sandstone. This unit can be observed at both west wall and east wall of the pit as it was a part of the anticlinal fold below the Penjom Thrust. The thrust movement remobilized carbonaceous material and caused it to mix-up with a thin layer of siltstone and sandstone along this fault. The western limb of the unit is not highly sheared but still contains a high carbon zone along the carbonaceous shale as shown by grade control carbon assay in Figure 3.6. This figure shows a dominant highly carbonaceous zone at RL 924 which is 55m below surface. Note that particularly sheared carbon material had posed some major setbacks to former cyanide in leach (CIL) processing plant to recover gold from cyanide solution.

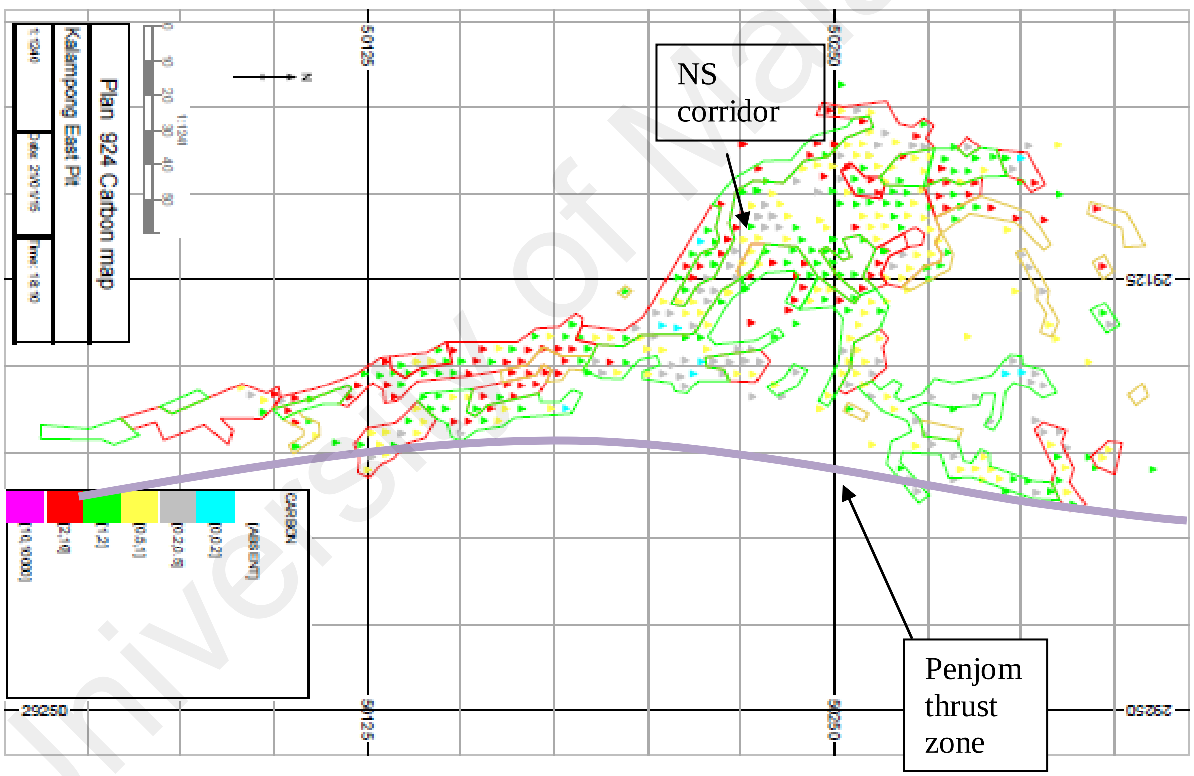

Figure 3.6: Carbon result (%) from grade control ore block 924mRL Grey dot is 0.2 to 0.5 %C. Ore mark-out string comprised of ore grade above 0.8 g/t, red string ore block is above 6 g/t. Continuation of the high carbon ore zones along the Penjom thrust and NS corridor (western limb of the main anticline/fold). High carbon content in the western limb is originated from carbonaceous shale.

3.4.7 Interbedded sandstone, carbonaceous shale and thin conglomerate (MMS 2)

The carbonaceous unit is gradually changed to a sandstone dominant unit. The sandstone unit is characterized by its rounded quartz grain and lithic particles (Figure 3.7). This unit is presently termed as sandstone rather than as tuff, as previously applied, in order to distinguish the sedimentary depositional environment rather than the pyroclastic (volcanogenic) origin.

A minor carbonaceous unit is usually thinly bedded and at many places was in-filled with laminated shear veins, which indicate that this unit had undergone repeated opening of the bedding slip shear. A grey conglomerate also occurred in this unit and overall comprises either a coarse or fine upward sequence (Figure 3.8 left). This sedimentary structure is referred as graded bedding.

Occasionally, lenses of dark grey quartz eye porphyry (dacite porphyry) are observed within this unit in both Manik and Kalampong north. This unit and the abovementioned carbonaceous unit made up the middle mine sequence. The alternating sequence of shale, sandstone and conglomerate is the main characteristic of this sequence.

3.4.7 Greenish/reddish tuffaceous siltstone, sandstone and conglomerate (LMS 1)

This unit comprised a thick and massive siltstone, sandstone and conglomerate and is commonly greenish in colour (Figure 3.8 right). The fine grain (siltstone) unit was previously thought by mine geologist as a pyroclastic rich sedimentary rock and previously referred to be of volcanic and dacitic in composition (VDA).The sandstone unit is not common and is normally highly silicified. Several segments of the conglomerate unit are reddish in colour (Figure 3.10). The thickness of the individual conglomerate unit can be up to 15m as in KE pit bottom and more than 20m at Kalampong North. A boundary with fine grained sediment is usually gradual.

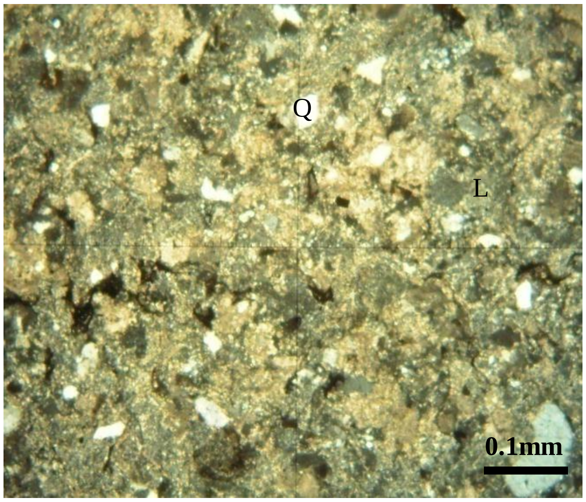

Figure 3.7: Photomicrograph of sandstone in MMS comprised of dominant, altered lithic (L) and quartz (Q) in sericitised matrix (location Western Limb 834mRL)

Figure 3.8: (Left) Light grey conglomerate of middle mine sequence underlying sandstone (SST) unit (location Western Limb 834mRL). (Right) Greenish grey conglomerate of lower mine sequence

The conglomerate is clast supported with a maximum size observed up to 20cm by 10cm. Fine grain sediments occur as a lens in the massive conglomerate. Elongated clasts have the same orientation with bedding strike. Chert clast is dominant over lithic clast. A location of samples for these units is showed in Figure 3.9.

Figure 3.9: Sedimentary rock of unit 8 (tuffaceous siltstone to conglomerate). A (Jalis corridor), B (Kalampong East fold axis), C (west wall). Looking to the north (photo May 2008)

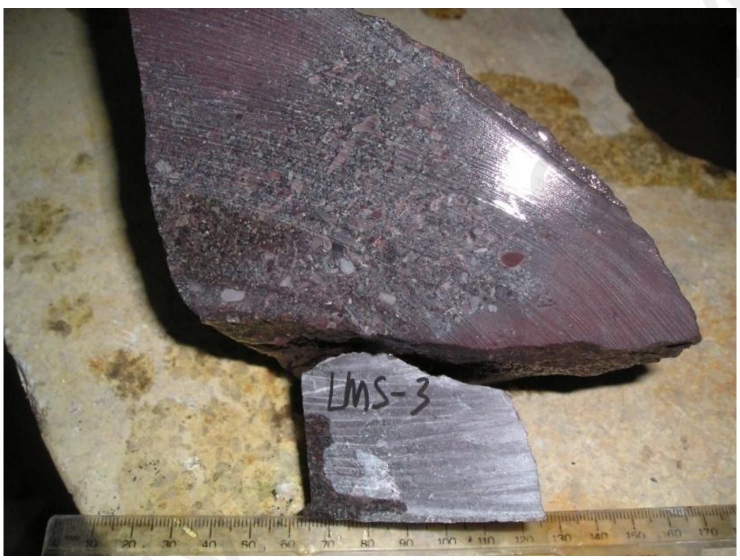

Figure 3.10: Purple/reddish granule size of pebbly sandstone graded to conglomerate usually forming up to 5 to 10m thick. This unit is part of lower mine sequences.

Another facies is greenish grey with well-bedded siltstone exposed at the west wall. This facies has a thickness of 200m but has locally interfingering relationship with conglomerate dominant unit at the northern side of the west wall, but as a fault boundary at the southern side.

3.5 Stratigraphy Sequences

A detailed description of the stratigraphy sequences are based on pit wall mapping and field observation. The mapped stratigraphic sequences of the Kalampong pit is generalised in Figure 3.11. In addition, two schematic stratigraphic profiles from the east and the west wall were respectively illustrated for comparison and correlation together with their associated bedding parallel vein, as shown in Figure 3.12:

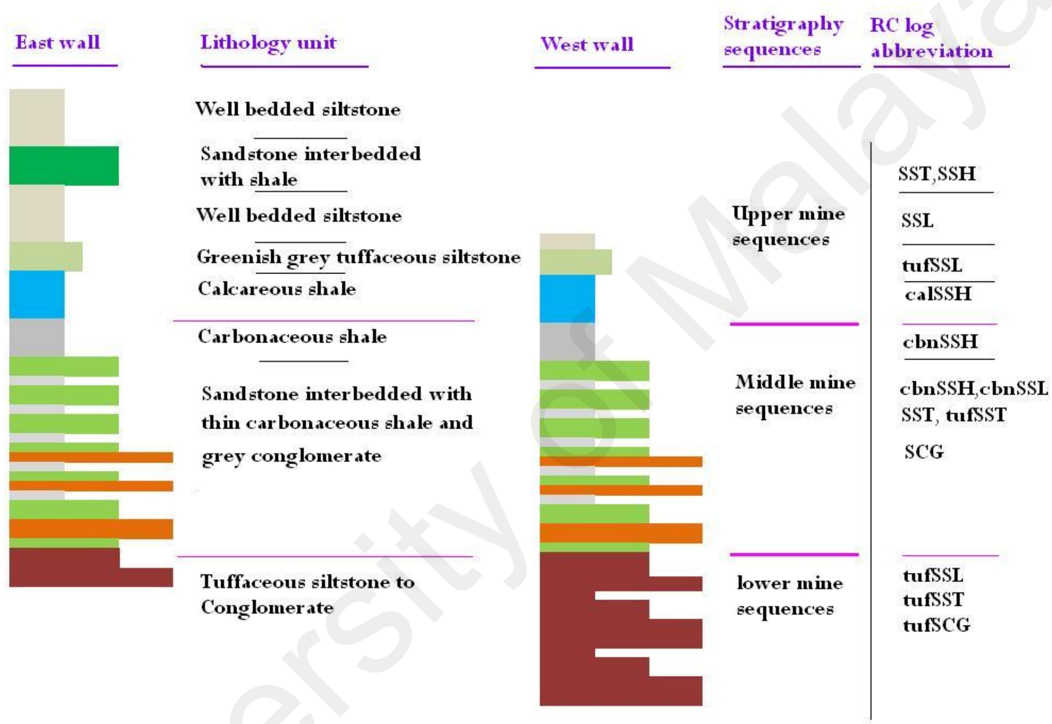

Figure 3.11: General stratigraphic profiles for the west wall and east wall of Kalampong East pit (not to scale) and not included the west wall of Jalis. (SST- sedimentary sandstone, SSH- sedimentary shale, SSL-sedimentary siltstone, tufSSL-tuffaceous sedimentary siltstone, calSSH-calcareous sedimentary shale, cbnSSH-carbonaceous sedimentary shale, SCG-sedimentary conglomerate

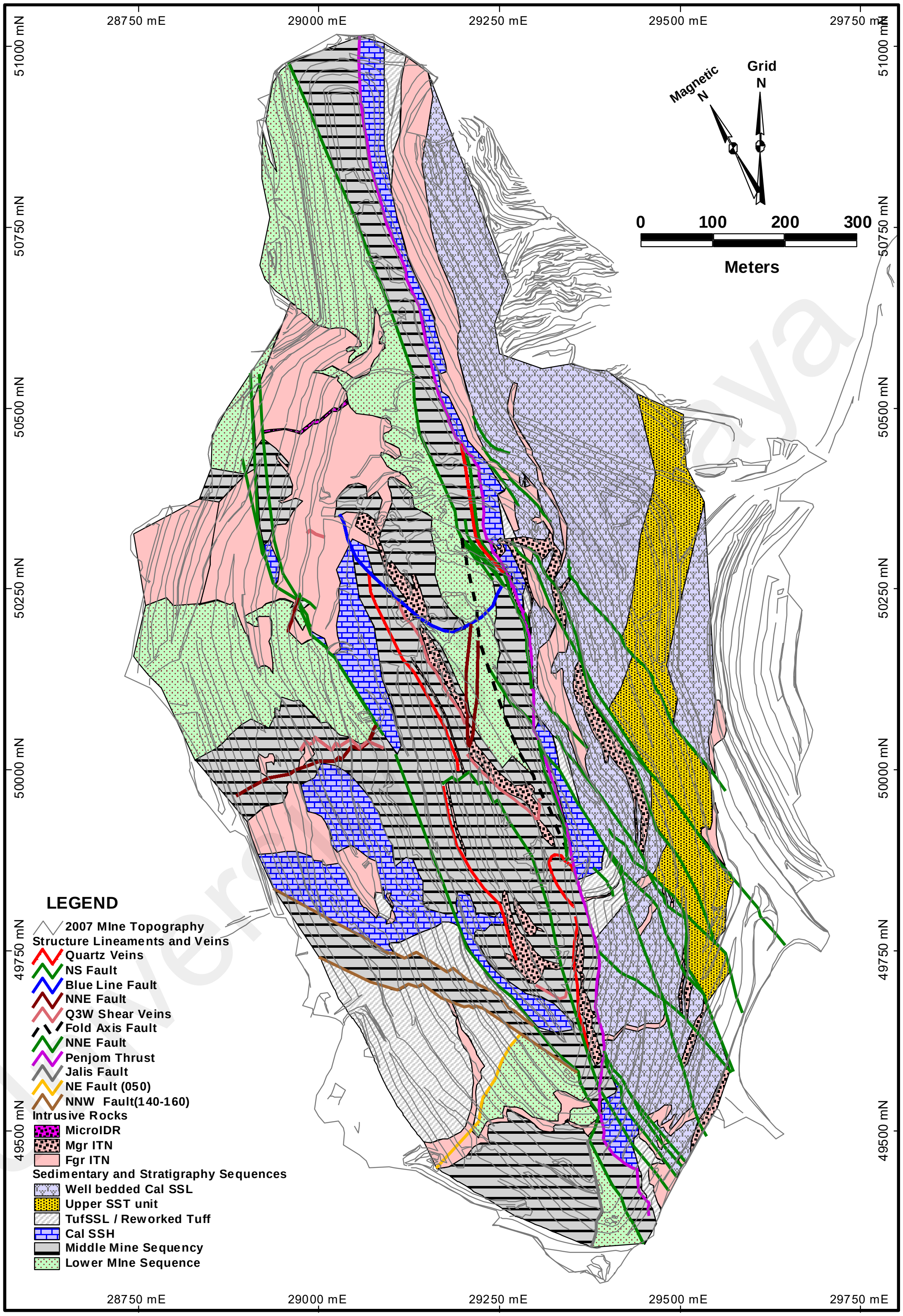

Figure 3.12: Stratigraphy distribution in Kalampong pit (2007).

3.5.1 Upper Mine Sequence (UMS)

The UMS comprised sandstone, laminated siltstone and calcareous shale units that represent the uppermost of the stratigraphic sequences on the east wall of Kalampong pit. This UMS is present as the hanging wall and footwall of the Penjom Thrust. Minor mineralized veins do occur at Hill 4 hanging wall area where medium-grained felsite cross cut the sequences at the contact margin of Penjom fault.

As for the footwall of Penjom Thrust, only the lower half of the UMS is exposed at the west wall of the pit. However, the upper sandstone unit is not exposed at the west wall as it is probably above the current topography. On the other hand, a unit of tuffaceous sediment grading from siltstone to minor medium-grained sandstone and agglomerate called reworked tuff was observed to be intercalated with the lower calcareous shale at Jalis Corridor (southwest wall of KE) formed as part of the UMS.

Most units in this sequence do not host mineralization even though they are below the Penjom Thrust.

3.5.2 Middle Mine Sequence (MMS)

The MMS is below the calcareous shale unit of upper mine sequence. MMS is the most favourable host rock for gold mineralization, most likely due to the competency contrast and geochemistry of this unit. It comprised predominant carbonaceous shale as the upper part of the sequence and changes to sandstone with thinly interbedded carbonaceous shale and greyish conglomerate at the lower part of the sequence. The conglomerate thickness is less than 2m and normally comprises 10 to 30 cm thick graded bedding of sandstone and shale.

The Kalampong West (KW) ore body which is hosted in the oxide MMS of higher elevation (from 990 to 1039mRL) can be correlated with MMS of lower elevation in KE.

This correlation indicates that the western host rock has been refolded and then further separated by the NS fault. The cutback of KW pit wall continues to expose this stratigraphic unit, which has been truncated and separated by the NS fault and massive felsite.

Local carbon remobilization may occur in the MMS. This remobilization is especially carbonaceous along the bedding slip shear and Penjom Thrust fault. Bedding parallel shear veins commonly occurr along lithology contacts especially along thinly bedded carbonaceous shale, while D2 extensional veins occurred at a high angle to the shear veins mainly limited to more competent massive siltstone, sandstone, conglomerate and felsite contact. Deformed veins occurred at areas intersected by D4-5 faulting.

3.5.3 Lower Mine Sequence (LMS)

The LMS comprises two groups of sedimentary facies. The first facies (LMS A) is greenish and purple fine-grained tuffaceous siltstone, sandstone and thick tuffaceous conglomerate. This unit is considered as a competent unit due to the lack of bedding structure and host less mineralization compared with the less competent MMS. However, the occurrence of small felsite at intercept along the NNE fault generates a series or network of extension veins with lower grade gold ore (e.g. northern and southern dyke) than the shear vein in carbonaceous host rock at the intrusive contact.

The boundary between this sequence and middle mine sequence is generally distinguishable by their colours in which the LMS tends to be more greenish or reddish in colour and has a thicker or massive bed without a carbonaceous shale unit. The colour is a consequence of detrital carbon particles. The exact boundary can be represented by a lowest thin layer of carbonaceous shale that is dominantly in-filled with a bedding parallel shear vein. Significant veins occur at the boundary in the form of a shear vein and discordant extension vein.

Another facies (LMS B) is a well-bedded siltstone and is exposed at Jalis-West Wall Corridor with thickness of up to 80m. The boundary with facies LMS A is a gradual contact at the north but is a fault contact at the southern part.

3.6 Stratigraphy and mineralisation

There is a close local relationship between stratigraphic units and the distribution of mineralization and associated quartz-carbonate veins. Several ore zones defined as a NS corridor are also categorized as stratigraphic concordant ore zones during the earlier geological modelling. These ores are characterized as bedding parallel, laminated to ribbon quartz veins and associated extension veins.

Gold-bearing quartz veins are summarised into three bedding parallel shear veins (Q1, Q2 and Q3) and its associated extensional veins, where all shear veins are within the middle mine sequence (Figure 3.13). E–W extensional veins are mostly associated with the third parallel shear vein zone (Q3W), locally in between Q3W and Q2W and in the LMS within felsites along NNE fault contact.

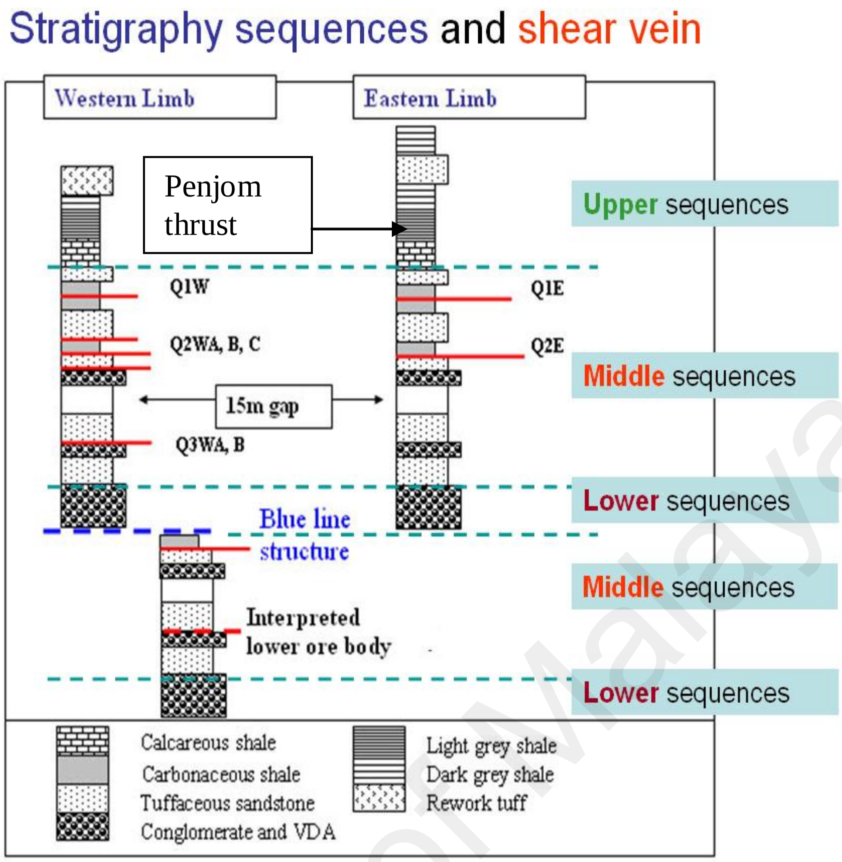

Figure 3.13: General stratigraphic sequences for eastern limb and western limb and the location of bedding parallel shear veins. Western limb shows stratigraphy repetition due to the E-W trending Blue Line Fault.

The schematic setting of these shear veins in the stratigraphic columns were shown in Figure 3.13. On the basis of the production records, more than 80% of ore zones that were mined in the Kalampong pit are hosted within the middle mine sequence, while the rest are hosted within the LMS commonly around faulted intrusive.

As a result, the former sequence, together with other specific factors, can be used as a guide in defining the continuity of the bedding parallel quartz carbonate shear veins (former NS fault) and in exploring other primary targets for near mine exploration.

However, not all shear veins host significant gold mineralization along the strike orientations. Rather some may function as a conduit to mobilise mineralization before trapping or deposition that occurred at favourable sites such as contact margins of felsite and below impermeable carbonaceous limestone and the NNE structure.

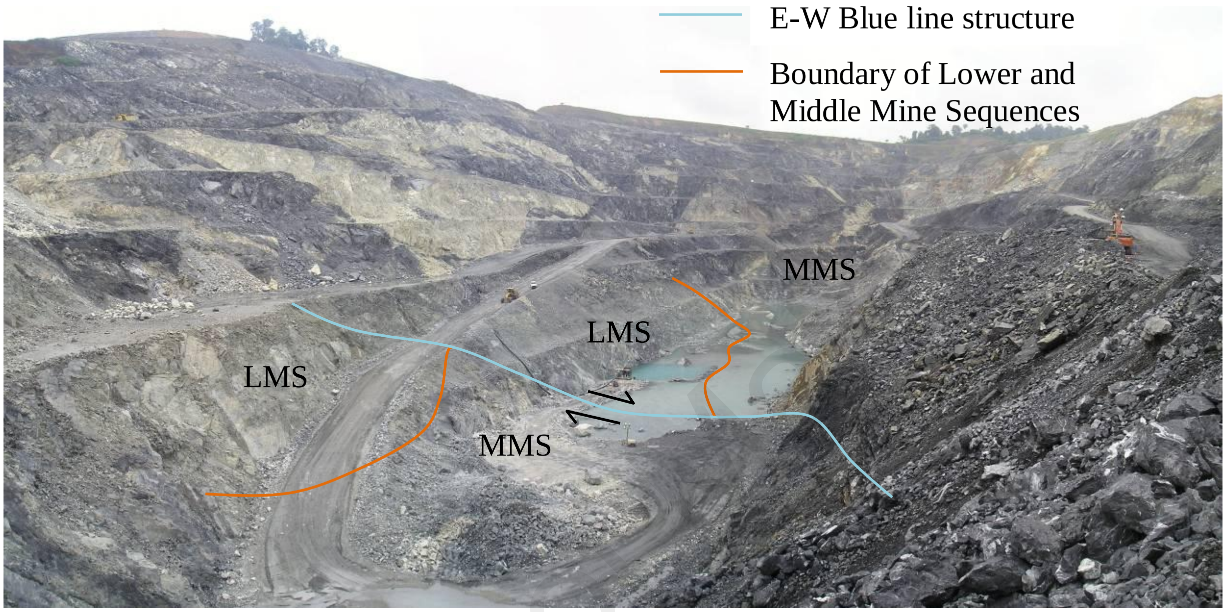

Figure 3.14: Looking southeast - Bottom of the pit, stratigraphic repetition as a result of displacement by Blue Line Structure (photo July 2008, bottom RL-792).

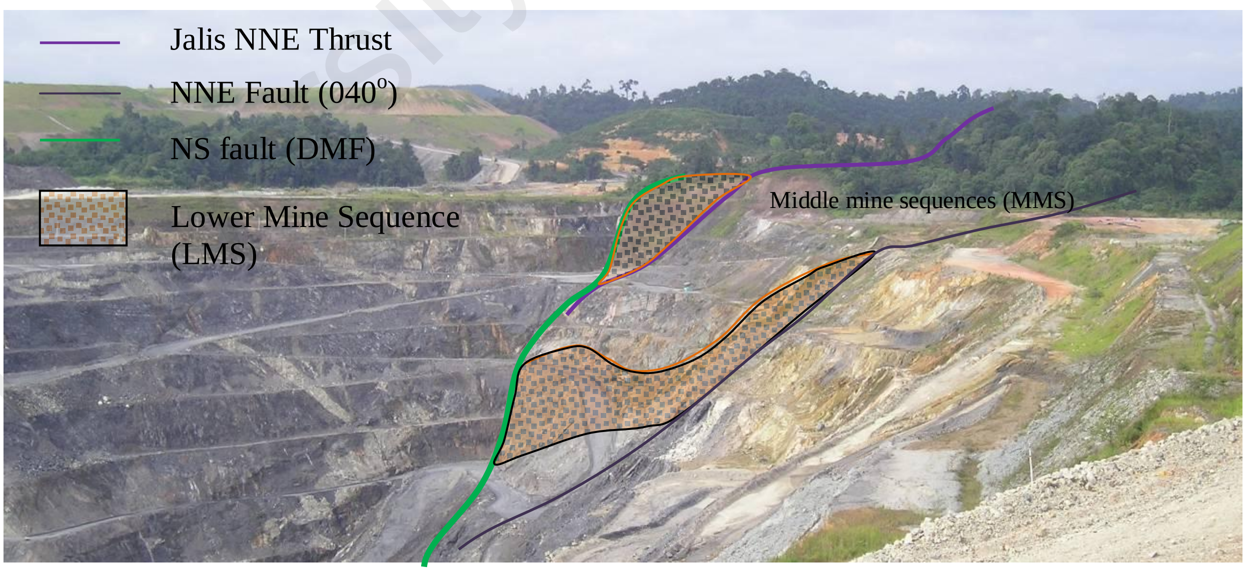

Figure 3.15: Looking south – Southwest wall of KE pit: Stratigraphic repetition indicated by lower mine sequence (LMS) comprised of massive conglomerate above carbonaceous dominance of MMS as a result of displacement by Jalis NNE reverse to dextral fault

3.7 Stratigraphic Repetition

Stratigraphic repetition is regarded here as the repeated sequence of lithology units found overlying or underlying each other in which the older sequence is placed above the younger sequence due to displacement by faulting and folding. For example, the stratigraphic repetition of the middle mine sequence occurred below the lower unit near to the fold axis owing to the displacement by the E–W fault referred at site as the Blue Line Fault (Figure 3.14).

Repeated stratigraphic sequences that were formed by a depositional sedimentary environment or by interfingers relationships between rock sequences can also result in stratigraphy repetition, but this kind of repetition is not observed in KE. Stratigraphy repetition in the KE pit is essentially caused by the displacement by the structures such as a reverse fault, oblique fault, right lateral fault, tight recumbent fold, etc. Stratigraphy repetitions related to reverse fault (Jalis fault) are shown in Figure 3.15.

3.8 Stratigraphic Break

A stratigraphic break is defined as a missing stratigraphic sequence resulting from a displacement by faults or by separation by massive intrusion (felsite). The displacement of stratigraphic sequences, especially by normal sense movement of NS faults during post-mineralization period also displaced the ore zones. This is also defined as a mineralisation break.

A general view of the three defined stratigraphy sequences based on the composite RC log profile is shown in Figure 3.16. This profile shows some occurrences of stratigraphic break and repetition as follows:

- UMS lying above LMS without intervening MMS or is having a very thin MMS (left side of the profile).

- UMS and MMS are missing in the top profile (right side of the profile)
- Thicker MMS due to displacement and repetition by both faulting and folding

3.9 Igneous rock

3.9.1 Introduction

The pit development exposed a variety of intrusions and a few types of hypabyssal rocks that intruded into the sedimentary rocks either as a sill, dyke and irregular or massive bodies. Igneous intrusive rock in PGM has been previously referred to as felsite, but is now referred to as tonalite by mine geologists.

3.9.2 Intrusive rock

3.9.2.1 Field occurrence

Several intrusive lithologies in PGM are fine grain felsite, medium grain porphyritic felsite and microdiorite. The first two lithologies have a yellowish green colour and appear as the same unit due to the colour similarity from the distance. Close up observation shows that both have different grain size. Field observation reveals that medium grain intrusive cross cut the fine grain intrusive, as can be observed in Hill 2 (west wall) and Hill 5 hanging wall.

Medium grain felsite has a thickness of up to 25m forming a sill with irregular shape at the southern part but cross-cuts the sequence at the northern and deeper parts of the KE pit. Grain size changes gradually from medium grain to fine grain along 1 to 2m from the contact. This chilled margin indicates a fast cooling process of magma at the contact as a result of the emplacement into cooler environment near the surface. The thermal aureole is also not well developed in the country rock contact, suggesting that the temperature gradient was low and the felsite sill was relatively small.

Many occurrences of medium grain felsites are parallel to the carbonaceous layer of the MMS suggesting that the emplacement of this rock may have been initiated by the ductile deformation event that was also responsible for dilation along the bedding plane. Fine grain felsites are observed in massive tuffaceous conglomerate of LMS, sandstone, siltstone in the northern area and cross cuts the sequence into the UMS to the east and south (Figure 3.17). It forms a massive body within the more competent LMS and a sill within the well-bedded UMS. In KE, this unit is not observed in carbonaceous dominance of the MMS, while in Jalis it intruded at the boundary of MMS and UMS to form a sill.

Microdiorite only can be observed in north of KE and occurs as an E–W trending 80^{o} north dipping dyke and is considered as the youngest intrusion. The thickness is less than 3m and this rock cross-cuts fine grained intrusive within the LMS rock. Continuation into the MMS and the hanging wall of Penjom Thrust is not found at the east wall.

3.9.2.2 Petrography

Under the microscope (Figure 3.18), felsite rocks especially medium-grain sizes are dominated by quartz (70%), plagioclase and minor alkali feldspar. The rock is classified as granodiorite to granitic intrusive. Many quartz phenocrysts are fine to medium grain and embayed or with resorbed margin. Samples from western limb have micro-cracks across the grains as a result of deformation.

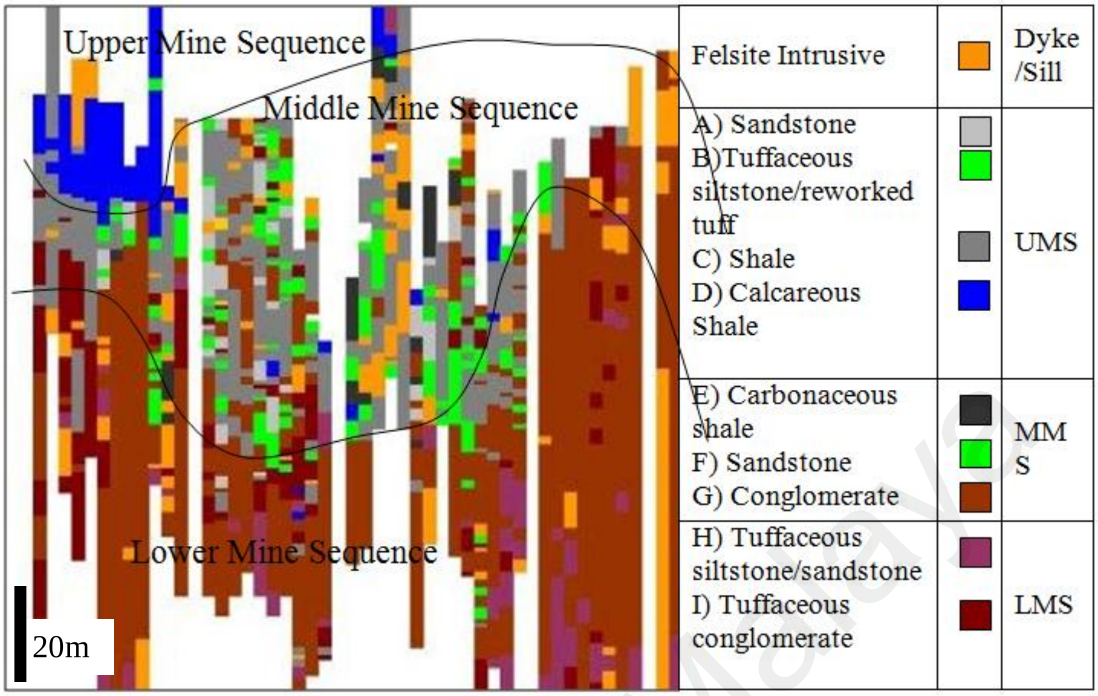

Figure 3.16: Stratigraphy from RC samples logging shows three sequences of lithology. UMS-upper mine sequences, MMS- middle mine sequences, LMS-lower mine sequences

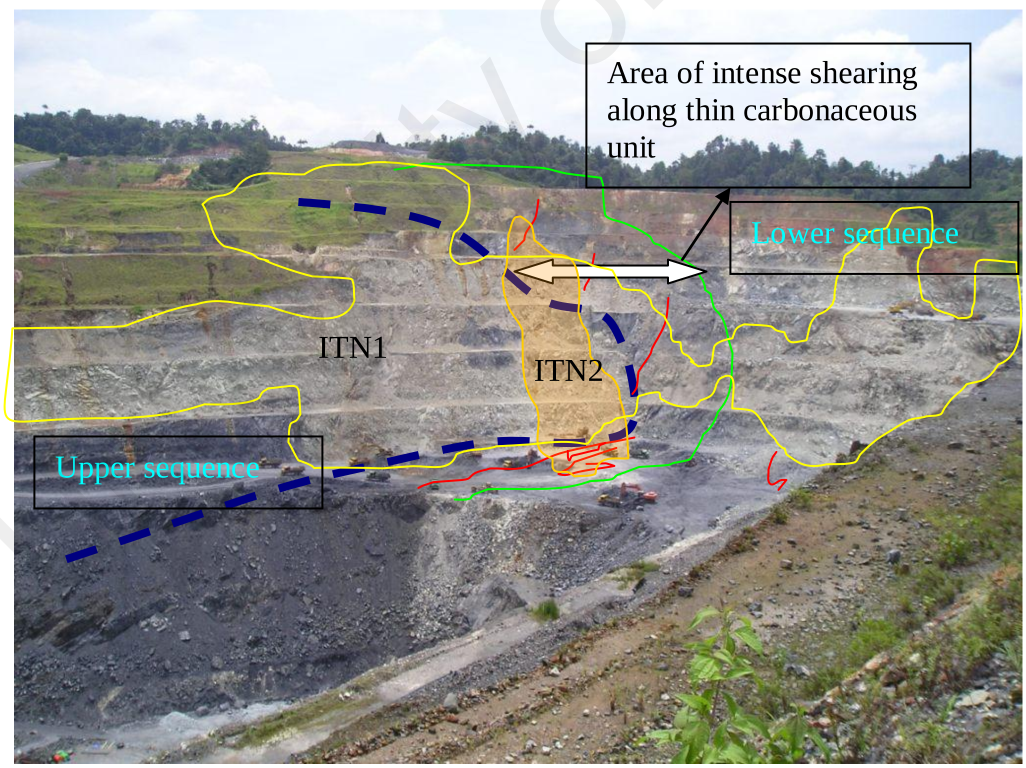

Figure 3.17: Felsites cross cut the host rock sequences (ITN1 & ITN2). Blue line represents approximate boundary between middle and upper mine sequences. Green line represent the boundary of middle and upper mine sequences.

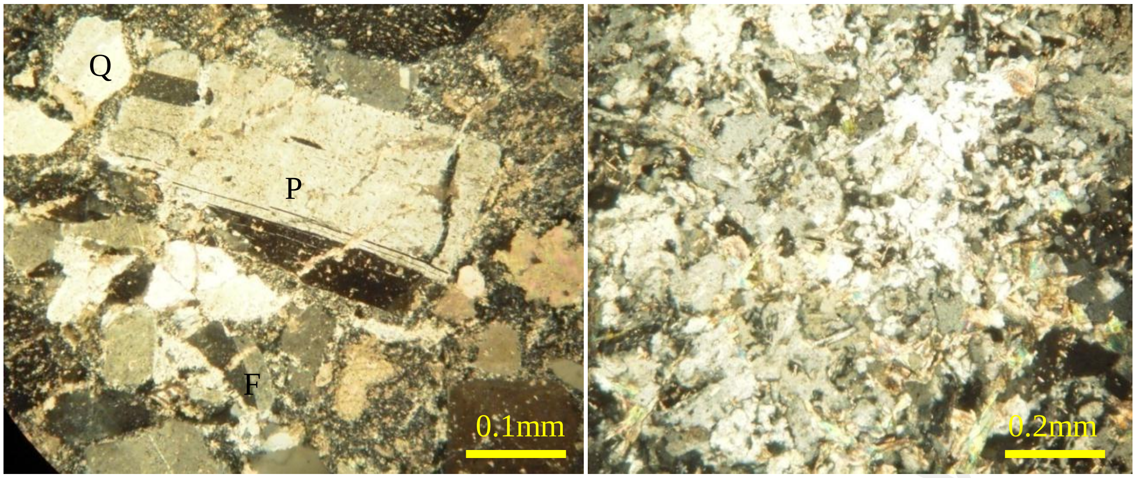

Figure 3.18: (Left) Photomicrograph of medium-grained felsites (ITN-1) with plagioclase (P) and quartz (Q) and minor alkali feldspar (F). (Right) Photomicrograph of fine grained felsite (ITN-2) comprised of quartz grain with some plagioclase. Thin section view in transmitted light.

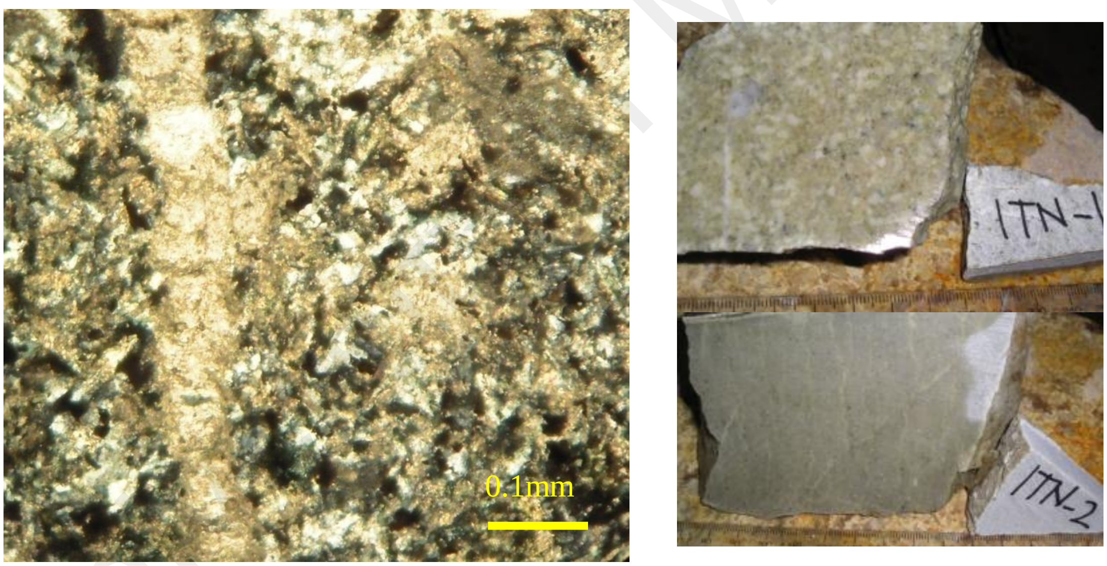

Figure 3.19**:** (Left) Photomicrograph of fine-grained microdiorite comprised of quartz and plagioclase with carbonate vein. (Right) Hand specimen of medium (ITN-1) and fine grained felsites (ITN-2). Thin section view in transmitted light.

For fine-grained felsite rocks, it comprises the same mineral and hence is classified as micro-granodiorite or aplit. Another fine-grained dyke comprises dominantly of plagioclase and quartz, hence is classified as microdiorite (Figure 3.19). Age of the Penjom felsite rocks is 222.4 +/- 1.8 Ma (Ng et al., 2015).

3.9.3 Volcanic rock

3.9.3.1 Field occurrences

Volcanic rocks observed are fine to medium-grained rhyolite and andesite. They occur within the sedimentary rocks as a sill and dyke. The thickness is commonly less than 5m and their colour appear to be almost similar to the host sediment and appear as greyish for a sill, while volcanic dyke appears as dark green.

Rhyolite unit can be observed in well-bedded shale of the LMS unit in the Jalis corridor. Andesitic rock can be found as dyke in the hanging wall of the UMS at Hill 6 of the KE pit and another fine-grain volcanic sill within the sandstone unit of LMS. In Manik pit, volcanic rock cross cutting the UMS and extended into MMS.

3.9.2.2 Petrography

Two types of volcanic rocks can be observed such as medium grain sill and fine grain dyke. Volcanic sill comprises dominantly of quartz (60%), some plagioclase and minor K-feldspar. This rock can be categorised as rhyolite to dacite porphyry (Figure 3.20). Another volcanic is a dyke of greenish grey with a patch of green minerals, possibly biotite. Plagioclase is the dominant mineral and hence is classified as andesite (Figure 3.21)

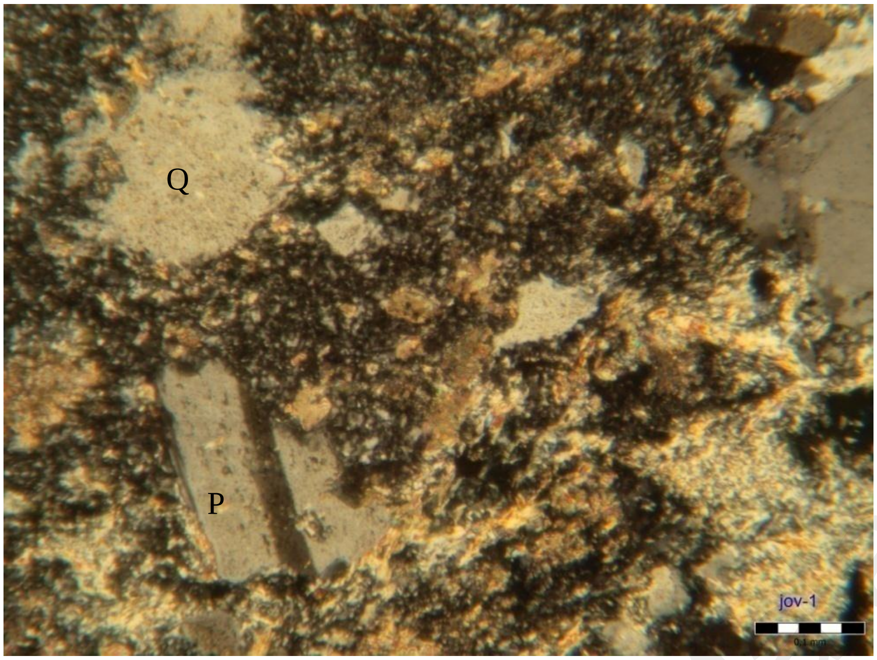

Figure 3.20: Photomicrograph of rhyolite to dacite porphyry comprises of dominantly of quartz (Q) with minor plagioclase (P). Thin section view in transmitted light.

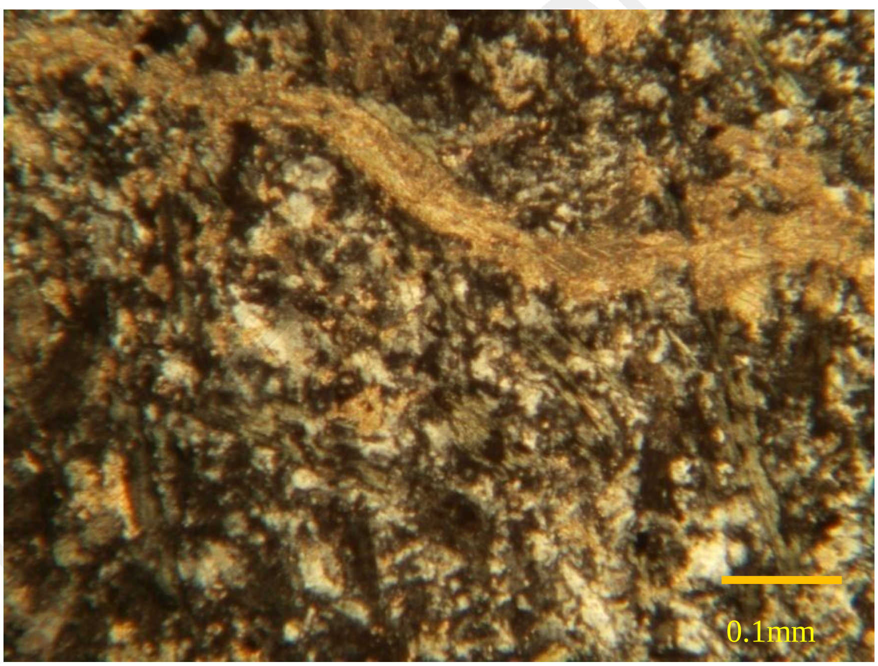

Figure 3.21: Photomicrograph of volcanic rock (andesite) made up by fine-grained of plagioclase and quartz. Stringer of carbonate vein cross cut the sample. Thin section view in transmitted light.

3.10 Discussion and conclusions

The study of rocks type is the first step in understanding the geological control of ore deposits. There is a clear relation between structural control and lithology in controlling the different types of veins. Three sequences of rocks namely UMS, MMS and LMS were established. MMS comprises of carbonaceous shale and host a majority of the ore in the sedimentary rocks as shown in Figures 3.22 and 3.23.

The upper sequence (UMS) is characterised by a shallow marine environment as indicated by flasser bedding, cross lamination and fossiliferous limestone unit. The MMS is consists of alternating beds of fine sediments, including carbonaceous shale, and coarse sediments with a turbiditic characteristics, which indicates a more distal marine environment or a deeper site. The lower sequence (LMS) is dominated by a thick conglomerate unit and is probably of a deepwater marine environment near to the slope resulted in the debris flow or as a basal part of turbiditic alluvial fan. Overall, the sedimentary sequences is characterised by deep to shallow environment.

Intrusive and volcanic rocks intruded into the host sequences as sills and dykes and were interpreted as pre-mineralization event as indicated by cross cutting relationship of structure and the host rocks. However, these intrusions may have been initiated during an earlier compressional event or during ductile deformation prior to peak deformation.

The sedimentary host rock sequence share common characteristics with many mesozonal orogenic gold deposits such as those found in Meguma Terrane, Canada (Mawer, 1987) or Lachlan Fold Belt, Australia (Bierlein et al., 1998) but the vein system also developed within the felsite intrusives below the Penjom Thrust. This close relationship has confused many geologists during the early pit development as they believed the felsites to be genetically related with mineralisation.

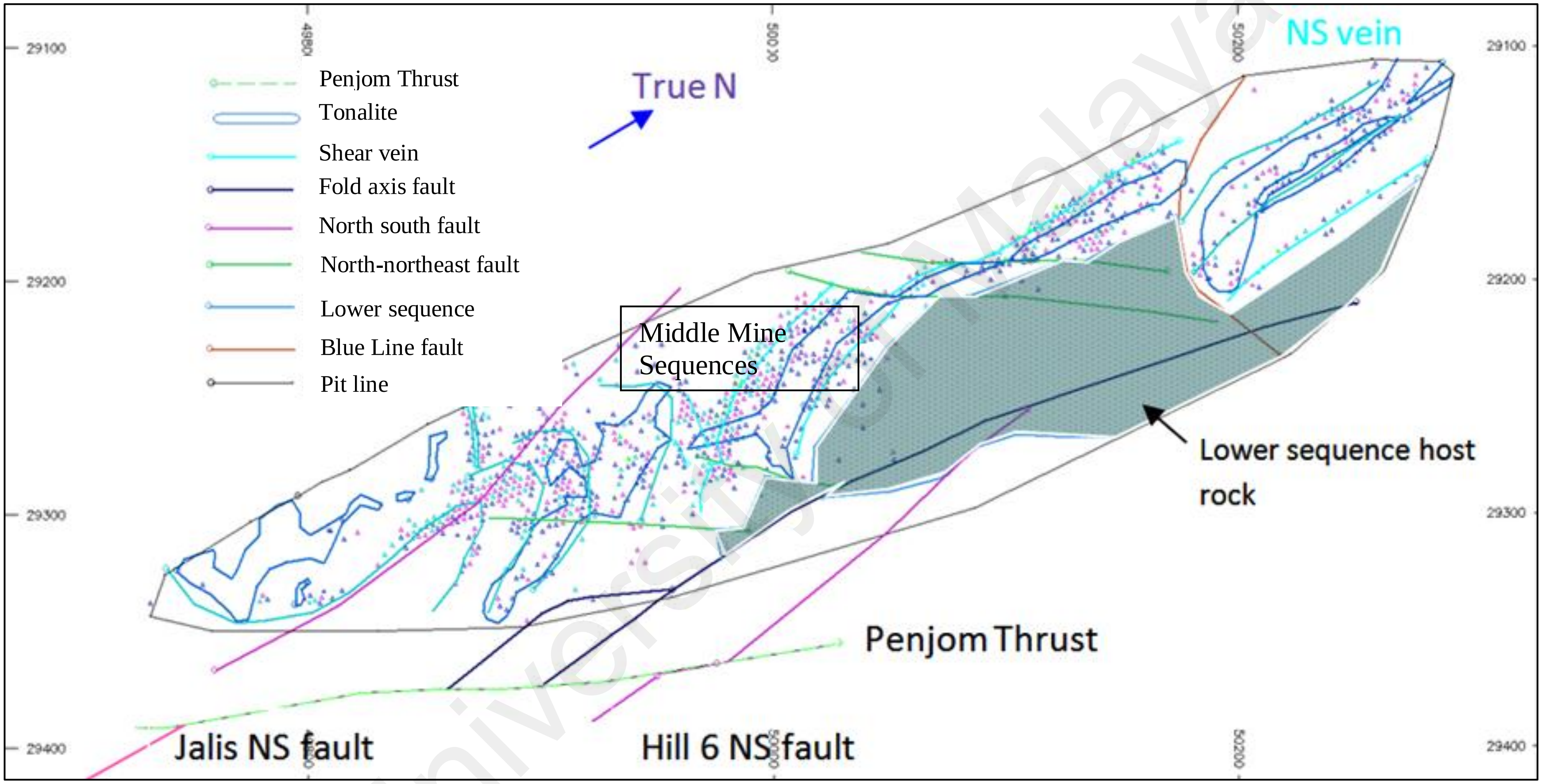

Figure 3.22: Lower sequences (LMS) sedimentary rock is not hosting significant ore bodies based on grade control assay data. (The blue and reddish dot represents the ore grade above 0.5 g/t). Ore dominantly within the Middle Mine Sequences (example from the main KE pit).

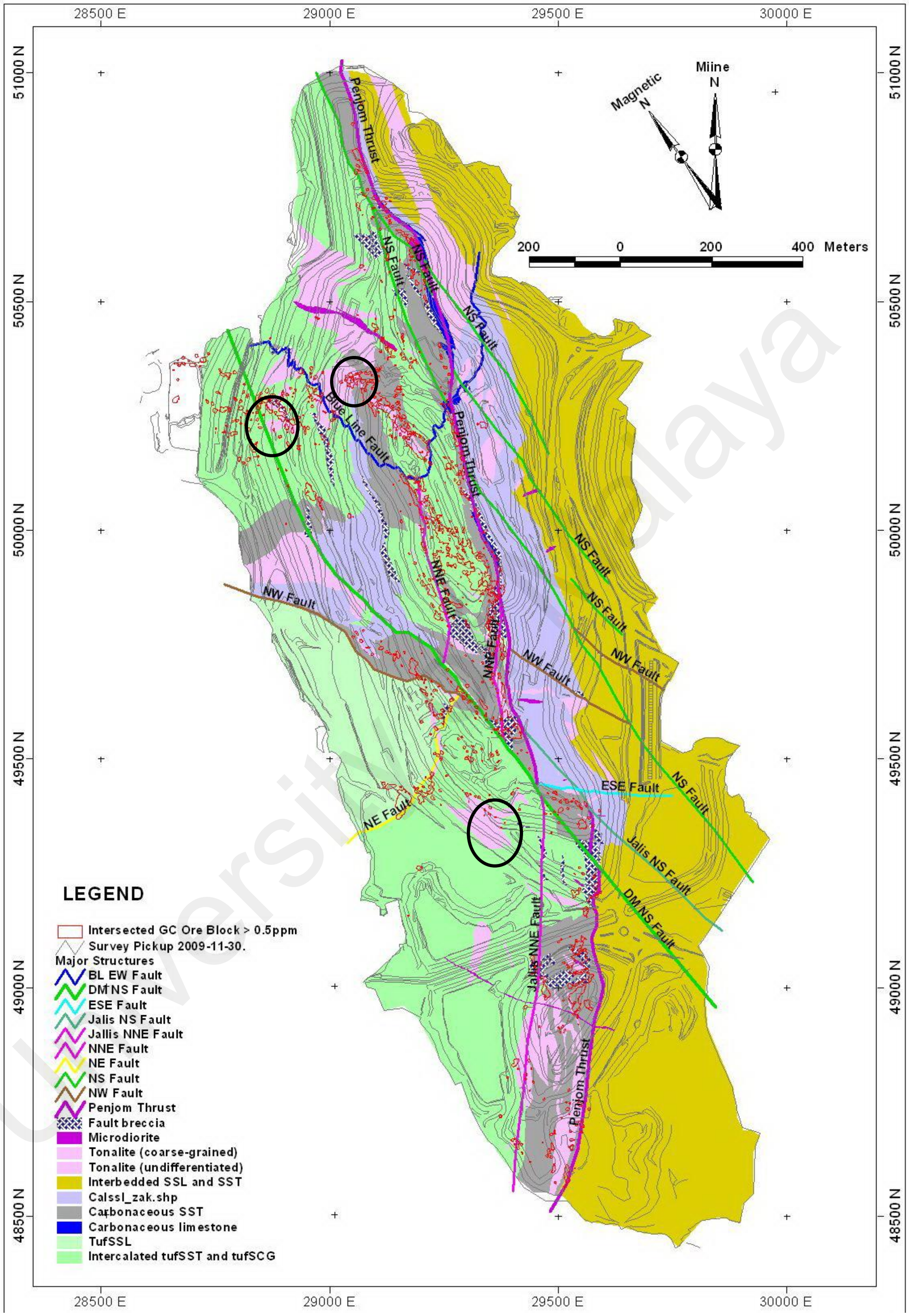

Figure 3.23: KE geological map. Mineralised outline (>0.5 g/t-red line) dominantly hosted in grey middle mines sequences. Some (in black circle) are hosted in felsite intrusive within the Lower Mine Sequence host rock.

CHAPTER 4.0 CARBONACEOUS ORE BODY

4.1 Introduction

Carbonaceous matter and organic carbon are important in mineral and petroleum exploration. Bio-mineralization, metal sequestration and reduction reactions can be active during all stages of syn-sedimentary to epigenetic ore formation, and therefore, they represent a potential key mechanism in metallization (Bierlein, 2001). In epigenetic lode gold, such as mesothermal or orogenic lode gold, there is a common association of carbonaceous matter and gold mineralization. However, its role, especially in chemical reactions, is a subject of on-going debates.

This chapter outlines the details as follows: (1) a comparison of the various types and the origin of carbonaceous matter in Penjom with those in other areas. (2) the significance of carbonaceous matter in the genesis of orogenic gold mineralization and (3) the factor controlling the reactivity of carbon in Penjom.

4.2 Various types and the origin of carbonaceous matter

Two origins of carbon in a host rock are as follows: from the sedimentary process, i.e. from either authigenic or terrigenous and epigenetic process, from metamorphic mineral or hydrothermal fluid. Authigenic sediment is sourced from (1) solid carbonaceous material reworked from older formations and (2) a particle of plant detritus that is transported and deposited as carbonaceous shale or siltstone before undergoing deformation or metamorphism.

An epigenetic source is related to metamorphic or hydrothermal fluid and occurs in the form of minerals such as graphite or hydrocarbon. Table 4.1 shows an example of carbonaceous sources and type of gold deposits.

Table 4.1: Different types of carbonaceous preg-robbing ore

Preg-robber/carbon type	Place	Sulphide content	Deposit type	References
High maturity carbon equal to or greater than anthracite coal and bituminous shale	Barrick Goldstrike Mines,N.E. Nevada	High sulphide	Carlin type, disseminated ore	Schmitz et. al. (2001)
Bituminous and pyrobituminuos carbon	Western Lachlan Orogen, Victoria, Australia	Low sulphide	Orogenic gold deposit	Bierlien (2001)
Hydrothermal/metamorphic graphite and ultra-fine pyrite	Macraes Gold Mine, New Zealand	Low sulphide	Orogenic gold deposit	Windle, S.J. (1999)
Sheared, detrital origin carbonaceous shale and minor anthracite	Penjom Gold Mine, Malaysia	Low sulphide	Orogenic gold deposit	Bogie (2002), this study

4.2.1 Sedimentary origin

Carbonaceous matter in Victoria (Western Lachlan Orogen) can be categorized as amorphous bitumens and pyrobitumen, distinguishable biological fragments and a rare graphite of metamorphic and detrital origin. Bitumens and pyrobitumens are derived from the degradation of organisms in an environment conducive to the formation of black shale, and in some places, they were remobilized into epigenetic structures during hydrothermal alteration and mineralization (Bierlein, 2001).

Another type of an organic particle in Stawell and Ballarat is a crystalline graphite flake that has high reflectance, anisotropy and is aligned along S_1 cleavage. Diessel et al., 1978 (in Bierlin, 2001) suggest that under temperature-pressure-chemical composition (T-P-X) conditions, the thermal alteration of kerogen can result in the formation of graphite via the oxidation or reduction of CH_4 and CO_2.

However, Springer (1985) suggests that shearing and fluid flow along foliation septa can trigger the graphitization of carbon on a shear plane under metamorphic conditions. Hence, the primary source of carbon in Stawell and Ballarat is still of allochthonous detrital origin.

Carbon in a high sulphide ore in Carlin, Nevada has been shown to be of high maturity state of carbon, equal to or greater than that of both anthracite coal (Schmitz et.al. 2001) and bituminous shale (Ratke & Scheiner, 1970). Tretbar (2000) reports that majority of the Carlin-type gold deposits of northeast Nevada are hosted in calcareous sedimentary rocks that contain naturally occurring carbonaceous material.

The reactivity of carbon vary depending on the geological characteristics of the deposit, i.e. original C content, sedimentary rock types, thermal history, extent of alteration, structural deformation and range of carbon maturity from poorly ordered amorphous phases to highly ordered crystalline carbon.

4.2.2 Carbon from metamorphic or hydrothermal origin

Graphite from Macraes Mine (Eastern Otago) and New Zealand was presumed to be of the epigenetic origin. The shear zone contains hydrothermal graphite, inferred to have been deposited from a methane-rich fluid (Windle et. al., 1999); thus, graphite only constrains within the shear zone and is highest in the mineralized zone (almost 0.5%).

McKeag et al., (1989) suggest that the metamorphic source of graphite based on the reflectance study which is almost identical to upper greenschist facies and amphibolites which is higher than that determined for the Macraes mineralization. There is a strong relationship between metallic mineralization and graphite-bearing schist, suggesting that the graphitic schist has had an effect on metal precipitation.

Gold recovery in the CIL processing plant at Macraes can drop up to 50% or lower because of preg-robbing by a certain component of ore, especially sheared carbon.

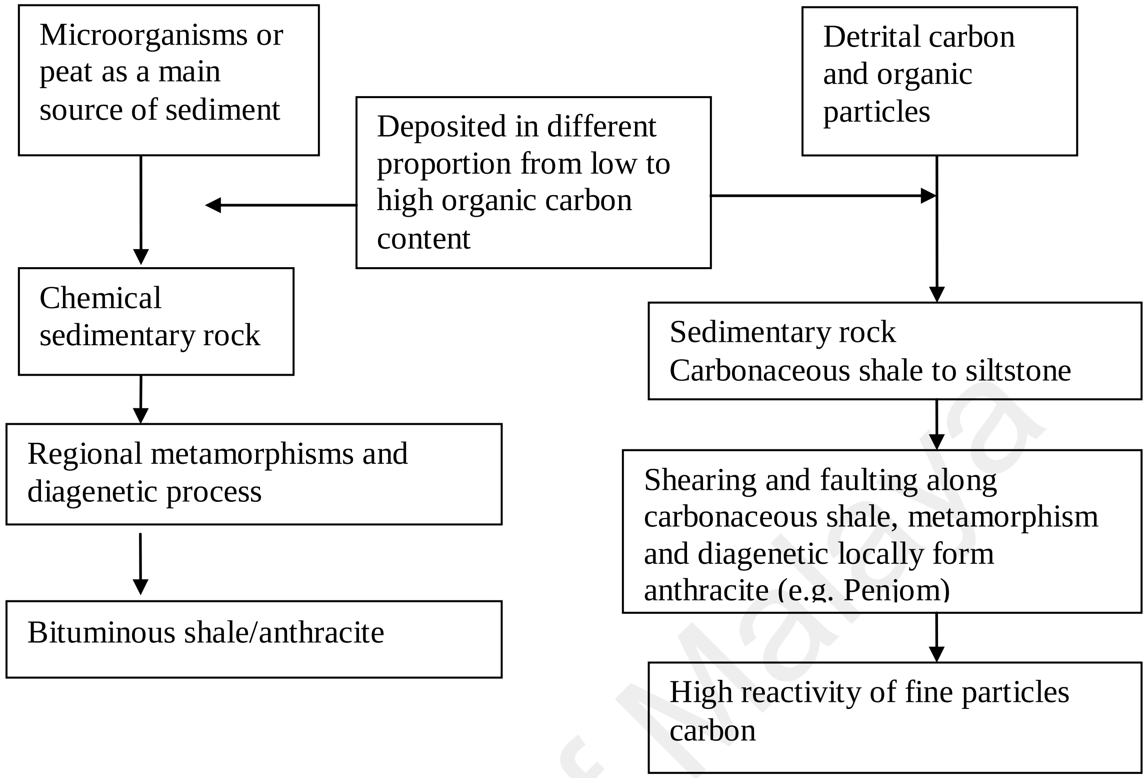

Figure 4.1 Different process of sedimentary origin of carbonaceous material (after Robb, 2008 and Bierlein, 2001).

4.3 Origin of carbonaceous material in Penjom

In Penjom, carbon in the host rock originates from the fine grain of organic material (fine amorphous carbon and so on) that was transported and deposited during a sedimentation process and through time was solidified as a sedimentary rock. Sedimentary origin is supported by the close association of stratiform features with carbon content. Different processes of sedimentary origin are shown in Figure 4.1.

In carbonaceous host rocks, carbon content is high in fine-grained sedimentary rocks, such as carbonaceous shale, and lower in siltstone and fine-grained sandstones. Medium-grained sandstones and coarse sedimentary rocks usually lack carbon particles. In carbonaceous shale unit, carbon can be found a localized glassy spot known as meta-anthracite and this was confirmed by carbon reflectance study in University Malaya.

Carbonaceous shale along the Penjom Thrust was also referred to as graphitic shale because of the platy and shining features along the sheared plane or the interface of the shear vein and carbonaceous shale. This graphitic shale has a gradual change to a coarse grain size, and thus suggests sedimentary origin or allochthonous detrital origin. Graphitization may be cause by shearing along the fine carbonaceous shale.

However, not all fine-grained rocks are carbonaceous. Fine-grained tuffaceous host rocks in lower mine sequences are from grey to green in colour and may have been deposited from different sources of materials.

Preg-robbing of ore generally corresponds with carbon content, but certain areas have higher reactivity, such as sheared carbonaceous host rocks along the fault zone. The shearing resulted to fine-particle carbon developed under pressure and heat, with a higher surface area and reactivity.

4.4 Carbonaceous matter and the genesis of gold mineralization

The importance of carbonaceous material in the genesis of gold mineralization can be divided into two categories: either physical or chemical control. This study does not cover the aspect of carbonaceous host rocks as a proto-ores or primary sources for gold that is now remobilized and subsequently re-deposited in the epigenetic structure during diagenetic, metamorphism or structural deformation (Large et al., 2011).

4.4.1 Physical control

Compression event and the Penjom Thrust produce a folding and the associated fold-related fault. Physical control is provided by lithology or competency contrast in which deformation occurs along the weak plane; especially thin carbonaceous shale, parallel to the bedding. The Penjom Thrust was reactivated on massive carbonaceous shale.

Repeated opening of the bedding-slip fault provides a channel way for fluid migration and intermittent quartz veining along this structure. Interaction with other factors such as intrusive body, geometry of the fold, competency contrast and intersection with the fault can provide a suitable place for metal precipitation and hence a high-grade zone.

4.4.2 Chemical control

The chemical control of a carbonaceous shale unit works in association with physical control to provide a reducing environment for fluid, which destabilizes sulphide complexes to precipitate gold.

A bedding-parallel quartz vein along thin carbonaceous shale could have provided channel ways for fluid or auriferous solution. The interaction of Au-bearing hydrothermal fluid with carbonaceous shale has been suggested as a possible primary cause of gold complex destabilization and native gold precipitation (Cox et al. 1991, in Bierlin, 2001).

4.5 Chemical analysis

4.5.1 Chromatography

Bogie (2002) analysed one sample to identify the type of carbon; either it is inherent to the country rock of carbonaceous shale or remobilized from hydrocarbons. The two chemical analyses are as follows: total organic carbon by high-temperature evolution and total petroleum hydrocarbons by fractions utilizing chromatography. Total organic carbon includes both free carbons and carbons present as hydrocarbons or other organic molecules.

Sample contains 2.15 wt% of total organic carbons; however, no hydrocarbon was above detection limit, and carbons were present as free carbons (Table 4.2). An XRD analysis was performed. The sample was then dissolved in concentrated HF to remove quartz. The insoluble residue was run over the main graphite peak at 26.6 degrees. The high background characteristic of poorly ordered graphite is not present, and a minimum degree of its crystallinity can be estimated as higher than the graphite D-3 structural state.

Table 4.2: Chromatography analysis of carbon in Penjom by SKM Consultant (2002) not detected any total hydrocarbon petroleum.

Sample	**Total organic carbon %**	**C_{10}-C_{14} Fraction (mg/kg)**	**C_{15}-C_{28} Fraction (mg/kg)**	**C_{29}-C_{36} Fraction (mg/kg)**
A	2.15	<50	<100	<100

4.6 Field classification of the carbonaceous zone

Plant processing can be affected by carbon level in the ore feed to the plant and process recovery can drop significantly as a result of preg-robbing activity. At 0.5% carbon content in an ore, plant process recovery with a chemical reagent is around 90%. Higher carbon content in the ore can reduce metal recovery as more carbon will take gold to tailings.

In order to control the carbon level of ore feed, ore mined has been stockpiled based on carbon content. Mining geologists will classify ore to be mined as either low or high carbonaceous content and will direct the ore to a specific stockpile. Based on field observation, ore at PGM can be divided into highly carbonaceous, moderately carbonaceous and low carbonaceous ores. Before 2009, all samples within the ore zone were analysed for carbon content that was used for field classification. Summary of vein type and structural corridor is as in Table 4.3.

Table 4.3: Carbon contains in different fold related shear vein ore zone.

Main ore zone and shear vein	Previous classification	Type of vein	Carbon level
Q1E/Penjom Thrust	Penjom shear/thrust	Ribbon, laminated and breccias	High carbon (>1.0%)
Q2E/ Penjom Thrust	Penjom shear/thrust	Laminated and discordant vein	Low carbon, partly medium to high carbon
Q1W	NS/jewel box corridor	Ribbon, laminated and breccias	High carbon (>1.0%)
Q2W	NS/jewel box corridor	Laminated and discordant vein	Low to medium (Q2WB), low to high (Q2WA) Discordant vein-low
Q3W	NS/jewel box corridor	Laminated and discordant vein	Low carbon
Overturn zone inclined fold	Northwest fault/tight fold	Laminated, stockwork and brecciated	Low to high carbon

4.6.1 Highly carbonaceous zone

A highly carbonaceous zone can be observed both in western (Figures 4.2, 4.3, 4.4) and eastern limbs (Figures 4.5, 4.6). This zone is made up by a thick carbonaceous shale unit interbedded with a thin sandstone unit. In the eastern limb, this zone has been reactivated by the Penjom Thrust movement and has further been reactivated by the normal to sinistral slip fault at a certain segment that produces highly sheared and graphitic host rocks.

Figure 4.2: looking north. West dipping mineralized carbonaceous unit of the western limb at contact with felsites.

Figure 4.3: Looking north view of the western limb thick carbonaceous host rock.

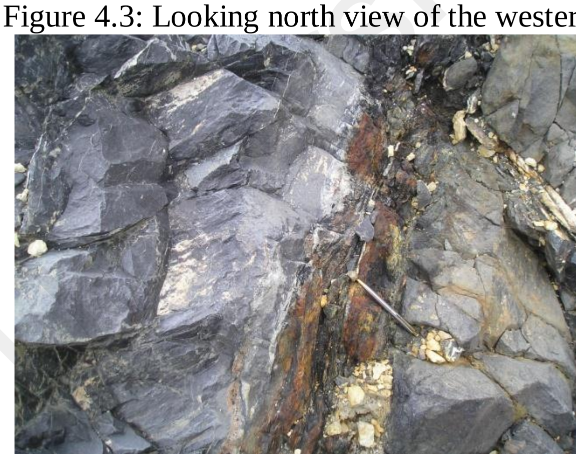

Figure 4.4: Close up view of the sampling in sheared carbonaceous shale and carbonaceous siltstone.

Figure 4.5: Kalampong North, Penjom Thrust reactivates along the carbonaceous unit of the east limb of the anticline.

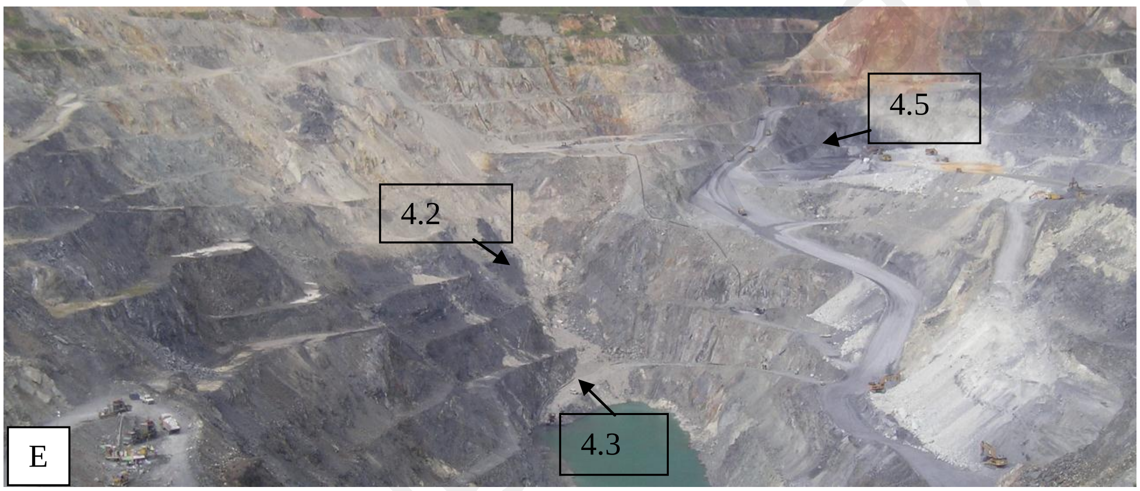

Figure 4.6: Overall picture of Figure 4.5 and location Figures 4.2, 4.3 and 4.5

On the west, only the bedding-slip fault reactivates along the carbonaceous unit so that the rock is less sheared, and furthermore, the veining process slightly reduces the carbon content by replacing the host rock.

4.6.2 Moderately carbonaceous zone

This zone is made up by interbedded alternate low and high carbonaceous host rocks (Figure 4.7).The overall carbon content is between 0.5 % and 1.0 % C and this material was stockpiled at the same place in a high carbon zone.

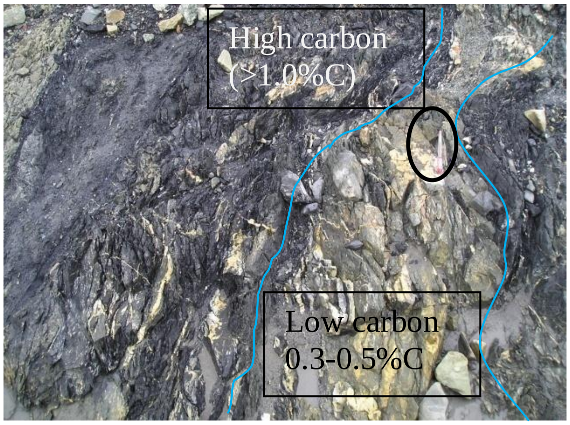

Figure 4.7: Interbedded of sheared carbonaceous shale with the small unit of low carbon sandstone (pen in the circle as a scale) will produce a moderate carbon content during ore mining.

Figure 4.8: Overall view of the photo A at south of KE, near the Penjom Thrust zone.

Other types of moderate carbon zones are carbonaceous siltstone (0.5% to 1.0%C) and fine-grained carbonaceous sandstone (0.3% to 0.8%C); where carbon content is usually lower than that in carbonaceous shale (more than 1% C). These sequences only can be seen in the middle and upper mine sequences. The lower mine sequence did not have carbonaceous material.

4.6.3 Low carbonaceous zone

A low carbonaceous zone is classified as the zone that has less than 0.5% C. Third shear vein (Q3W, see cross section figure 5.9 to 5.12) is hosted within this zone that is at the bottom of the middle mine sequence. Lithology is made up from thin carbonaceous shale interbedded with sandstone, conglomerate, fine-grained tuffaceous shale or siltstone and at felsite contact.

Intense quartz veining, such as quartz stockwork, reduces the carbon level of the carbonaceous ore zone. Table 4.3 shows the ore zone, the shear vein and different percentages of carbon level.

4.6.4 Distribution of the high carbon ore in geological setting

A close relationship between fine-grained sedimentary rock and carbon content in the middle and upper mine sequences make the style of folding as an important structural element controlling the distribution of carbonaceous material.

In Penjom, the thick carbonaceous unit with an interbedded thin sandstone unit is the main part of the high-carbon ore body that represents the upper unit of the favourable host rock. In other units, the thin carbonaceous unit interbedded with sandstone and conglomerate also made up the moderate carbonaceous ore block, especially near the fault zone. Hydrothermal alteration has also bleached the colour of the carbonaceous unit so that it appears as grey colour.

The distribution of the carbonaceous host rock can be divided into three areas, as shown in Figure 4.9 (cross section) and Figure 4.14 (plan view):

a) Fold nose and near fold axis (zone A)

b) East limb (zone B)

c) West limb and refolded western limb (zone C)

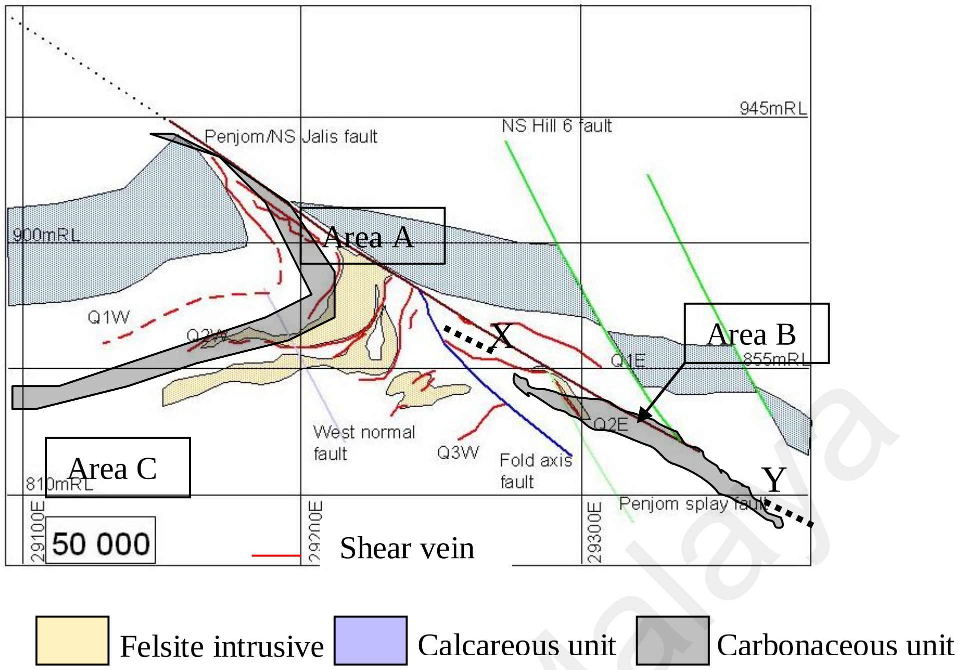

Figure 4.9: Cross section at 50 000 (looking north) show distribution of the main highly carbonaceous unit (>1.5% C). High carbon along thrust is made up by western limb carbonaceous sequences. The ore zone along the thrust (area A) is also considered as part of western limb sequences (part of NS corridor of the previous interpretation and can be correlated with area C, usually separated by fold related fault). Area A also comprised of a low carbon ore. Area B is eastern limb sequences.

Further to the south, area A also comprised the eastern limb carbonaceous unit, which made up the high carbon ore. This area can be referred to as the tight moderately inclined fold with faulting accommodates between two limbs. This fault is considered as a fold-related fault (D2 deformation), which also increases the intensity of quartz veining. The normal fault (NS Jalis) was further reactivated along this fault.

Figure 4.9 shows the cross-section of the shear vein system. Area ‘A’ comprises high carbonaceous zone that host the Q1W shear vein and moderate carbonaceous zone host to Q2W shear vein close to the thrust and extends into the western limb corridor/jewel box. Detail of shear vein is discussed in chapter 5. The vein along the thrust is more brecciated as the thrust increases the dilution space and superimposes with the earlier shear vein, as indicated by the laminated vein at the margin.

East limb carbonaceous hosted shear vein (area B in Figure 4.9) continues down dip and the grade still consistent along the strike. However, in a certain segment, carbonaceous and mineralization breaks occur because of structural (displacement), stratigraphy or natural breaks.

4.7 Carbonaceous break

Since the high carbonaceous zone originates from the host rock, certain places affected by the structures or by the natural occurrence as described below can result in carbonaceous and mineralization breaks.

4.7.1 Structural break

This occurrence can be observed in several places, as indicated in Figure 1 (areas X and Y). The carbonaceous unit become thinner because of the cross-cutting of fault at low angle to the carbonaceous unit or thrust zone.

A series of the northerly normal extension fault is either reactivates along the thrust and carbonaceous unit or cross cut the carbonaceous unit and resulted to the carbonaceous break or becoming discontinuous. Several faults, including NS Jalis fault (responsible for area X, reactivated along the thrust), Hill 6 NS fault (responsible for area Y) and another network of fault in Hill 4 of Kalampong north responsible for area Z, are shown in Figures 4.9, 4.10, 4.11B and 4.12.

The tightening of the fold because of the thrusting movement also resulted in faulting parallel to bedding and the thinning of this unit.

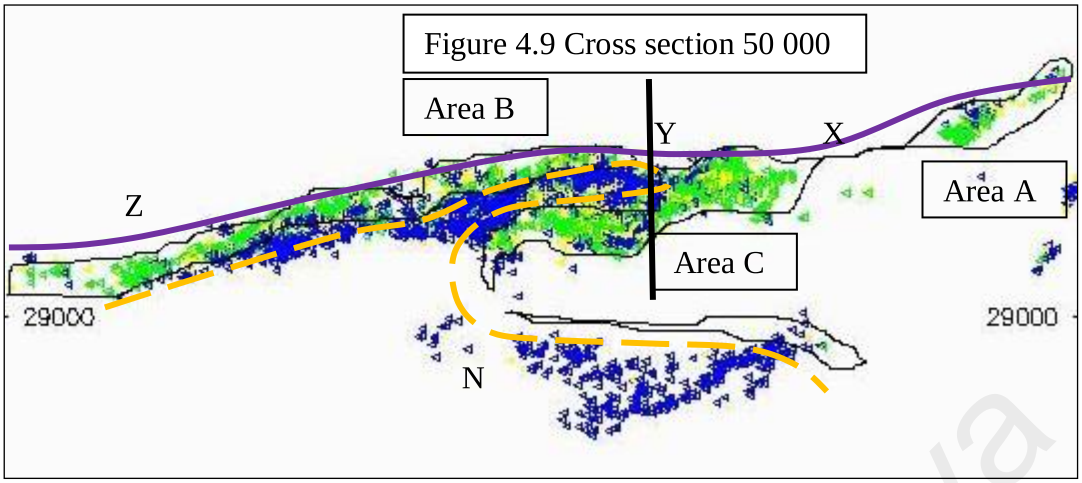

Figure 4.10: Distribution of the mineralized zone (>0.5 g/t Au) for high carbonaceous zone (green, >0.5%C) and low carbonaceous zone, <0.5% C (blue) from Kalampong East pit. Data is from 945 to 960mRL.

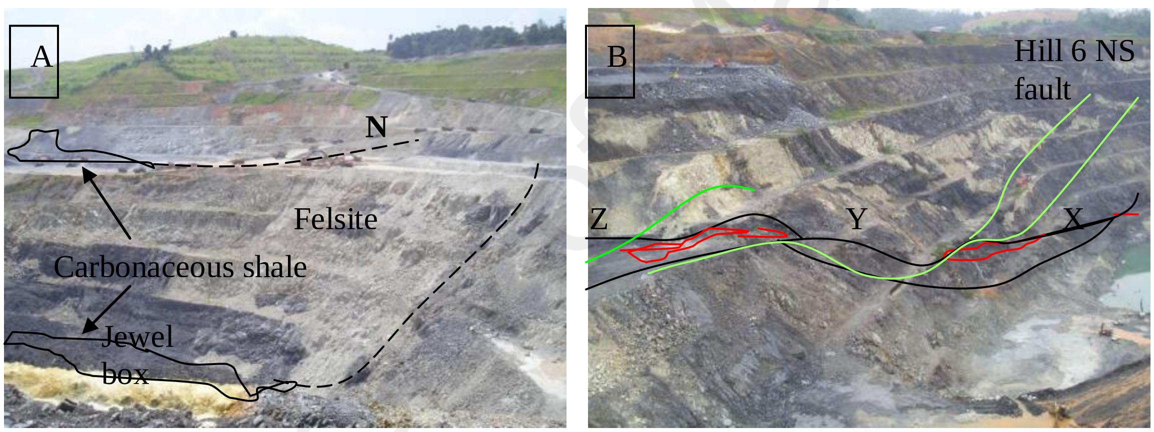

Figure 4.11: (A) Natural break (area N) of the carbonaceous unit due to the massive felsite, Hill 7 and Hill 2 (west wall). (B) Structural break of carbonaceous and mineralization (east wall) due to fault displacement.

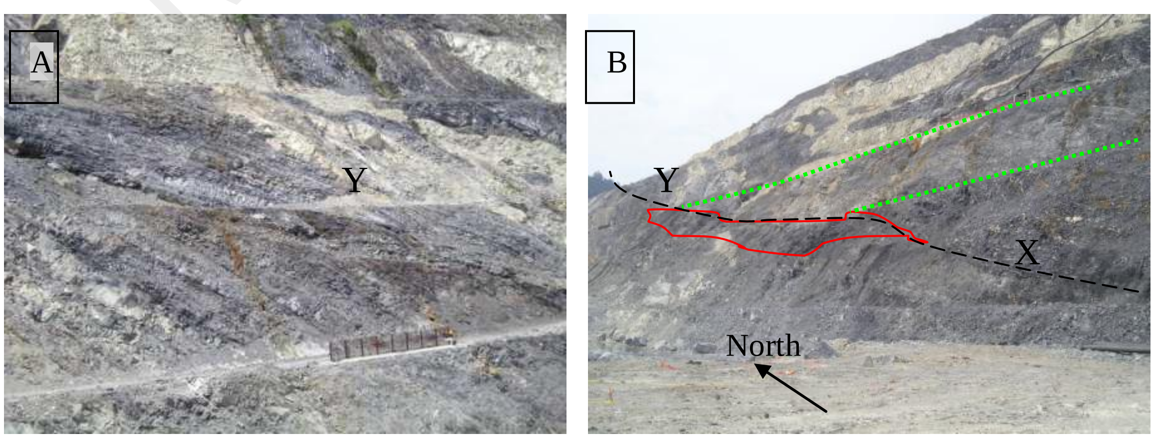

Figure 4.12: (A) Close up view of area Y (east wall), carbonaceous and mineralization break by the structure, (B) Overview of area X and Y, Penjom fault (dash line) responsible for area X and Hill 6 NS fault (dot line) reactivate along main fault responsible for area Y.

4.7.2 Natural break

Massive felsite body is responsible for the natural break of the carbonaceous unit, such as in Hill 3 (Figure 4.11A-area N). The “Jewel box” that comprises the highly carbonaceous unit and Q1W shear vein terminates in this area. Thus, the carbonaceous unit becomes thin, and shearing continues in the felsite with the thin carbonaceous unit inside the felsite.

4.8 Remobilisation of carbon

Along the Penjom Thrust, which is parallel to the eastern limb of the fold, the host rock is highly sheared. The shearing resulted in the mixing of the massive carbonaceous shale and thin, less carbonaceous sandstone and siltstone along this shear zone. The dissolution and loss of silica or carbonate, has possibly increased the carbon content of the carbonaceous host rock. Hydrothermal solutions can also responsible for the remobilization of carbon as evidence in the infill breccias texture, where carbon is infill in fractured quartz. However, this process does not result in a significant increase of the carbon level.

Another zone of high carbonaceous unit is along the western limb and is less sheared. In this zone, the alternating layer of the carbonaceous shale, siltstone and sandstone is preserved. The carbon content is dominantly higher in shale and less in conglomerate. The increase of grain size normally coincides with the carbon content.

4.9 Mineralisation break

The mineralization break of the high carbon unit coincides with the structural break of the carbonaceous unit. There are two east-dipping shear veins: Q1E hosted within the thick carbonaceous unit and Q2E hosted within the thin carbonaceous unit, which is locally in contact with felsite and mostly mined as a low carbonaceous ore. Q2E is not considered as a part of this zone, although in certain places, Q2E also made up the moderate carbonaceous unit.

4.9.1 Structural break

The carbonaceous break area usually does not host mineralization. This is because of the timing of quartz veining formed during the bedding-slip activity and thrust along the carbonaceous layer as an earlier episode. Any later displacement of the carbonaceous unit by faulting resulted in the break of this zone and mineralization.

Several areas were identified as the structural break, such as areas X, Y and Z in Figures 4.9 and 4.10.

Main structural event	**D2 Deformation**	**D3-5 Deformation**
Bedding slip fault along the carbonaceous unit Near fold, east limb and west limb	→	
Penjom Thrust Near fold (area A) and east limb (direct shearing, increase dilution zone, vein slightly deform) Increase carbon reactivity. Other fault, fold related fault	→	
Shear vein, extension vein and mineralization	⇢	
Extensional fault, vein deformed, Further increase a carbon activity Responsible for carbonaceous and mineralization break		→

Figure 4.13: The main structural event affected the carbonaceous unit.

4.9.2 Natural break

A quartz vein that continues into the limb but is not followed by good mineralization is considered as a natural break. There is another factor that controls the grade and could be other syn-deformational structure, fluid flow characteristic, chemical and physical contrast. In a certain area, quartz vein such as on the limb is getting smaller, and this also resulted in the mineralization break. In many places, the occurrence of localized felsite along the carbonaceous unit influences the size and intensity of a vein in a form of brecciated, stringers or bulk quartz, as well as the grade.

A natural break can be unpredictable along the strike because of the occurrences of other factors that control the mineralization, especially felsite intrusive; however, a structural break is usually more consistent along the strike.

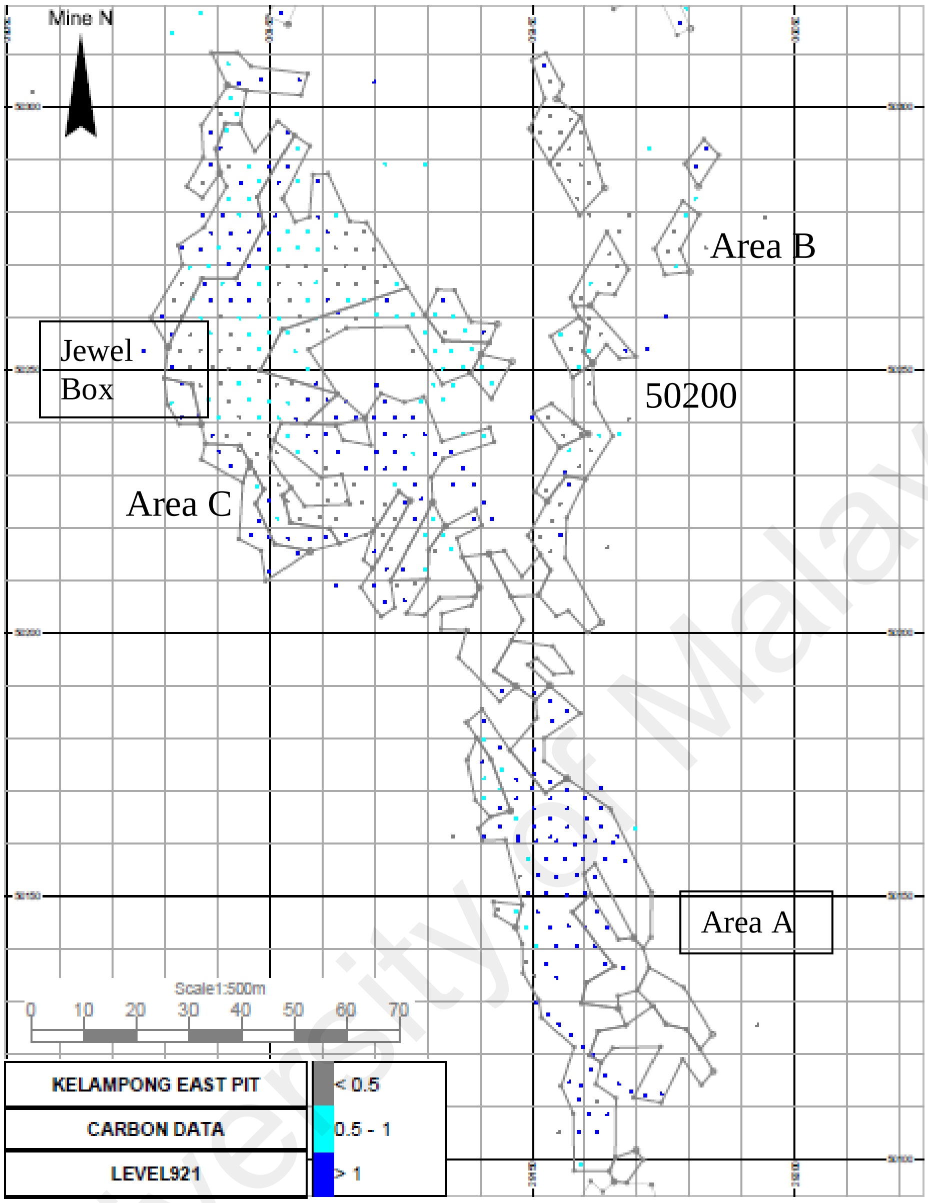

Figure 4.14: Grade control ore block (above 0.8g/t). NS corridor (Jewel Box/Area C) is also high carbon content.

4.10 Different types of carbonaceous shale and percentages of carbon.

Different forms of carbonaceous shale are calcareous carbonaceous shale (A), carbonaceous fault gouge (B), sheared carbonaceous shale (C) and silicified carbonaceous shale (D) with different carbon and sulphur contents (Figures 4.15 A to B and Table 4.4). Sheared carbonaceous shale at the margin is of a finer grain size and usually appears as shiny graphitic shale. Based on the Penjom Metallurgical test work, the highest recovery among the carbonaceous ore was from the calcareous carbonaceous shale, and the highest organic carbon is carbonaceous fault gouge and sheared carbonaceous shale. Secondary calcite in calcareous shale cemented the carbon particle that makes carbon less reactive.

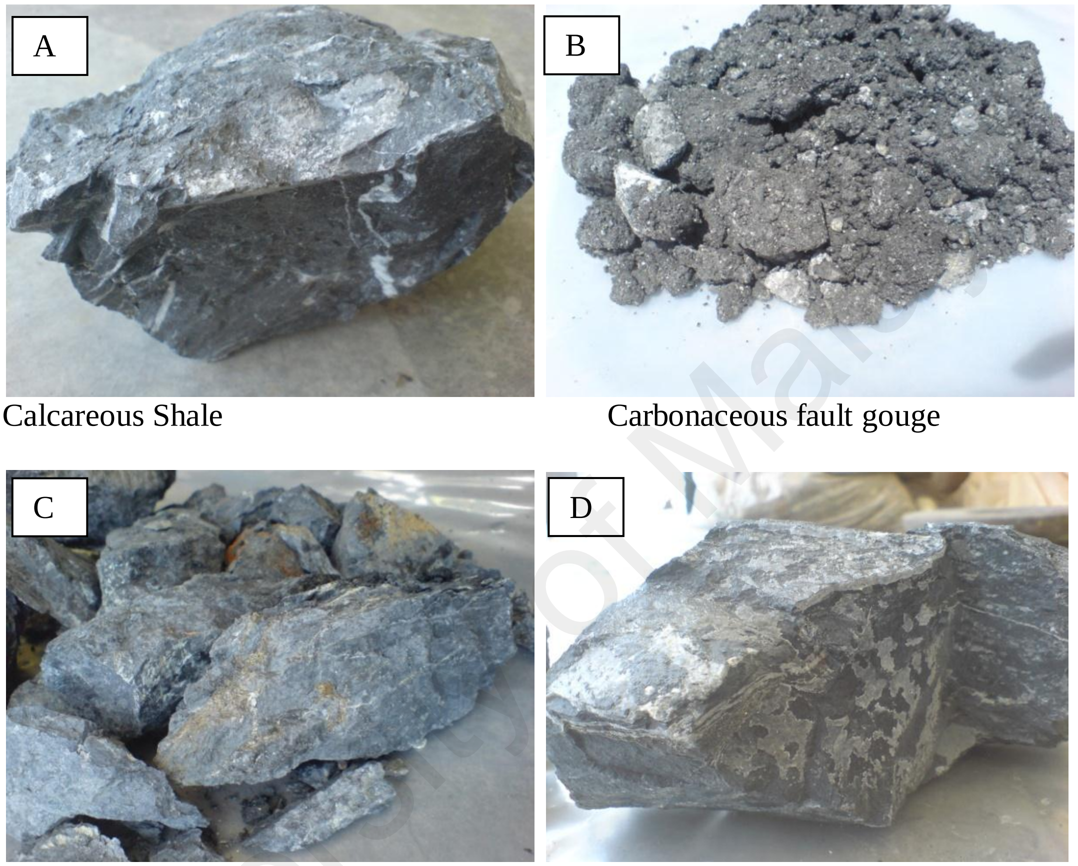

Calcareous Shale — Carbonaceous fault gouge

Sericitized sheared carbonaceous shale — Silicified carbonaceous shale

Figure 4.15: Various types of carbonaceous shale. See explanations in text.

Table 4.4: Various type of carbonaceous shale and result of carbon content and sulfur (as analysed at Penjom Lab).

Activity	**Calcareous Carbonaceous Shale**		**Silicified Carbonaceous Shale**		**Sheared Carbonaceous Shale**		**Carbonaceous fault gouge**	
	ppm	**%**	**ppm**	**%**	**ppm**	**%**	**ppm**	**%**
Gold, g/t	1.01		1.5		1.55		15.13	
Organic C		0.58		0.5		1.44		1.32
Sulfur		0.15		1.3		1.61		1.6

4.11 Other organic matter (meta-anthracite)

A significant streak of volcanic glass appearance can be observed in a carbonaceous shale unit cemented with quartz vein (Figure 4.17 left) and was identified as meta-anthracite. This is based on the analysis of carbon reflectance measurement, which shows a very high reflectance of 4 to 6 (Figure 4.16). It dominantly occurs parallel to foliation or bedding and rarely infills discordant tension fracture or irregular shape. Carbonaceous shale is a common host to this material. Framboidal pyrite can also be observed in a polished section (Figure 4.18)

4.12 Conclusion

Sedimentary host rock in Penjom, particularly in the middle mine sequence, is composed of low to highly carbonaceous rocks and contain a minor quantity of anthracite especially in highly carbonaceous unit. During earlier interpretations, carbonaceous rocks were believed to be mobilized along the thrust from deeper sources based on the high-carbon ore body along the thrust. The thrust at the same time acts as a barrier to the mineralization.

Bogie (2002) proposes that a high carbon material is inherent to the country rock and not from the deep sources and hence is regarded as a free carbon of sedimentary origin. Carbonaceous shale acts as a weak plane for the thrust to develop along this unit. Fold occurs below the thrust, and bedding-slip fault accommodates along this unit. The distribution of carbonaceous material is not only along the thrust but also in the westward dipping of the western limb of the fold and along the same refolded stratigraphy unit towards the south.

Carbonaceous shale is also referred to as graphitic shale along the Penjom Thrust because of the shining black shear surface, but it was still the detrital sedimentary origin that suffered transformation because of structural deformation. The reactivation by the faults parallel to this unit has further thermally altered, reduced the grain size and weakened the strength of this unit. The sheared rock resulted in finer textures after the milling process and higher surface reaction to adsorb dissolved gold and hence resulted in a higher reactivity of the carbonaceous ore.

A carbonaceous shale is very important in the ore genesis process as a physical characteristic that provides competency contrast and acts as a strain accommodator during structural deformation. Chemical characteristic was also being highlighted as carbon can provide a reduced environment for gold precipitation from ore fluid. The carbonaceous material as a proto ore and later enrichment during metamorphic dehydration requires further detailed study.

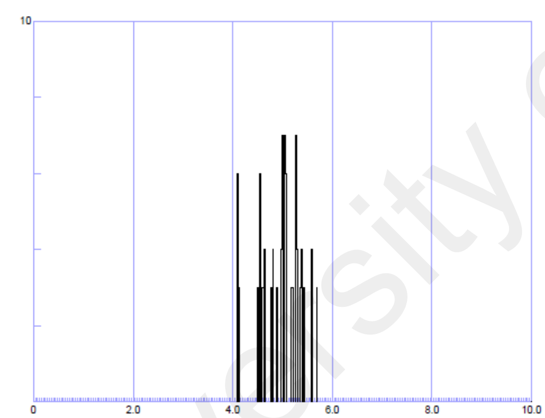

Number	= 30	Measure Date	22/03/2010 16:20
Mean Rm	= 4.936 %	User	wha
s	= 0.414	Date	30/04/2010

4.08 - 4.10 % R	6 %	5.00 - 5.02 % R	7 %
4.12 - 4.14 % R	3 %	5.04 - 5.06 % R	7 %
4.50 - 4.52 % R	3 %	5.06 - 5.08 % R	6 %
4.54 - 4.56 % R	6 %	5.18 - 5.20 % R	3 %
4.58 - 4.60 % R	3 %	5.20 - 5.22 % R	3 %
4.60 - 4.62 % R	3 %	5.26 - 5.28 % R	7 %
4.64 - 4.66 % R	4 %	5.28 - 5.30 % R	4 %
4.76 - 4.78 % R	3 %	5.36 - 5.38 % R	3 %
4.80 - 4.82 % R	4 %	5.38 - 5.40 % R	4 %
4.88 - 4.90 % R	3 %	5.42 - 5.44 % R	3 %
4.96 - 4.98 % R	4 %	5.58 - 5.60 % R	4 %
4.98 - 5.00 % R	4 %	5.68 - 5.70 % R	3 %

Figure 4.16: Reflectance scale of 4.5 to 5 indicates organic carbon is meta-anthracite.

Final reactivation of sinistral, oblique to the normal fault has further increased the shearing of carbonaceous material along the thrust. This reactivation is also responsible for deformation of the veins and carbonaceous shale. The structural event that affected the carbonaceous unit is summarized in Figure 4.13. It can also be concluded that structural and natural breaks that are responsible for the displacement and discontinuity of the highly carbonaceous body are also responsible for the localisation of mineralisation.

Figure 4.17: (Left) Anthracite cemented by quartz vein infilled dominantly parallel to rock fabric in silicified carbonaceous shale. (Right) Polish section image of meta-anthracite (A) in carbonaceous shale and framboidal pyrite under reflected light.

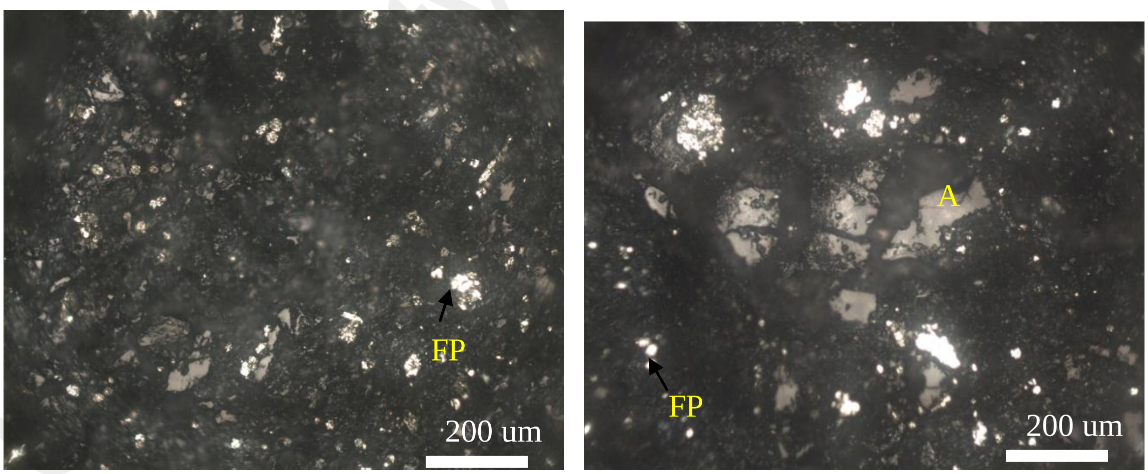

Figure 4.18: (Left). The occurrence of framboidal pyrite (FP) (bright reflectance) associated with anthracite under reflected light. (Right). Meta-anthracite is observed with vesicles indicative of thermally altered. Framboidal pyrite is also observed.

CHAPTER 5.0 STRUCTURAL GEOLOGY AND VEINS SYSTEM

5.1 Introduction

Penjom is classified as orogenic gold (Flindell, 2003) after Groves et al. (1999) and has many characteristics that are common with other orogenic systems such as the Victorian gold fields (Eastern Australia) and the Meguma terrain (Nova Scotia, Canada). These systems have a similar structural environment-controlling veins system related to compressional and transpressional regimes that produce folds, reverse and strike slip faults.

5.2 Regional structural geology

Penjom Gold Mine is situated in the Central belt of Malaysian Peninsula in an area with the topography elevation lower than 300 m, except several granitic hills such as Bukit Lima and the Benom Complex. Despite this low topography, a series of strike-ridge lineaments coupled with negative lineaments trending NNE-SSW to NS can be seen on radar set images. Penjom is situated along one of the splays of the Bentong–Raub suture (Kidd and Zainuddin, 2000), about 30km east of these main sutures.

Due to lack of exposure, structural study is always limited in coverage, but an attempt to interpret the regional structural geology by radar set images has been made (Tjia and Harun, 1985). NS and NNW faults are reported to be the most common faults direction in the Malaysia Peninsula, compared to the NNE-trending fault. However, within the West Pahang, NS trending lineament and NNE splay are easily seen on the radar-sat image.

Structural deformation of peninsular Malaysia is summarized by Shuib (2009) as shown in Table 5.1. Late Triassic-Early Jurassic has been highlighted as an important period that applicable to the study area.

Table 5.1: Summary of deformation events in Peninsular Malaysia (Shuib, 2009)

	Western belt	**Central belt**	**Eastern belt**
Early Cambrian	Uplift and deformation		
Early to Mid-Devonian	?Deformation, metamorphism, uplift		
Pre-Early Permian			Dextral transpressive deformation, metamorphism, uplift
Post-Early Permian			Transpressive deformation and transtensional opening of continental pull-apart basins
Mid-Devonian to Mid-Permian	Rifting, extension		
Mid-Permian to Early Triassic	Dextral transpressive deformation, metamorphism	Dextral transpressive deformation, metamorphism, uplift, subsidence & further dextral transpression along Bentong-Raub Suture Zone	Dextral transpressive deformation, metamorphism
Middle Triassic-Late Triassic	?Extension/?Transtension	Dextral transpressive/transtension deformation	
Late Triassic-Early Jurassic	Dextral transpressive deformation, metamorphism		
Latest Triassic to Createaceous	Transtensional opening of dextral pull-part basins		
Mid to Late Cretaceous	Sinistral transpressive deformation	Sinistral transpressive deformation, metamorphism (Stong Complex)	Sinistral transpressive deformation
Early to Middle Eocene	Late brittle faulting		

The most prominent structure in the Central Belt is the Bentong–Raub Suture along the eastern footwall of the Main Range Granite. It has been interpreted as the subduction line between the Sibumasu and Indochina Blocks (Hutchison, 2009; Metcalfe, 2000, 2013) and is correlated toward the north as Nan Uttaradit and Sra Kaeo sutures of Thailand.

Tectonic and magmatic events are summarized by Metcalfe (2013) as shown in Figure 5.1. The Bentong–Raub Suture represents the closure of the Palaeo-Tethys and is made up of suture lithologies including oceanic radiolarian cherts recording the age from Devonian to Upper Permian, melange and serpentinite (Metcalfe, 2002, 2013).

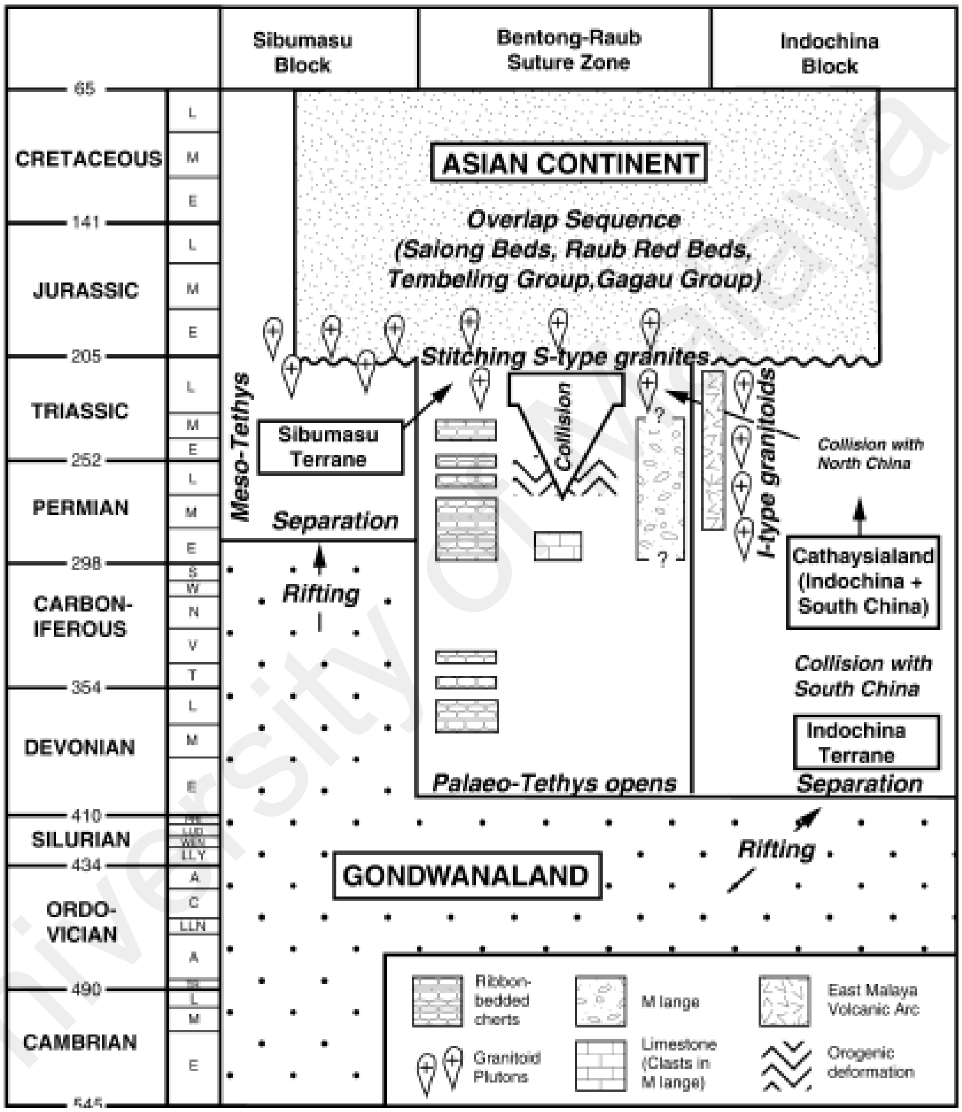

Figure 5.1: Tectonic-magmatic event involving the collision of Sibumasu-Indochina terrain (Metcalfe, 2013).

5.3 Previous studies

5.3.1 Geological modelling 1 (1997–1999)

NS-trending mineralization made up the NS corridor, which hosts laminated to ribbon quartz (Corbett, 1997), and the thrust zone hosts sheared ribbon quartz. At higher elevation, both ore zones are high in carbon or carbonaceous content, but only the thrust zone has been recognised and highlighted as a high-graphitic ore zone during that period and characterized as the Penjom Thrust ore body.

The NS fault (now classified as quartz-bearing NS trending bedding-parallel shear related to folding episode) was interpreted as hosting and control mineralization or as the main conduit for fluid at depths.

5.3.2 Geological modelling 2 (2000–2001)

A second geological modelling reinterpreted and recognises the laminated vein-bearing NS corridor as a new element of bedding slip fault so that it emphasizes more on stratigraphy control. However, the NS fault is still maintained in the model and considered to a certain extent as responsible for reactivating the bedding slip fault and partly hosting the mineralization. The role of the NS fault is unclear, but this structure is still maintained and inferred as the structural conduit. Ore zones in Kalampong East during this period were classified as:

1) Penjom Thrust ore zone
2) Stratigraphy concordant ore zone at certain structural setting
    a. Felsite sill-hosted ore zone
    b. Stratigraphy parallel ore zone
3) Minor NS-bearing ore zone.

Around the jewel box, the previous NS corridor has been re-classified to a bedding-parallel zone; however, in other area away from this area, the earlier element of NS shears/fault hosted ore is still maintained. The change of NS-trending quartz-bearing bedding slip fault, previously classified as the NS fault mined during earlier pit development (geological model 1), to a stratigraphy concordant or bedding-parallel veins (geological model 2) has downgraded the previous theory about the role of the NS fault as the main controlling factor in mineralization.

5.3.3 This study

This study upgrades the second geological modelling with a focus on the genesis and structural setting of the bedding-parallel veins and several stages of the extensional veins. Setting of the shear veins are shown in the map as depicted in Figure 5.2. The relationship between these two veins types were also described in detail. The shear and the extensional veins can occur in a single ore zone normally in areas where a competency contrast unit exist, for example the contact of carbonaceous shale with sandstone, conglomerate or felsite intrusive. The bedding-parallel veins were interpreted as occur during flexural slip folding during the D2 compressional event (Endut and Teh, 2010; Endut et. al, 2014; Endut et. al, 2015a). With this new understanding, this structure is only considered as a trap and not the conduit at depth. The conduit may have been provided by the main thrust, parallel structure, splays and associated fractures during the deformation. Another phase of faulting is responsible for a second stage of extensional veins.

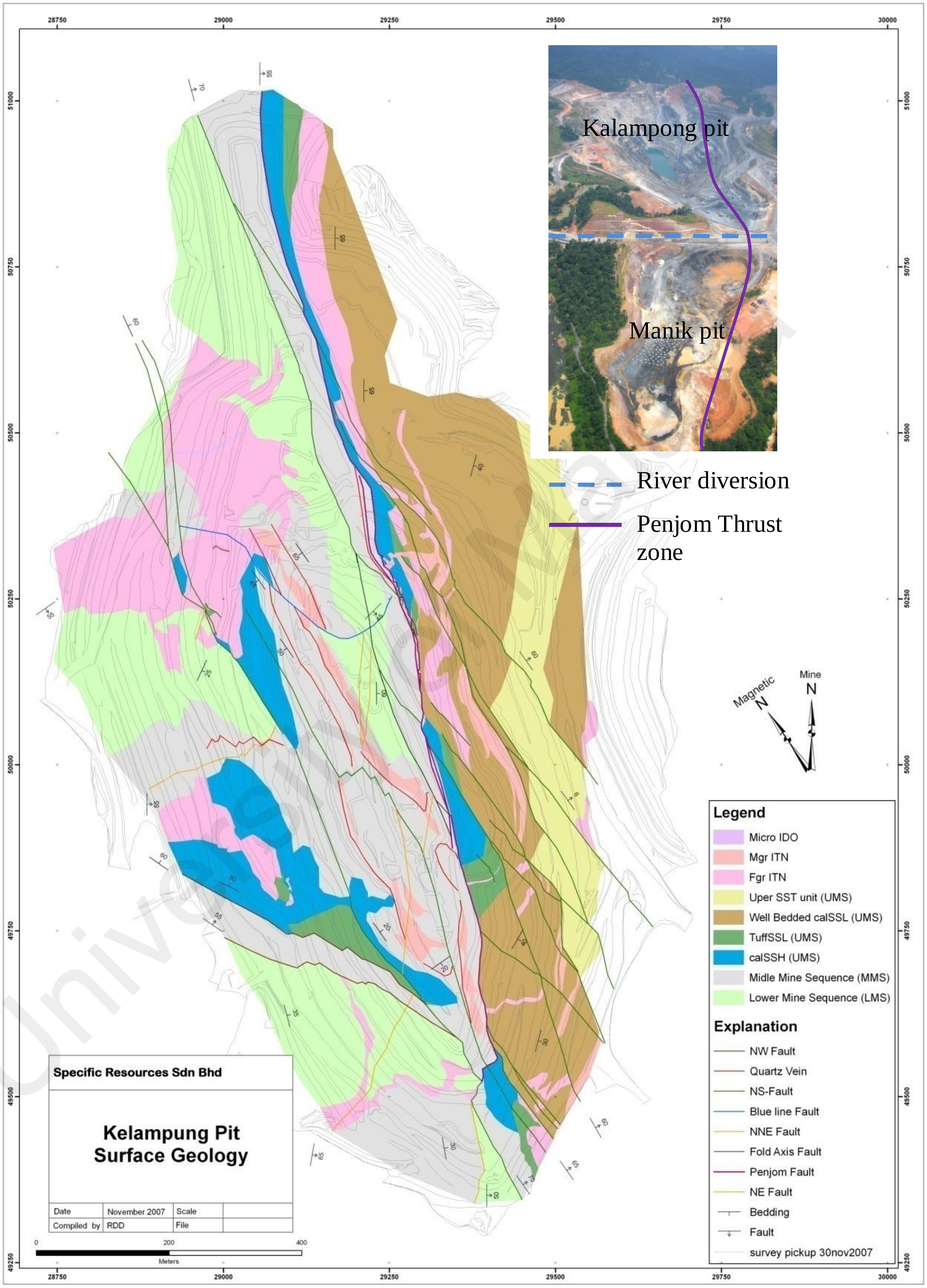

Figure 5.2: Geological map of Kalampong pit (2008), inset photo shows bird eye view of Kalampong and Manik pit.

5.4 Folding

5.4.1 Introduction

Folds can be divided into two phases. The overall east-dipping sequences developed during the D1 event that is part of regional folds, and Penjom is located at the eastern limb. Local re-folding of the sequences forming anticline–syncline sets associated with the Penjom Thrust structure can be seen in the Kalampong pit. Folding was certainly the earlier structural event, and this episode was modified and overprinted by the movement of the thrust-parallel structure with reverse and dextral sense of movement and later by the sinistral to normal sense of movement by the northerly trending fault. The fault also accommodated along the fold axis that separates the eastern and western limbs. Both limbs formed two separate corridors that host two significant ore bodies along the same rock unit. The photo of north and south walls with the structural outlines are shown in Figures 5.3 to 5.6.

Other corridors are tight-incline folds, which are along the fold axis and the refolded western limb which hosts Kalampong West, Manik and Jalis ore zone particularly along the fault zone or shear vein. Study of fold-related structures other than the veins includes bedding outline, stratigraphy correlation (fold geometry) and fold related products such as cleavage.

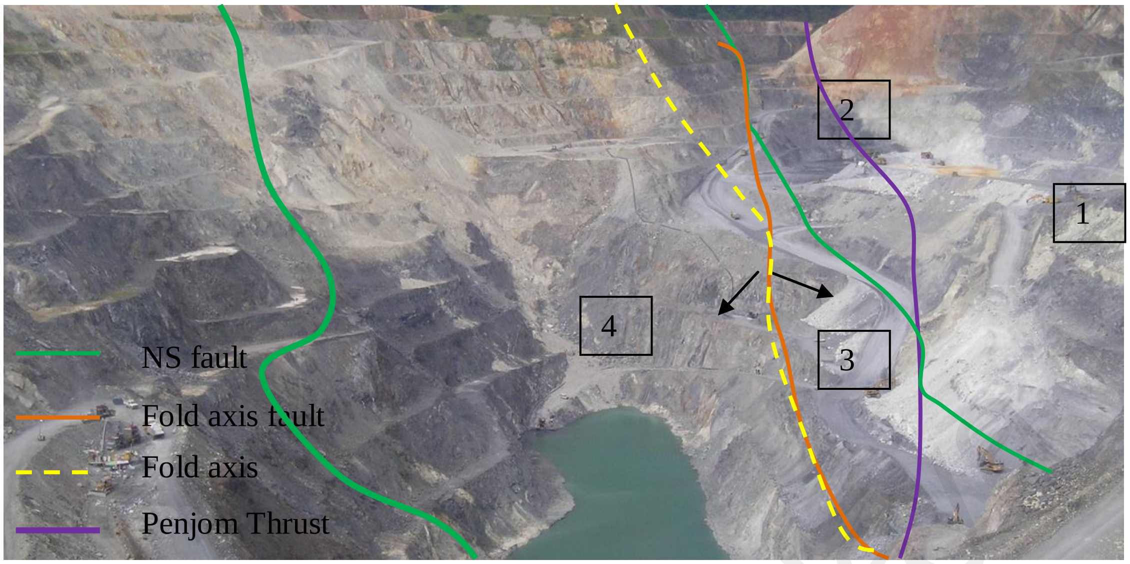

Figure 5.3: North wall as current pit slope (2009). Area for the bedding analysis plotted in stereonet. Bedding at area 1, 2 and 3 are dipping east and area 4 is dipping west.

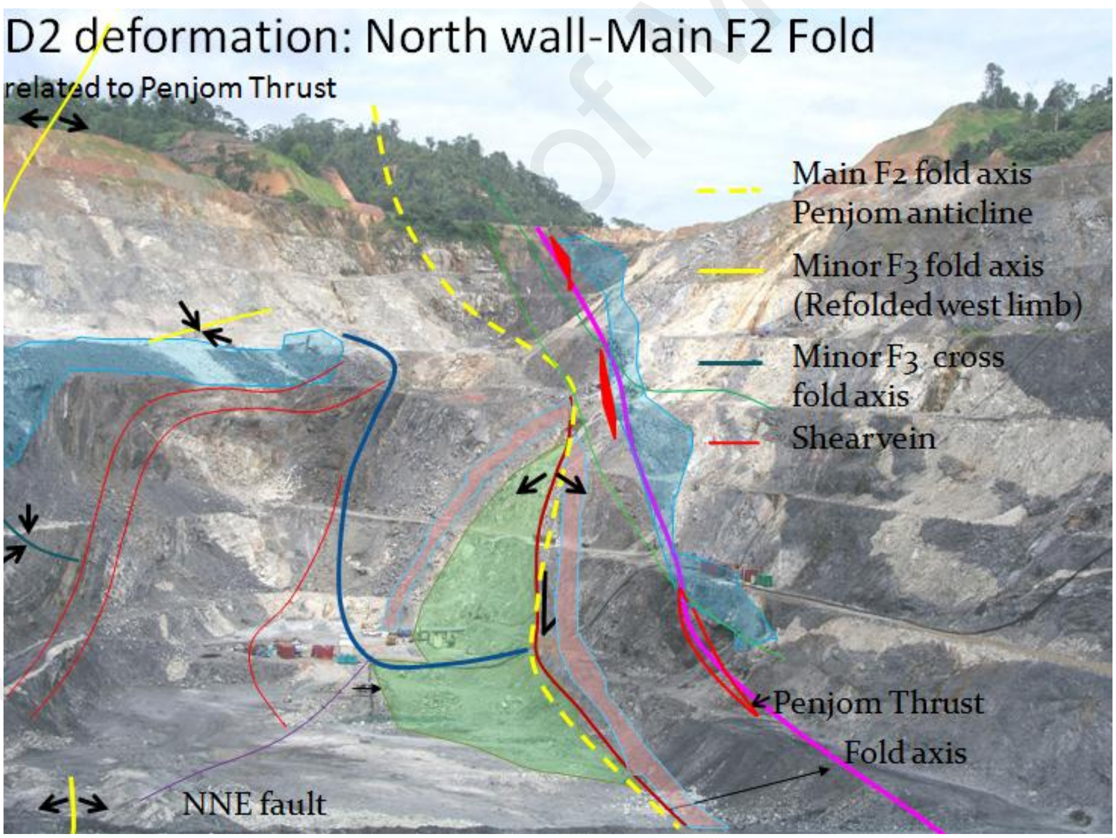

Figure 5.4: North wall before cutback shows the same style of folding.

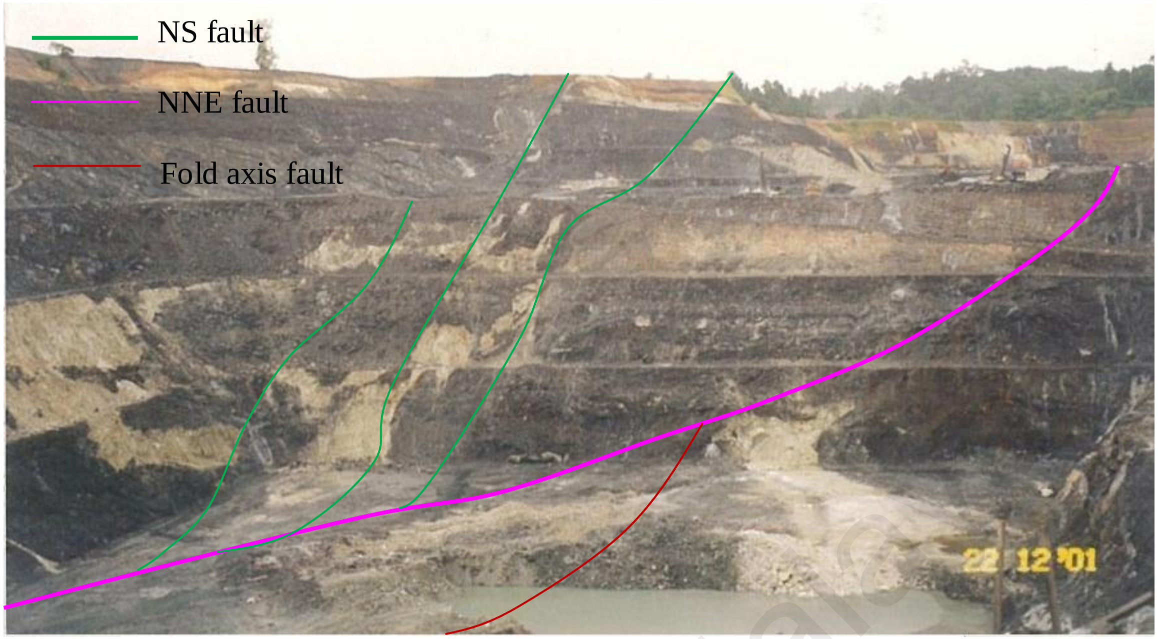

Figure 5.5: South wall during third cutback. Hill 6 NS fault intercepted along the eastern limb.

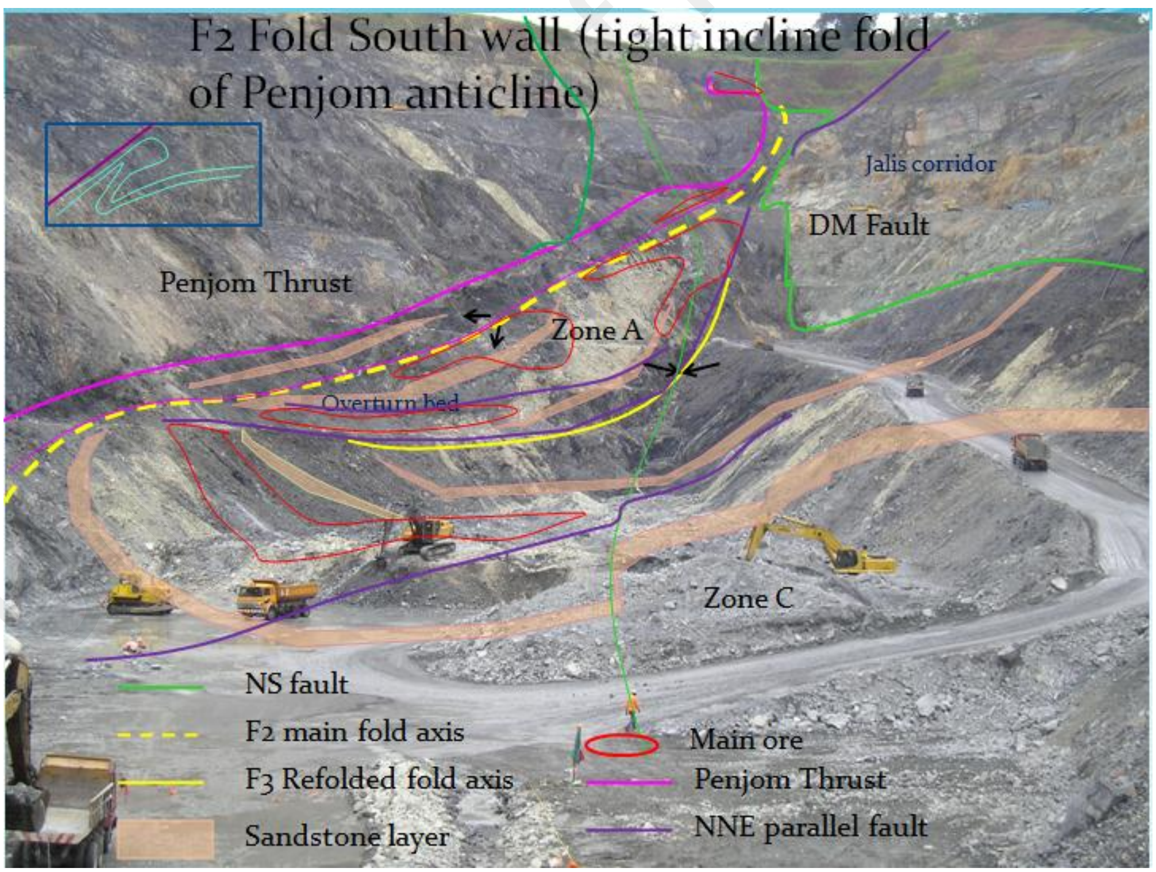

Figure 5.6: South wall of Kalampong pit before 2009 cutback shows recumbent fold of tight inclined fold.

5.4.2 Bedding

Bedding should not be thought as a passive surface during deformation. It is commonly an ideal accommodator of strain, especially progressive shearing strain (Davis, 2005b) which results in bedding slip fault as indicated by the slickenside surface along the bedding shear. The bedding can be an active surface during deformation as a result of its physical and mechanical properties such as lamination and, in particular, layering of fine grain sediment in between coarse grain sediment. The process is usually associated with the folding process and is also referred to as flexural slip fault.

5.4.2.1 Bedding analysis

Bedding orientation around the pit has been measured and plotted on stereonet. Data collection has been divided into two structural domains referred to as hanging walls and footwalls. Footwalls represent the overall east-dipping sequence that undergoes a compressional event resulting in the host rock being folded in the pit area to an antiform-synform couple below the main thrust. The Jalis thrust reactivates along synform and is probably responsible for another fold that is currently to the west of the current pit.

Figures 5.7 to 5.8 show stereonet plot for the dip and the dip direction of bedding in various parts of the Kalampong pit. Based on the geometry of the fold, comprised of anticline-syncline at the footwall, the dip direction of the bedding can be divided into three main groups such as east-dipping eastern limb parallel to the main thrust (Area 1-3), west dipping western limb (Area 4) that is part of the Kalampong anticline and east dipping sequence that forms a synform that hosts Jalis–Manik corridor (Area 5). Tight incline fold around the fold axis also has an east dipping bedding.

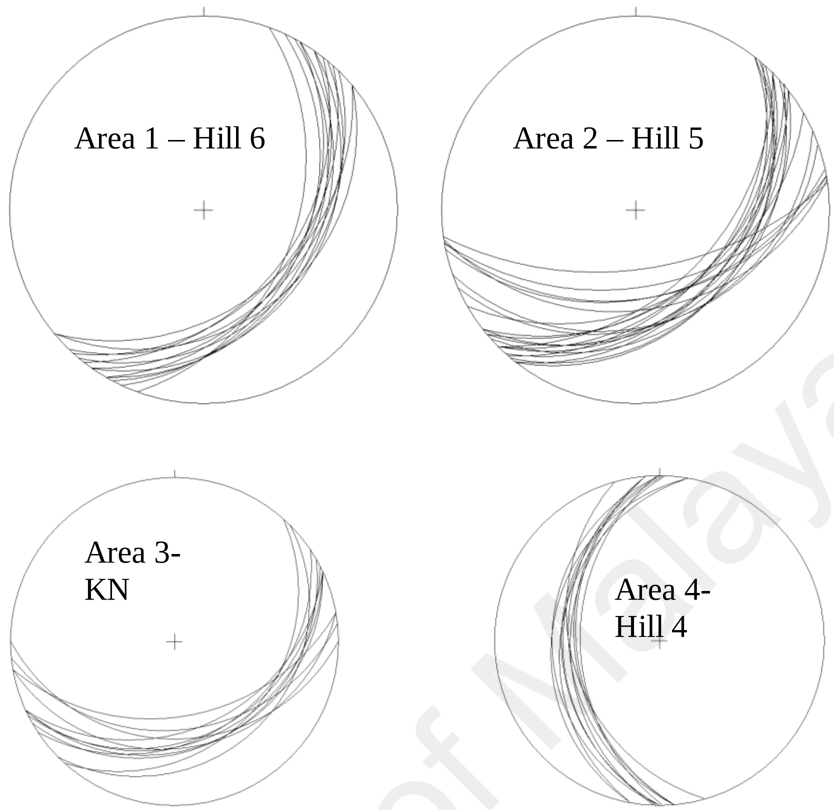

Figure 5.7: Hanging wall, Area 1 - Hill 6: Mean Orientation = 44/126 (Dip/dip direction). Area 2 – Hill 5: Mean Orientation = 46/147 (Dip/dip direction). Foot wall, area 3 (zone B) - Eastern Limb near fold axis: Mean Orientation = 38/157. Area 4 (zone C) – West wall North: Mean Orientation = 64/277.

Figure 5.8: Jalis-Manik corridor. Stereonet plot of bedding at Jalis west wall shows mild cross fold of the east dipping bedding: Mean Orientation = 30/094

Stereonet analysis shows that the structure of folded rocks in the footwall of the Penjom Thrust changes from open fold to tight-incline fold towards the south. The Western limb becomes refolded in the western side, resulting in the east-dipping sequence of the sediment from the west wall of Kalampong towards Jalis and Manik.

5.4.2.2 Stratigraphy correlation and style of the fold

A complete understanding of the stratigraphy is essential to understand the style of the folded rock. Detailed explanation of the stratigraphy unit is covered in chapter three. The overall stratigraphy sequence in Penjom can be divided into three sequences to enable simplified geology to be incorporated into the fold analysis. The cross-section of the ore body is shown in Figure 5.9 to 5.12, and this provides the overview of the fold geometry. Several important stratigraphy units are calcareous shale, thick carbonaceous units and thick conglomerate units. The occurrence of mineralized bedding-parallel vein and felsite also helps in determining stratigraphy correlations on the smaller scale.

Main fold is considered as folded rock associated with the Penjom Thrust that has resulted in antiform and synform couples below the main thrust from Janik to Kalampong North. Around the Kalampong anticline, fold settings of the ore domain can be divided into a tight-incline fold (zone A), eastern limb (zone B), western limb (zone C) and west limb of the synform (zone D). Western limb (zone C) is also known as a NS corridor because of the same strike direction. Areas for this zone (A to D) were shown in Figure 5.9 to 5.12. Figure 5.13 shows a plan view of pit geology and stereonet plot of the fault direction. The active bedding slip shear at the western limb contributes to the intense west dipping fault.

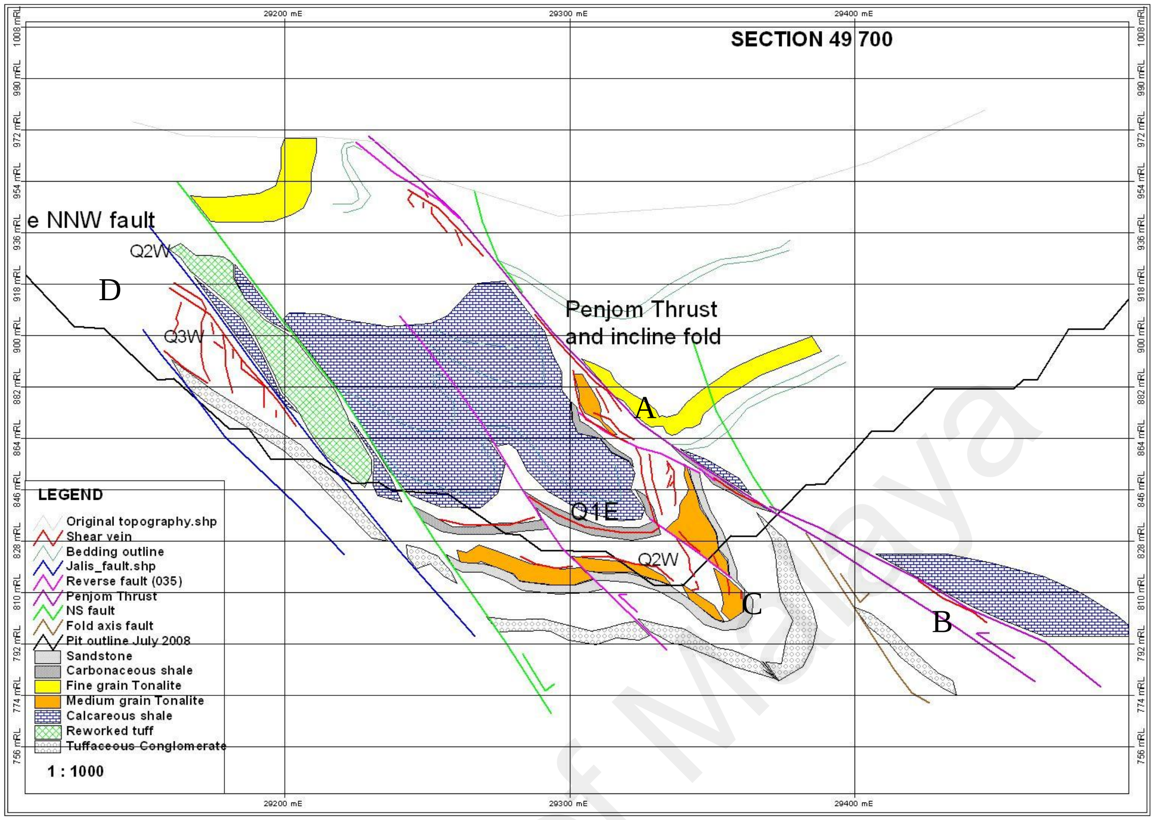

Figure 5.9: Cross-section at 49700.

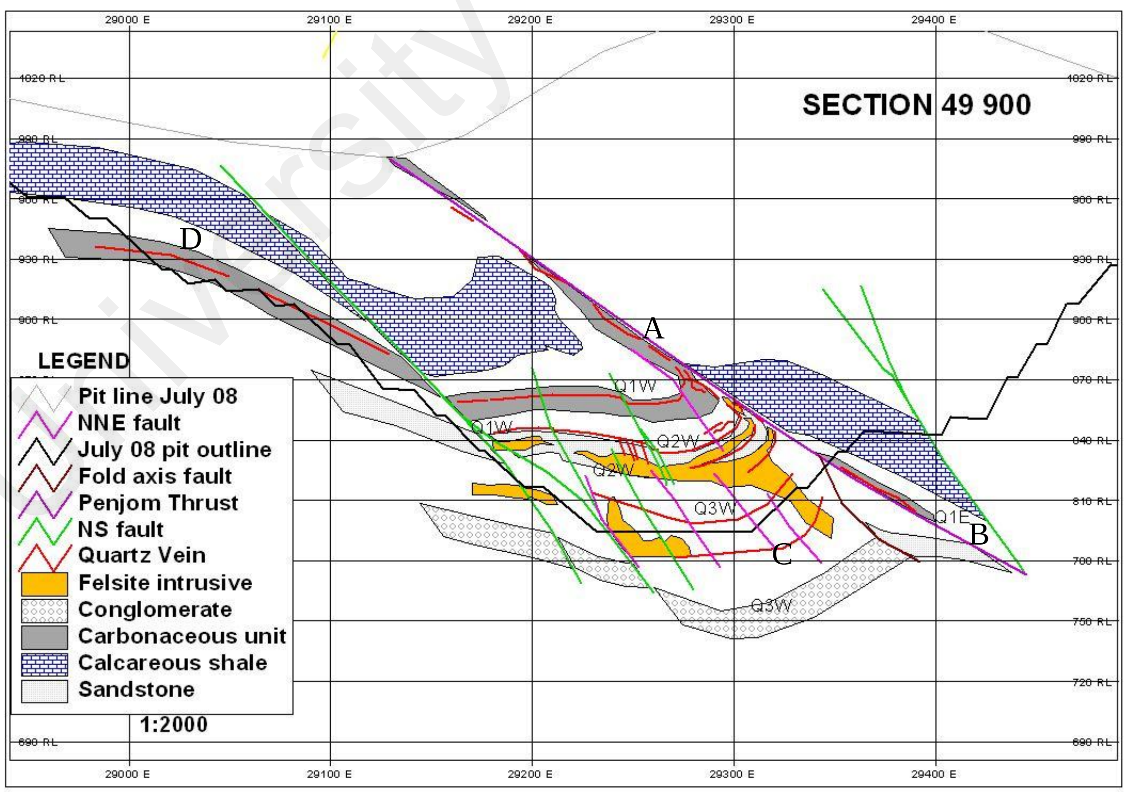

Figure 5.10: Cross-section at 49 900.

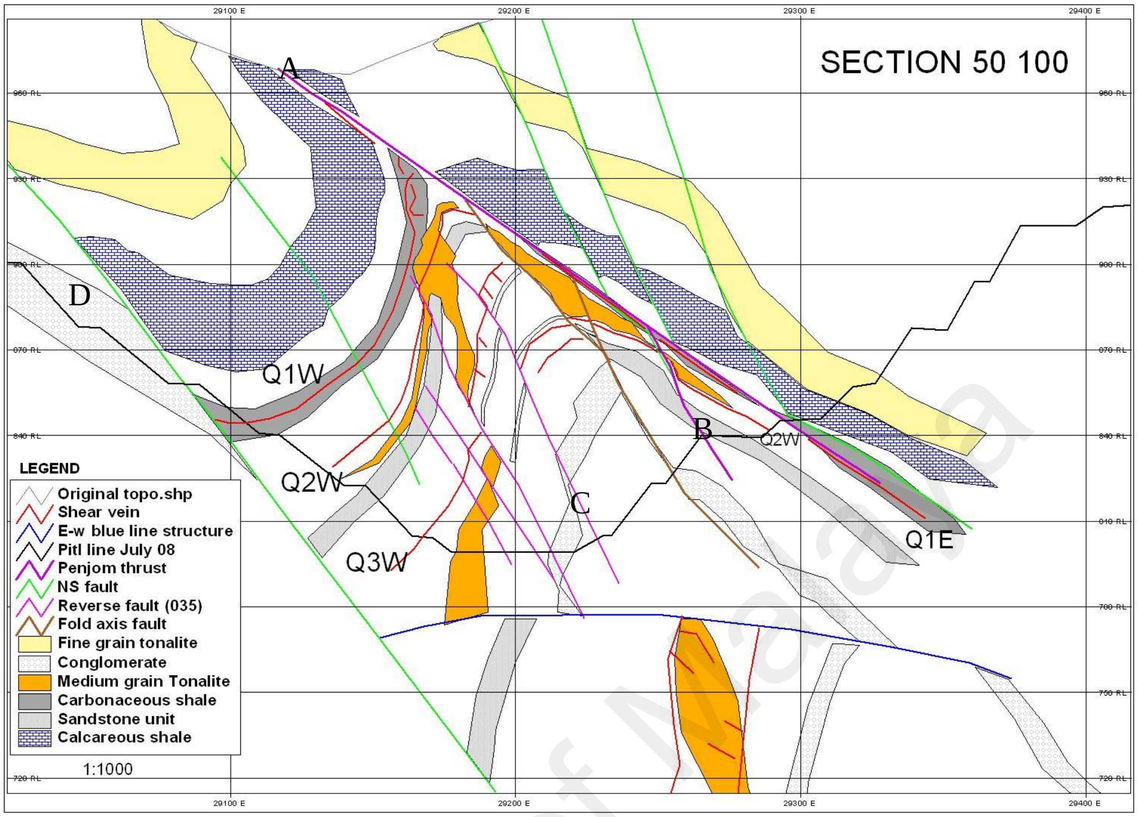

Figure 5.11: Cross-section at 50100.

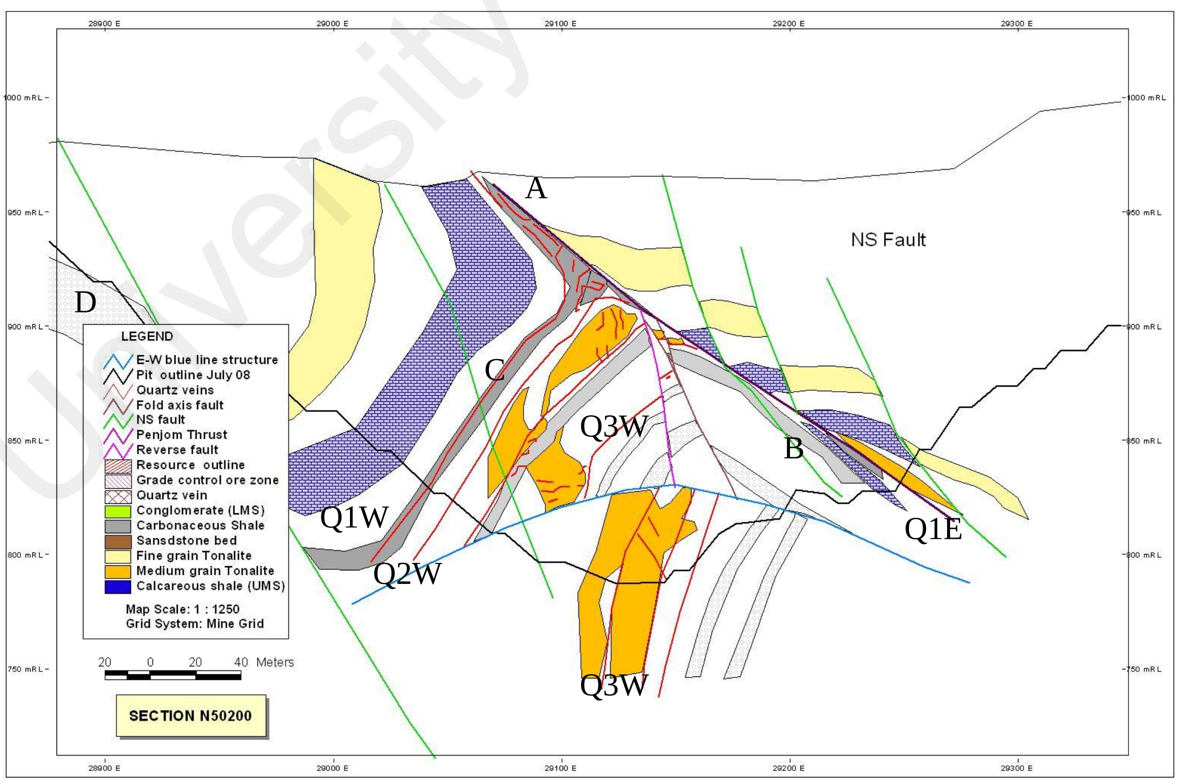

Figure 5.12: Cross-section at 50 200.

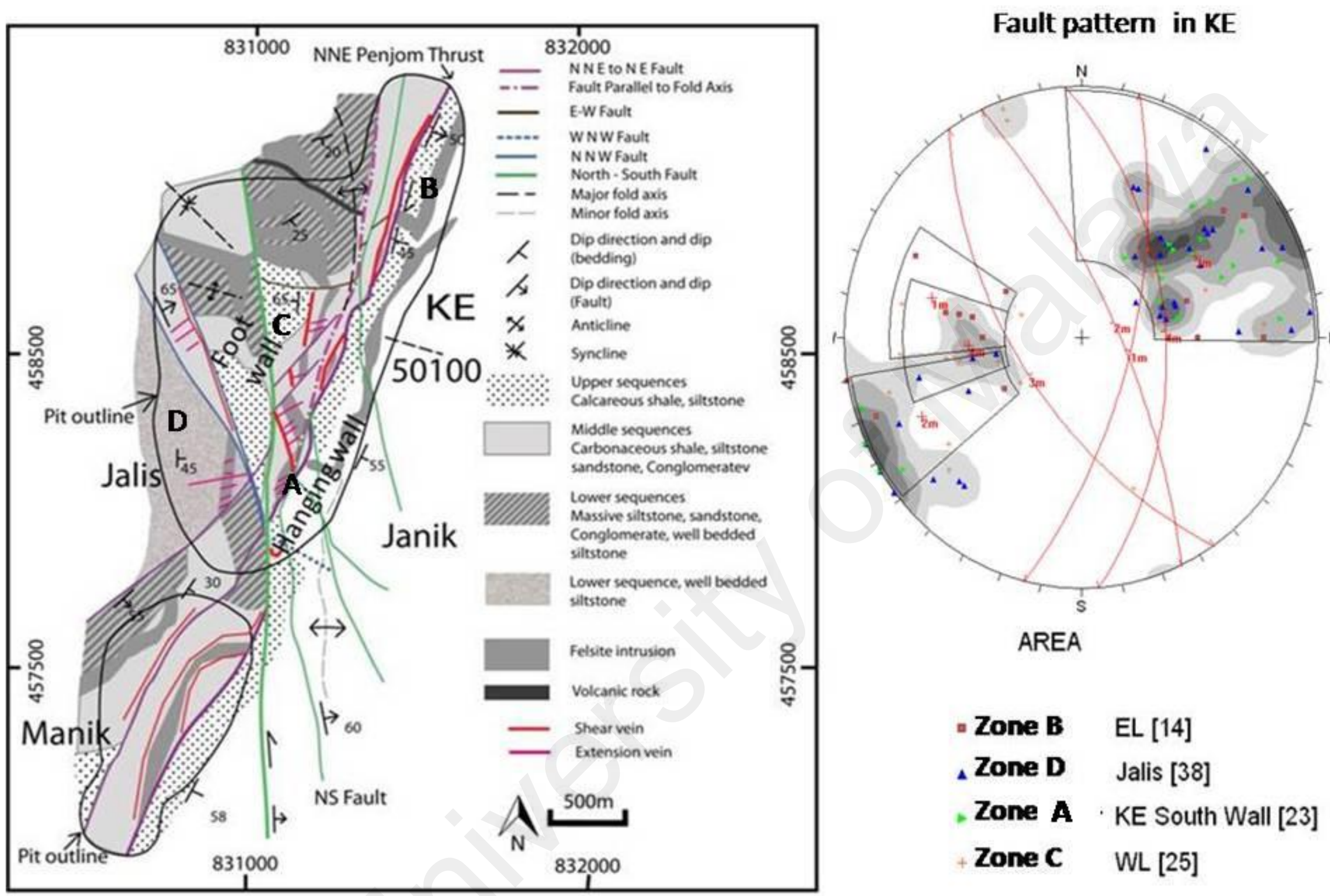

Figure 5.13: The stereonet plot of fault orientation in several zones. Numbers of data are in bracket.

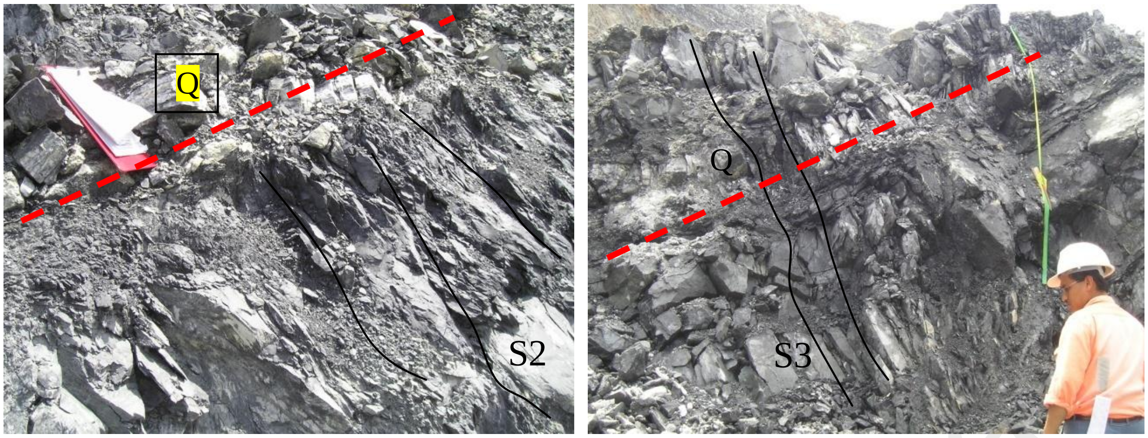

Figure 5.14: (Left) Undeformed shear vein with fracture cleavage S2 below the vein (western limb). (Right) S3 fold axis cleavage also affected the shear vein (refolded western limb).

5.4.3 Cleavage development

Cleavage consists of penetrative planar rock fabrics that are developed during deformation and formation of folds. Their intensity is commonly heterogeneous across various scales, and shear zones represent zones of cleavage intensification (Davis, 2005b).

The occurrence of cleavage will help to understand the effects of folds and faults on the host rock and veins in order to constrain the time relationship between the structure and mineralization. Several styles of cleavage can be observed within the Kalampong Pit, either developed locally or broadly across the fold axis, such as bedding-parallel cleavage or foliation, fractured cleavage, crenulation cleavage and pressure-solution cleavage.

Bedding-parallel cleavage S_1 develops during the regional deformation event before refolding related to Penjom thrust. Fracture cleavage (S_2) that is perpendicular to the bedding locally developed below the bedding parallel shear vein is formed during the D2 fold activity (Figure 5.14 left). Northerly strike-fractured cleavage S_3 probably formed during the later stages of compressional event or refolded activity associated with fault. It forms below the NNE reversed fault that cross cut the earlier bedding-parallel shear vein (Figure 5.14 right).

Bedding-parallel cleavage is more intense in inclined fold and also well developed in conglomerates, especially along reactivation of the fault. Similar fractures can also be observed in small felsite sills (Figure 5.15 right) as a result of reactivation along the shear vein. Contact of felsite intrusive and shear vein during the veining process, as in Figure 5.15 (left), is only shows a narrow deformed rock.

Figure 5.15: (Left) Shearing at contact of felsite intrusive as indicate by shear vein V1, intrusive is undeformed. (Right) Shearing as a result of reactivation of the fold at contact with intrusive produced parallel fracture in narrow sill (refolded of the western limb)

Figure 5.16: (Left) S_2 develop in refolded fold below incline fold. (Right) Close up view of northerly strike parallel fracture cleavage. Dash line is bedding outline.

The occurrence of the fault along the fold axis that separates the east and west limb of the fold has probably accommodates the stress during deformation so that less intense S2 fracture cleavage is developed along the main axis of the anticline within the competence unit such as felsite intrusive. The other fracture cleavage S3 develops adjacent to the D3 fault (Figure 5.16).

5.5 Fault

5.5.1 Introduction

Fault is not always a straight line or plane. It bends or splays from the main fault plane forming a network of faults. The direction of fault can locally change from NNE to NS-trending so that classification of fault is based on the direction only could result in misinterpretation of the fault system.

Several steps of studying the fault, in particular the major fault, start with the study of individual major faults at the pit wall and across the pit. Direction of the fault can be in the range of 30 degrees and, direction-based classification should be done with regard to this range. For example, Fold Axis Fault has a NS direction to the south but a NNE direction to the north. The fault is also assigned a specific name to differentiate among a series of faults.

After the individual fault has been recognized, sense of movement for every fault will be determined based on marker-bed displacement and slickenside direction. The fault will be grouped based on the direction and sense of movement. The strike direction takes into account certain ranges of the fault orientation.

Based on the study, several fault orientation can be observed; including NE to NNE reversed and lateral fault, E-W, NNW and NS trending lateral to normal fault. At least four mine-scales NE to NNE reversed faults and several NS normal faults with a minor component of lateral strike slip have been recognised. Based on crosscutting relationships, three groups of faults and structural deformation can be established (Figure 5.17).

5.5.2 Fold related fault

The Penjom thrust is a fold-related structure developed after initial folding and characterized by occurrences of tight-incline folds to open folds at the footwall of the structure. The Penjom Thrust appears as highly carbonaceous because it is reactivated along the carbonaceous shale and has physically remobilized the carbon along the fault.

The Kalampong anticline that developed below the Penjom Thrust has a fault accommodated along the fold axis that is referred as fold-axis fault. This fault has a normal sense of movement that separates the east limb and west limb of the open fold and is thus classified as a fold-related fault. Direction of this fault is NS near to the thrust and turns NNE towards the north.

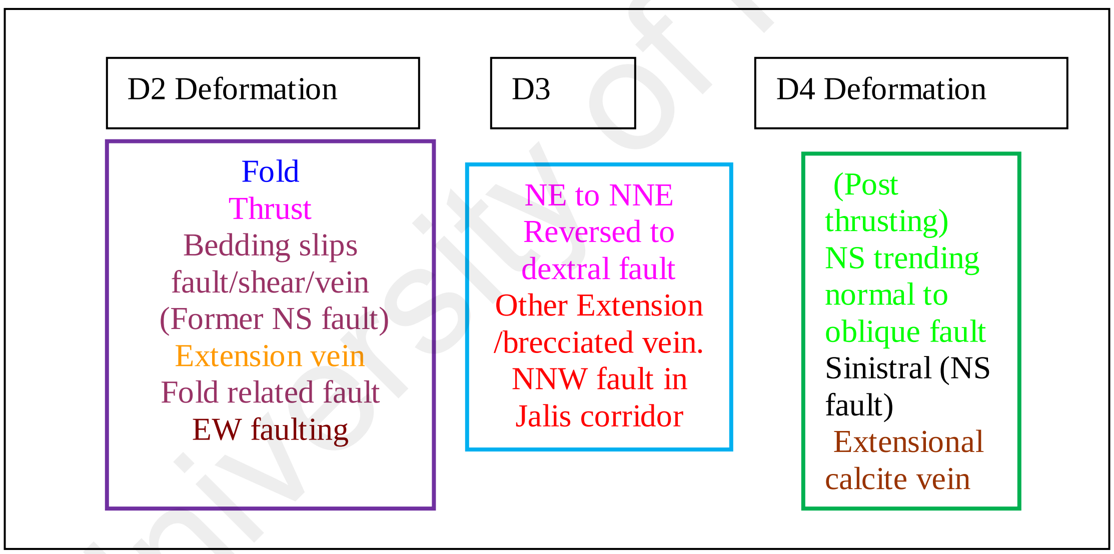

Figure 5.17: Structural classification for Kalampong East (KE) Pit shows three main structural events.

5.5.3 Compression fault

Several series of NNE to NE fault can be observed in the Kalampong pit cross cut the western limb of the fold. This fault is referred to as the R1 to R5 reverse fault (Figure 5.18 to 5.19). The R1 fault in the north is likely to be a part of the Jalis-reversed fault with reverse slickenline as exposed in the south and this structure has been displaced by the NS DMF fault. The NNE faults are very important and control the extension veins at fault-intrusive contact even though the veins mostly yields a lower grade ore but a larger zone if at felsite contact. Displacement by this fault can be up to 20 m such as the R1 fault (Figure 5.18), and the other fault has a displacement of less than 5 m.

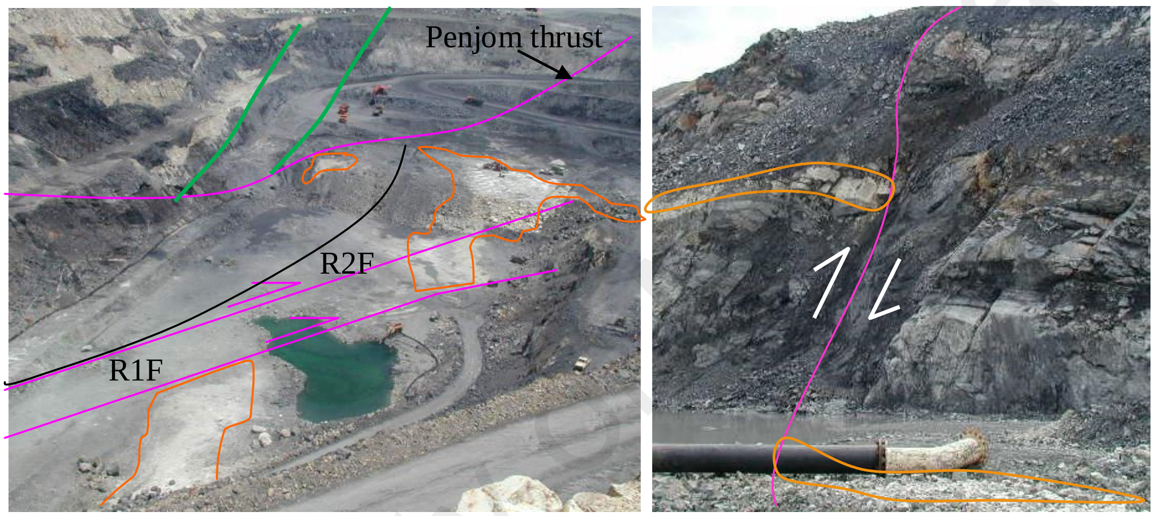

Figure 5.18: (Left) R1F and R2F displace felsite body, looking south (852mRL). (Right) R1F as expose on the wall.

Figure 5.19: (Left) R4F (NNE fault) displace felsite rock in incline fold zone, base level 834mRL (looking south) after cutback. (Right) Close up view, intense quartz below R4F at contact with felsites intrusive.

5.5.4 Strike slip regime

Based on observations of the slickenside on the fault plane, several faults show multiple movements such as reverses with dextral (e.g. NNE to NE faults) and normal with sinistral movement (NS fault).

5.5.4.1 Dextral fault

Some of the NNE and NE faults have a component of dextral and oblique-reversed movement as shown by the R2 fault; a steep NNE fault and a NE fault in the Jalis corridor. This movement is thought to occur after the reverse sense of movement when the stress changes from compressional to transpressional.

5.5.4.2 Sinistral fault

Sinistral movement can be observed along the NS Jalis fault at southern wall of the Kalampong pit but normal to oblique normal sense of movement is prominent along a series of Hill 6 NS fault, as indicated by the movement of marker bed and fault striation.

NS Jalis fault is considered here as a major sinistral to normal fault and not responsible for the folding but reactivating along Penjom thrust parallel to the fold axis. NS Jalis fault has downthrown all the sequences and reactivates along the Penjom thrust. This explains why the younger sequences have occurred above the Penjom thrust (not vice-versa) along the fault reactivation.

5.5.5 Extensional regime

Several normal to oblique-normal NS-trending faults can be observed to reactivate, diffract and cross-cut the Penjom Thrust zone. From east to west, these faults are recognized as Hill-4 NS fault (slickenline as in Figure 5.20), Hill-6 NS fault, NS Jalis and Dancing Man

Fault (DMF) (Figures 5.21 and 5.22). These faults are well defined above the Penjom Thrust. Other small-scale NS-trending normal fault cross cut the horizontal D2 bedding-parallel vein with a normal sense of movement (Figures 5.23 and 5.24).

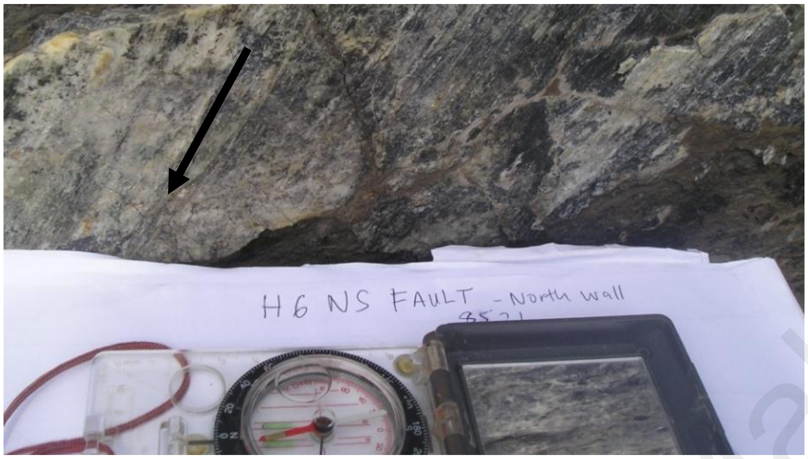

Figure 5.20: Slickenline striation on Hill 6 NS fault plane shows slightly oblique normal fault

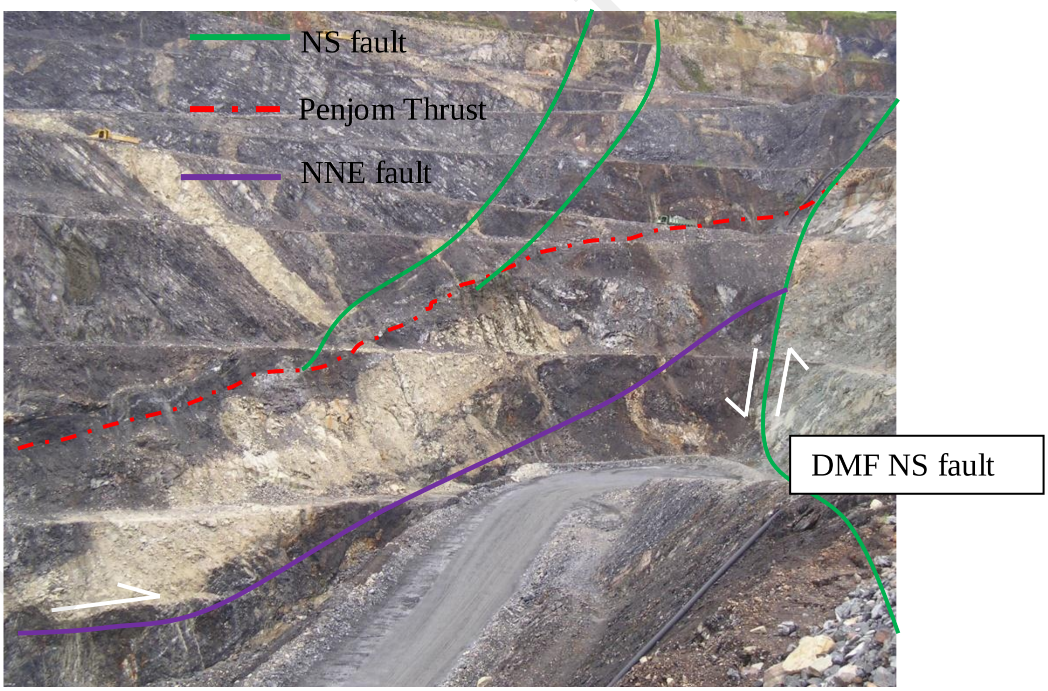

Figure 5.21: At the southernmost part of the Kalampong pit, a steeply dipping N-S normal fault (DM Fault) (right side of the picture) cuts the gently dipping NNE-SSW reverse fault and high carbon zone. Another normal fault (NS Jalis) at left side reactivates along Penjom Thrust.

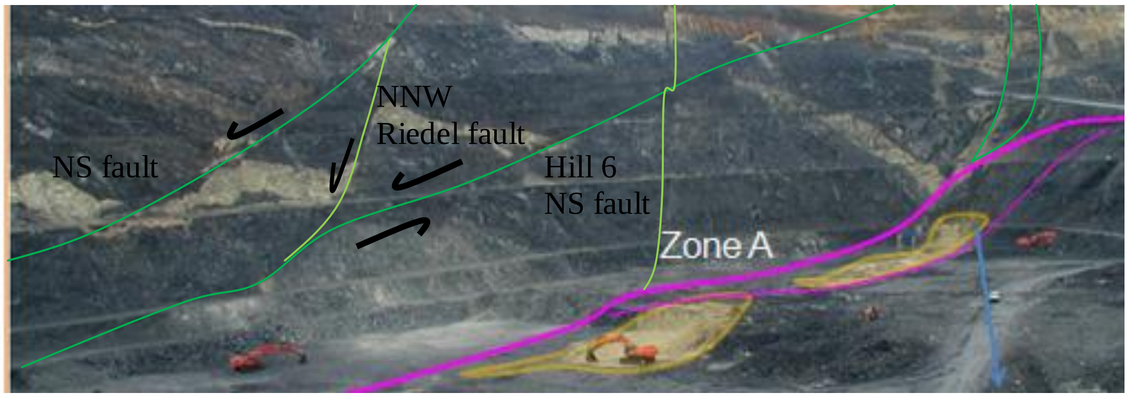

Figure 5.22: NNW fault developed as a Riedel fault in between NS indicating normal sense of movement.

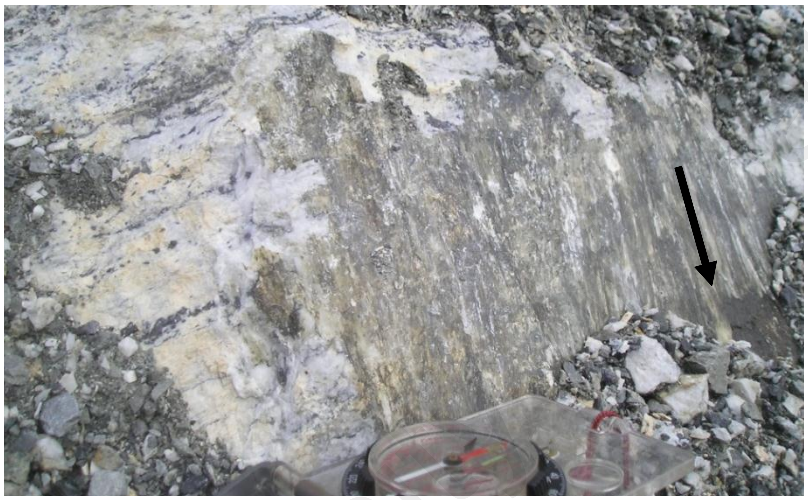

Figure 5.23: Fault striation indicate normal sense of small scale NS fault cross cut quartz-carbonate shear vein.

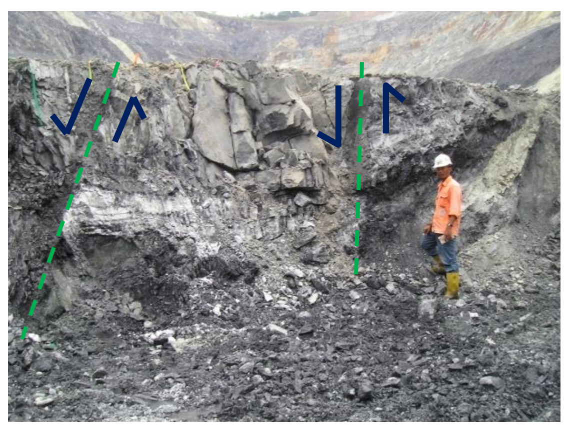

Figure 5.24: (Left) Normal north south fault displace flat dipping high grade laminated vein (looking south, 834mRL). (Right) Close up view of normal NS fault displace a flat bedding parallel vein.

5.5.6 Summary of the new structural framework

Structural deformation can be divided into at least five structural episodes, from compressional and transpressional (D1 to D3), which also involves strike-slip movement and later transtensional regime (D4-D5). The first episode is responsible for the regional fold followed by a local fold, thrust activity and later stage NNE to NE-reversed fault after the fold has locked up. Further deformation episodes involving dextral movement (strike slip) of earlier NNE to NE structures and Jalis corridor NNW trending fault with apparent sinistral fault movement. NNW fault is not prominent in Kalampong pit and only occurs in Jalis corridor sub-parallel to the carbonaceous shale unit. Final D4 deformations are the NS-trending cross-cutting faults with sinistral and reactivated as normal and oblique normal sense of movement. The faults also reactivate and diffract along Penjom Thrust mainly after veining and mineralization events. The summary is shown in Table 5.2.

Table 5.2: Summary of structural event in PGM indicates two main structural events. D2 to D3 deformation involving compression to transpressional event and D4 to D5 extensional period.

Events	D2 Deformation	D3 Deformation	D4-5 Deformation
Fold and fold related fault	---------------		
Penjom Thrust	--------------		
NE to NNE reverse fault	------	----------	
NE to NNE dextral		----------	
NNW sinistral and reverse fault (Jalis corridor)		------------------	
EW Lateral fault		------------	
NS sinistral fault		---	-?----
NS to NNW Normal			-------------------

5.6 Quartz-carbonate vein system

5.6.1 Introduction

Quartz veins are derived from the hot hydrothermal fluid from deeper levels or from dissolution from the host rock, deposited into confining spaces such as faults, bedding-parallel faults, dilational spaces and extensional fractures. Veins are important components of most epigenetic hydrothermal ore systems. Understanding their formation and different styles of quartz veining is the key to unraveling the structural controls on these ore systems (Davis, 2005b and Robert and Poulsen, 2001).

Many researchers regard quartz veins as a tectonic fossil which records the structural control on gold mineralization so that any structural studies must be able to explain vein formation. Some reasons to study such veins are as follow (Mawer, 1987).

- Veins have considerable potential as indicators of at least part of their host rock's strain history.
- The fluid inclusions they invariably contain represent a direct sample of vein-forming fluids.
- Veins generally represent paths of focused fluid flow.
- Quartz veins contain precious metals such as gold.

It is very important to study episodes of vein formation to distinguish features due to vein formation and superimposed features caused by later deformation. Vein classification is based on Davis (2005b), Hodgson (1989), Robert and Paulsen (2001) and Ramsay and Huber (1987). Veins that host gold indicate that they come together with veins and remobilized during the ongoing deformation and brecciation of the veins (Davis, 1998) so that some gold appear as infilling fractures in veins.

In Kalampong pit, several vein-hosted ore bodies have been given a names such as "highly graphitic Penjom shear", "jewel box", "high carbon North-South (NS) corridor", "low carbon NS corridor" and "the North-West (NW) corridor ore body". Despite specific references made to these high-grade ore bodies, the boundaries between them and the vein formation has not properly been discussed.

The structural classification of veins helps in the discussion of how the vein was formed and the relationship to mine scale structural deformation. Relative chronology of the structure and vein formation can be related to the initial development of thrust and fold, and later development of reversed fault after the fold had locked up. Continuous movement resulted in dextral slip of parallel faults. Two main groups of veins are the veins associated with folds and thrust that is mainly shear veins and associate discordant veins and those associated with faulting as reactivated shear vein and other types of extension veins.

5.6.2 Different style of quartz veining

Two systems of quartz veining can be observed such as shear veins with associated extension veins and extensional veins related to fault. The latter is a different term from extensional fault which commonly related to basin development and normal fault. Fault controlled veins also include reactivated bedding parallel shear veins by fault such as along the Penjom Thrust and shearing along carbonaceous shale close to this fault.

Based on the structural control of the vein system, the main setting of the quartz veins hosted mineralization are mainly developed during the fold, thrust and parallel fault activity. The movement of thrust has reactivated several series of bedding slip fault along the massive and thin carbonaceous shale before the faulting has further reactivate and channeling the auriferous fluid into the vein structures.

The movement of the bedding slip fault and other fault subsequently followed with the quartz veining referred as shear vein and within the extensional site referred as extension vein.

Veins have become the main subject of discussion related to mineralization and deformation as early as in first geological modeling at PGM. Corbett (1997) describes vein as laminated to ribbon quartz characterize the NS corridor and Fillis (2000) redefined this vein as bedding parallel vein. Endut (2004, Internal memorandum), Endut and Teh (2010) propose that bedding parallel vein was developed during the folding and thrusting and not during extensional faulting. Davis (2005a) recognized this style of veins and confirmed the D2 structural deformation for this event.

Different stylolitic features and texture suggested bedding parallel shear veins along the thrust and refolded western limb have been reactivated as a result of ongoing deformation.

5.6.3 Thrust and fold (D2) related veins

Shear veins were formed as a result of shear opening of the structure including bedding and carbonaceous layers and intermittent veins deposition. They were formed under high differential stress and a local compressional environment. Two geological features that host this vein are exclusively along the Penjom Thrust zone and bedding-parallel shear. The shear veins continue across the felsite dyke. Several types of extension veins are associated with these shear veins, including sheeted extension veins, breccias and stockworks. Breccias and stockworks can be observed within the same ore body.

5.6.3.1 Penjom Thrust shear vein

The Penjom Thrust was reactivated along the eastern limb of the Kalampong anticline, in particular, along a thick carbonaceous shale unit which may already hosted earlier bedding-parallel veins (Figures 5.25a and 5.25b) and formed shear vein type 1 (Table 5.3). This is a common feature where a reverse fault is rooted along the bedding plane. Reactivation by the thrust has further created new textures in the form of ribbon, breccias, boudinage, fold and shear. Furthermore, the vein infills the shear fabric with a thickness of individual vein up to 10 cm but at very close spacing of less than 10 cm and formed a discontinuous pinch and swell veins structures. The Penjom Thrust ore zone can be divided into two areas with respect to its location within the fold axis or the limb of the Kalampong anticline as follows:

- Within fold axis

The style of folding around the main fold axis at the southern half of KE is a tight recumbent fold, in the northern area as an open fold (Figure. 5.26). Saddle reef type or style of gold mineralisation is present in the fold nose of the dominant carbonaceous unit above the felsic intrusive body and extends as quartz stockwork or irregular veins inside the intrusive close to its contacts. At greater vertical depths within the fold, the veins become narrower at the intrusive–shear vein contact and are less developed in the intrusive. Veins are massive at the fold nose with ribbon textures at the veins margin indicating repeated opening of the structures and introduction of fluid into the local low mean stress area normally above the rigid competent unit such as an intrusive (felsic) body.

- Within fold limb

This is a deeper Penjom Thrust ore zone parallel to the eastern limb and forms linear ore bodies made up of veins from massive shear-parallel veins to narrow ribbon quartz veins. The main mineralised area is observed when there is an embedded small scale intrusive body enveloping massive carbonaceous shale that increases the physical and chemical contrast. Veins in this area are variably deformed because of the reactivation of the late NS trending sinistral to normal faults along the thrust. This reactivation was also responsible for the thinning of carbonaceous material at certain segments and the localisation of ore zones along the thrust.

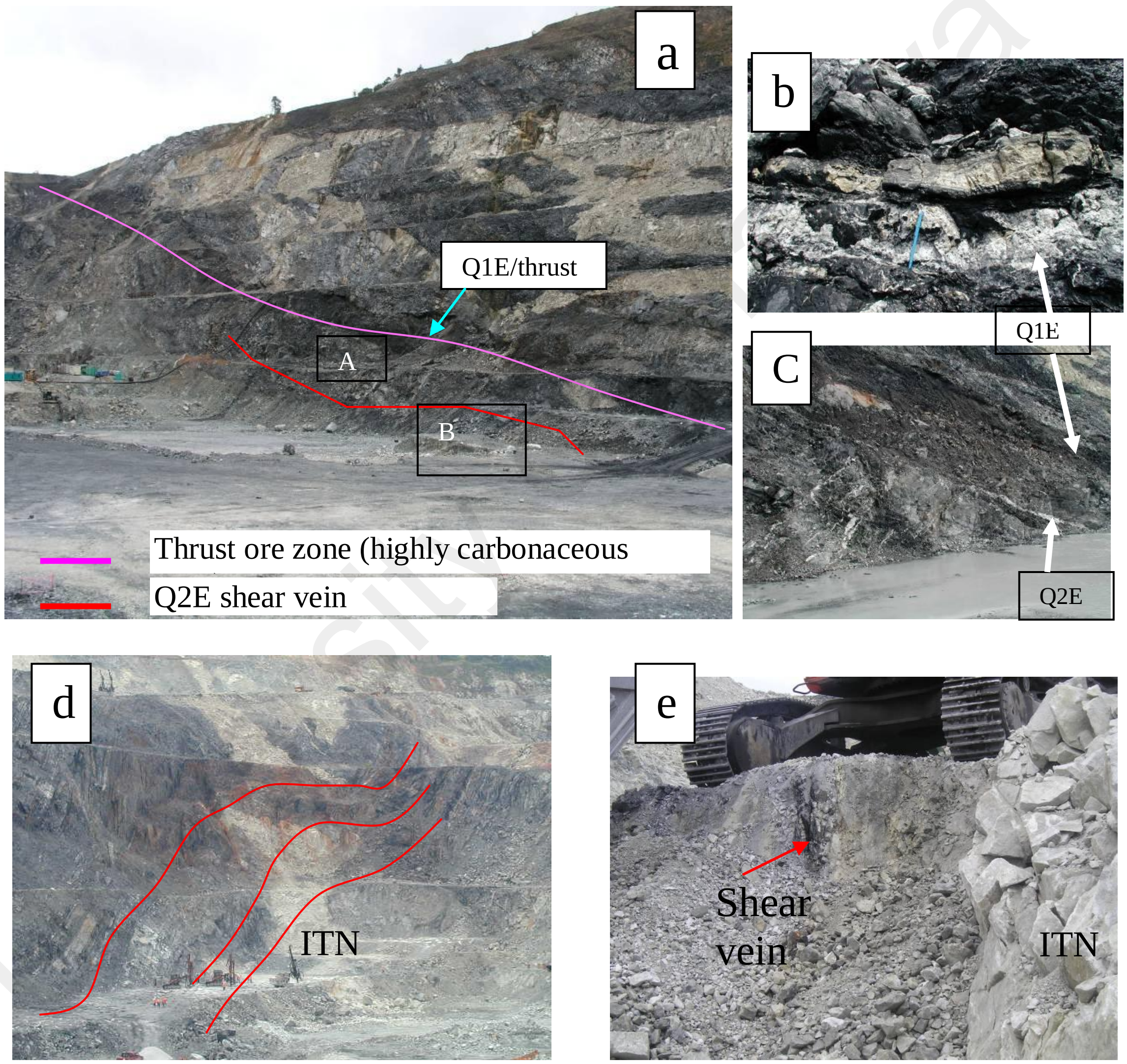

Figure 5.25: (a) Penjom Thrust ore zone trending NNE and subparallel to bedding. (b) Close up of area ‘A’ shows a laminated to ribbon quartz. (c) Another bedding parallel vein below the thrust ore zone (after further digging of area ‘B’ in photo ‘a’. (d) Ore zone comprised of shear veins (black zone), cross cutting through intrusive rock (ITN). (e) Q2W shear veins as shown by slivers of host rock in sheared intrusive. Blocky intrusive on the right side lack quartz veining.

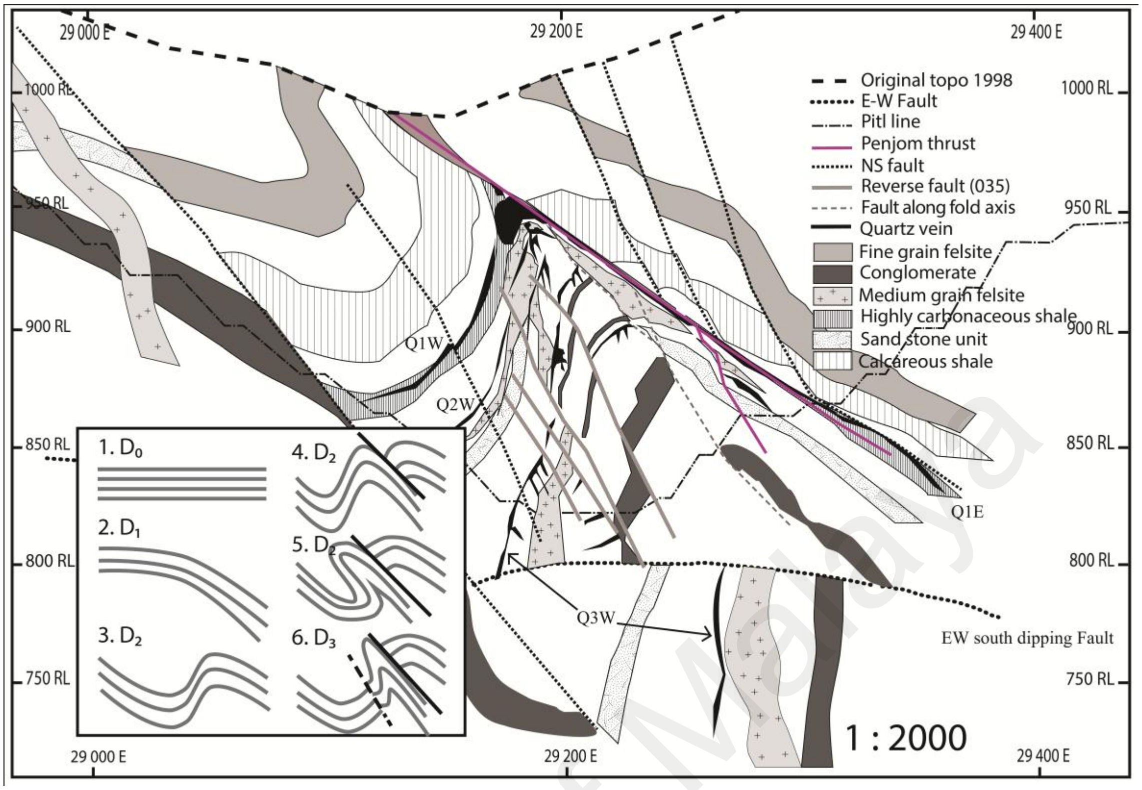

Figure 5.26: Looking mine north (35^o from true north), cross section at 50100 at the center of Kalampong Pit, shows structural framework of shear veins (Q1W, Q2W and Q3W) in the fold setting of the Kalampong Anticline. Inset figure is an evolution of the folding.

5.6.3.2 Bedding-parallel shear veins

This type refers to quartz veins infill along carbonaceous shale units and represents an active bedding plane-slip fault or flexural-slip fault with an intermittent deposition of shear vein type 2 (Table 5.3). This process occurred during fold activity to form a ribbon or lamination texture. Recrystallization of quartz occurs along the shear plane where a band of fine quartz grains represented an active plane (Davis and Hippert, 1998). Remnants of the carbonaceous layer represent multistage opening of the structure through an episodic opening during fluctuation of stress and fault-valve behaviour (Cox et al., 2001; Sibson, 2001). This type of vein is structurally classified as shear vein (Hodgson, 1989). The presence of slip lineations, slickensided and lamination surfaces are attributed to shear opening of the veins during the folding process. The fault striations commonly show reverse movement, indicating flexural slip during folding. As shown in Figure 5.26, there are at least five bedding-parallel shear veins identified within the Kalampong pit. Two are along the eastern limb and three within the western limb sequences. This bedding shear vein cut across the felsite unit with remnant carbonaceous material Figures 5.25d and 5.25e and that the term bedding parallel shear vein in felsite unit can be confusing if overall understanding and genetic of the structure is not properly understood.

These veins, in particular, are very important as they host a majority of high-grade ores in Penjom gold mine, particularly gravity recoverable gold. Ribbon quartz which is a part of a shear vein was previously recognised as high-grade veins (Corbett, 1997; Endut and Teh, 2010) and forms the NS trending mineralisation. However, certain segments of the same vein, particularly on the limb and away from the intrusive body, are very low in gold content. Field observation shows that high-grade laminated veins can be observed close to or at the contact with the intrusive, along the fold axis and the Penjom Thrust. Thus, chemical and physical conditions of ore fluids, interactions with host rock and structural control play important roles in controlling gold precipitation.

Three different morphologies of veins are recognised as follows:

- Planar laminated (<20 cm)

Planar, thin (<3 mm) graphitic or carbonaceous material of irregular thickness comprise the lamination within these veins. Laminations can be at different angles to an earlier veins-wall-parallel lamination. Q2W and Q3W (Figure. 5.27) are fine examples of these veins and as a narrow shear vein (<20cm) associated with a zone of discordant extension vein. Q3W has significant carbonate (mainly calcite as analysed by XRD) as well as galena and sphalerite either along the lamination or within the buck or thicker segment of the veins. Host rock comprises very thin carbonaceous shale and siltstone units interbedded with a sandstone unit. Carbonaceous material could also have been leached out and become lighter colour.

- Roughly laminated (ribbon texture)

This is a common bedding-parallel vein in dominant or thicker carbonaceous shale interbedded with minor sandstone units. It is also referred to as ribbon quartz. The graphitic layer that forms the ribbon varies in thickness and is irregular and undulating in nature as the upper part of the vein (Figure. 5.27a). Furthermore, this vein is commonly associated with different forms of stylolite, either the planar or wavy type. It is roughly laminated as a result of continuous deformation and in many places it is associated with vein breccias.

- Massive bedding-parallel quartz (>20 cm)

This form of thick quartz occurs parallel to bedding and localised at the intersection with dominant felsic rocks and at the fold axis. Host rock remnants within these veins occur similar to the case of vein types 1 and 2 with a few stylolites at the vein margin. The upper part of the shear vein is comprised of thicker vein with massive appearance or quartz dominated. In the other parts, massive quartz can be brecciated, form a gradual boundary with the host rock or become veins stockwork. Quartz grains within the thicker and massive portion are typically coarse with variable size and exhibit a buck texture.

- Foliation-/cleavage-parallel veins

This is a minor type of vein and is commonly associated with bedding-parallel shear veins. This vein type is hosted in sandy silt to shale units, forms a laminated texture and is parallel to the main shear vein. This vein is thought to fill a weak plane along the foliation or bedding-parallel cleavage as the shear vein developed. The overall thickness of such veins is less than 5 cm at a very close spacing of 1 mm. These veins were formed by the crack-seal mechanism in which the vein grew in thickness by the reopening of wall rock and progressive deposition of minerals.

5.6.3.3 Sheeted extension veins

Different styles of extension veins reflect the structural control and physical properties of the host rock during vein formation. These veins were formed by extensional filling particularly for extension vein array or sheeted and quartz stockwork. Vein direction is broadly East–West parallel to maximum compressive stress, vertical to sub vertical and either formed an individual zone or dangling below bedding-parallel shears (Figures. 5.25c, 5.27b and 5.27c).

Minor vugs and comb textures are locally observed in this vein type. Many of these veins can occur together in one zone and are usually controlled by movement of shear veins or faults that produce different extension veins type in different lithological units. The different styles of extension veins are described as follows:

A) High angle EW extensional veins array

Zones of extension veins type 1 (Table 5.3) can be up to 15m wide at a vein spacing of up to 1 m. Individual vein thickness can be up to 8 cm. This set of veins is only weakly mineralised, and based on a 3 m sampling for ore mining, commonly returns grade values less than 0.5g/t. The main reason to classify this vein as formed during similar compressive event is the EW direction parallel to the maximum compressive stress. Quartz is the main vein component with rare carbonate. This style of vein can be observed locally along the fold axis within the competent lower mine sequences of either massive siltstone or thick conglomerate.

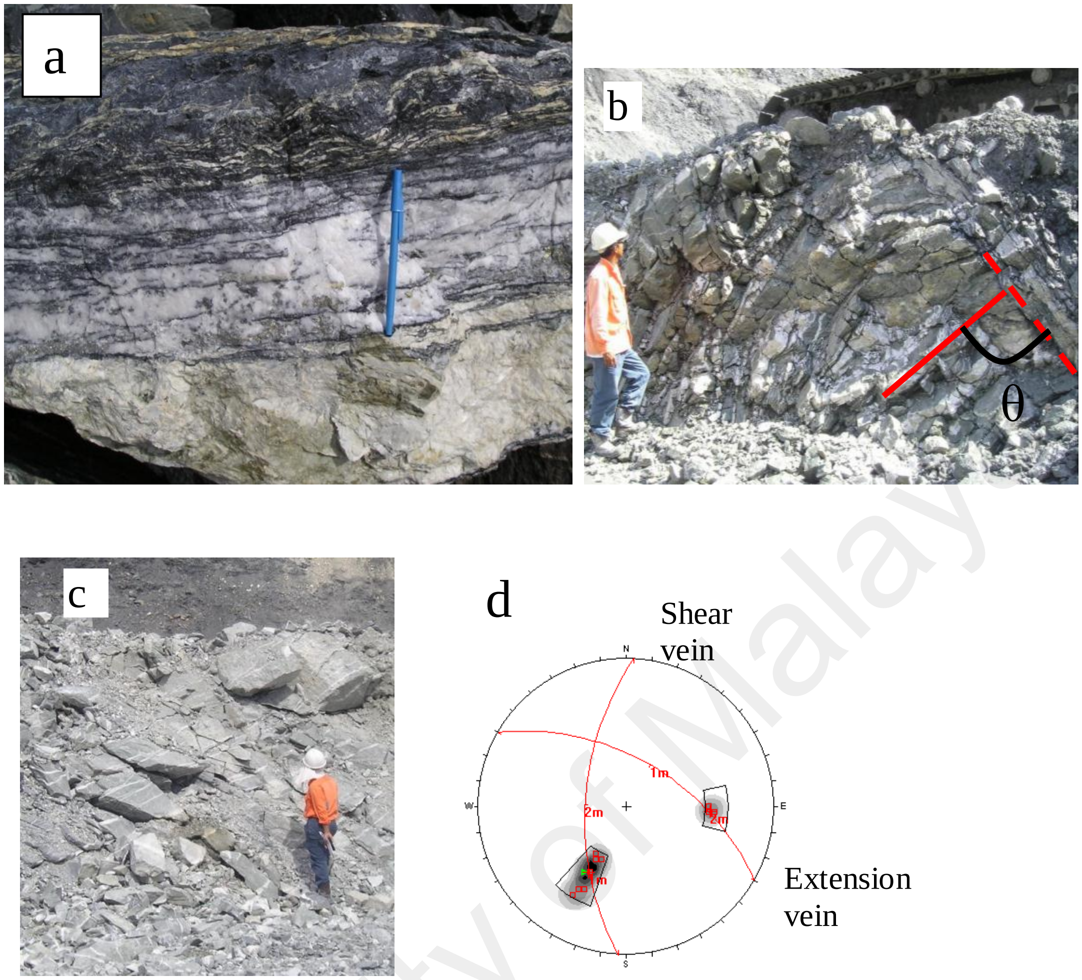

Figure 5.27: (a) Roughly laminated veins in carbonaceous shale unit with more planar laminations inside the veins. This shear vein type 2 in Table 1 was formed through shear induced lamination. (b) E-W extension vein array type 2 or planar sheeted vein developed at θ equals to 90^{o} below the main shear vein (red dash line), looking south and at level 840mRL. (c) A series of E-W striking sheeted veins (extension vein array type 2) exposed after the excavation of the main shear veins (looking east, at level 834mRL). (d) Equal area, lower-hemisphere stereographic projection showing the average dip and dip-direction and pole to vein.

B) Moderate angle EW extensional vein array

This vein array is mainly characterised by a moderate to steeply dipping, sheeted parallel vein set aligned EW. The veins in the array are sub-vertical to the bedding and commonly below the bedding-parallel shear veins (Figure 5.27b). The occurrences and intensity of extension veins are very important to represent the thickness of the overall ore body below the main and higher grade shear quartz veins. There are two lithological settings of this extensional vein array occurring in Kalampong pit: hosted either in a stiffer sedimentary unit below thin carbonaceous-hosted shear vein or brittle intrusive host rock.

In both lithologies, vein orientation is parallel to maximum compressive stress and axes of incremental shortening (dZ) or perpendicular to the elongation (dX) as a result of shortening (Robert and Poulsen, 2001). The veins extend from the sediment into the intrusive rock with no change in orientation indicating similar direction of stress acting on both host rocks and that the intrusive event predates the deformation giving rise to the vein set.

- In a harder rock unit (sediment) below shear veins (D2 event)

This extension vein type 2 (Table 5.3) is the main source of ore, in particular, for the less carbonaceous host rocks. Sheeted veins occur as extensional veins below a laminated vein and trend sub vertical to a bedding-plane-slip fault (Figures 5.27b and 5.27c). Widths can be up to 20 cm at a spacing of 5 cm to 2 m with bulk gold grade varying from low to high. No quartz occurs above laminated veins unless in between two bedding-slip faults; this suggests a coeval relationship between these two types of veins.

- In brittle host rock (intrusive)

The felsite unit within the ore body hosts this extension vein type 3 (Table 5.3) similar to the case of the harder rock unit. These veins extend from the sediment and into the felsic rock in almost a similar direction; however, the veins developed in the felsite unit can be more intense (Figure 5.28). Thickness of the veins can be up to 15 cm, and the veins predominantly comprise more quartz than carbonate. Furthermore, the EW striking veins are a dominant set compared to the other direction.

5.6.3.4 Quartz breccias

Quartz breccias are defined as a body of quartz vein in which country rock fragments exceed the vein volume. It can be divided into two categories: hydrothermal quartz breccias which normally form in dilatants zones along bedding-slip faults and fault breccias which form as a result of shear movement and are part of the shear veins. Movement of two closely spaced bedding-slip shear veins at a competency contrast unit or near a fold axis provides space for the development of hydrothermal breccias, particularly in the competent felsic unit (Figure. 5.29a). Vein also developed in the sedimentary rock around the boundary forming a localised jog along relatively narrow shear vein. The hydraulic fracturing mechanism is involved during the formation of brecciated veins due to high fluid pressure and fluid volume (Cox et al., 1991).

5.6.3.5 Quartz stockworks

Quartz stockworks (extension vein type 4- Table 5.3) are associated with shear veins and are described as a network of more than two set of veins that commonly occur in competent units such as felsite. The individual veins can be up to 10 cm thick. This vein type is mainly formed in the localised felsic sill within the eastern limb shear vein or along Penjom Thrust ore zone forming linear ore shoot, whereas at other places, it is more localised along the interception with bedding-parallel shear veins.

5.6.4 Fault (D3) related veins

Faulting events that are active after fold lock-up are not observed as hosting the laminated or ribbon vein. The fault is occasionally infilled with very thin quartz with a thickness of less than 3 cm and does not make up a significant ore zone. This fault system generates either sheeted, brecciated or stockwork extension veins at the interception with brittle units such as the felsic rocks and dominantly in the felsite unit and to a lesser extent in other rock types. This constitutes felsite-hosted ore body which has a good grade near the fault plane. Furthermore, the intensity of the veins is important to form higher grade ore.

5.6.4.1 Sheeted extension veins

A) Sub-vertical sheeted veins

Sub-vertical veins in brittle host rocks, commonly felsic bodies, are formed at the contact with a fault. Parallel sheeted veins (planar extension vein array) with an individual thickness of less than 10 cm occur perpendicular to the fault and the fold axis, striking from 90° to 120°. Vein intensity also increases in the narrow felsic rock (Figure. 5.28b) compared with surrounding host rock. As a result, the trend of economic mineralisation at several places follows the shape of this intrusive rock. Several other vein directions associated with the vertical set; however, the vertical set is commonly much more dominant over other directions.

Figure 5.30a shows stereonet plots of EW sheeted veins at three different localities. Overall orientations of bedding and sheeted veins are in Figures 5.30b and 5.30c respectively. Strike direction of the veins is normally parallel to the main compression force (Robert and Poulsen, 2001, Figure 5.31 left) acting in the EW direction. Figure 5.31 (Right) shows the example of the vein in the felsite unit at fault interception in which the EW direction is dominant over other directions at a ratio of 30:1.

B) Low-angle sheeted extension veins

Low-angle sheeted extension veins Type 3 (Table 5.03) with a maximum thickness of 10 cm perpendicular to the wall occur in sub-vertical narrow felsic intrusives of less than 5 m to 8 m width (Figure. 5.28a). In Kalampong East pit bottom, felsic dyke near the fold axis is cross cut by a series of NNE trending fault. Deformation induced by the faulting; but, the trend of parallel fractures with the veins infilled may have been controlled by the wall contact that produced flat, dipping veins perpendicular to the felsite contact. Within the intrusive near the shear or fault plane, veins grade into stockworks (Figure. 5.28c). Transition to other forms can be observed as shown in the same Figure 5.28a and Figure 5.29. This type is locally observed along the western limb of the felsic dyke that extends toward the fold axis, particularly where there is a cross-cutting NNE trending fault or shear veins.

5.6.4.2 Quartz breccias

Quartz breccias were formed within the narrow felsite bounded by two faults. The occurrence is similar to the shear vein of D2 fold-related hydrothermal quartz breccias; however, this vein is exclusively hosted within the felsite intrusive along the fault contact and rarely extends outside the felsite into sedimentary rocks. Fault breccias is defined in cases where the wall rock fragments exhibit evidence of rotation and are dominant with respect to quartz fragments. However, it can be quite common, that further inside the zone, the quartz becomes dominant over the wall rock fragments in which case it is referred to as hydrothermal quartz breccias. Overall, both hydrothermal quartz breccias and fault breccias exist within the same ore zone.

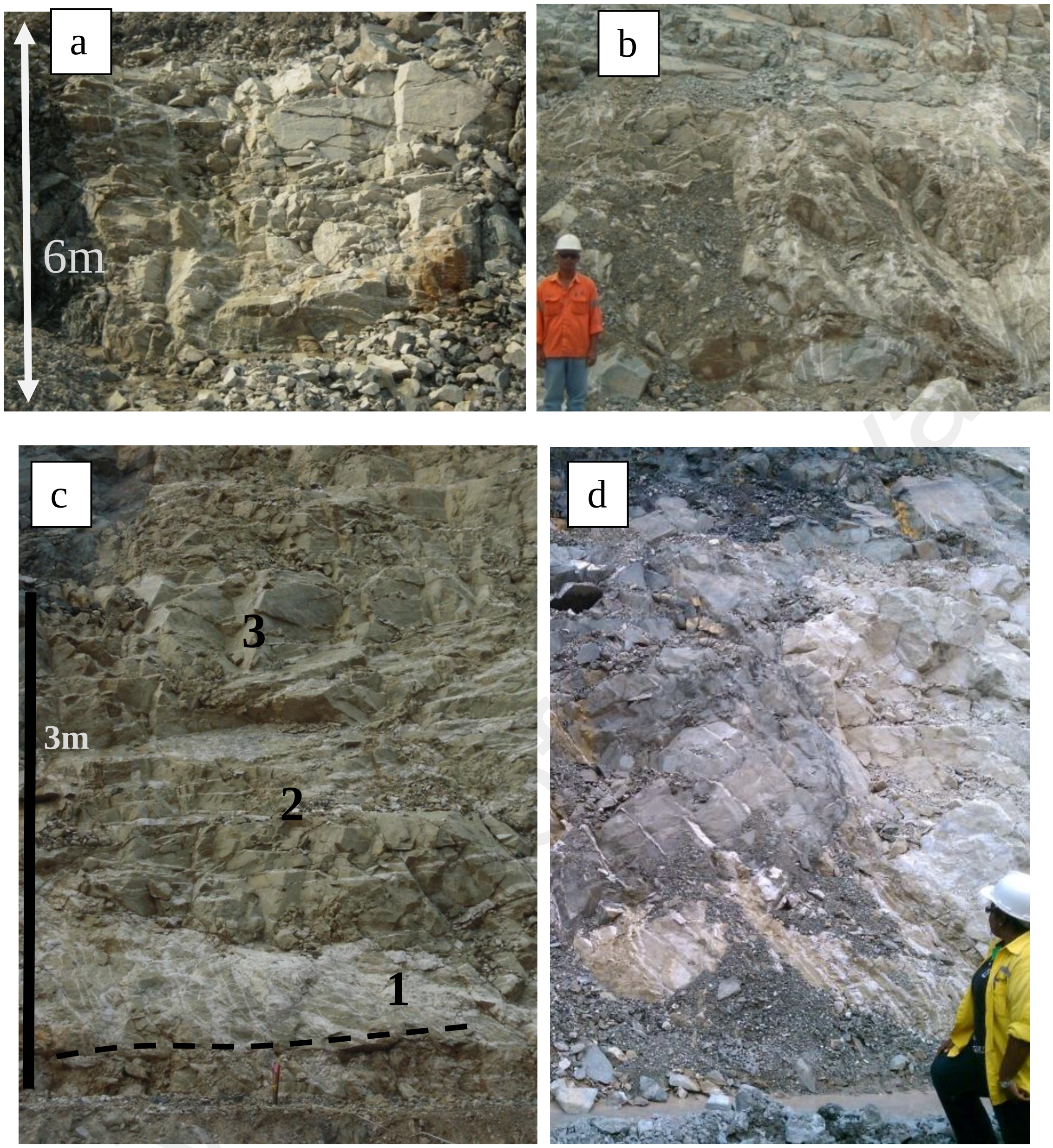

Figure 5.28: (a) Dominant low angle extension veins Type 3 in felsite dyke perpendicular to contact, bedding and fault. Location: north of KE pit; Spacing: from 5 to 50cm; Thickness: from 1 to10cm. (b) Dominant vertical E-W extension veins Type 1 across the bedding and felsite intrusive at Jalis West Wall. Spacing: from 5 to 50cm; Thickness: from 1 to 20cm. Vein intensity increases in intrusive. (c) Dash line represent west dipping shear plan across felsite. 1-vein stockwork near shear plane (D2 deformation), 2-vein infilling parallel fracture resulted to low angle vein array, 3-less vein away from the shearing. (d) Vein across the lithology contact.

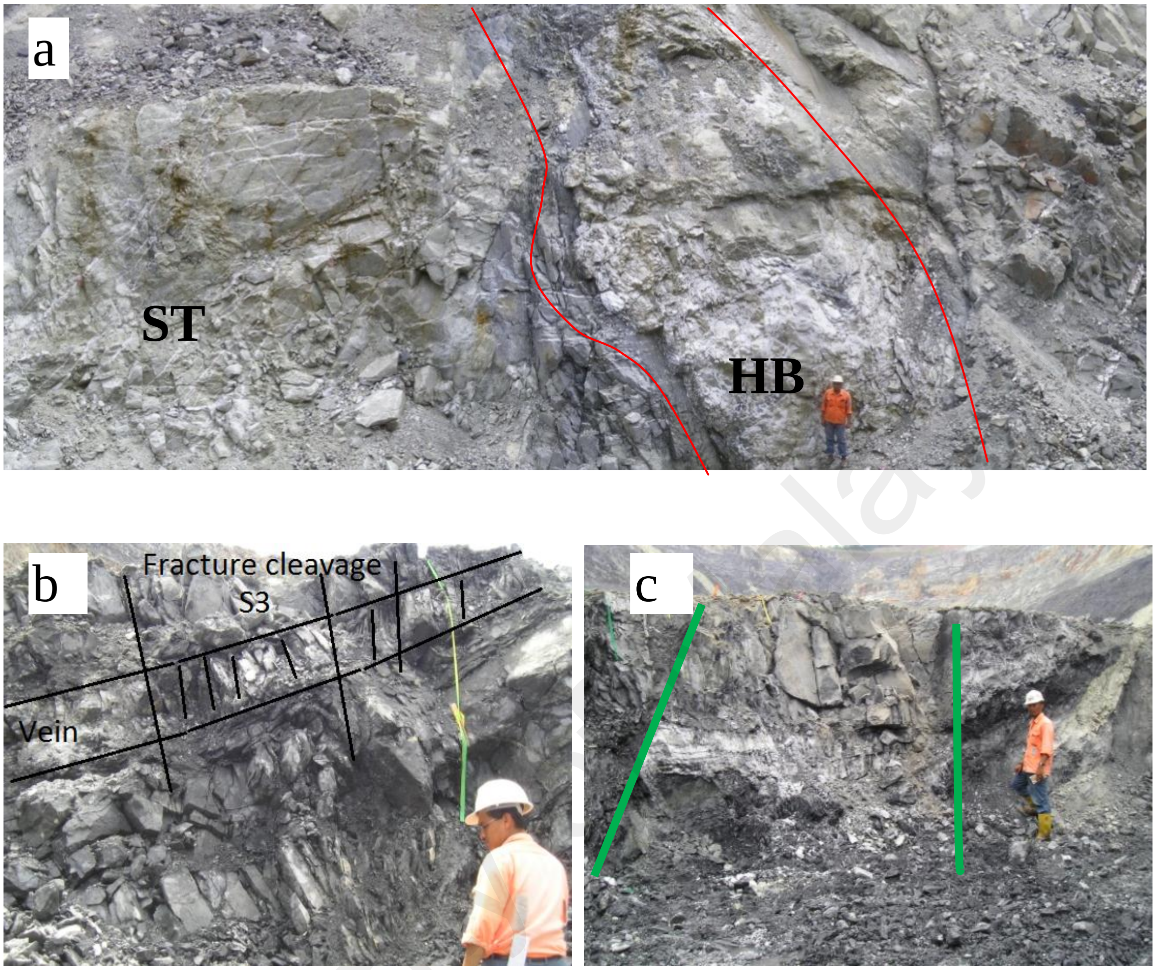

Figure 5.29: (a) Stockwork (ST) veins (extension vein Type 4) in intrusive rock below North-South trending West dipping shear veins (red line) and hydrothermal breccias (HB) in between two shear veins in intrusive and siltstone. (b) Fractures cleavage (S3) locally developed below NNE D3 fault affected the D2 shear vein. (c) Normal D5 fault (green line) displaces flat dipping along synform axis D2 shear vein.

5.6.4.3 Quartz stockwork

A faulting event also generates quartz stockworks mainly in felsite units at fault intersection. At several places, a dominance NNE reverse-dextral fault generates multi directional set of vein directions.

5.6.5 Structural explanation of veins formation

Most of the quartz veining in the Penjom gold mine occurs within the sequences of thick or thinly bedded carbonaceous shale and occur as several bodies of low to high-grade veins along, below or between active bedding-plane-slip faults. Fault-generated veins mostly occur at the intersection with intrusive rocks.

The overall shape of the Kalampong Fold can be explained as an antiform–synform couple in the foot wall of the Penjom Thrust. Parallel to the main thrust are several series of NNE faults including the Jalis Reverse Fault southwest of the Kalampong pit. Bedding-parallel shear veins and associated vein stockwork and sheeted veins are mainly hosted in the middle mine sequence and at the boundary of the middle–lower sequence. This boundary is characterised by thin to thick layers of carbonaceous shale which normally become the site of type 1 and type 2 laminated veins. Structural control of these veins is comparable with other bedding-parallel veins particularly in fold- and thrust dominated areas elsewhere in the world such as at Bendigo (Schaubs and Wilson, 2002) and Meguma Terrane (Mawer, 1997), as summarised in Table 9.2. The Bendigo area exhibits a superimposed reactivation by faulting, after the fold has locked up as a consequence of the folding process. The shear vein can further be described as being similar to the backbone structure of Cox et al. (2001) and the discordant extensional vein as the dead end or a dangling extensional vein. Additionally, the high-grade shear vein hosts abundant early sulphide mineralisation including pyrite and arsenopyrite with or without a base metal.

Structural classification of veins provides an indication of the manner in which the veins were formed and their relationship to mine-scale structural deformation. The relative chronology of the structures and vein formations is characterised by initial development of thrusts and folds (D2) and later development of reversed faults (D3) after the folds have become locked up. Continuous movement resulted in dextral strike slip on several D3 faults including splay faults and NNE faults. Sinistral strike-slip movement and normal to oblique-normal fault reactivation of NS faults is interpreted from fault striations.

Interpretations of structural control indicate that the various vein arrays were mainly developed during folding and thrusting (D2). The movement of the thrust fault has reactivated several series of bedding-plane-slip faults along the massive and thin carbonaceous shale forming the type 1 and associated type 2 veins. Reactivation of faulting during D3 deformation continues to channel auriferous fluids into the vein structures following fold lock up forming only type 2 veins. In summary, two structural settings of vein formation can be discussed such as fold- and thrust-related D2 and later phase faulting D3 events.

5.6.5.1 Fold- and thrust-related veins (D2)

The Penjom Thrust and associated Kalampong Fold are responsible for bedding-slip activity throughout the Penjom pit particularly along the carbonaceous unit. Quartz veining that subsequently follow the movements of the bedding-plane-slip faults and other faults is referred to as a shear vein type (same category as fault fill vein, Robert and Poulsen, 2008), whereas within the extensional site, it is referred to as an extension vein type. Sheeted extension veins, stockworks and breccias associated with bedding-parallel shear vein (Table 5.3) are also considered fold-related veins.

Veins were formed during repeated opening of the structures particularly along bedding-plane-slip faults (D2) which produced lamination and ribbon texture in the veins. The western limb ore zone is the main area for these types of veins and is the main ore zone mainly during earlier pit development. On the veins surface, slickenline or fault striation is commonly observed and this is indicative of continuous deformation particularly flexural-slip movement.

The fold related veins system forms several ore zones, whereas the intensity and grade are controlled by several other factors such as fold geometry, either on the limbs or around the fold axis. High-grade veins occur at the fold nose above the intrusive rock. On the limb, mineralisation is still very good at the contact of bedding-parallel shear veins and felsic intrusives. The shear veins become narrower on the far limb, and veins associated with brittle fracturing due to faulting, such as extension veins array or sheeted veins within small intrusives, become more dominant.

5.6.5.2 Fault-related veins (D3)

Except for the Penjom Thrust, structures including reverse, oblique-reverse or dextral strike-slip faults which control the second stage of vein development are classified as D3 deformation. These faults are mainly NNE trending reverse to dextral strike-slip faults (Figure. 5.18) which occurred during the late stage of folding after the fold had locked up. Locally, fracture cleavages are well developed below this fault and disrupt the early high-grade shear veins of the D2 deformation (Figure. 5.29b). NNW fault controlled significant mineralisation at the west-dipping sequence in the west wall of the Jalis corridor marks the reactivation of a fault sub parallel to the western flank of the synform. This fault is probably a splay or conjugate fault to the main NNE fault.

Faults trending dominantly NS (Figure. 5.21) as recognised above the hanging wall of Penjom Thrust are diffracted, cut across or reactivated along the thrust. Based on a slickenline direction observed on few faults, these faults exhibited sinistral strike-slip movement but on the other faults, normal to oblique-normal movements are dominantly exhibited. These faults are locally associated with calcite veins mainly on the hanging wall. Reactivation of these structures resulted in the deformation and displacement of earlier formed quartz veins; however, no economic mineralised veins are associated with these structures. A normal fault that separates the eastern and western limbs of the fold is an exception; it occurs as a splay from the Penjom Thrust and is considered as an accommodation of the folding process.

As in the case with fold-related veins, fault-related veins are also classified as shear or extension veins. Faults that are not parallel or sub-parallel to bedding or within the lower mine sequence were not observed to host laminated or ribbon shear veins. This characterises the brittle movement of this fault as a late stage event after the fold had locked up and also indicates that this structure is a brittle event related to fault valve behaviour (Sibson, 2001). The types of vein included in this structural event are quartz breccias and sheeted vein as either low to steeply dipping veins. Veins are best developed at the contacts inside intrusives near this fault.

A) North–northeast (NNE) fault-related veins

The NNE parallel fault is a secondary structure which overprints the Penjom Thrust and its associated folding and was active after the fold was locked up. It is more prominent along the western limb of the open fold and the tight inclined fold that is discordant to bedding at the intercept with an intrusive body. This structure might also reactivate the earlier fold related structures.

Veins associated with this fault are usually flat dipping extension veins in a narrow felsite intrusive body but are always discordant to the wall, massive, stockwork, brecciated veins and irregular vein arrays mostly at contacts or close to intrusive rocks. The overall grades of the veins are usually lower compared with those of the bedding- or shear-parallel ribbon quartz but can form larger zones with erratic grades especially in the more competent rocks. However, patchy high-grade veins can be locally observed close to the intersection of faults and intrusives; at such sites, galena and pyrite are also developed.

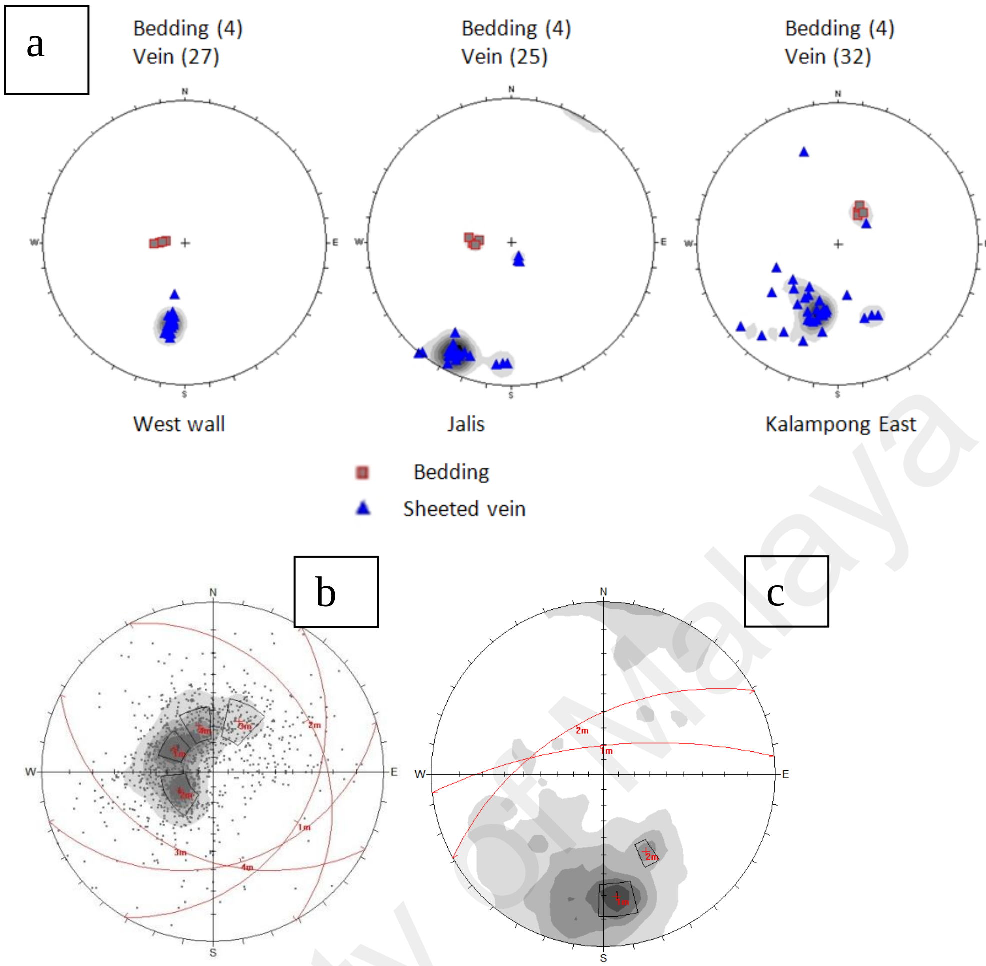

Figure 5.30: Lower hemisphere equal-area of sheeted veins orientation (poles plot of dip direction and dip) shows dominant steeply north dipping extension veins discordant to bedding from three areas. (b) Overall lower hemisphere equal-area of bedding orientation (poles plot of dip direction and dip, n = 1187), (c) Vein (poles plot of dip direction and dip, n = 797), 0.5% interval.

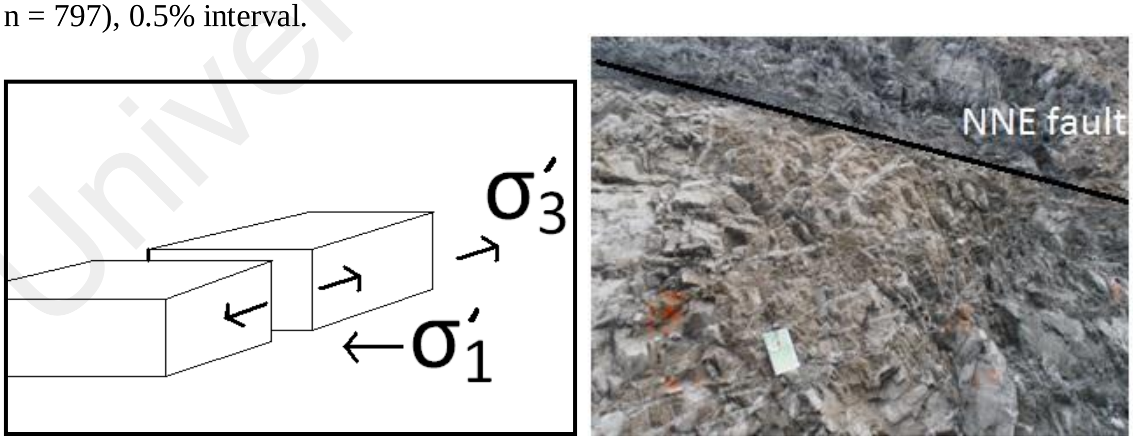

Figure 5.31: (Left) Stress field diagram shows relationship of extensional fractures perpendicular to maximum compressive stress. (Right) Dominance E-W sheeted extension vein Type 2 in felsite unit at fault intercept. Looking east at east wall.

B) North–northwest (NNW) fault-related veins

NNW trending faults oriented sub parallel to the bedding host high and low-grade gold-mineralised extension and shear veins parallel to bedding and shearing in the Jalis corridor. Shear veins occur within carbonaceous shale in the middle mine sequence and commonly yield higher gold grades compared with other vein types. Bedding-parallel veins with ribbon texture within this zone may have already been developed during fold-related bedding-plane-slip before the reactivation of NNW faults that generated more veins within this zone. This is particularly the case around competent intrusive bodies mainly at sites of low stress such as dilational jogs between two NNW faults.

5.6.6 Role of competence contrast

Several vein hosted gold deposits are hosted in extension veins in competent units such as dyke-like felsic intrusives at the St. Ives goldfield (Sibson, 2001). Competency contrast refers to different rock properties where strong brittle or competent units are juxtaposed with weaker units such as carbonaceous-rich host rock or shear zones. Maximum compressive stress is normally perpendicular to the weak plane, and strain partition results in a fracture array parallel to the shortening direction.

Frictional drag along the contact reduces the minimum principal stress in the competent unit (Sibson, 2001). This results in an increase in hydraulic pressure in the brittle unit causing shear failure especially in narrow competent units embedded in less competent rock. Veins are commonly formed as narrow veins within the shear failure zone but can be intensive in the narrow embedded competent unit in the form of extensional veins such as breccias, stockwork or sheeted veins. In Penjom gold mine, shear veins within the mineralised ore body at many places contain higher gold grades than in extension veins indicating shear failure and pressure drop play a significant role in concentrating gold bearing solutions and creating favourable sites for deposition.

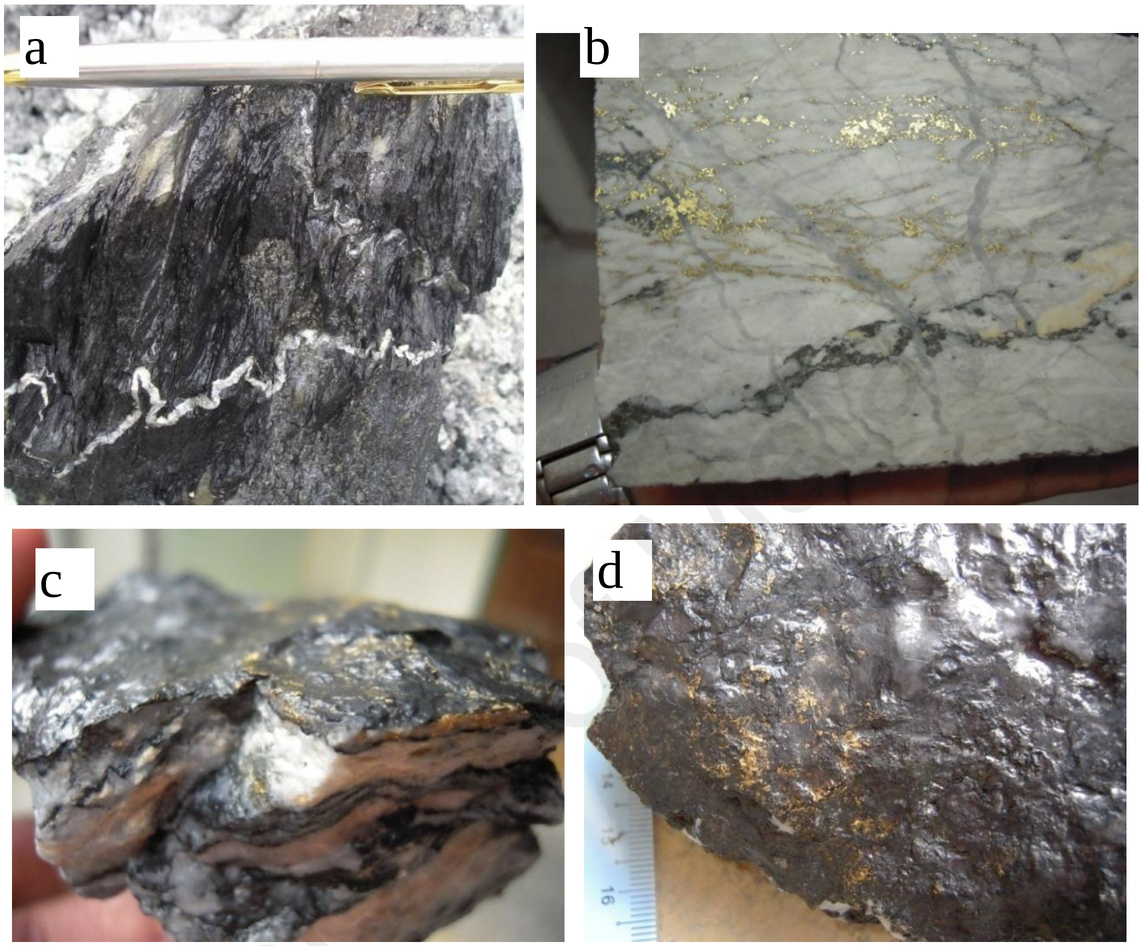

Figure 5.32: (a) Crenulated extension veins as a result of the ongoing deformation that also produced the cleavage at high angle to veins. (b) Late vein stringers across gold network within brecciated calcite vein. (c) Ribbon quartz from the side view with gold along vein margin. (d) Laminated veins with sign of fault striations affecting the gold itself on the vein margin.

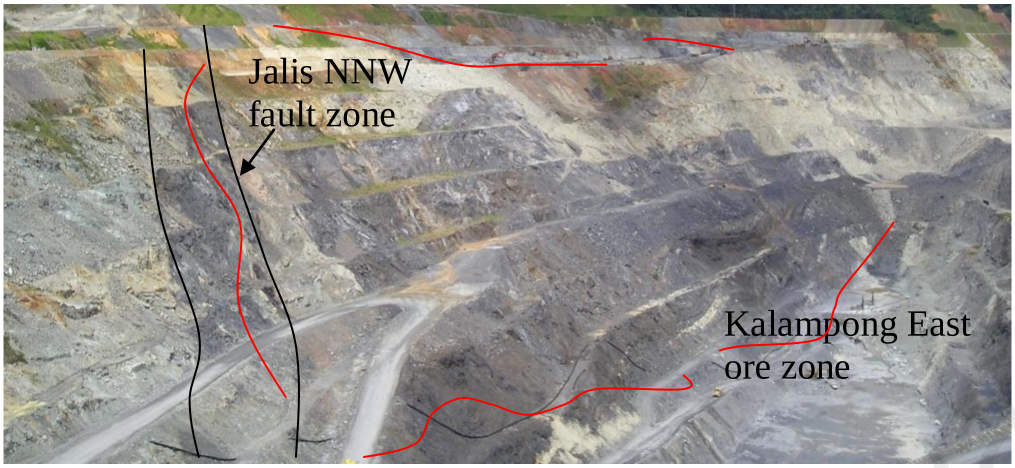

Figure 5.33: Location of Jalis NNW Fault Zone sub-parallel to carbonaceous shale (looking north). Red line is an outline of the shear vein within and outside the fault zone. Economic mineralization (ore body) localised at intercept with dominant felsic host rock.

In contrast to the above condition, mineralised veins mainly occur in the weaker zone at contact with massive competent units, such as the bigger intrusive rock, massive conglomerate or thick silicified rock. These units behave like rigid bodies, providing resistance to stress, and contain only minor vein networks around the contact. The weaker zones are deformed and provide more space or dilational sites for mineralised veins. A fold hinge or saddle reef style ore body above the massive felsic rock are the main examples of this ore body.

5.7 Relative roles of fold and fault on quartz veining

Structurally controlled veins exhibit varying degrees of deformation. It is important to distinguish primary textures of initial vein formation from textures developed by secondary processes or post-vein deformation. Several features of post-vein deformation can be observed at Penjom such as folding of veins, vein margin striations, breccias, internal deformational fabrics such as stylolites and various micro-scale structures. EW extension veins were buckled (Figure. 5.32a) along the cleavage development as a result of on-going compressional deformation parallel to σ1. Even the gold itself is striated along the shear margin (Figures 5.32c and 5.32d), indicative of very late stage reactivation along the shear vein margin. Veinlets crosscut the gold streak (Figure. 5.32b) indicating the vein formation outlast the gold mineralization event.

In the KE pit, the presence of bedding-parallel veins in both the eastern and western limbs of the Kalampong anticline and the western flank of the Kalampong synform suggest that they were formed during the folding process. Ore zones in thick carbon-rich (>1.0% C based on 3 m sampling) units occur in both the eastern and western limbs although veins close to intrusive rocks are more mineralised. This indicates the additional influence of the rheological and chemical contrast provided by country rocks in controlling the development of gold mineralisation. Penjom Thrust hosted veins in carbon-rich host rocks are highly deformed as a result of the reactivation compared to the less deformed primary shear veins in carbonaceous rocks of the western limb. This highlights the post-vein deformation that occurred along the eastern ore zone.

Reverse and dextral strike-slip faults belonging to the deformation phase D3 followed by D4 and D5 deformation of sinistral and normal faults displace bedding-parallel quartz veins. However, intense extensional quartz veining has been observed at the contact between intrusives and sediments near the NNE reverse/dextral faults (e.g. R1and R2 faults, Figure 5.18). These observations suggest that reverse faulting occurred during late stage compression after the development of bedding-parallel veins but subsequently still reactivated and channelled the mineralised fluid. NS sinistral and normal faulting (D4 and D5) were observed to not commonly generate quartz veining in intrusives and sediments compared to the bedding-slip, NNW and NNE faults.

These important roles in controlling the vein system provide evidence for interpreting bedding-parallel shear veins associated with fold and thrust, and later faults including NNE and NNW (Figure 5.33) faults are a continuous event that controls gold mineralisation. In contrast, sinistral and normal to oblique-normal faults including Hill 6 NS Fault and Jalis NS Fault occurred at a very late stage, displacing earlier veins (Figure 5.29c) and occurring after the mineralising episode but may also have been responsible for at least some remobilisation of gold.

5.8 Conclusions

Gold mineralisation at the Penjom gold mine is hosted within quartz-carbonate veins that display varying degrees of overprinting events developed during episodic failure in ductile–brittle environment. The two main types of vein identified are shear and extension veins. The dominant shear veins in Penjom gold mine are either bedding-parallel or fault-hosted sub parallel to bedding such as the Penjom Thrust ore zone. Associated with these dominant shear veins are extension vein arrays such as sheeted discordant extension veins, stockworks, irregular veins and brecciated veins. This group of veins was formed during folding and thrusting. Other vein systems were developed during the later stages of deformation and may represent reactivation of the earlier formed shear veins. Later fault movements, particularly reactivation of sinistral to normal mainly those extending from the hanging wall faults, disrupt a majority of both quartz veins and gold mineralisation.

Table 5.3: Classification of vein types, host rock and superimposed reactivation by later fault

Veins		Morphology or Type	Lithology site	Reactivation by later fault/process	Type
Shear veins		Ribbon, roughly laminated, massive	Carbonaceous shale	Parallel reactivation resulted to fault/shear fill vein	Shear vein Type 1
		Planar to roughly laminated	Thin carbonaceous shale	No parallel reactivation	Shear vein Type 2
			Carbonaceous shale at felsites contact or cross cutting	No parallel reactivation	Shear vein Type 2
		Vein septa/book texture. (Hodgson, 1989)	Siltstone below shear vein	No parallel reactivation	Associated with Type 1 and 2
Extension veins	Sheeted veins (high angle)	Planar	Competence rock including massive siltstone and conglomerate.	Strike parallel to σ1. No parallel reactivation	Extension vein Type 1
	Sheeted veins (high angle)	Planar	Competent rock below shear vein including felsites	No parallel reactivation. Stress induces by shear vein or other shear.	Extension vein Type 2
	Sheeted veins (low angle)	Planar	Mostly in sub-vertical felsites dyke/sill	At or near fault contact	Extension vein Type 3
	Stockwork	Multi directional	Mostly in felsites rock	Fracture induce by shear vein or fault	Extension vein Type 4
	Hydrothermal breccias	Non rotated angular wall rock fragment	All rock except massive conglomerate	At intercept of shear vein/fault with rheological contrast unit	Associated with shear vein type 1, 2 and other faults

CHAPTER 6.0 MINERALOGY, TEXTURE, SULPHIDE AND GOLD MINERALIZATION

6.1 Vein mineralogy

Vein mineralogy is dominated by quartz and minor calcite, ankerite and sulphide minerals. Veins are characterized by quartz only, a mix of quartz and carbonate, carbonate (mainly calcite), minor ankerite and barren calcite vein. This reflects several stages of fluid mobilization into the opening system related to structural control. Based on field observation and cross-cutting relationships, mineralized quartz and carbonate veins occur in four different mineralogical phases within one episode of structural event to form single sync-genetic quartz veins.

6.1.1 Quartz veins

Quartz veins comprises grey to watery quartz veins and milky quartz veins. Early quartz (I) along shear plane appears as grey quartz due to insoluble carbon because fluid migrated through the shear opening of carbonaceous shale during repeated bedding slip faulting. Without the insoluble carbon, early quartz appears as watery quartz.

Boundaries with milky or white quartz are usually difficult to identify but can be recognized along ribbon and laminated quartz, because later milky white quartz can be seen crossing carbonaceous parting and grey quartz (Figure 6.1). In shear veins, grey quartz occurs along the ribbon or at the margin and milky quartz normally within the buck quartz. Minor quartz cross-cut the laminae along the micro-fault (Figure 6.1 Right).

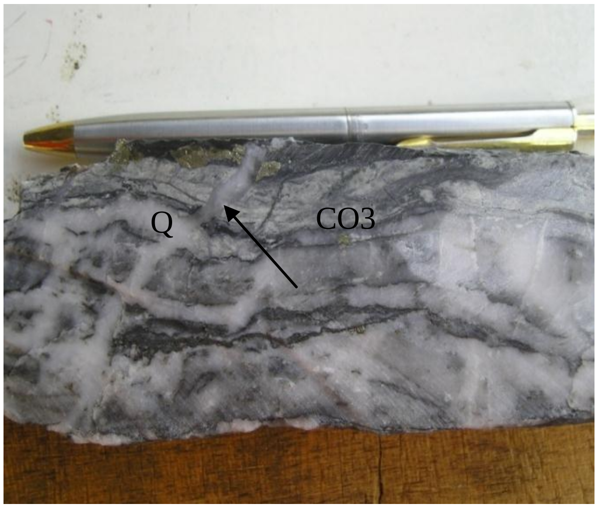

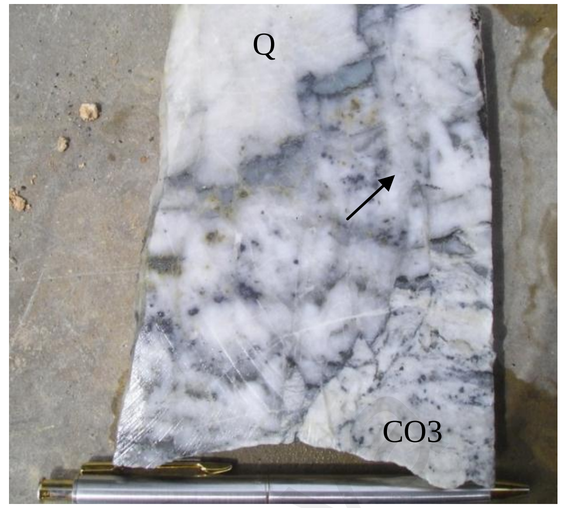

Figure 6.1: (Left) Late stage of a white quartz infill along lamination but also cross-cuts laminations of gray quartz and carbonate veins (CO3). (Right) Milky quartz and micro-fault truncated stylolite, a band of grey quartz and carbonate (CO3) veins.

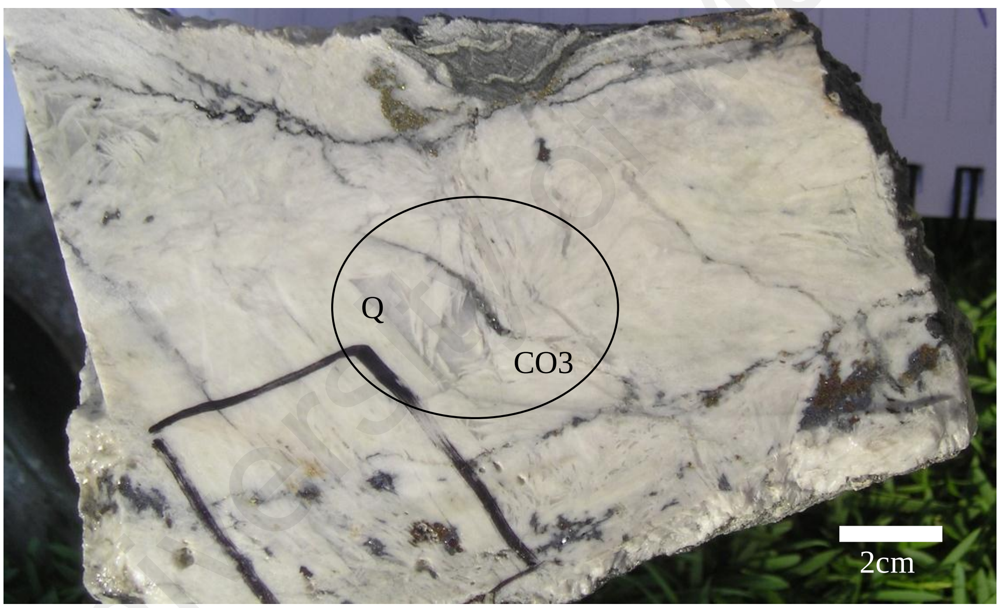

Figure 6.2: Intergrowth of prismatic carbonate (calcite dominance based on XRD analysis) and quartz in quartz carbonate veins.

6.1.2 Quartz carbonate veins

Theses veins comprise of quartz and carbonate in which at many parts were seen to have intergrown into each other as a result of the fluids that formed the veins containing an equal amount of silica and carbonate. Both were crystallized almost at the same time, and there were no clear crosscutting features between both minerals. Carbonate, dominantly calcite, locally crystallizes as prismatic shape such as in Figure 6.2. In certain parts such as at Q3W in contact with intrusive, carbonate proportion relative to the quartz is usually higher and coincides with a higher gold grade. This can be observed in Hill 2/3 (jewel box), certain segments of Q2W and Q3W as well as in associated extension veins. Carbonate veins also forms lamination texture along carbonaceous parting together with thin watery or grey quartz. Even though carbonate in place shows a close relationship with gold, sphalerite and galena, gold itself can be observed in many carbonate free laminated quartz.

6.1.3 Carbonate veins

Calcite (mineralised veins): various forms of calcite can be observed forming a minor component of veins crystallized at different episodes from quartz but within the same vein. Calcite occurs as veinlets (up to 1 cm) across earlier quartz (Figure 6.3), infill along the ribbon (Figure 6.4) or cross cutting the early laminated quartz. Though some late stage quartz veinlet is observed as cross cutting the earlier calcite vein. Early mineralized calcite veins have the conchoidal surface and lack a cleavage plane (refer to Figure 6.14), possibly due to the modification by deformation. The different morphology such as the early calcite required a confirmation with XRD analysis (as in Chapter 7).

Ankerite: within the extension quartz, carbonate (ankerite) filled along the margin of the vein and commonly appears to be reddish as a result of the oxidation of the iron in the carbonate (Figure 6.5 Left). Rare occurrences of ankerite as replacement in host rock, but the majority of it is related to late-stage deformation events related to faulting. Networks of ankerite veins are common and cross-cut the earlier veins. Locally pyrite is the only sulphide associated with this mineral.

6.1.4 Late calcite veins (gold barren)

Late calcite veins have rhombohedral form with a well-developed cleavage plane. Their colour is usually white, but sometimes it is a clear, colourless crystal. Calcite is not hard, it can be scratched easily and is easy to break compared with other carbonates such as ankerite, which is often intergrown with or infills fractures in quartz veins.

Most calcite veins occur as extension veins up to 5 cm thickness along bedding, as indicated by fibrous growth against the wall that is a well-developed crystal cleavage (Figure 6.5 right). This kind of vein is common in calcareous shale and laminated calcareous siltstone of the Upper Mine Sequence. Some of the veins infilling normal to sinistral North–South faults, particularly at hanging wall. Late small stringers of north dipping E–W extension veins less than 2 mm locally develop discordantly to the strike of bedding (Figure 6.6) and are not affected by the displacement.

Late calcite veins are also locally associated with coarse grains or massive galena, but have no significant gold mineralization. These late calcite veins are hosted locally along the normal fault above the Penjom Thrust and locally within the Penjom Thrust at the interception with the NS trending cross cutting fault. No other sulphide is found associated with this calcite. As a result, at several places along the Penjom thrust, the barren calcite occurs within the mineralized orebodies. Several galenas from these zones have been collected for lead isotope and trace element analysis to differentiate the genetic and timing of that galena. Trace element analysis and lead isotope of various phases of galena were described in Chapter 8.

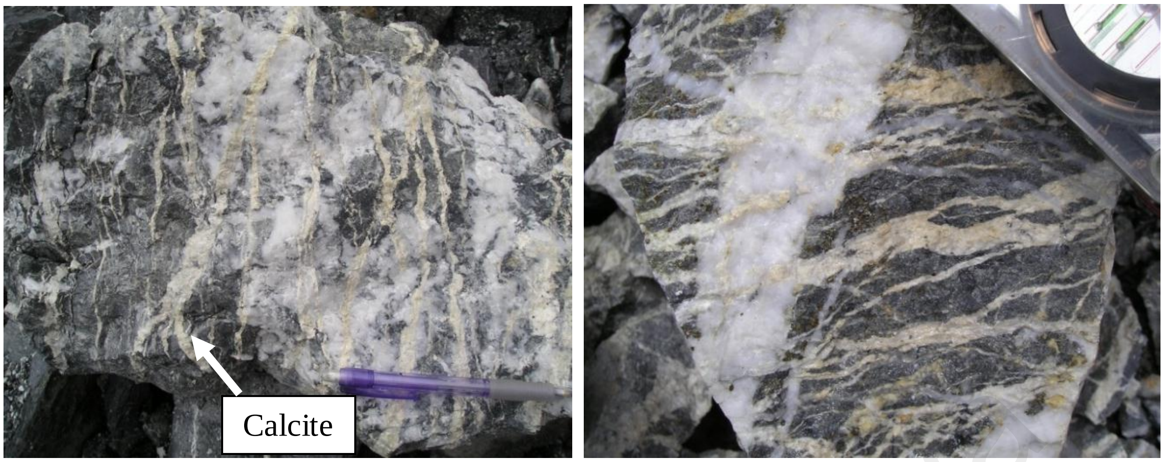

Figure 6.3: (Left) Ribbon to laminated vein comprised of carbonate (calcite) at the bottom and quartz on top. (Right) E-W sheeted carbonate veins cross cut the brecciated quartz within the veins but not forming outside the vein body.

Figure 6.4: Quartz-carbonate veins, ribbon quartz on top and carbonate bottom.

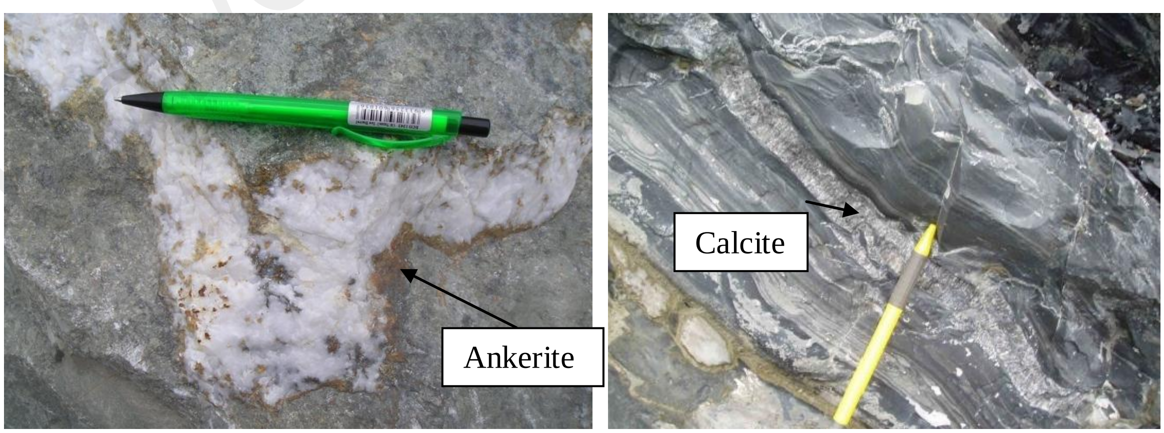

Figure 6.5: (Left) Ankerite appears as red after expose to oxidation for a certain period. (Right) Calcite extension vein parallel to the bedding with fibrous of the veins growth perpendicular to veins wall

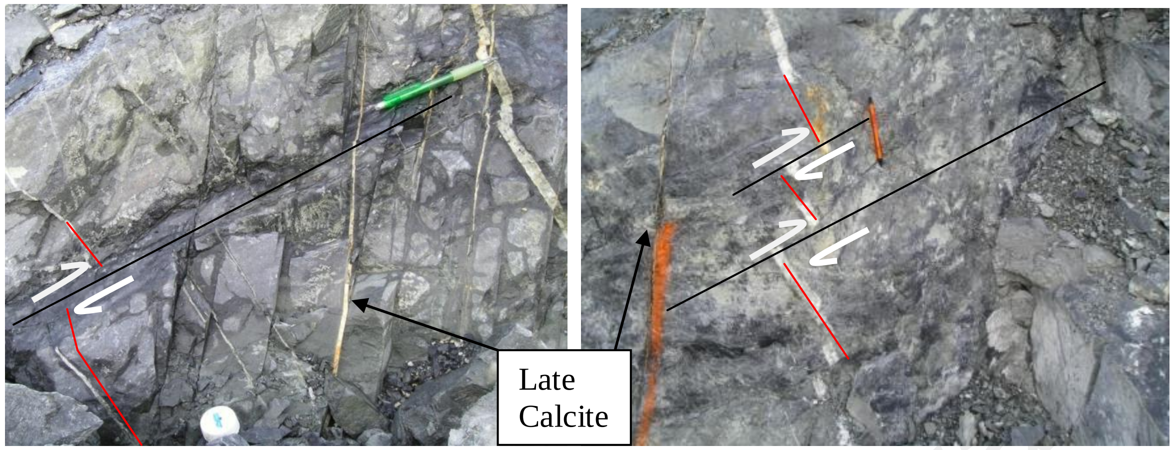

Figure 6.6: Late calcite veins at different phase with sheeted quartz carbonate veins. Reverse sense of movement were evidence in both photo.

6.2 Veins texture

6.2.1 Introduction

Different gold deposits which define different tectonic settings have consistent correlation with particular quartz veins textures (Dowling and Morrison, 1989). Veins are the main component of many hydrothermal systems because fluid that carries metals and variable sulphide minerals are rich in silicate and also carbonate mineral.

Description of vein textures is based on terminologies from Dowling and Morrison (1989) from their study in North Queensland gold deposits. They introduce eleven classes of quartz texture, which are defined by the degree of crystallinity, grain size and form, density of crystal packing, preferred orientation of the grain, deformation and recrystallization.

Vearncombe (1993) introduces a simplified scheme to categorize quartz veins morphology based on the quartz addition in veins that produce the vein texture. The controls are face-controlled (comb, some fibres), displacement-controlled (fibres), parallel-controlled (crustiform, cockade), radiating (plumose), non-directional control (buck, saccharoidal), replacement (pseudomorph, lattice texture) and modified-controlled (stylolite, breccias).

The main objective of the study here is to identify different characteristics of veins texture, including the primary and superimposed in different local structural setting and host rock lithology.

6.2.2 Textural classification

Two major textural groups can be recognized on the basis of the on hand specimen with aids from thin section study that is based on grain size, preference of grain orientation and form:(1) primary textures, which represent initial veins fill and (2) superimposed textures as a result of deformation, overprinting, dissolution, hydrothermal brecciation and recrystallization (Dowling and Morrison, 1989).

Different structural setting of veins can have different quartz texture. As classified in the previous chapter, veins were classified as shear veins if the vein was associated with a shear or fault movement and extensional veins if the veins were infilling an open space. Due to the on-going deformation, shear veins have superimposed structure but the associated extension veins had a primary quartz texture as the quartz infilling the open space in either sheeted, stockwork or massive buck quartz. However, post vein emplacement movements could occur along the extension contact and for this case superimposed structures may also be observed.

In Penjom, primary quartz show comb textures, either fine or coarse commonly developed in sheeted extension veins, euhedral and anhedral buck quartz in massive veins either fault controlled of shear vein controlled. Secondary quartz textures are lamination, ribbon, stylolite, spider veinlet, breccias and shattered quartz texture (Endut et. al, 2012).

6.2.2.1 Buck texture

Buck refers to massive quartz containing milky and vitreous veins, which consist of tightly packed interlocking grains of highly variables size and orientation. Buck texture implies high confining pressure, where anhedral quartz is deposited under the compression and euhedral quartz under tensional stresses. This texture is categorized as non-directional controlled (Vearncombe, 1993), with no obvious geometrical control on the addition of quartz.

Extensional veins show euhedral textures. Continued deformation can result in recrystallization and that anhedral textures may also develop. Small scale extensional veins commonly shown comb texture in thin section. In thick shear veins, ribbon or laminated textures developed along the margin and the rest of the vein was massive (Figure 6.7 A and B); the latter exhibits buck texture. Based on microscopic studies, recrystallized, very fine grain of quartz occurs at the shear margin (Figure 6.7C). In the massive shear veins both anhedral (Figure 6.7D) and euhedral buck developed in one vein.

6.2.2.2 Comb texture

This texture is commonly developed in E–W direction sheeted extension veins comprising an individual crystals that can easily be recognized in hand specimens. Alignments of the crystals are perpendicular to the vein wall or the c-axis. Crystal size varies and can be further classified as fine comb, medium comb or coarse comb. Comb texture found locally in the Jalis corridor shows crystal growth in an open space, as shown by individual crystal and open space in an extension vein (Figure 6.8).

Vugs and druses are also common in the Jalis corridor vein, especially in the extension vein hosted in the intrusive rock. However, carbonate free vein within the shear zone less than 15 m deep from the surface, which has the vugs and druse are as a result of the dissolution of the carbonate component in the vein and not the primary features. Massive veins associated with reactivated shear veins also have minor vugs textures.

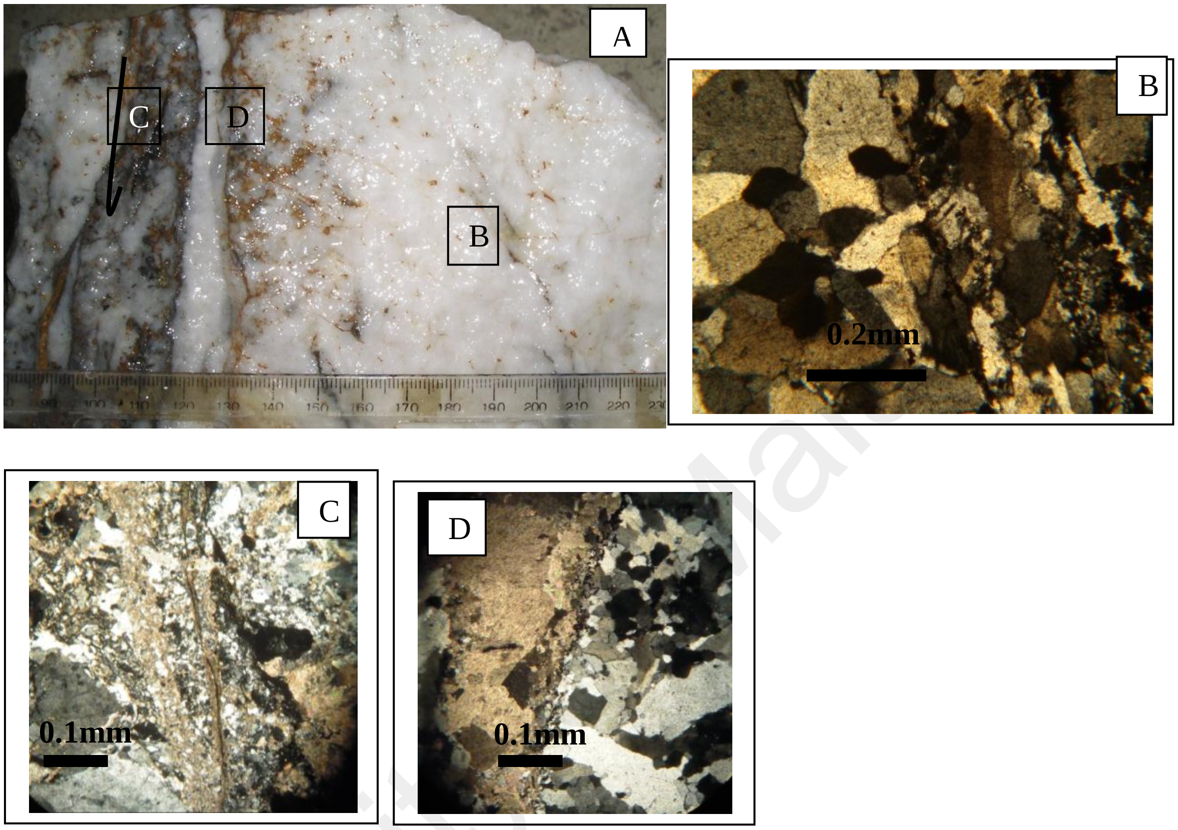

Figure 6.7: (A) Ribbon quartz and massive inside the vein. (B) Coarse grain quartz inside the vein made up the passive grain. (C) Fine grain along the laminated vein represents the active plane. (D) Anhedral to euhedral quartz grain close to carbonate vein along ribbon.

Figure 6.8: (Left) Medium comb with crystal growth perpendicular to vein margin, (Right) Coarse comb but with a more random crystal growth texture.

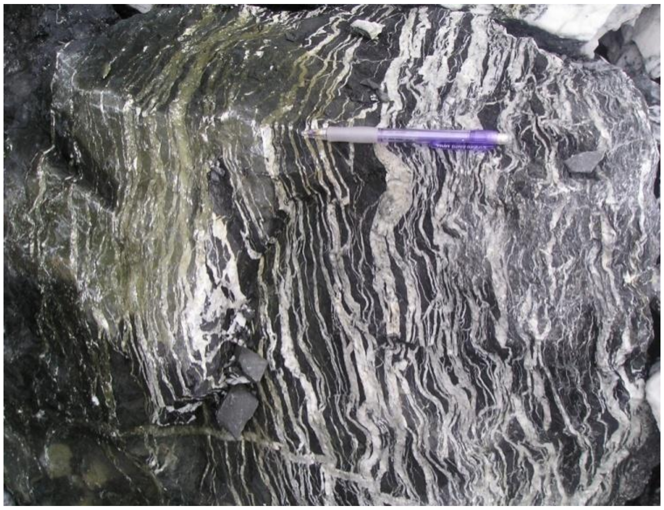

Figure 6.9 Parallel veins in siltstone with multiple veins to form laminations or septa. Vein crystals align parallel to the wall and with no fibre or comb quartz are indicative of veins forming in confined space.

6.2.2.3 Lamination texture (vein septa)

Lamination is a term where crystal growth is parallel to the vein margin (Thrush, 1968 in Dowling and Morrison, 1989). The term here is restricted to the bands of quartz or laminations parallel to vein walls (Figure 6.9) with interlocking of an equal size of quartz grain. Vearncombe (1993) described lamination as a term to refer to multiple parallel quartz veins containing slabs, slivers or bands of wall rock by opening, reopening and eventual merging of veins.

In Penjom, this texture is referred to parallel quartz in between thin host rock, and can be observed locally in carbonaceous shale and siltstone below the shear veins. Veins possibly infilling the weak planes along the foliation or bedding parallel cleavage and can structurally be referred to as extension vein. It differs from the ribbon textures in terms of deformation state involving the opening but not shearing. Continuous deformation results in veins become folded or buckled.

6.2.2.4 Ribbon texture

Ribbon texture is a superimposed structure due to the repeated opening and shearing that is characterized by laminations or ribbon developed by the thin country rock or insoluble material within quartz or carbonate vein. Quartz grains show an evidence of deformation along the ribbon and intensive development of sub-grains (Figure 6.7C). Wall rock ribbon is commonly discontinuous or undulating as a result of an on-going deformation. Ribbon referred not to quartz, but to the host rock that makes the ribbons inside the vein. Later, reactivation by late faults results in further deformation along the ribbon with intensive recrystallization (Figure 6.10).

In Penjom, ribbon textures characterized the shear veins and developed mainly parallel to bedding along carbonaceous shale. Two morphologies can be observed in either very fine remnant of wall rock, commonly in very thin carbonaceous shale such as in Q3W sample and thicker wall rock or ribbon in highly carbonaceous zone of thick carbonaceous shale. The former was also referred as laminated with occasional undulating form due to the thin line of wall rock remnant in the veins.

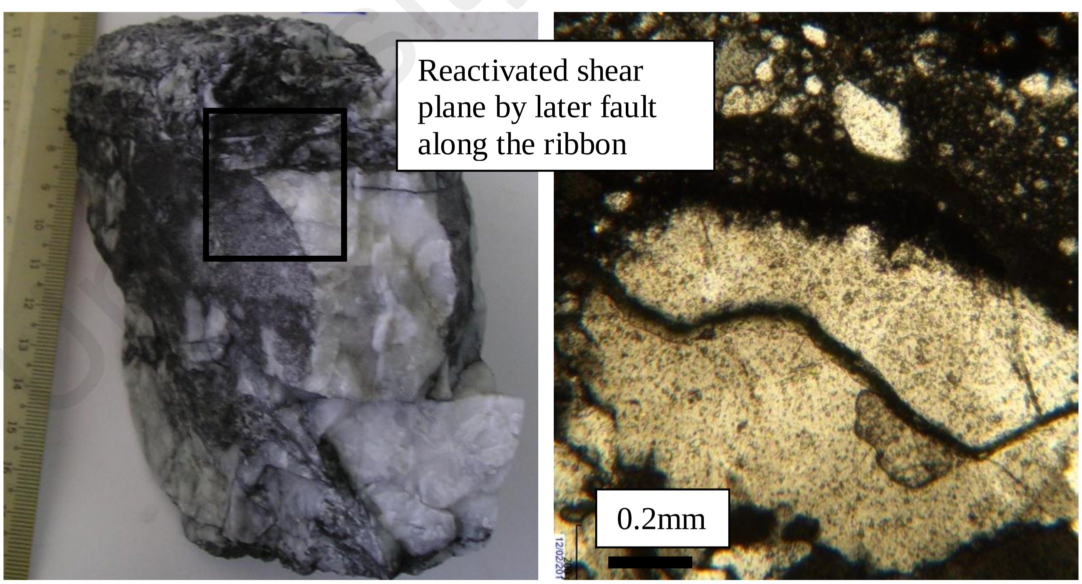

Figure 6.10: (Left) Reactivated shear on ribbon (in box) that produced the cataclasite quartz grain and massive anhedral buck below the ribbon. (Right) Photomicrograph of fine abrasive quartz represents the mill grain and anhedral buck quartz below the shear.

6.2.2.5 Stylolite texture

Stylolite texture is defined as dark lines of insoluble material such as carbon or sulphide. This line can be parallel to the vein margin (Figure 6.11 Left), fractures pattern (Figure 6.11 Right) or irregular line as a product of the pressure solution of the insoluble carbon. The host quartz can be recrystallized to form a sub-grain because of deformation. This texture is considered as a secondary or modified texture due to the on-going deformation, especially shear vein along the thrust that is referred as reactivated shear vein.

6.2.2.6 Breccias texture

Breccia texture refers to the deformation features related to faulting or shearing, resulting in recrystallized grains. This term should be differentiated from undeformed hydrothermal breccias or deformed fault breccias, which is characterized by rotated angular host rock fragments in veins or faults. Breccias texture is a superimposed feature defined as either a vein network in host quartz or a complex of angular fragments of host quartz in a semi-continuous matrix with common sub-grain development and partial resorption of the quartz fragment (Dowling and Morrison, 1989). They introduced two sub-classes of breccias texture: such as infill and aggregate. The former is characterized by a vein network as a later phase and resorption and recrystallization is minimal.

In hand specimen, infill breccias texture can be observed in massive parts of shear veins along the Penjom Thrust. The breccias or fracture systems were infilled with a dark later phase fluid which contains insoluble carbon that was introduced into the fracture system as a result of pressure solution and remobilisation of carbon. This differs from the texture mentioned by Dowling and Morrison (1989), which involved silica bearing fluids as a later phase. However, in this case, the later phase is fluid containing insoluble carbon.

Breccias aggregates are the result of progressive fracturing and modification. Resorption of fragments and sub-grain development can be observed on vein at fault contact showing the shattered and recrystallized quartz grain. The same process can occur on earlier formed infill breccias Figure 6.12 (Left) resulted to irregular line of black stylolite as in Figure 6.12 (right). During this brecciation process, a certain amount of gold was introduced either from a residual hydrothermal fluid or remobilized from the local system.

6.2.2.7 Minor veinlet texture

In slightly deformed zones, it is quite common to have thin veinlets comprising quartz and minor calcite of less than 0.5 cm crossing the earlier shear vein (Figure 6.13) and stylolites either perpendicular or sub-parallel to the shear fabric which are irregular. Based on limited samples available, these veinlets cross cut sulphide minerals and also visible gold (Figure 6.14 and 6.15). These veinlets were emplaced late during the deformation.

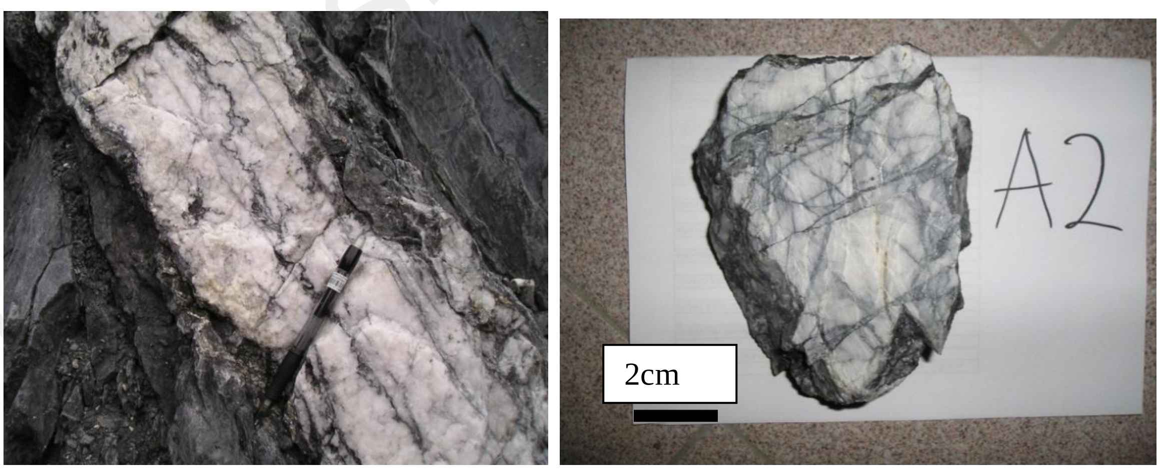

Figure 6.11 (Left): Bedding parallel shear vein with parallel wavy style stylolite. (Right) Shear vein with fractured fill stylolite or infill breccias texture.

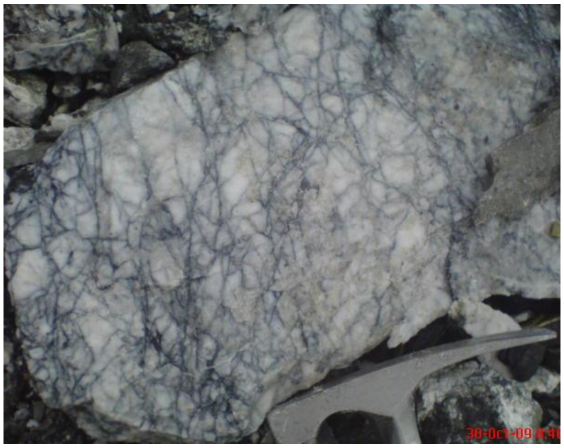

Figure 6.12: (Left) Fractured stylolite or infill breccias texture. (Right) Superimposes features of aggregate breccias in shear vein can be originated from recrystallized fractured stylolite or infilled texture (sample half core HQ).

6.3 Application of quartz texture

At the field scale, the identification of textures can be used to gain a better understanding of vein formation and structural interpretation. The analysis of structural control on ore deposit must first take into account the structural classification of veins and textural classification can further define the environment, physicochemical conditions and the timing of gold during a long period of veins formation.

Study of textures can also help to define the deformation effect on veins, either synchronously with mineralization or as a post mineralization event. In orogenic gold deposits, the introduction of gold is always regarded as late, but still within the time of vein formation that is during the development of both primary and secondary textures. Gold can also be deposited earlier with early sulphide and veins and redistributed into the superimposed deformation features.

On the deposit scale, a detailed study by Dowling and Morrison (1989) concluded that gold deposits have several associations of vein textures while, at the same time, other textures are absent. Table 6.1 shows a list of vein textures at different gold deposits (Dowling and Morrison, 1989). Vearncombe (1993) further studied Archaen lode gold and suggested that crustal depth indirectly controls quartz textures. This is based on the textures commonly found in young epithermal deposit and in older Archean lode gold such as those in Western Australia.

In Penjom, vein textures are predominantly euhedral and anhedral buck quartz, ribbon, laminated vein and comb quartz type, a typical orogenic gold (Slate Belt) assemblage of vein textures. Veins have been further superimposed by syn-vein deformation such as breccias texture and post-vein structural deformation such as deformed, fractured or mylonitized and destruction of vein texture with no indication of addition of fluid.

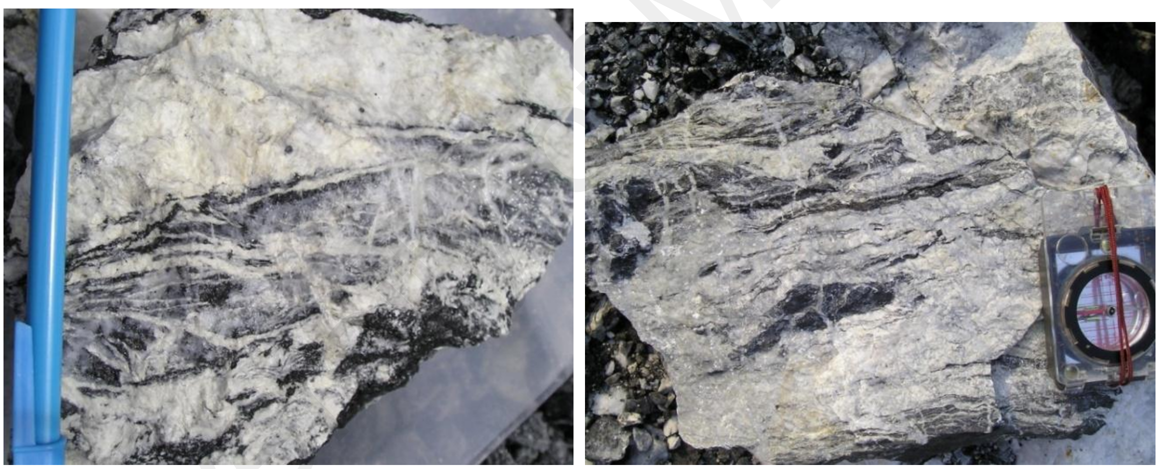

Figure 6.13: Quartz carbonate veins near to fold axis and Penjom Thrust has a network of thin veinlets overprint the earlier ribbon texture.

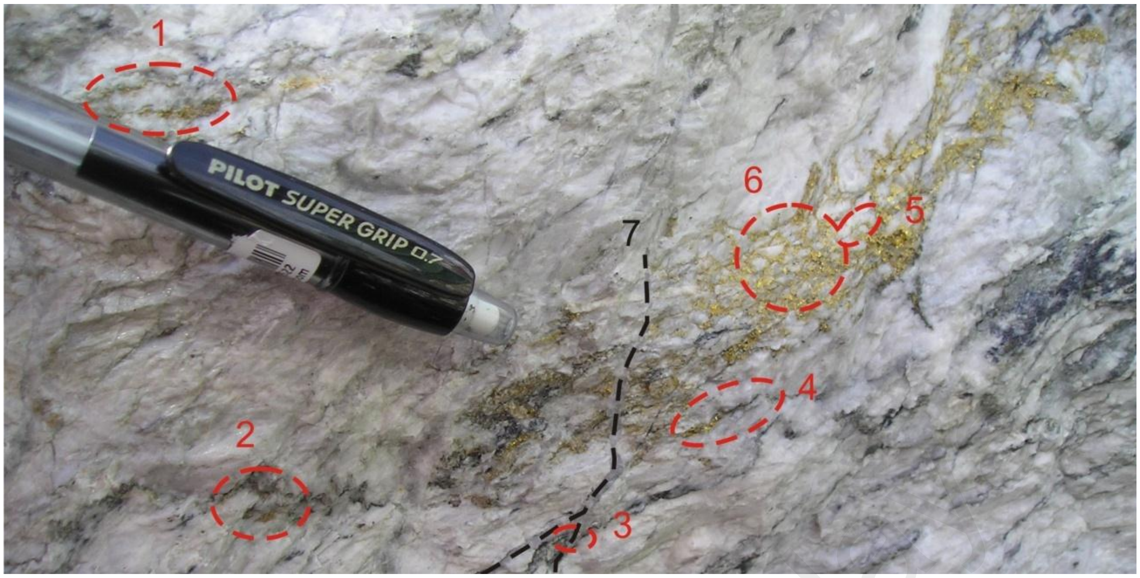

Figure 6.14: Gold infilling the local breccias texture in reactivated shear vein as in circle 1, 5, 6 and along stylolite in circle 2 and 4. Discordant veins (black line 7) as a late stage veins cross cut the massive brecciated veins and gold.

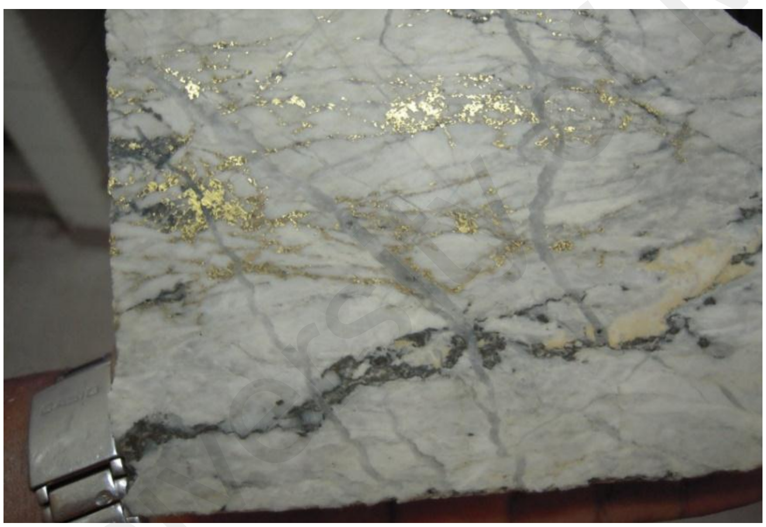

Figure 6.15: Discordant quartz veinlets as a late stage event cross cut the stylolite and gold. Stylolite made up of soluble carbon and sulphide.

Table 6.1: Quartz texture types for different deposits environment (Dowling and Morrison, 1989). Blank-absent, 1-rare, 2-present, 3-common, 4-abundant, 5-predominant.

TEXTURE ORIGIN	TEXTURE TYPE	Epithermal	Porphyry	Plutonic	Slate belt/ (Orogenic)
PRIMARY GROWTH	1 BUCK				
	1a Anhedral				5
	1b Euhedral		1	5	
	2 FIBER				2
	3 LAMINAR		4		
	4 SACCHAROIDAL	2	1		
	5 CRYSTALLINE				
	5a Coarse comb	2	1	3	2
	5b Medium comb	2	2	2	1
	5c Fine comb	4	5	2	
	5d Zoned crystal	3	1	1	1
	6 BANDED				
	6a Crustiform	5	3		
	6b Colloform	5			
	6c Cockcade	3	2	1	
	7 CHALCEDONIC				
	7a Massive	4			
	7b Banded (agate)	4			
SUPER-IMPOSED Deformation/ Dissolution	8 RIBBON			2	4
	9 STYLOLITE			2	3
	10 SPIDER				
	10a Comb spider	1	1	2	3
	10b Phantom spider			1	2
	11 BRECCIA				
	11a Infill	4	1	2	3
	11b Aggregate			2	2
RECRYSTALLI-ZATION	12 MOSS	3			
	13 PLUMOSE	3			
REPLACEMENT	14 MOLD	2			
	15 BLADED				
	15a Lattice bladed	3			
	15b Ghost bladed	1			
	16c Parallel bladed	2	1		

6.4 Ore mineralogy

6.4.1 Introduction

The purpose of this study is to document a paragenesis of sulphides mineral based on field observation and microscopic study. A list of samples for polished section is shown in Table 6.2. The field study is based on the observation in the pit on different ore bodies with limited core logging since 1997. A better understanding of the styles of quartz veining, distribution of veins in the pit, mineralogy and different chemistry of host rock, especially carbonaceous shale, contributes are better understanding the geological and structural control on mineralization.

This study also focuses on the texture of the mineral; especially deformation related feature based on samples taken from every shear veins and in comparison with the same veins near the fault zone to determine relative deformation and mineralization.

These studies focus on five common sulphide minerals found accompanying the mineralization of minerals: pyrite, arsenopyrite, galena, sphalerite and chalcopyrite. The better constrain relative timing of structure and mineralization, minerals such as early pyrite and arsenopyrite with late galena are compared with the occurrences of veins and gold. This has been the main focus for this study.

However, only undeformed to slightly deformed samples were prepared for polish sections. Samples close to the fault zone are usually deformed and cannot be successfully prepared for polished sections. The deformation effect is considered as a post vein and structurally post mineralization event. A sample rich in gold and sulphide was not prepared for the polish section. The study of sulphide-gold bearing vein, vein mineralogy, textural and structural classification of vein, detail pit observations and review of previous core logging significantly improve the understanding mineralization control and paragenesis. The previous site based study of sulphides and gold mineralization paragenesis is limited on the observation such as by Gunn et al, (1993) and Arrifin (1994) during the exploration stage.

Table 6.2: List of the polish section samples.

Sample ID	Location	RL	Mineral	Vein zone	Nearest fault
Q3W1	West limb	824-KE	Ga, Sph, Au	Q3W	NNE
Q3W2	West limb	824-KE	Py, Au, Ga	Q3W	NNE
Q3W879	Near fold axis	789-KE	Sph, py	Q3W extension vein	NNE to NE
Q3WH4	Near fold axis	789-KE	Py, ga, sph	Q3W	NNE
Q3WA	West limb	786-KE	Apy, ga, Au	Q3W	NNE
Q3WB	Near fold axis	789-KE	Ga, py, cpy	Q3W extension vein	NNE
Q3WL (E)	Repetition west limb	786-KE	Py	Q3W extension vein	Blue line structure
FQ1	East limb	888-KE	Py, apy	Q2E	Penjom Thrust, FAF
JN1	Fold axis	894-JN	Ga, Sph?, Py	Q1E	NW, Penjom Thrust, NS
JN2	Fold axis	894-JN	Py, Ga	Q1E	NW, Penjom Thrust, D2 NS
MNQ2A	Manik	924-MN	Apy	Q2	Penjom Thrust
MNQ2B	Manik	924-MN	Apy, Au	Q2	Penjom Thrust
QMN1	Manik	927	Au,ga	Q2	Jalis RF
Q3D	KE west limb	792	ga,Au, py	Q3W	R1 and R2, DMF
A1	Janik	882	ga	Q1	
JNA	Janik	888	py	Q1	
Q3W3	KE west limb Hill 6	792	Py,ga	Q3W	
GA1	Janik	888	Ga,Au	Q1	
ZP3	KE west limb	792	Ga, Au, py	Q3W	

6.4.2 Previous study

Previous studies of sulphides mineral has been undertaken by Gunn et al. (1993), Ariffin (1995) and Abdul Aziz (2002) during the exploration stage. The first two studied the diamond drill core, and the latter had selective drill core and field observations. This study covers more site occurrences of the sulphide and the effect of deformation event.

6.4.3 Sulphide mineral

6.4.3.1 Pyrite

6.4.3.1.1 Field observation

Pyrite occurs in the shape of microscopic framboid (py_0): idiomorphic or cubic shapes mainly in carbonaceous shale and siltstone (py_0),cubic pyrite (py_1) disseminated in the wall rock adjacent to the quartz vein within the altered zone and as aggregates of sub-hedral grains in the quartz (py_1) (Figure 6.16), commonly intergrown with other sulphide minerals. Pyrite (py_1) is related to hydrothermal event and quartz veining. Disseminated pyrite (py_0) hosted within carbonaceous host rock is commonly related to early diagenetic processes or as early syn-sedimentary. Locally, fine grain cubic pyrite (py_2) occurring in a certain layer and seen as post to S_1 cleavage is considered as later in the deformation event.

Within shear veins, pyrite occurs at the margin of the vein, in the slivers of host rock in the quartz itself. Shear movement along the margin of the bedding parallel vein can be seen affected the pyrite (Figure 6.17 Left) and is responsible for pyrite deformation indicating that the pyrite already deposited in quartz vein during or prior to the bedding slip fault activity. Some veinlets was crosscut the early pyrite (Figure 6.17 Right), and the mild refold of pyrite band (Figure 6.18) indicate an on-going deformation of the vein and sulphide.

Pyrite can be observed in all mineralized areas associated with arsenopyrite and base metal. In the high carbon zone along the thrust, pyrite in quartz veins is much more associated with arsenopyrite and lacks base metal sulphide except in Janik Zone B Upper/fold hinge where it is associated with galena, but not sphalerite and chalcopyrite.

6.4.3.1.1 Microscopic study

In polished sections, pyrite appeared with a yellowish colour and is altered. Coarse grained pyrite in shear veins along carbonaceous parting is usually highly fractured and brecciated. Fine grain euhedral pyrite also commonly occurs in this zone along the vein margin as alteration pyrite. The occurrence of broken and finely cataclastic pyrite by tectonic stresses indicates that this mineral is formed earlier in mineral paragenesis and in geological event.

In extensional veins, pyrite also can be fractured along micro faults and infilled with galena and chalcopyrite (Figure 6.19). This sample was taken near to the NNE fault; thus, it was assumed that this micro-fault developed synchronously with this fault.

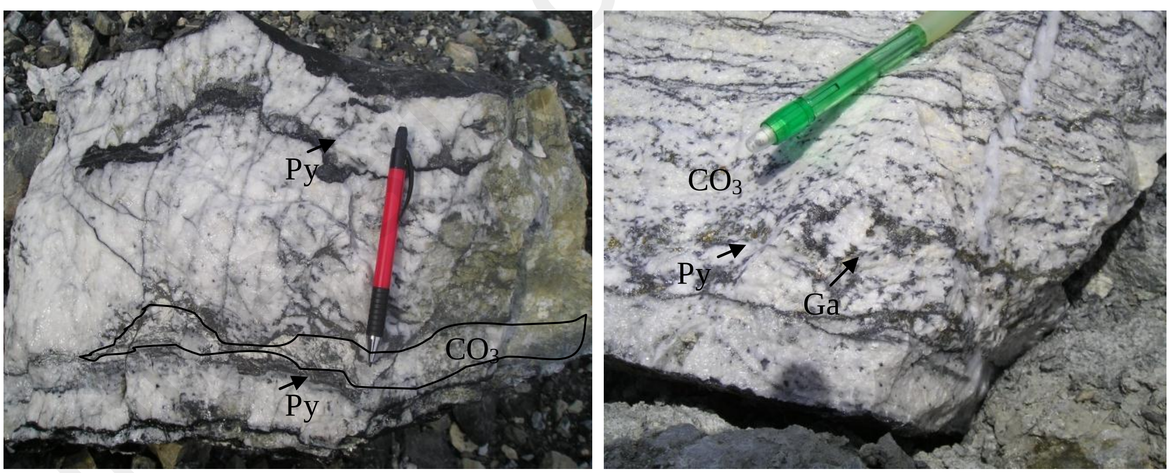

Figure 6.16: Pyrite py_1 hosted along the host rock remnants in vein and along mineralogy boundary. (Right) Pyrite Py1 is more randomly distributed in carbonate (CO_3) vein.

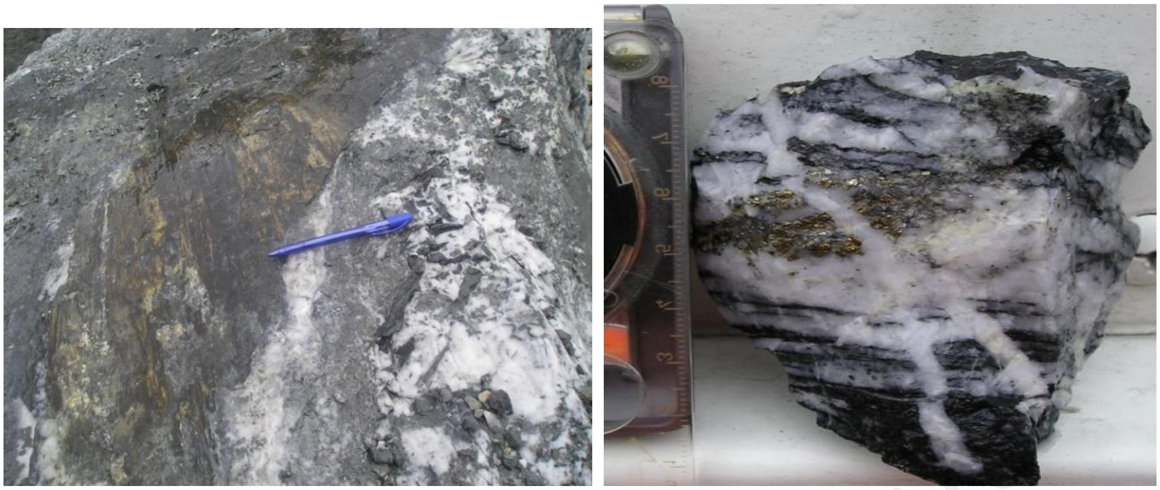

Figure 6.17: (Left) Deformed pyrite as indicated by shining yellowish surface as a result of the fault (KE, Q2W shear vein). (Right) Late stage quartz vein (v1b) cross cut lamination and pyrite py1 aggregate.

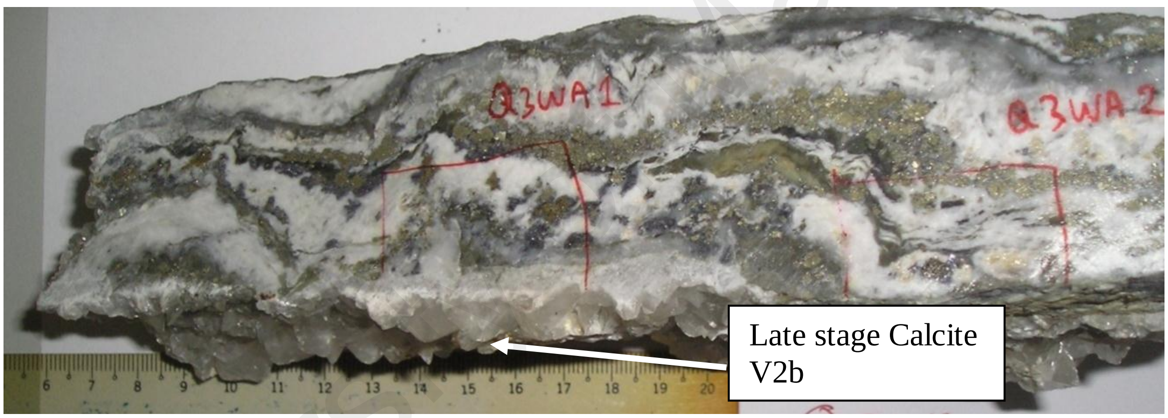

Figure 6.18: Mild refolded of shear vein (V1) (Q3W shear vein) hosts to pyrite (Py_1) and galena (Ga_1), Calcite crystal growth on the shear plane during the later stage not associated with any sulphide mineral.

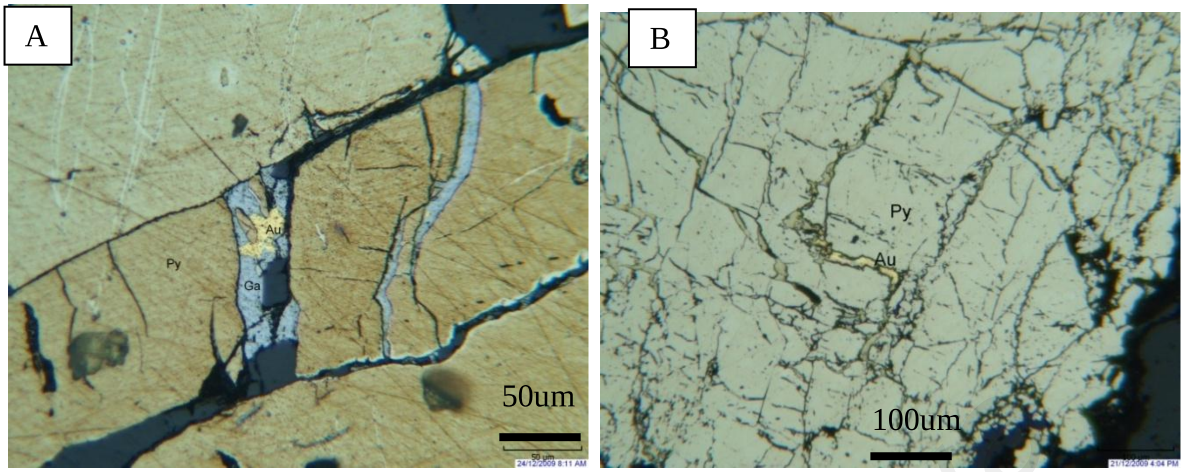

Figure 6.19: (Left) Extension vein-Gold (Au) and galena (Ga) infilling fracture in pyrite (sample q3w879- Q3W near to fold axis). (Right) sample Q3WB gold and chalcopyrite infilling cracks and fractures in pyrite.

6.4.3.2 Arsenopyrite

6.4.3.2.1 Field observation

Arsenopyrite appears silver in colour; commonly occurs disseminated in wall rock (Figure 6.20) and in the quartz veins within the ore zone (Figure 6.21), commonly with pyrite. It forms sub-hedral grains in the quartz veins to rhombic shape in wall rocks and up to 5 cm in size as minerals aggregates. Coarse aggregates in extension veins, usually not associated with high gold grades compare to shear veins.

Arsenopyrite is dominant in shear veins compared with the extension veins. In the wall rock, it occurs along the vein forming a narrow sulphidized wall rock. The dominant of arsenopyrite can be observed along the Penjom Thrust (highly carbonaceous shale) especially in Manik and Janik pits located at the south of the KE pit. In the ribbon quartz along bedding parallel shear, arsenopyrite can be seen as deformed. This indicates that the movement of bedding slip faults during ductile movement still continues after mineral emplacement.

Fault related veins (D3 deformation) also host this mineral and can be observed in veins related to the NE trending Jalis fault. This suggests two episodes of arsenopyrite during the D2 and D3 faults. In other places, it is relatively difficult to find an arsenopyrite in fault (D3) related veins.

6.4.3.2.2 Microscopic study

Three samples of arsenopyrite-bearing shear veins were collected for polish section analysis in the western limb (Q3W shear vein), eastern limb (Q2E shear vein) and Manik pit (shear vein). The cataclastic texture is a very common form of arsenopyrite, especially in bedding-parallel shear veins and reactivated shear veins (sample FQ1 and MNQ2A). FQ1 sample have been undergoing the deformation effect as shown by the refolding or buckling (Figure 6.20B) of this shear veins resulting to the fracturing of pyrite and arsenopyrite. In other samples, deformation is due to the on-going development of shear vein. Pyrite in this sample shows the same deformation characteristic.

Gold as an inclusion in arsenopyrite can be observed in sample MNQ2B (Figure 6.22 Left) indicative of a temporal relationship of gold and arsenopyrite. Kamar Shah (1995) also reports gold as an inclusion in pyrite and arsenopyrite. Arsenopyrite is also found at the corroded margins of pyrite suggesting that pyrite was emplaced before arsenopyrite. (Figure 6.22 Right). Arsenopyrite at the same time shows deformation effect along the shear margin (Figure 6.23). Gold has also infilled the cracks or fractures in arsenopyrite together with later phase galena and chalcopyrite (Figure 6.24) through chemical adsorption on early sulphide or as a result of remobilization of gold from solid solution in early sulphide during the on-going hydrothermal activity and alteration.

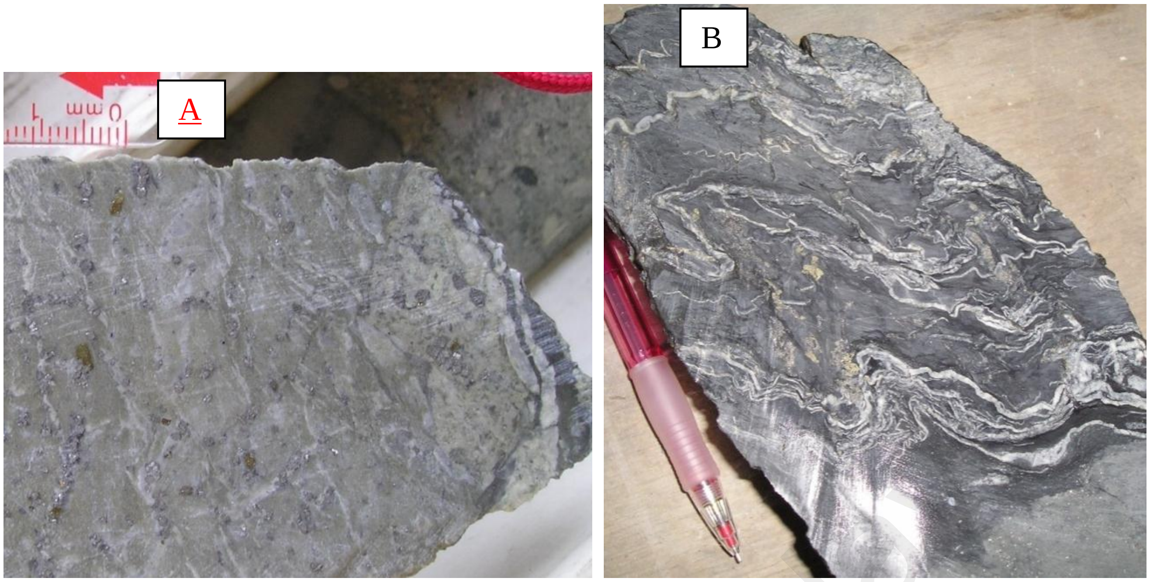

Figure 6.20: (Left) Disseminated subhedral to anhedral arsenopyrite around thin network of quartz veinlet in tuffaceous shale. (Right) Thinly bedding parallel veins has been buckled-up as a result of the ongoing deformation (sample FQ1) also affects the sulphide.

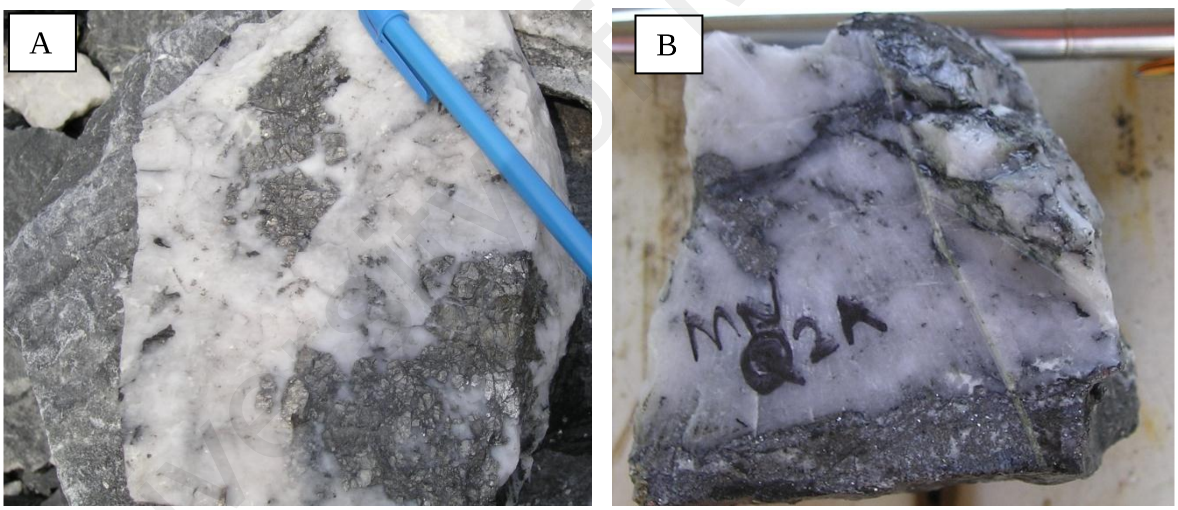

Figure 6.21: A. Aggregates of arsenopyrite in extension vein. B. Band of cataclasite arsenopyrite at lower contact of shear vein along slivers of carbonaceous shale (sample MNQ2A).

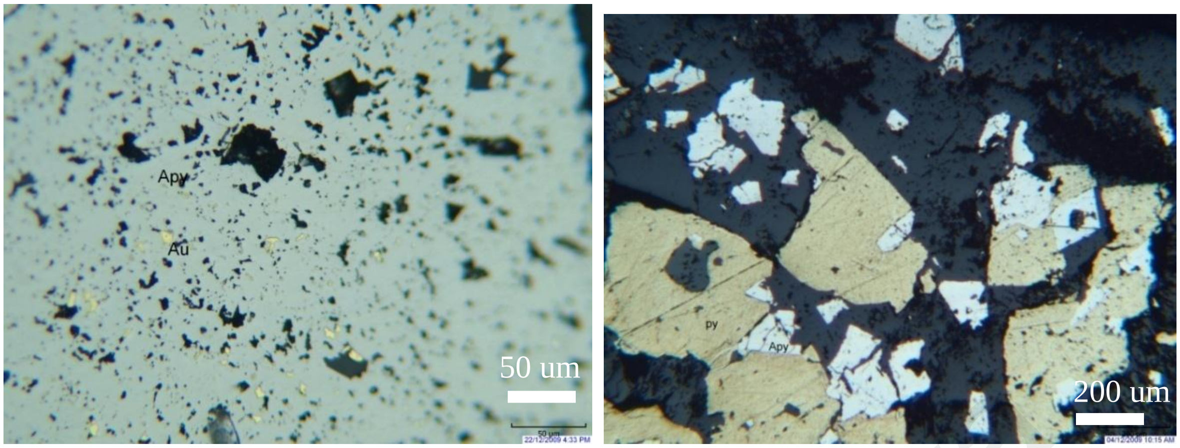

Figure 6.22: (Left) Photomicrograph of gold occurs as inclusion in arsenopyrite. (Right) Photomicrograph of the shear vein FQ1-Arsenopyrite intergrowth with pyrite and also in corroded pyrite. Reflected light.

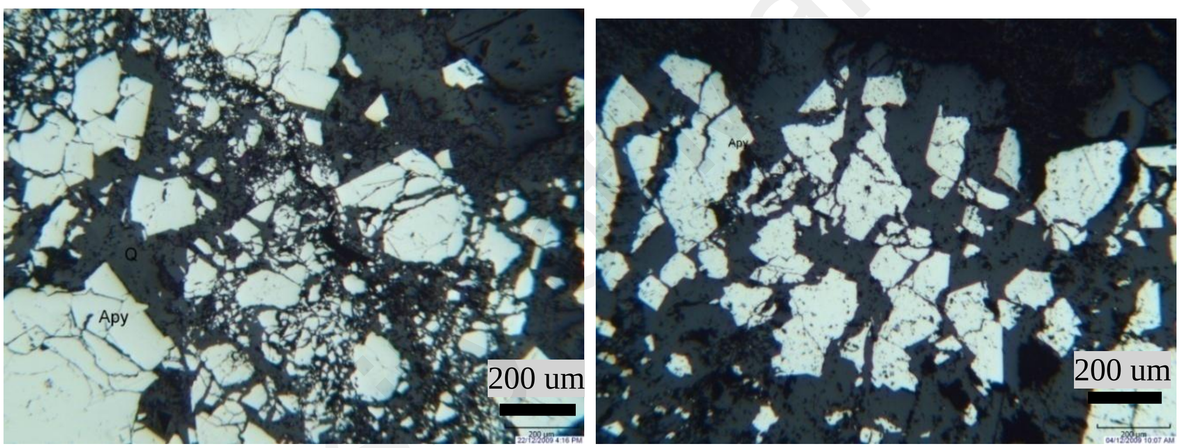

Figure 6.23: Photomicrograph of sample MNQ2A in Manik (left) and FQ1 (right) in the eastern limb of the fold (KE) shows cataclastic features of arsenopyrite along the active shear plane. Reflected light.

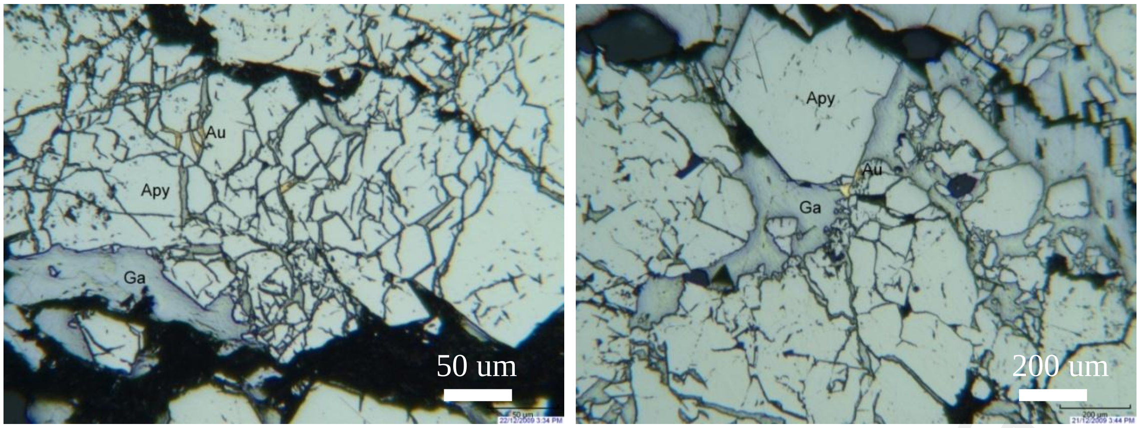

Figure 6.24: Photomicrograph of Q3WA shows galena (ga) at a margin and infilling fractured arsenopyrite (apy) in Q3W quartz carbonate-early sulphide and base metal. Reflected light.

6.4.3.3 Sphalerite

6.4.3.3.1 Field observation

Sphalerite appears honey red in colour, forming an aggregate up to 2cm and as a discrete grain in carbonate and quartz vein. This mineral is commonly intergrowth with galena, pyrite and minor chalcopyrite. This mineral can be dominantly found at the western limp hosted Q3W shear vein, either as infill or along laminations (Figure 6.25), stylolites or patches in extensional vein. However, it is not found on bedding shear surfaces as pyrite is, thus the temporal relationship with bedding shear activity is not certain and was most probably was precipitated at a late stage of ductile movement.

6.4.3.3.2 Microscopic study

Sphalerite appears grey under reflected microscope with irregular shape, size and with corroded boundary. Several samples were collected from western limb within Q3W shear vein and extension vein. The sample of the extension veins near NNE fault shows that the sphalerite was also fractured and infilled with second phase quartz, galena and chalcopyrite

(Figure 26). Pyrite in this sample is sub-hedral and corroded in places with sphalerite occupying the pits and as inclusions.

The exsolution and inclusion of chalcopyrite in sphalerite is very common and can be seen under reflected light in almost all sphalerite bearing polished samples. Based on the style of occurrence and deformation features, sphalerite is precipitated after the first stage pyrite and arsenopyrite but predates galena and chalcopyrite.

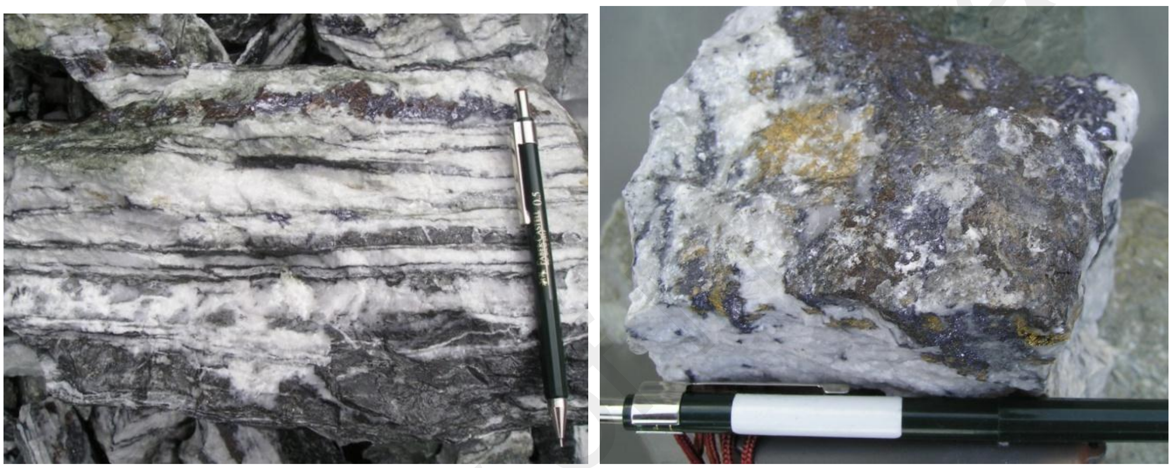

Figure 6.25: (Left) Laminated vein Q3W shear vein with galena (black) and sphalerite (honey red) occupy along the lamination. (Right) Visible gold (yellow), sphalerite and galena along the lamination.

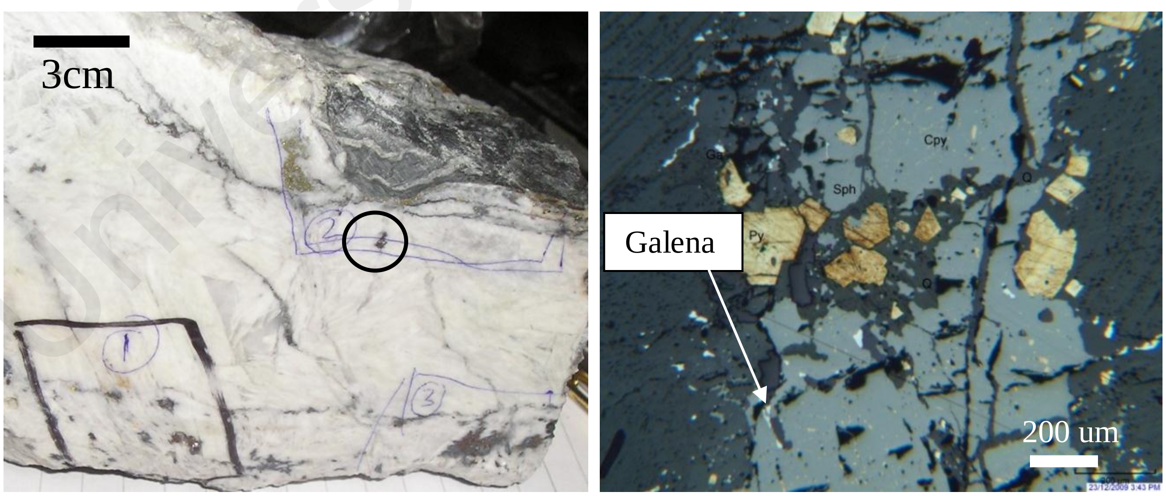

Figure 6.26: (Left) Small pieces of sphalerite in quartz carbonate vein in circle have been prepared for the polish sample. (Right) Photomicrograph of chalcopyrite diseases occur in sphalerite as a fine bleb. Fine particles of galena surrounding the fractured sphalerite. (Reflected light).

6.4.3.4 Chalcopyrite

6.4.3.4.1 Field observation

Chalcopyrite is the least abundant mineral among the five sulphide minerals. It can be found together with pyrite, galena and sphalerite hosted in D2 shear veins and faults (D3) related veins in low carbonaceous host rock such as sandstone dominant around the western limb of the Q3W ore zone and in felsite. It is not always associated with the occurrences of carbonate veins such as in Figure 6.27.

Chalcopyrite occurs as small blebs within laminated shear veins and as coarser grains in extensional quartz veins. It is commonly hosted in milky quartz and rarely in earlier grey/watery quartz. Chalcopyrite appears greenish in the form of an emulsoid on the vein surface. Locally, the abundance of this mineral is high but contains little gold.

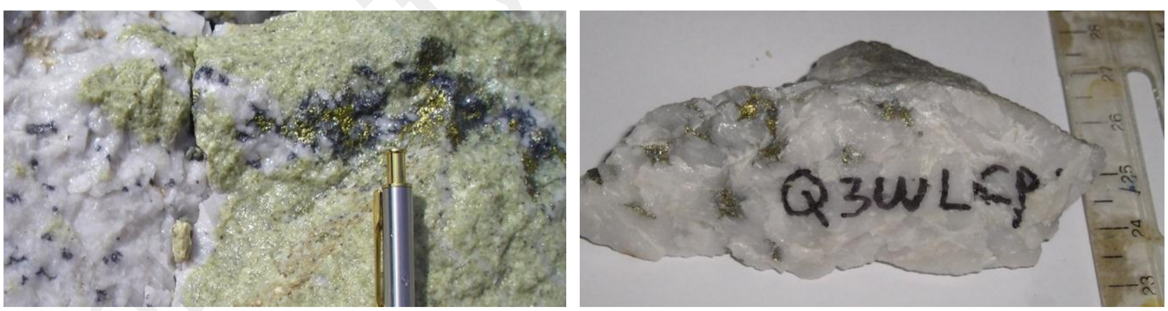

Figure 6.27: (Left) Occurrence of galena and chalcopyrite in extensional veins within intrusive rock. No association with carbonate veins. (Right) Spot of pyrite and chalcopyrite infill the fracture in quartz.

6.4.3.4.2 Microscopic study

Chalcopyrite appears light yellowish in the polish section in irregular form and size. This mineral is commonly observed with pyrite, galena, sphalerite and rarely with arsenopyrite. Most of the samples from Q3W veins that contain sphalerite also have small blebs (Figure

6.26B) or narrowly oriented blades of chalcopyrite in it as exsolution lamellae. This texture is also known as chalcopyrite disease.

Several researchers describe this intimate relationship of these minerals as a result of the replacement of Fe-rich sphalerite with by Cu-rich hydrothermal fluid (Bortnikov et al., 1991). However, other researchers (Kojima, 1990 in Bortnikov, 1991) suggest that the relationship of these two minerals is due to co-precipitation. This is based on the microprobe study of sphalerite in chalcopyrite diseased areas and compare to other areas, in which the iron content in sphalerite is the same. Chalcopyrite also infills fractures or cracks in stage 1 pyrite, arsenopyrite and sphalerite, together with gold indicates that it was formed later than those minerals.

6.4.3.5 Galena

6.4.3.5.1 Field observation

The occurrence of galena in mineral paragenesis is usually late. Its distribution is sparse in shear veins within the highly carbonaceous zone such as the Penjom Thrust (along the east limb and the western limb zone of Q1E and Q2E), and is relatively common in low carbonaceous ore zones of the Q3W western limb ore zone. However, only at Janik, galena together with pyrite and arsenopyrite can be observed relatively abundance in carbonaceous zone.

Galena hosted within quartz carbonate veins usually associated with other base metal sulphides such as sphalerite and chalcopyrite with pyrite and locally arsenopyrite while in veins containing less carbonate, it is usually associated with pyrite. Fine grained galena, also commonly found, accompanies visible gold in quartz carbonate veins. In veins, galena occurs as interlocking fine grains and filling along lamination features (Figure 6.25), or fractures in shear veins. Locally, galena infills the local breccias within the shear veins that dominated by milky quartz and forms dendrites (Figure 6.28 Left). Barren galena associated with coarse galena as in Figure 6.28 (Right). Galena shows a close correlation with visible gold but in the Janik area, Q1E shear vein is rich in galena but visible gold can be hardly found.

6.4.3.5.2 Microscopic study

Galena appears bluish white in polish section and occurs as fine to coarse aggregates infilling interstices in between grain boundaries as fine particles in quartz or carbonate and as filling of micro fractures in veins. Galena from the western limb of the fold shows almost no deformation features, but samples from Janik shear vein show a low degree of fracturing (Figure 6.29 Left) due to fault reactivation in that area. In Q2W galena is not observed within the active shear/ribbon but occur as small blebs in passive thicker part of shear vein (Figure 6.29 Right).

Figure 6.28: (Left) Band of dendritic galena infilling local breccias in a milky quartz vein. (Right) Coarse grain galena associated with calcite but not associated with gold.

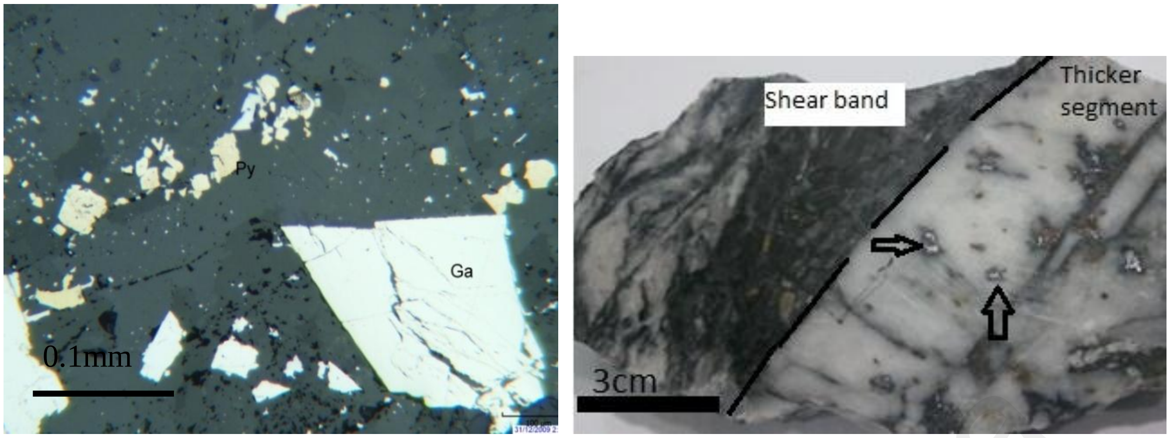

Figure 6.29: Left. Photomicrograph of galena (ga1b) in Janik area near the fold hinge is observed as fractured (reflected light). (Right) Sample Q3WL: Galena in thicker segment of vein and absent in the ribbon quartz.

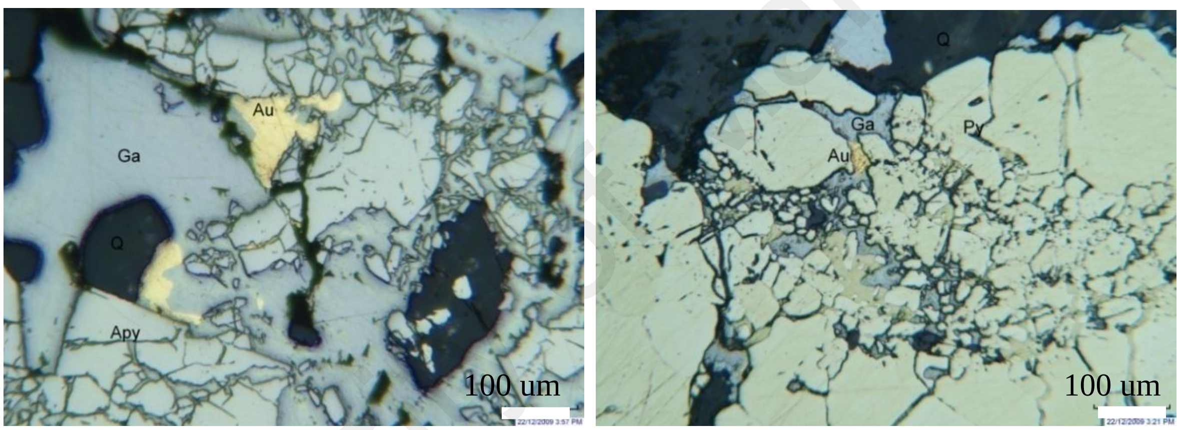

Figure 6.30: (Left) Photomicrograph of gold and galena infilling fractures in arsenopyrite. (Right) Photomicrograph of gold and galena infilling pyrite.

Galena from the western limb (Q3W) can be observed as infilling the shear margin as a tiny blebs (Figure 6.26 Right), infilling the fracture in pyrite, arsenopyrite and inter-grown with sphalerite (Figure 6.30) and chalcopyrite.

6.4.4 Gold

6.4.4.1 Field observation

Shear parallel veins in particular along or near the Penjom thrust (shear) host the main high grade and visible gold (Gorbett, 1999). These veins with laminations and ribbon texture are the earliest structure recognized in Penjom (Corbett, 1997; Fillis, 2000) and are later identified to be parallel to the bedding. Gold can be found along laminations and shear vein margins, replacing slivers of host rock (mainly carbonaceous shale) in veins or fractures inside veins. In the eastern limb, gold along the shear margin can be seen as effected by the movement of the shear, indicating that the shear process is still active after the gold deposition.

Gold occurs in three styles as free gold in veins, as interlocking grains or inclusions in sulphides (mainly pyrite and arsenopyrite) and as gold alloy such as electrum (gold with silver) and telluride (gold and tellurium). The last two can only be identified under microprobe study (Kamar Shah, 1994). Visible gold can be seen either in quartz only or in quartz-early carbonate (calcite) veins but not in late calcite vein.

Gold is closely related with pyrite, arsenopyrite with galena and sphalerite in the Q3W western limb, but in other areas such as eastern limb-Penjom Thrust, visible gold is associated with pyrite and arsenopyrite. There is a high correlation of gold with arsenic and this is supported by previous geochemical studies that suggest some early gold was introduced during the formation of arsenopyrite.

6.4.4.2 Microscopic study

Gold appears as bright or golden yellow in the polished section with irregular shape and size. As gold is very ductile and physically strong, it appears solid with no fractures compared with pyrite and arsenopyrite. Gold occurs as inclusion in quartz or early sulphide minerals such as arsenopyrite and pyrite. Gold also fills cracks in early sulphide (Figure 6.30), interstices and grain boundaries of quartz or local breccias, fractures (Figure 6.31) or micro-faults in quartz carbonate veins and along carbonaceous partings or laminations (Figure 6.32 Left).

Gold as inclusions in arsenopyrite and pyrite suggests the genetic and temporal relationship of gold with early sulphide minerals (Ramdohr, 1980). A similar observation was reported by Ariffin, (1994). Later veins process crosscutting the gold streak-bearing vein (Figure 6.32 Right) indicates that some early gold has been deposited during the development of shear veins before the brittle setting and later fractured infilling veins.

Figure 6.31: (Left) Gold in quartz carbonate shear vein forming a layer parallel to vein margin. (Right) Gold infilling fractures or breccias in vein that part of shear vein

.

Figure 6.32: (Left) Gold along the lamination has faulted/sheared effect indicating gold synchronously deposited during repeated opening and shearing of the bedding. (Right) Gold associated with pyrite within the wall rock inclusion and late quartz cross cutting the early quartz and gold band.

6.5 Vein and mineral paragenesis

6.5.1 Sulphide-gold paragenesis

Table 6.3 and Figure 6.33 summarises the structural paragenesis, including sulphide assemblages, mineralogy and structural events controlling gold-vein mineralization. The overall relationship improves previous mineral paragenesis studies by Ariffin (1994) and Corbett (1999).

6.5.2.1 Disseminated early syn-sedimentary and diagenetic pyrite

Disseminated subhedral to cubic pyrite occurs profusely in carbonaceous siltstone and shale and sparsely in other lithologies including intrusive rocks, especially on the footwall of the Penjom Thrust. Different host rocks occur in the hanging wall. The broad zoning of this sulphide is not related to quartz veining and possibly began as syn-sedimentary pyrite often associated with carbonaceous shale. Grain size is less than 1 mm and host rock bearing this mineral yields sulphur percentages of up to 1.0% (based on grade control assays). Framboidal pyrite can still be observed in carbonaceous shale (refer to Figure 4.19).

6.5.2.2 Quartz +/− carbonate-early sulphide gold (Fe, As, S +/- Pb, Zn) - Assemblage A

Pyrite and arsenopyrite were emplaced early and commonly show deformation features such as cataclasite, fractures, alteration, vugs, dissolution and corroded boundaries. However, pyrite and minor arsenopyrite also can be seen in fault related veins indicating multiple phases of sulphide. Shear veins from arsenopyrite rich Manik pit reveal some microscopic gold disseminated in arsenopyrite with grain size of less than 10 µm.

Pyrite occurs in all ore bodies and is closely associated with arsenopyrite. Gold occurrences are also commonly associated with pyrite, with or without base metal sulphides. Based on pit observations and the review of many core logs, high grade veins and all gold intercepts are usually rich with early sulphide minerals. Pyrite and lesser arsenopyrite are dominant as an aggregate in quartz veins ore and also disseminated in the altered zone outside the veins.

Free gold is common in shear veins either along carbonaceous parting, infilling fractures or local breccias in veins, compared with sheeted veins and in fault-related veins suggesting the consistent higher grade of these veins. Similar relationship can be observed in previous core logging by Penjom geologist during the exploration stage and by Corbett (1998). Vein structures that hosted early sulphides were described in early (exploration stage) core logging as graphitic parting, parallel vein, layering or shear zone indicates the ongoing deformation during ribbon vein formation.

Gold as inclusions is considered to have a temporal relationship with the host sulphide (Ramdohr, 1969). This interlocked gold contributes to some refractory ore in plant processing. From the Penjom experience, refractory ore is usually less than 5-10% can increase up to 10-15 % if the source is from Manik pit and is relatively moderate in Janik. Both ore bodies are considered to be structurally shallow. Silver content is also high in Manik pit, and the fineness of gold bullion can be as low as 780 if the plant feed are from Manik. No proper observations have been made in other areas. The study by Abdul Aziz (2007) indicates that the fineness of gold decreases from south to north. Based on structural understanding it could be from top to bottom as Manik is considered shallow ore.

6.5.2.2 Quartz carbonate-pyrite, minor arsenopyrite, base metal and gold (Fe, As, Pb, Cu, Zn, S) - Assemblage B

Quartz and carbonate occur as intergrowth or a separate band within single quartz carbonate vein in which carbonate can be occasionally slightly dominant compared to quartz. Galena, sphalerite, and chalcopyrite are common base metal sulphides associated with pyrite and minor arsenopyrite. Distribution of this assemblage is obviously significant in the third zone of the western limb (Q3W) shear veins and associated extensional veins. Galena can also locally be found in other areas such as in a Janik pit (around the apex of the folded carbonaceous shale).

Microscopic study shows that the base metal, typically galena, overprints the early sulphide within the deformed zone. In high grade veins, gold can be seen filling fractures in early sulphide and quartz together with galena. Visible gold is also quite common in this zone and always occur free or associated with pyrite, arsenopyrite, galena and to a lesser extent, sphalerite.

The dual relationship of gold with both early sulphides and later base metal mineralization suggests two mechanisms or times of gold emplacement. Gold that was already deposited as early gold, or in solid solution in early sulphide, was subsequently remobilized to form the gold interlock and later free gold. A second episode during continuous metamorphism or structural deformation together with late phase hydrothermal event has further remobilized the particulate gold or early free gold and deposited it a short distance along fractures in sulphides or quartz veins together with later stage base metal.

Reactivations of early shear vein structures, which could occur during both D2 and D3 events, provides the common pathway for the later base metal sulphide deposition. In this case, gold can be considered to have been transported by the later phase fluid, together with base metals. The very late stage fluid or residual fluid may still have precipitated the late base metal (chalcopyrite or galena) together with the gold that is commonly associated with vein modification and deformation, result in the late stage textures associated with the D3 deformation event.

6.5.2.3 Calcite galena veins

Calcite veins are a commonly found in filling brittle extensional (normal) faults within calcareous shale, but are also locally found filling fractures in other rock type or cross cutting earlier quartz carbonate veins. Calcite veins infilling extensional faults above the Penjom Thrust are locally associated with fine grained to massive galena (Figure 6.28 Right). Massive galena with calcite can also be found along the Penjom Thrust at the reactivation of the extensional fault along the Penjom Thrust ore zone.

This galena in calcite veins is without significant gold content and is considered to have been emplaced after gold mineralization. The geochemistry of the galena has been study in further detail by trace element analysis and lead isotopes.

Table 6.3: Structural phases, description of veins, gold content of the ore zones and the occurrence of sulphides. Ore grade – low: 0.5 to 1 g/t; medium: 1 to 3 g/t; high: 3 to 6 g/t; very high: >6 g/t). Py: pyrite; Apy: arsenopyrite; Ga: galena.

Deformation and vein		**Vein Type**	**Thick (cm)**	**Microscopic and primary mineralogy**	**Gold content**	**Sulphide**
Late Fault D4-D5	12	Fault fill veins (extensional)	0.1 to 15	Rhombohedral calcite, minor white quartz	Barren	Rare Ga,
	11	Phantom veinlet	0.1 to 0.3	White quartz or calcite	Barren	
Fault related vein D3 (Reverse-Dextral	10	Stockwork (competent/felsite unit at fault contact)	< 15	Euhedral to Subhedral, White to milky buck quartz	Low to medium,	Py, base metal, minot Apy
	9	Low to high angle sheeted vein	< 15	White to milky quartz, minor comb and euhedral to subhedral	Low to Medium,	Py, base metal, minor Apy
	8	Massive/thick extension vein	< 300	Massive, subhedral to euhedral, coarse grain, rare vug	Low to medium,	Py, base metal
	7	Brecciated bedding parallel shear reactivated by fault	< 100	Subhedral to anhedral, grey and milky quartz with carbonate vein, locally with dark straight line of stylolite, overprinted on D2 vein	Medium to very high,	Py, base metal, Apy (mainly in wall rock)
Fold and Thrust related vein D2	6	Bedding/ shear parallel vein (laminated only)- thin carbonaceous shale	<0.2	Anhedral, grey, milky quartz and carbonate with parallel stylolite	Low to high,	Py, Apy, base metal
	5	E-W sheeted vein (spatially not related to vein No 1, 2, 3, 4)	0.1 to 20	Euhedral to subhedral, milky quartz and minor carbonate, occasional comb texture	Low to medium,	Minor Py, base metal,
	4	Extension vein related to bedding shear vein	0.1 to 20	Euhedral to subhedral white quartz and carbonate, minor vug, (mainly E-W trending)	Medium	Py, base metal
	3	Sheeted vein in felsite and locally stockwork	0.1 to 30	Milky quartz, less carbonate except with occurrence of vein No. 7. Part of it are extension from vein No. 4	Low to medium,	Py, base metal
	2	Penjom Thrust shear vein	< 300	Anhedral, subgrain, neocryst, grey and milky quartz with carbonate (mainly calcite) vein,	Medium to very high,	Py, Apy
	1	Bedding parallel shear vein (Laminated, ribbon), thick carbonaceous unit	0.5 to 200	Grey, milky, anhedral quartz, polygonal subgrain, minor calcite in vein,	Weak to very high,	Py, Apy

Geological chronology					D0-D1	D2		D3	D3	D4-D5
					Regional metamorphism Early compression	**Fold and Thrusting**		**Reversed NNE parallel**	**Lateral NNE, NNW fault**	**Sinistral,Normal to Oblique NS fault**
					S_2 cleavage	**Early S_2**	**S_2**	**S_3**	**S_3**	
Stages		**Vein phase**	**Mineral occurrence**	**Gold Sulphide**						
Late	Stage 5	Calcite, quartz vein	Vein and veinlets	Cubic Ga						
	Stage 4	Phantom quartz	Veinlets							
Middle	Stage 3	Quartz Carbonate vein	Shear and extension vein	Py, Ga, Sph, Cpy, Au, APy						
	Stage 2c	Milky white quartz	Shear and extension vein	Py, Apy Ga, Sph, Cpy						
	Stage 2b	Grey and watery quartz	Shear vein	Py, Apy Au						
	Stage 2a	Sericite Pyrite-arseno-pyrite veins	Alteration and veins	Py, Apy						
Early	Stage 1	Early Pyrite	Diagenetic	Py						

Figure 6.33: Summary of several phases of structure, veins and sulphides mineral paragenesis. Py-pyrite, Apy-arsenopyrite, Ga-galena, Sph-sphalerite, Cpy-chalcopyrite.

CHAPTER 7 GEOCHEMISTRY OF VEIN AND ORE

7.1 Introduction

The geochemical analysis of vein, ore and host rock was conducted to understand the characteristics of vein and mineralization fluid. The geochemistry analyses are:

- Fluid inclusions of quartz vein
- Mineralogy of carbonate vein
- Wall rock alteration
- Multi elements (XRF)

7.2 Fluid inclusions

7.2.1 Introduction

The micro-thermometry study of fluid inclusions provide information on the temperature, depth of formation and pressure during vein formation and can be used to indicate the environment of mineralization. During the crystallization of vein material or overgrowths, fluid inclusions are trapped within the crystal as a cluster or along the growth zone. These inclusions are classified as primary inclusions. Fluid inclusion (FI) resulted by fluid trapped by the healing of fractures by later fluids is classified as secondary inclusion. These appear as linear features following healed cracks. Pseudo-secondary fluid inclusions are those which are trapped in cracks healed during crystal formation. They are not parallel to crystal boundaries but form internally within the crystal. Inter-granular fluid inclusions are similar to secondary inclusions, but could also be formed from a residual fluid left over after early crystallization. As the gold and sulphides are mostly associated with veins, analysis of vein features such as fluid inclusions provide the physico-chemistry information related to the ore forming fluid.

7.2.2 Previous fluid inclusions studies

The fluid process group (1992) report primary inclusion dominated by two phase aqueous (H_2O-salt) inclusion. Occasionally two or three phase carbonic (H_2O-CO_2-salts) inclusions are also present. Homogenization temperatures indicate fluid temperatures in excess of 200^{o}C which is cooling temperature during quartz precipitation and hence possibly during mineralization.

Ian Bogie (2002) reports primary inclusions in ankerite with homogenization temperatures as 410^{o}C and two patches of secondary inclusion with homogenization temperatures of 240-300^{o}C and 140-170^{o}C respectively. Given the higher homogenization temperatures of the primary inclusions, it is likely that these temperatures reflect condition during uplift and unroofing of the deposit rather than of the mineralization.

Makoundi (2012) reported many CO_2 bearing fluid inclusions in Penjom with salinity of 6 to 8 %NaCl and homogenization temperature of 250^{o}C to 300^{o}C. Laser Raman analysis also revealed a high content of CO_2 (up to 100 mole %) and one sample with N_2 rich (100 mole %).

7.2.3 Samples selection

Samples were taken from two stages of veins interpreted as having formed during folding and faulting events. Details of samples are given in Table 7.1. The mineralised veins host two common sulphide assemblages (assemblage A and B) from three types of vein structures as well as veins without the sulphide. They are early sulphide (assemblage A:

pyrite-arsenopyrite) and late sulphide (assemblage B: wall rock pyrite +/- minor Arsenopyrite + base metal in a vein).

Table 7.1: Sample for fluid inclusions represents different vein type and sulphide assemblage. Stage 1 vein is controlled by D2 deformation, Stage 2 vein by D3 deformation. Vein type based on Table 5.03. Sulphide assemblage as described in Chapter 6.5. Py-pyrite, Apy-arsenopyrite, Ga-galena, Sph-sphalerite.

Sample No	Vein Type	Vein description	Sulphide association observed	Sulphide assemblage	Veins phase
Z1	1	Shear vein, laminated, 5cm thick, white and grey, Q2WL	Py	A	Stage 1
Z2N	2	Extension vein stockwork, related to shear vein Z1.	Apy- Py (wall rock). Gold in quartz	A	Stage 1
Z3L	2	Extension vein, stockwork related to Q3WL shear vein	Sph, Ga, Py (wall rock)	B	Stage 1- reactivated during D3?
Z4EX3	2	Extension, sheeted vein in the felsite	Py in wall rock, Sph, Ga, Cpy in vein	B	Stage 1- deformed by D3
Z5JLA	3	Extension vein, sheeted vein below NE-NNE fault Jalis	Py, Ga, Sph, cpy	B	Stage 2
Z7Q2W	1	Shear vein, laminated, bedding parallel. Massive/white and ribbon/grey	Apy	A	Stage 1
Z8F	3	Extension vein, hydrothermal breccias vein along NE fault	Py, Ga, Py wall rock	B	Stage 2

Assemblage A is commonly found in shear veins (stage 1) and assemblage B in extensional veins (stages 1 and 2) but also in shear veins. A summary and description of seven samples containing fluid inclusion are tabulated in Table 7.1. Other samples are quartz vein at the hanging wall (Z14HW) and two calcite veins representing brecciated calcite (ZX4) and late calcite (ZX6). No significant fluid inclusion can be found in calcite samples and only very small one phase inclusions are found in hanging wall veins. A total of ten samples were prepared by double polished wafers for analysis of fluid inclusions. SEM Cathodoluminescence (CL) imaging analyses were also conducted on these samples. Analyses were conducted at the Earth Science Department, James Cook University, Townsville, Australia.

7.2.4 Fluid inclusion petrography

7.2.4.1 SEM- CL imaging and crystal growth

All doubly polished wafers of quartz were examined under optical microscope to locate fluid inclusions. The best fluid inclusion populations were marked for SEM CL analysis and thermometry analysis. Scanning electron microscopy-cathodoluminescence (SEM-CL) is used to study crystal growth that cannot be observed in SEM alone, and is used for comparison with optical images of the same area showing the pattern of fluid inclusions. Vein growth and the pattern of inclusions indicate whether the fluid inclusion trail or cluster is secondary or primary. Two D2 extensional vein samples (sheeted vein) show the crystal growth such as in Z4EXT (vein with base metal sulphide) and Z2N. The latter is highly deformed with fractures and shear planes. No fluid inclusion patterns match the growth zone. CL imaging shows later fluid seals many of the earlier vein fractures. Zone of trails that coinciding with fracture planes can be observed in many earlier veins. Shear veins with ribbon texture (Z1) do not show any crystal growth, possibly due to crystallization of finer grained quartz associated with shearing and fractures. CL images shows fractures being sealed similar to other extensional vein samples and coincides with the zone of inclusions trail (Figure.7.1). However, deformation could be by the ongoing shearing along the shear vein and can be categorized as D2 deformation. Less deformed Z3L (vein with base metal) samples show only a massive appearance, possibly due to coarser quartz grains and lack of systematic vein growth during crystallization in confined space, texturally described as buck quartz.

7.2.4.2 Microscopic observation

The majority of the inclusions are less than 4um and not suitable for micro-thermometry analysis. Recommended size for the fluid inclusion study is more than 4 micron (um) for two phases (Shepherd, et. al, 1985). However, several samples contain at least one sizeable inclusion for micro-thermometry study. Several images of fluid inclusions are shown in Figure 7.2. Fine fluid inclusions forming trails dominantly in D2 veins such as Z1, Z2N and Z4EX3 commonly intercepting each other (Figure. 7.2A) are classified as secondary inclusions. A few coarse and measureable inclusions occur along this trail. Clusters of intra-granular inclusion ranging in size between 5.5 and 11 microns can be observed inside the rims of very fine inclusions and can be used for micro thermometric analysis, such as in Z3L, Z7Q2W and Z5JA. In these samples, variables sizes of the vapor phase were observed. L: V ratios in between 6:1 to 1:3. Rare CO_2 monophase vapors of Type 4 were also observed (Figure 7.2G). Only a few fluid inclusions are bigger than 8um and are vapor rich, such as in samples Z7Q2W (Fig. 7.2II) and Z3L with L: V ratio 1:1 to 1:2. Several inclusions are irregular shape and necking down is indicative of deformation effect.

7.2.5 Distribution of fluid inclusions

The occurrence of inclusion can be observed as a zone or trail across the grain, along the grain boundary, or are inter-granular or a cluster within the quartz grain or intra-granular. The size of the quartz grains is variable. Four types of fluid inclusions as observed at room temperature in decreasing order of abundance are:

a) Type 1 inclusions: Liquid-vapor (H_2O) L>V
b) Type 2 inclusions: CO_2 bearing (CO_2>H_2O)
c) Type 3 inclusions: CO_2 bearing (CO_2<H_2O)
d) Type 4 Monophase H_2O
e) Type 5 inclusions: Monophase or dominant carbonic (CO_2+/-CH_4)

Type 1 and Type 5 occur in all samples either as cluster or intra-granular (Figures 7.2 D, F), inter-granular or zone of trail within or across the grain boundary indicative of primary, pseudo-secondary or secondary fluid inclusion respectively. Inter-granular made up of very small inclusion and are not suitable for analysis. Vein not containing sulphide also lack measurable fluid inclusions and absent of CO_2 bearing fluid inclusions.

7.2.5.1 Shear vein (stage 1)

In a part of shear vein (Z1), fractures zones were observed which coincide with an inclusion trail. Inclusion trails in shear veins are interpreted as related to ongoing movement or shearing, and are formed during the introduction of residual fluid sealing the fractures during the same or a later event. All inclusions studied in this sample are small type 1 inclusion (<3 to 6um). Some Type 5 (Monophase H_2O) inclusions occur as a cluster, zone or trail within the grain or along the grain boundary indicating primary, pseudo-secondary or secondary inclusion origin.

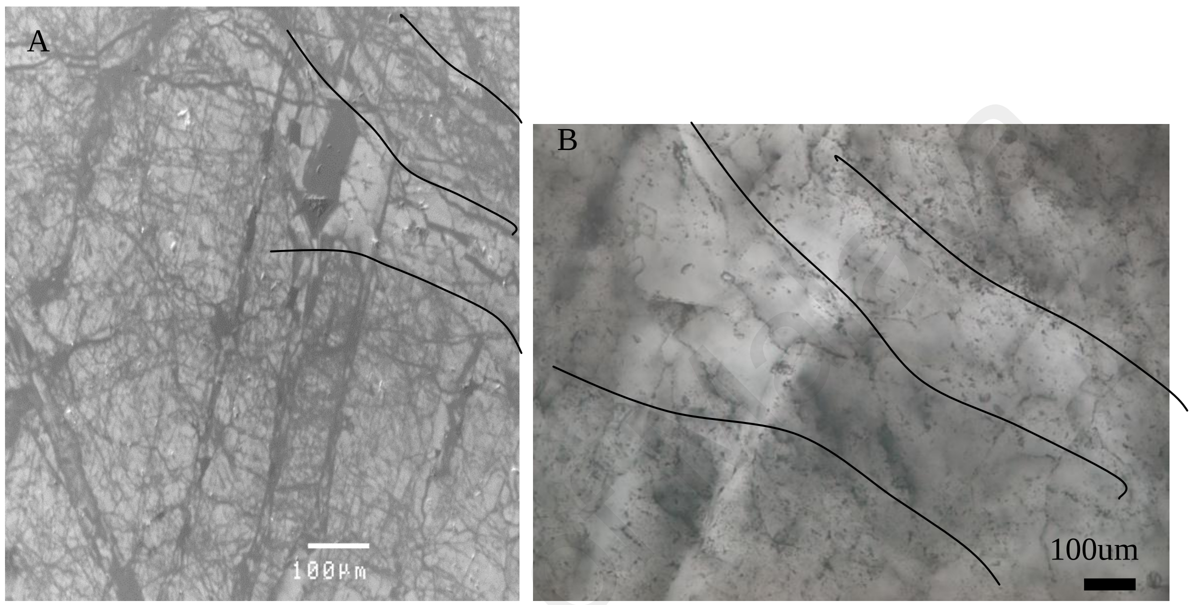

Figure 7.1 Fractures zone in shear vein shown by low angle string outline and overlapped with zone of trail inclusion. Vertical fractures are less coincided with zones of trail. (A) SEM CL image. (B) Under reflected light.

On polished wafer specimen Z1, a whitish late carbonate veinlet can be observed cross-cutting the shear or laminae (refer to Fig. 6.13) fabric and are neither deformed nor host to any visible inclusions. The veinlet is considered to be post shearing, or related to a phantom veinlet. Another shear vein sample Z7Q2W is host to arsenopyrite and pyrite along the laminated portion. 21 measurements were made on large inclusions (5.5um to 11.5um). Both Type 2 and Type 3 CO_2 bearing inclusions in addition to Type 1 can be observed. Total homogenization of CO_2 liquid and vapor can be easily seen in type 3, but only thin double bubbles are shown in type 2. Both are characterized by higher Temperatures of Final Homogenization (T_h final). Very few vapor CO_2 dominant fluid with dark rims of aqueous or carbonic vapor, identified as Type 4, can be observed in this sample (Figure 7.2 G and 7.2H). Many of the CO_2 inclusions are scattered within intra-granular zones and rarely along trails indicative the primary nature of these inclusions.

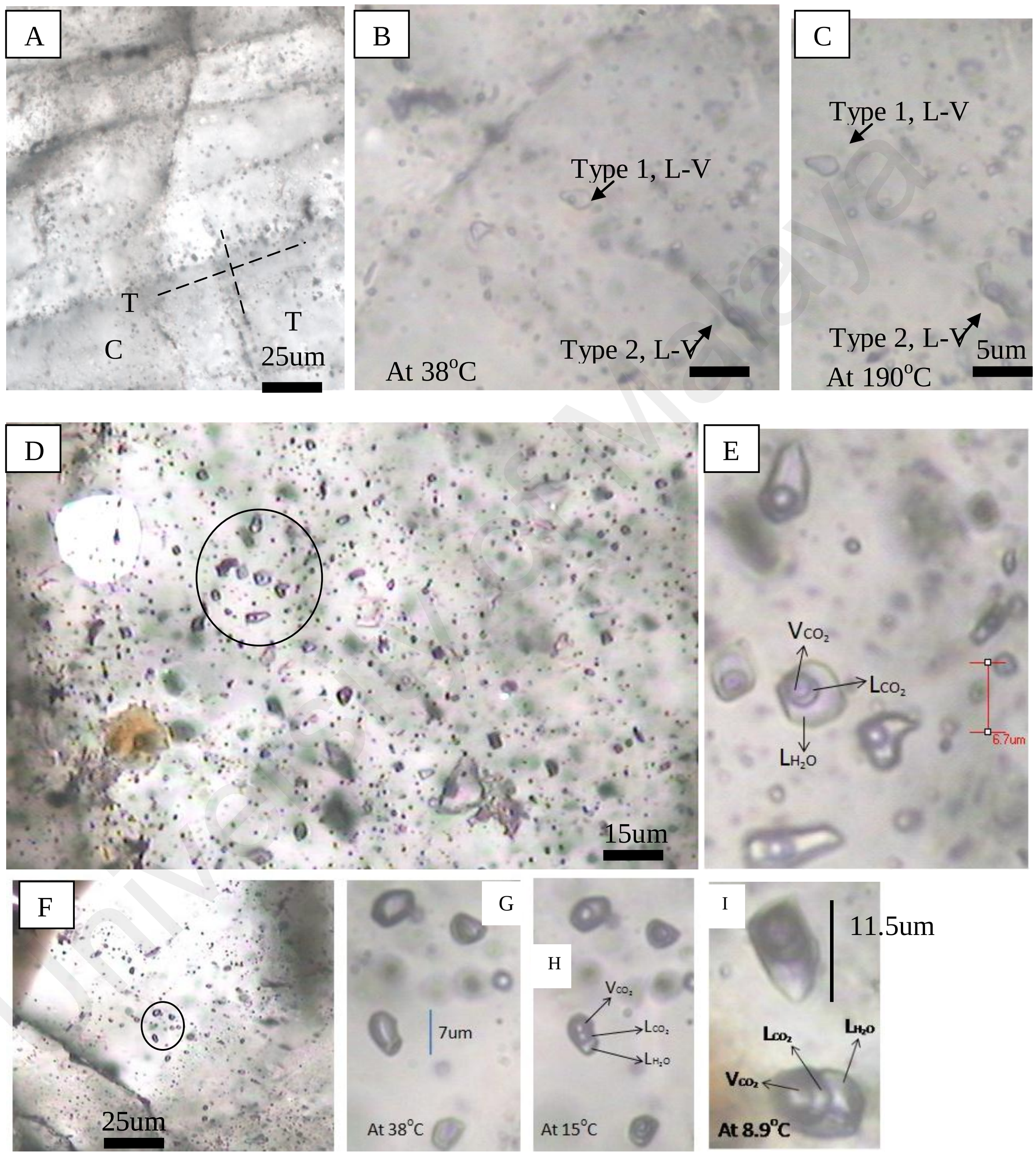

Figure 7.2 (A) Sample (Z2N), extension vein-Stage 1: Several trails (T) of inclusion and cluster (CL) within the grain. Trail mainly L-V of Type 1 inclusion and cluster made up of L-V of Type 1, 2 and 4. (B) Extension vein, stage 1: Occurrence of both Type 1 L-V and Type 2 L-V inclusion along trail. (C) Similar sample: Type 1, L-V homogenized at 189°C and Type 2, L-V still preserve the inclusion. (D) Shear vein, stage 1: Cluster of Type 2 and

Type 3 L-V inclusion. (E) Close up view of photo D: Coexistence of Type 3 L-V with double-bubble of CO_2 inclusion and Type 2 L–V with dark rim. (F) Shear vein, Stage 1: Overall view of photo G and H containing inclusion forming as a cluster. (G) Close up of photo F. Top two inclusions are vapor rich of Type 5 and bottom two are Type 3 V-L. (H) Inclusion at 15^oC showing the formation of CO_2 liquid and vapor in all inclusions.

7.2.5.2 Extension veins (Stage 1)

Z3L is a sample of extensional hydrothermal quartz breccias related to bedding plane shear, hosting sphalerite and galena, which represents the base metal sulphide vein with pyrite disseminated in the wall rock. This sample is host to several bigger inclusions mainly type 2 and type 3. A total of 28 measurements were taken and at least 12 CO_2 inclusions were identified as evident by double bubbles forming at 15^oC and higher CO_2-H_2O final homogenization temperatures. Type 2 and Type 3 CO_2 inclusions were found mainly in clusters or in intra granular spaces but some type 2 inclusions were found as trails (Figures 7.2B and 7.2C). Type 1 inclusion (L>V aqueous) also occurred in similar patterns and in trails. Z2N is from an extensional vein infilled brittle fracture related to the interception of shear veins and felsite intrusion. Fine inclusions of type 1 and type 5 occur in inter granular zones and in trails parallel to micro fissures.

CO_2 bearing inclusions of type 2 occur in intra granular space or in clusters and are characterized by higher clathrate melting and final total homogenization temperatures (Th). Nine measurements were taken with this sample, including one Type 3 inclusion and six Type 2. Sample Z4EX3 is from an extensional vein in a felsite intrusive and host to galena and sphalerite, with pyrite in wall rock contact. Inclusions are small and only three measurements were taken, one Type 1 aqueous inclusion and two Type 2 CO_2 bearing inclusions were measured. The latter is characterized by higher T_h (>300^oC) and were found in a cluster or in intra granular space. Other inclusions are small and were mainly Type 1 and Type 4 inclusion found in trails related to all stages of deformation events.

7.2.5.3 Extension vein (Stage 2)

Sample Z5JLA is from a sheeted extension vein related to the NNE faulting event (D3) within The Jalis Corridor. 23 measurements were taken, twelve from CO_2 bearing inclusions as indicated by higher clathrate melting T_mClath (3 to 6.7^oC) including five Type 3 CO_2 bearing inclusions having liquid and vapor CO_2 (double bubbles) at a temperature of 15^oC. The rest of the inclusions observed were Type 1 which occurs in inter-granular space, and as trails, as well as intra-granular clusters. Sample Z8F was taken from hydrothermal quartz breccia related to the NE fault in the Jalis corridor, representing the D3 deformational event associated with base metal sulphides. Only a small portion of the vein contains sizeable inclusions suitable for measurement. The majority are small either monophase Type 4 or Type 1 inclusions. Both occur as intra-granular or cluster. Seven two phase inclusions measured from the sample show T_h in between (220-320^oC) hence are regard as CO_2 bearing Type 3.

7.2.6 Thermometric measurement and results

Thermometric experiments are using a petrographic Carl Zeiss binocular microscope equipped with LINKAM MDS600C heating and reducing stage capable of +/-2^oC accuracy (Figure 7.3). Liquid nitrogen was used to lower the temperature in the chamber through a vessel where a small chip was placed. The temperature raised by an electric current that heated the air in the chamber. The temperature was monitored to an accuracy of 0.1^oC at the expected phase transition. Calibration is based on synthetic inclusions with last ice melting of 0.3°C and T_h of 374.8°C. To avoid decrepitating, freezing experiments were carried out first before heating. Temperatures were also regularly lowered to 15°C to identify double bubbles indicative of CO_2 bearing inclusions.

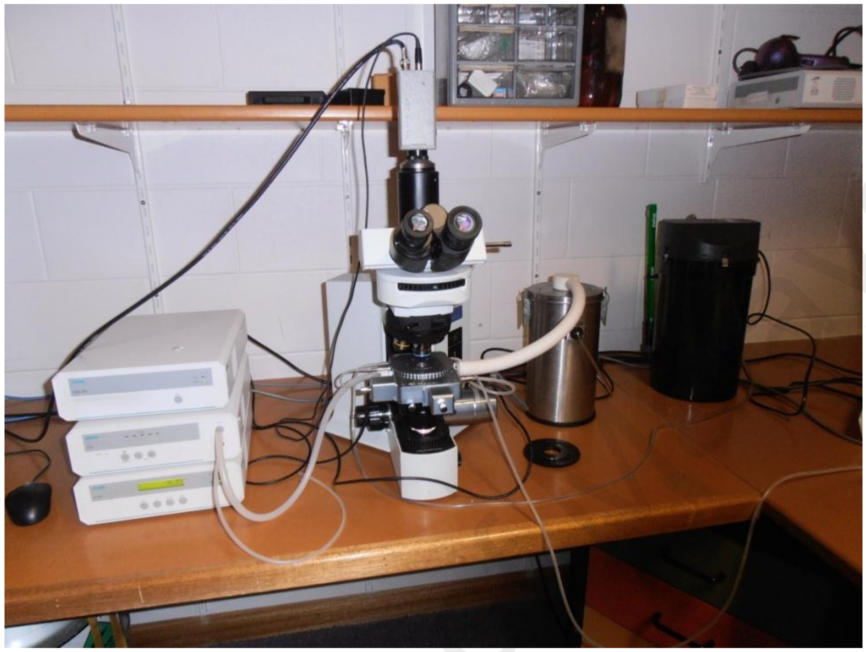

Figure 7.3: Thermometric experiment of fluid inclusion is using LINKAM MDS600C with Olympus camera attached.

Temperatures where phase transitions inside the inclusion were observed as well as physical observations including shape, size and phase ratio. Various phase transition seen during freezing and heating are:

1-First melting of ice ($T_m$ice).

2-Last melting of ice and clathrate (T_m ice/$T_m$clath).

3-Total homogenization temperature of CO_2 inclusion (T_hCO_2).

4-Final homogenization temperature of liquid-vapor or H_2O-CO_2 (T_hFinal).

Observations were focused on inclusions more than 5um in diameter which were the suitable size to study the fluid inclusion accurately especially for CO_2 bearing inclusion.

Despite the lack of inclusion of such size in certain samples, several important samples yielded sizeable and good inclusions for micro-thermometry such as Z3L, Z7Q2W and Z5JLA, representing veins from two different phases of deformation and two types of sulphide assemblages. Ninety-nine measurements were been recorded in all seven samples. Summary of results as in Table 7.2 are plotted in several histograms and graph. Figure 7.4 shows a plot of temperature of final homogenization for all result.

Table 7.2: Summary of micro-thermometry results

Type	**Type 1**	**Type 2**	**Type 3**	**Type 4**	**Type 5**
Shear vein-Stage 1	T_mIce-9 data (-8 to -0.6^{o}C) T_hFinal-8 data (140 to 278^{o}C)	T_mClathrate-9 data T_hFinal-9 data	T_mClathrate-8 data (1 to 6.7^{o}C) T_hCO_2-8 data T_hFinal-8 data (250-378^{o}C)	T_hCO_2-2 data (23.3-23.5^{o}C)	No record
Extension vein-Stage 1	T_mIce-10 data T_hFinal-10 data	T_mClathrate-14 data (0 to 8.0^{o}C) T_hFinal-14 data	T_hCO_2-5 data 23.3-26.7^{o}C		
Extension vein-Stage 2	T_mIce-11 data T_hFinal- 11 data	T_mClathrate-12 data T_hFinal-12 data	T_hCO_2-4 data		

7.2.6.1 Freezing and heating experiments

Condition of inclusions at room temperature was observed and photographed for comparison with other phase transition during freezing and heating. Temperature was lowered to around 15^{o}C and phase changes of the inclusions were observed. CO_2 bearing Type 3 inclusions transformed to double bubble as CO_2 liquid-vapor in a H_2O aqueous. Type 2 display a dark rim surrounding the vapor while other H_2O liquid-vapor inclusions remained unchanged. The temperature was then reduced gradually down to -90^{o}C. At this stage H_2O +/- CO_2 froze to solid ice and normally the shape of the inclusion becomes distorted, the boundary becomes irregular or it shrinks smaller size compare to the shape at room temperature.

Type 1 inclusions:

On heating, the first melting of the solid phase can be observed at -20^{o}C. However, the change is difficult to observe and this measurement was not systematically recorded. The temperature of last ice melting ($T_m$ice) and other transitional phases upon heating was recorded. In all samples, many small inclusions from 4.5 to 9 micron can be observed as Type 1 with $T_m$ice less than -1^{o}C, indicative of H_2O-NaCl fluid composition. The Last Ice Melting ($T_m$ice) is indicated by the restoration of the distorted inclusion back to its shape at room temperature. Continued heating to 140 to 200^{o}C causes the liquid phase homogenized into the vapor phase. This temperature is recorded as Temperature of Final Homogenization ($T_h$final).

Type 2 inclusions:

The inclusions are characterized by a dark rim at temperatures around 18^{o}C. The first ice melting is not clearly observed and was not recorded. The temperature of last ice melting is higher than those obtained in Type 1. The temperature of final homogenization is also higher than Type 1 (commonly above 200^{o}C). This inclusion may contain clathrate CO_2-H_2O composition as a phase.

Type 3 inclusions:

These inclusions can be up to 11.6 µm in size. The condition at room temperature was recorded and photographed. On cooling to 18^{o}C, double bubble would appear, indicating a Type 3 inclusion. When frozen to -75^{o}C, the fluid freezes into a single solid phase. First melting of solid CO_2 occurs at around -57^{o}C. Similar to type 1, the physical changes at this temperature are not clearly observed, hence is not routinely recorded.

Clathrate formation overshadows the last ice melting so that the $T_m$ice was not visible. Last clathrate melting ($T_m$clath) is at a range between 3.2 to 6.7^{o}C. In Type 3 inclusions in which CO_2 liquid-vapor are visible, after further heating, the homogenization temperatures of the two phases are recorded. All CO_2 inclusions normally homogenize into the dominance phase of either liquid or vapor between 23.5 to 26.8^{o}C. Vapor rich inclusions are dominant, and have higher $T_h$final from 250 to 350^{o}C. Inclusion with invisible CO_2 liquid-vapor phase boundaries at 15^{o}C shows $T_m$clath in between 0^{o}C to 8^{o}C. These inclusions have fluid compositional of H_2O-NaCl-CO_2.

Type 4 Monophase (L or V) aqueous fluid inclusions

Monophase aqueous inclusions do not show any phase change during the experiment hence no thermometry data were recorded. These inclusions are usually small <2 µm) and occur in variable conditions indicate their formation during vein growth, during grain boundary fluid migration and later healing of fractures in veins.

Type 5 Monophase/ vapor dominant (CO_2 bearing) fluid inclusions

In arsenopyrite bearing shear veins, several inclusions with a dark rim around the inclusion were observed as being vapor rich. In a few inclusions a very thin meniscus of the aqueous phase is developed around the vapor inclusion and is considered as Type 4: Dominant vapor. Upon cooling to 15^oC, two phase (liquid and vapor) were formed, indicating that inclusions are dominant CO_2 bearing. The size is in between 6 to 8um with oval shape. Upon cooling, a slightly distortion in shape can be observed. Final clathrate melting can be observed at 4^oC and the homogenization of CO_2 bubble at 23^oC. The thin rim disappears at 292^oC and this marks the temperature of final homogenization ($T_h$final). Other rare Type 4 monophase inclusion without the rim of an aqueous phase shows a vapor bubble at 15^oC which again indicates a CO_2 bearing inclusion. Temperature of CO_2 homogenization is recorded at 23.5^oC.

A plot of T_m (ice)/Clathrate vs. T_h final indicate three populations of fluid inclusions (Figure 7.5). Population 1 shows high Th (more than 200 to 350^oC) and positive T_m clathrate. Population 2 shows low T_h (140 to 200^oC) and $T_m$ice of below 0^oC (-4 to -1^oC). Population 3 has $T_m$ice or clathrate similar to population 1, but $T_h$final similar to population 2. This population might be considered to be transitional between the two main populations. The data recorded is as follows: high $T_h$final and low $T_m$ice (278^oC and -2^oC, 250^oC and -0.6^oC) or low $T_h$final and high $T_m$ice/clathrate (185^oC and 4^oC, 150^oC and 3^oC, 190^oC and 3^oC, 165^oC and 0.5^oC, 178^oC and 2.2^oC). 10 data falls into this category.

7.2.7 Discussion

7.2.7.1 Fluid composition

As can be seen in Figures 7.5 and 7.6, two main groups of thermometric measurement data can be obtained with a few transitional in between them. These ranges of temperature represent H_2O-NaCl-CO_2 for population 1 and H_2O-NaCl for population 2. The equations used by Diamond (1992) were used to calculate salinity calculation for CO_2-bearing and aqueous inclusions respectively. Plots of salinity data against temperature of final homogenization are in Figures 7.5 and 7.6. Plot shows two groups of data cluster indicate two possible fluid compositions. Co-existence of two fluid compositions may indicate the involvement of fluid un-mixing during the mineralization process. The equation salinity for CO_2 bearing aqueous Type 2 and 3 inclusion as follow:

Salinity (wt% NaCl) = 15.6192 - 1.1406 T_{mClath}- 0.035 (T_{mClath})2 - 0.0007 (T_{mClath})3

(T_{mClath}=Temperature of last ice melting)

The equation for Type 1 aqueous inclusions is as follow:

Salinity (wt% NaCl)= (-1.78T_m)-(0.00442T_m^2)-(0.000557*T_m^3)

(T_m=Temperature of last ice melting)

a) NaCl-CO_2-H_2O (+/-CH_4)

Inclusions in both arsenopyrite and base metal sulphide bearing quartz veins contain this fluid composition. Both shear and extension vein contain fluid inclusions that give similar results, indicating that early and later stages of vein emplacement are both associated with CO_2 bearing fluids. By using the above formula, the salinity of CO_2 bearing aqueous inclusions of Type 2 is in a range from 8.9 to 15.6 wt% NaCl with one data of 3.9 wt% NaCl and Type 3 between 6.2 and 11.6 with one inclusion at 14.4 wt% NaCl. Low T_mClath corresponds with higher salinity.

b) H_2O-NaCl

Thirty one inclusions have low last ice melting Temperature (T_mIce) from -8 to -0.6^oC, indicative of an aqueous-salt system. Seven inclusions have temperature of final homogenization in between 207^oC and 278^oC. Based on the above equation, the salinities of the aqueous inclusion are in the range of 1.0 and 11.6 wt% NaCl.

The CO_2 and H_2O are believed to be from the same fluid and trapped simultaneously together during the formation of mineralised veins. Except for secondary H_2O inclusions which occur as a trail, the other H_2O inclusions can be primary and coexist with the CO_2 bearing fluid. The former gave lower T_h compare to the CO2 bearing inclusions inclusion.

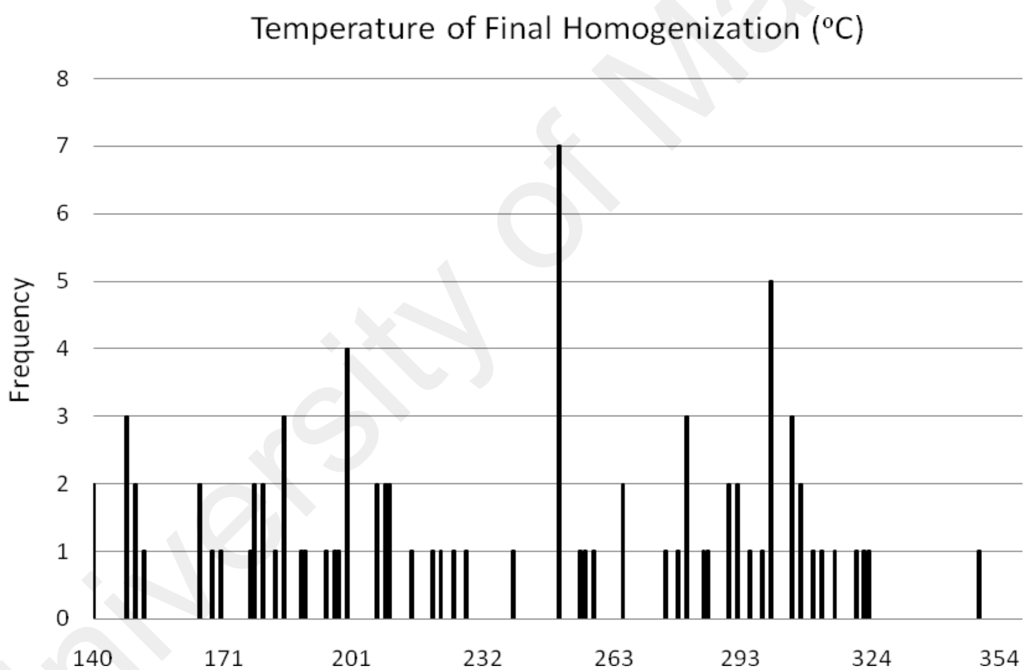

Figure 7.4: Temperatures of final homogenization (T_h) obtained from all samples (85 data).

7.2.7.2 Temperature and pressure condition

Thermometry measurement from H_2O-NaCl system may represent trapping temperatures of the inclusion during the formation of vein. However for NaCl-CO_2-H_2O system, the temperatures of homogenization only represent the minimum trapping temperatures. The temperatures of final homogenization obtained are from 195°C to 323°C (means 264°C). Depth of formation and pressure cannot be directly calculated from micro-thermometry data because no data was recorded for first melting temperatures of CO_2 bearing inclusions. Based on Figure 7.6, ore fluid mechanism involved is mainly an isothermal mixing (after Shepherd et al., 1985).

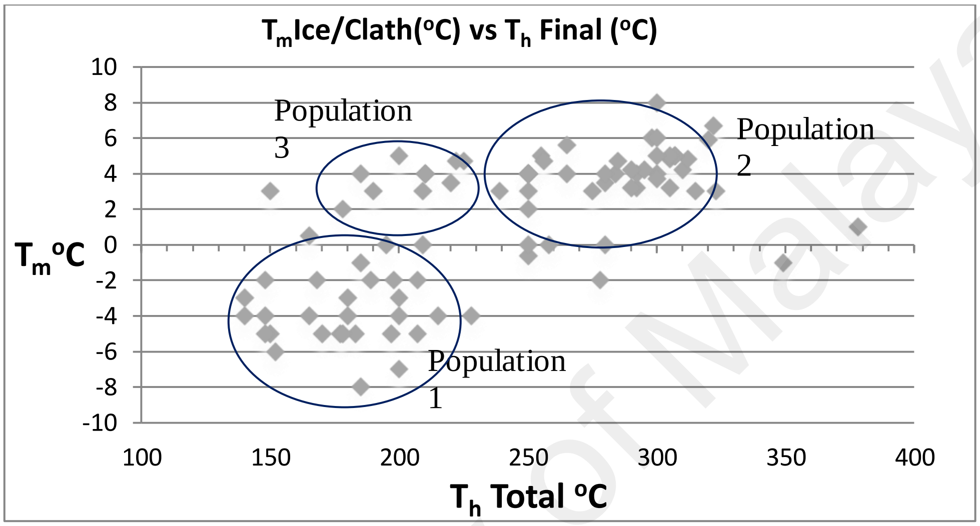

Figure 7.5: Final melting temperatures of Ice and Clath (T_m) plotted against temperatures of final homogenization (T_h) (85 data).

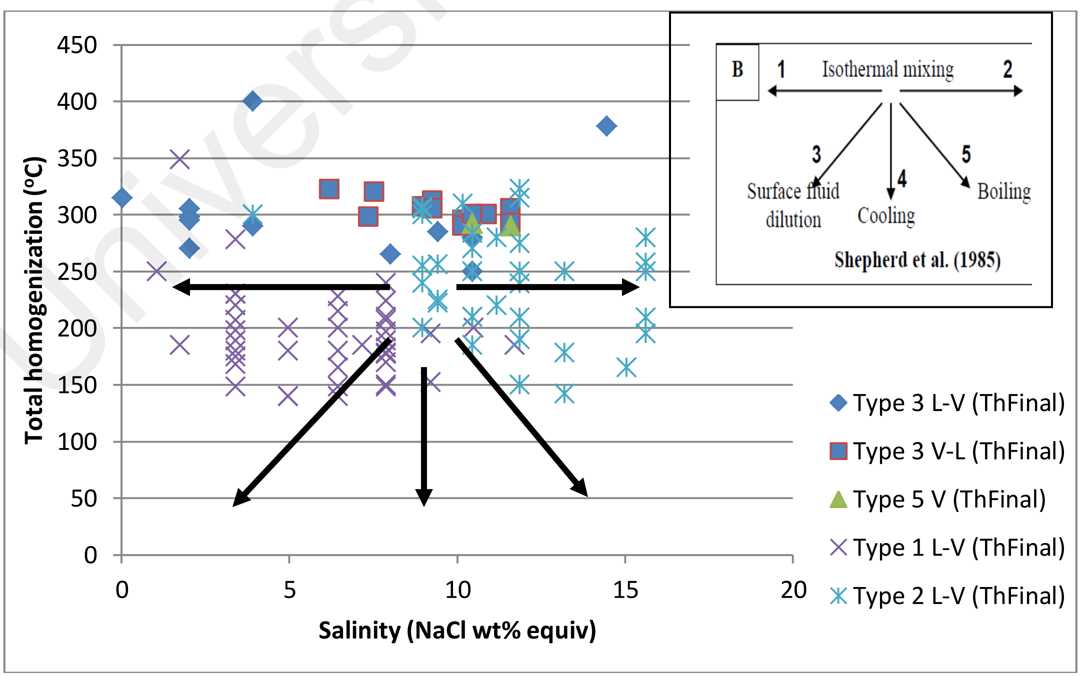

Figure 7.6: Final homogenization temperatures (T_h) plotted against salinity.

7.3 Geochemistry analysis of carbonate minerals in veins

7.3.1 Introduction

At many places at Penjom, carbonates are associated with quartz in veins in varying proportions. In some places, carbonate was emplaced earlier and cross cut by later quartz. Macroscopic and microscopic observation has been described in chapter 6 (mineralogy). Geochemical analyses of quartz carbonate veins were conducted to confirm visual observation by utilizing XRD analysis at the Geology Department, University Malaya.

7.3.2 Quartz carbonate vein

These veins contain mineralised quartz and carbonate which in many places are intergrown, embedded within quartz or cross cut each other. Calcite is usually the dominant carbonate within the vein, but dolomite has been detected through XRD analysis. Result of XRD analysis is summarized in Table 7.3. Analysis of total carbon and organic carbon of certain vein samples has been carried out to determine the content of inorganic carbon in vein that represents the carbonate carbon (Table 7.4). This analysis was conducted at Penjom gold mine lab. Ankerite associated with quartz vein has been reported by Bogie (2002). However, this XRD study confirmed calcite as the most common carbonate mineral while ankerite only occurs as thin networks infilling fractures within the vein.

7.3.3 Samples for analysis

Details of the analyses of the samples from the main ore body and hanging wall area are shown in Tables 7.3 and 7.4. The Q3WL vein is the main calcite dominant quartz carbonate vein located in the KE pit bottom. Analysis shows that higher inorganic carbon indicates higher carbonate content, which in turn correlates with higher gold grade. Carbon content determination was performed at Penjom lab by using the ELTRA CS 800 (Carbon Sulphur Analyzer). Figures 7.8 to 7.10 show the results of the XRD analysis. Calcite is also the main carbonate mineral in the hanging wall and along the post mineralisation fault (ZX6 and ZX7). Samples Q1Jn (Figure 7.7) and Q2Jn are also from mineralized zone.

Table 7.3: Results from XRD analysis. Some of the vein samples are the same with Table 7.2.

Sample No	Mineralogy from XRD	Sulphide	Area
Q3WL (1)	Quartz, Calcite, Ankerite	Sphalerite, galena	Mineralized zone
Q3WE	Quartz, Ankerite	Pyrite	Mineralized zone
Q3WL (2)	Quartz, Calcite	-	Mineralized zone
ZX6	Calcite, high Magnesium Calcite	-	Hanging wall, barren
ZX7	Calcite, high Magnesium Calcite	-	Hanging wall, barren
Q1Jn	Calcite, Dolomite, Ankerite	Galena	Mineralized zone
Q2Jn	Quartz, Calcite, Dolomite	Galena, pyrite	Mineralized zone

Table 7.4: Total carbon percentage in vein sample reflected the inorganic carbon from quartz carbonate vein in various ore zone (analysis at Penjom Lab).

Sample No	Au (g/t)	% Total Carbon	% Organic Carbon	% Inorganic Carbon	% Sulphur	Area
Q3WL	131.4	7.41	0.13	7.28	0.24	KE
Q3WA	11.4	0.74	0.14	0.6	0.94	KE
Q2Mn	11.4	2.46	0.16	2.30	2.05	Manik
Q1Jn	10.26	4.28	0.16	4.12	0.49	Janik
Q2Jn	0.58	1.49	0.12	1.37	0.59	Janik
Q2E KN	7.62	3.81	0.37	3.44	0.53	KN

Figure 7.7: Calcite vein with gold. Gold infilling brecciated portion of the vein (sample Q1jn).

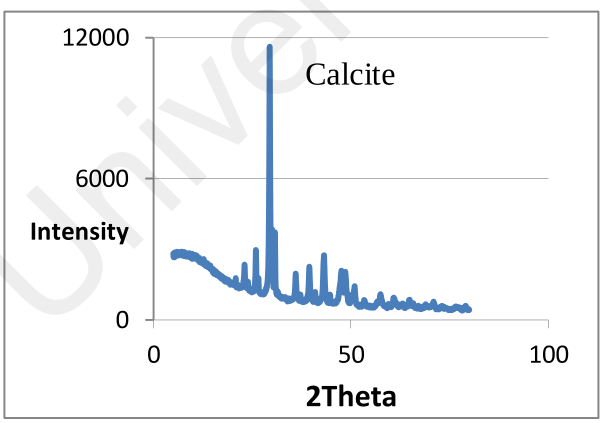

Figure 7.8: XRD analysis of sample Q1jn with higher calcite peak.

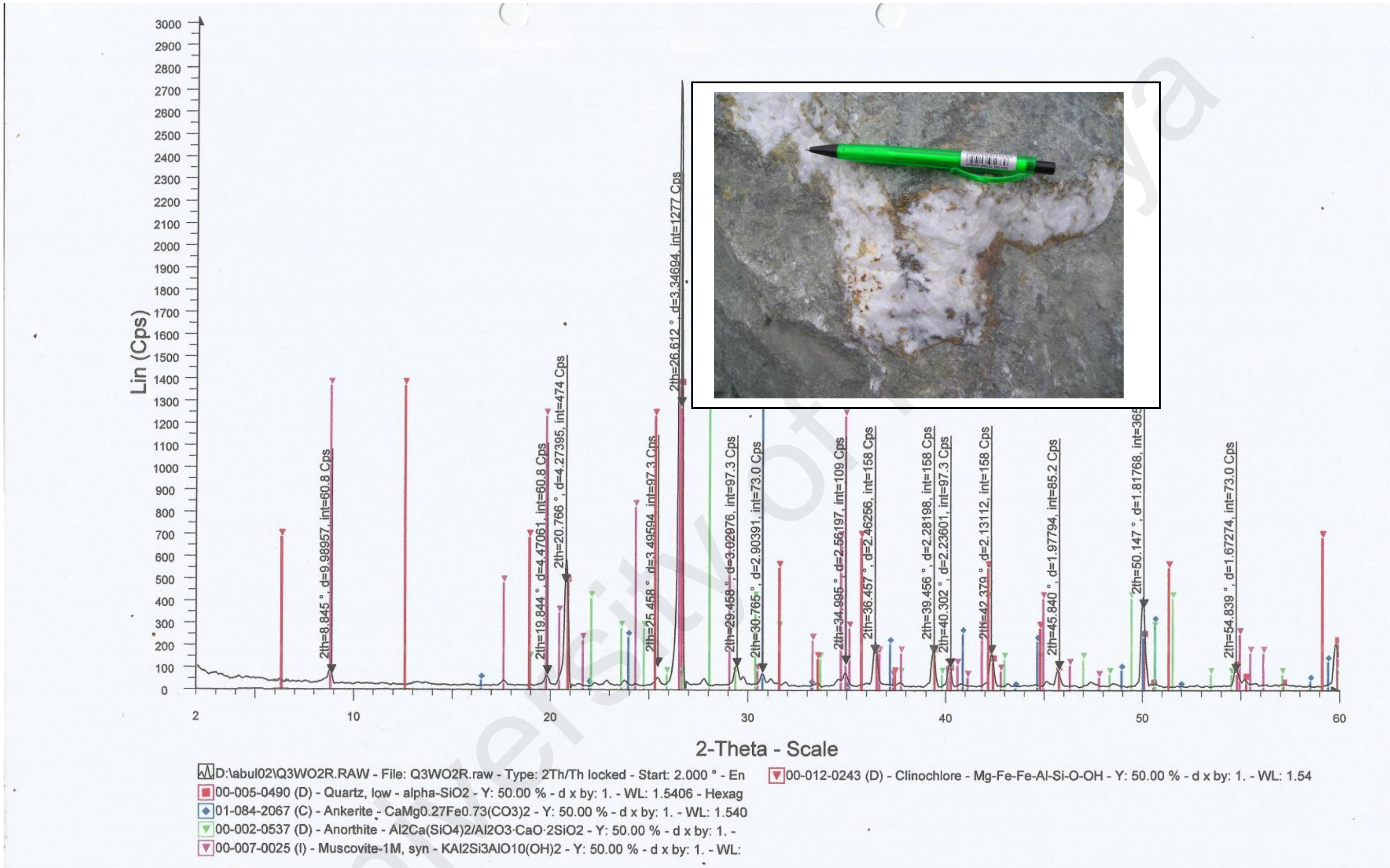

Figure 7.9: Extension quartz carbonate vein with a reddish color after expose to oxidation at the edge of the vein (inset photo) confirmed from XRD analysis as ankerite. Sericite alteration detected as indicated by occurrence of muscovite.

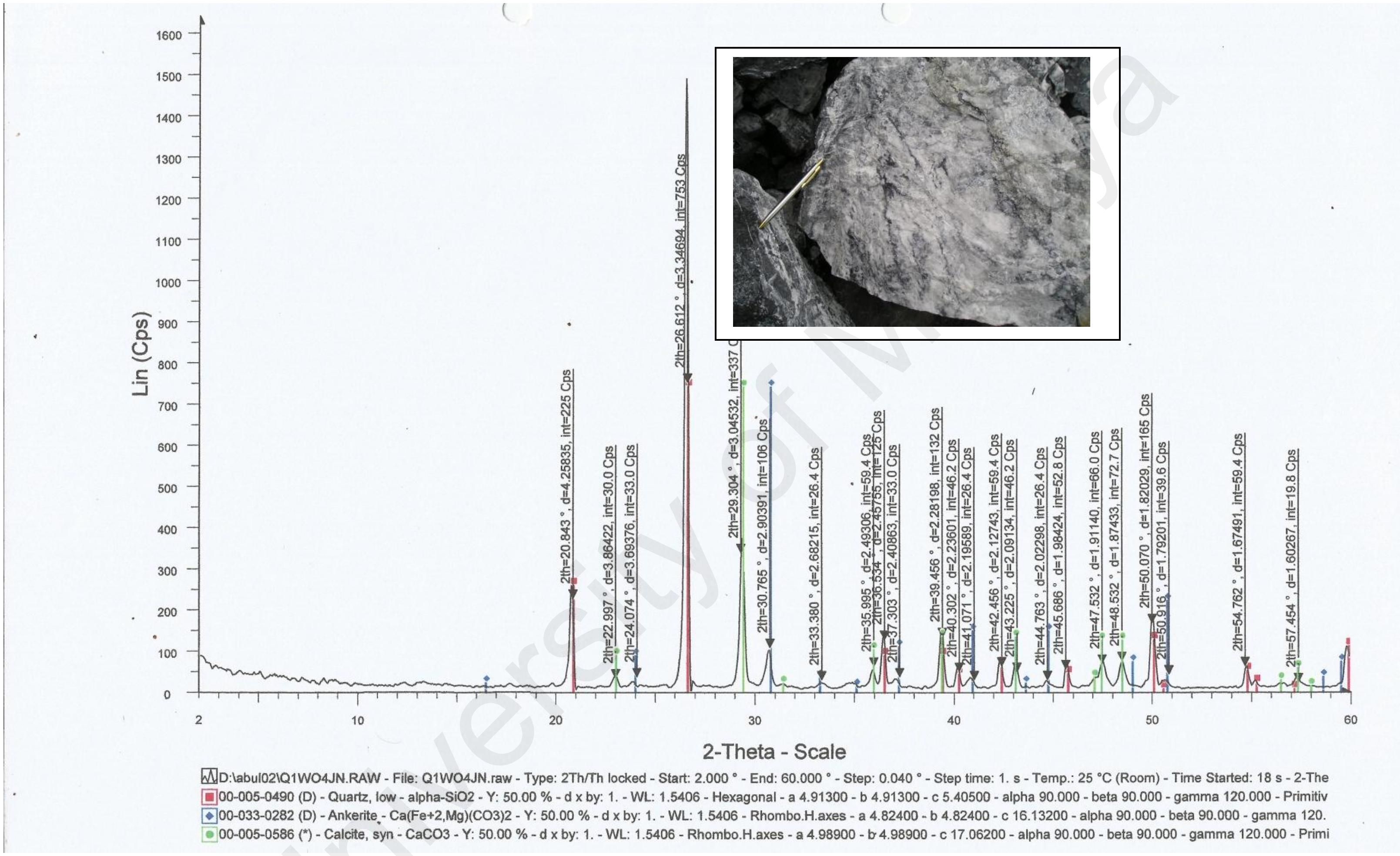

Figure 7.10: Deformed shear vein from Penjom Thrust zone at Janik hosted in high carbon zone have quartz carbonate vein of ankerite and calcite.

7.4 Alteration of wall rocks

7.4.1 Introduction

Hydrothermal alteration involves the reaction of hydrothermal ore fluids and the wall rock. Understanding the chemistry of the altered wall rock reveals the characteristics of the ore solution associated with ore deposition.

Mainly due to the characteristic of the host rock, turbidite hosted orogenic gold deposits were historically believed to lack such diagnostic alteration haloes and their study has long been neglected (Bierlien, 1998). More recent wall rock alteration studies of this type of deposit has incorporated geochemistry, including major and minor element plus identification of alteration mineral using XRD and optical petrography.

Limited wall-rock alteration has been studied in Malaysian gold mine. Only Purwanto (2002) had studied some aspect of wall rock alteration at the Penjom Gold Mine. Study of wall rock alteration in orogenic gold deposit also includes the dissemination of sulphide surrounding the vein in addition to the common wall rock alteration such as sericitization (phyllic alteration), de/silicification, chloritized and argillic alteration.

7.4.2 Difficulties in studying alteration in Penjom

The Penjom main deposit is hosted within alternating sequence of carbonaceous shale, sandstone and conglomerate in between calcareous shale and tuffaceous conglomerate and massive siltstone. The trend of orebody which is sub-parallel to parallel with the lithology sequence even though the main lode is occurs at the interception of intrusives and bedding-parallel shear veins or faults, any sampling traverse across the ore zone will also cut across the lithology sequence, and this contributes variability in geochemistry. .

This problem is not unique to Penjom but is also present at other turbidite hosted deposits elsewhere. According to Bierlein (1998), the degree of reactivity of the meta-sediment will influence the extent of any chemical reaction and alteration halo. Variation in porosity and permeability may be also responsible for variability.

Another reason for this lack of an alteration halo in turbidite deposits is that the ore bearing fluid may have been in chemical equilibrium with the host rock, as equilibrium conditions are likely to have been attained during peak metamorphism (Cox et.al., 1983) and Bierlein et al. (1998).

7.4.3 Wall rock alteration

Wall rock sulphidation by pyrite and arsenopyrite can be observed enveloping the mineralized vein system. Pyrite distribution is more widespread compared to arsenopyrite especially in the carbonaceous unit. Other common alteration minerals are fine grain muscovite, chlorite and illite that are typically characteristic of phyllic alteration.

XRD analysis has been performed to confirm alteration mineral especially clay mineral and mica group. Several results of the analyses are shown in Figures 7.13, 7.14 and 7.15 and summarized in Table 7.5.

Table 7.5: Summary of XRD analysis of vein and wall rock alteration mineral of several main ore bodies which are typical of phyllic alteration.

Ore body	**Vein mineralogy**	**Alteration mineral**	**Sulphide mineral**
Shear vein (Q3W)	Quartz, Ankerite, Calcite	Muscovite (fine grain sericite) Chlorite	Pyrite, Arsenopyrite Galena
Extension vein (north)	Quartz, Ankerite	Muscovite	Pyrite, Arsenopyrite
Penjom Thrust zone Figure 8.23, 8.24	Quartz, Calcite	Muscovite, Illite	Pyrite, Arsenopyrite minor galena
Extension quartz (South)-figure 8.25	Quartz	Muscovite, Chlorite	Pyrite

7.4.3.1 Pyritization

Pyrite is the most widespread sulphide mineral and can be of several different origins either syn-sedimentary, diagenetic or deposited by a hydrothermal/metamorphic fluid. etailed discussion of the origin of pyrite is in chapter 4. Only hydrothermal or metamorphic pyrite is considered to be related to wall rock alteration in which pyrite occurs disseminated around veins (Figures 7.11 and 12) as well as in the vein themselves.

Disseminated pyrite occurs as euhedral cubic of up to 2 mm in size around both shear veins and extension veins. At many localities, pyrite is disseminated in a bleached zone of sericite alteration at the vein margin. However, within the carbonaceous zone, pyrite distribution is wider, forming several bands of pyrite following the stratigraphic unit or enriched along macro fractures with no direct relationship with individual vein and not forming an economic ore zone. Pyrites also sparsely disseminated in felsite intrusives along the shear contact, in which sulfur content can be up to 0.5%.

Sulphidation such as pyritization of wall rock is effective way of reducing HS^- concentration and is a frequently proposed mechanism for the genesis of orogenic gold deposits, where there is spatial relationship between gold and pyrite (William-Jones et al., 2009)

7.4.3.2 Arsenification

Arsenification is characterized by occurrences of disseminated arsenopyrite in the wall rock along mineralized veins forming a surrounding halo of up to 50 cm in width. Cubic rhombohedra are common and always form bands along foliated siltstone or shale. Pressure solution, forming face controlled fibres along the grains are common features indicating ongoing deformation.

Disseminated arsenopyrite is more abundant in Janik, Manik, Kalampong North and Kalampong upper ore bodies especially around shear vein in the medium to high carbonaceous ore zones. In low carbonaceous and felsite host rocks and extensional veins, pyrite is more dominant.

7.4.3.3 Phyllic alteration

Bleaching of color can be observed in less carbonaceous host rocks along the main ore zone at different intensities but are not so obvious in medium to highly carbonaceous host rocks zone. Based on XRD and microscopic analyses, the bleached host rock is dominated by sericite or fine grain muscovite. Chlorite is also present in XRD analysis, but greenish spots that characterize this mineral are not observed and it is not considered a dominant alteration type.

The XRD analysis of the vein and wall rock along the Penjom Thrust ore zone indicates the occurrence of muscovite and illite without chlorite mineral (Figure 7.14). The presence of muscovite or sericite, minor chlorite and illite is characteristic of phyllic alteration (Bogie, 2004). This alteration is caused by acid to near neutral fluids at temperatures between 230^{o}C to 400^{o}C, which is a typical characteristic of orogenic gold deposits.

7.4.3.4 De-silicification

Based on hand specimen and thin section, the addition of secondary quartz around veins or ore zones was not clearly observed but many grain particles, especially lithic fragments have been replaced by sericite. Dissolution of existing quartz particles may contribute to the vein forming process and is referred to as de-silicification. However, the thickness of veins forming through this process is usually less than 10 cm (Bierlein, 2001).

7.4.5 Discussion

During the gold mineralization event, the influx of hydrothermal fluids enriched with silica and various types of carbonate into the structural trap forms quartz and minor carbonate veins. Calcite is the main carbonate mineral along with ankerite and minor dolomite. Cross-cutting between calcite and quartz reflects multiple fluid infiltrations during the vein formation. Barren calcite veins were emplaced during late faulting with different morphologies compared the early calcite veins. The occurrence of calcite indicates the source of fluid is possibly CO_2 rich, generated from the local carbonaceous shale, and mixed with another source of silica rich fluid. Quartz predominates over calcite above 300^{o}C to form a mineralized quartz carbonate veins and vice versa at or below 150^{o}C (Sharp, 1965). The lower temperatures veins are usually barren.

Alteration assemblages indicate phyllic alteration, as indicated by assemblages of muscovite (fine-grained sericite), illite and minor chlorite. This alteration suite is typical of orogenic gold associated with a vein system.

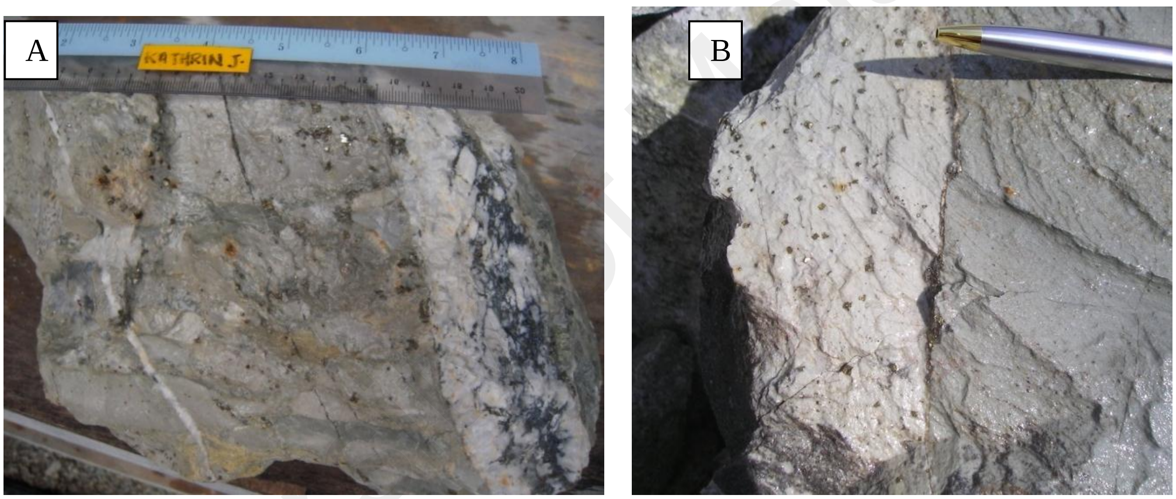

Figure 7.11 (A) Sulphides in vein comprised of mainly pyrite and a black shining galena and disseminated pyrite in altered wall rock zone. B: Altered wall rock and disseminated pyrite.

Figure 7.12: Disseminated pyrite in felsite intrusive within the bleached altered host rock around the vein.

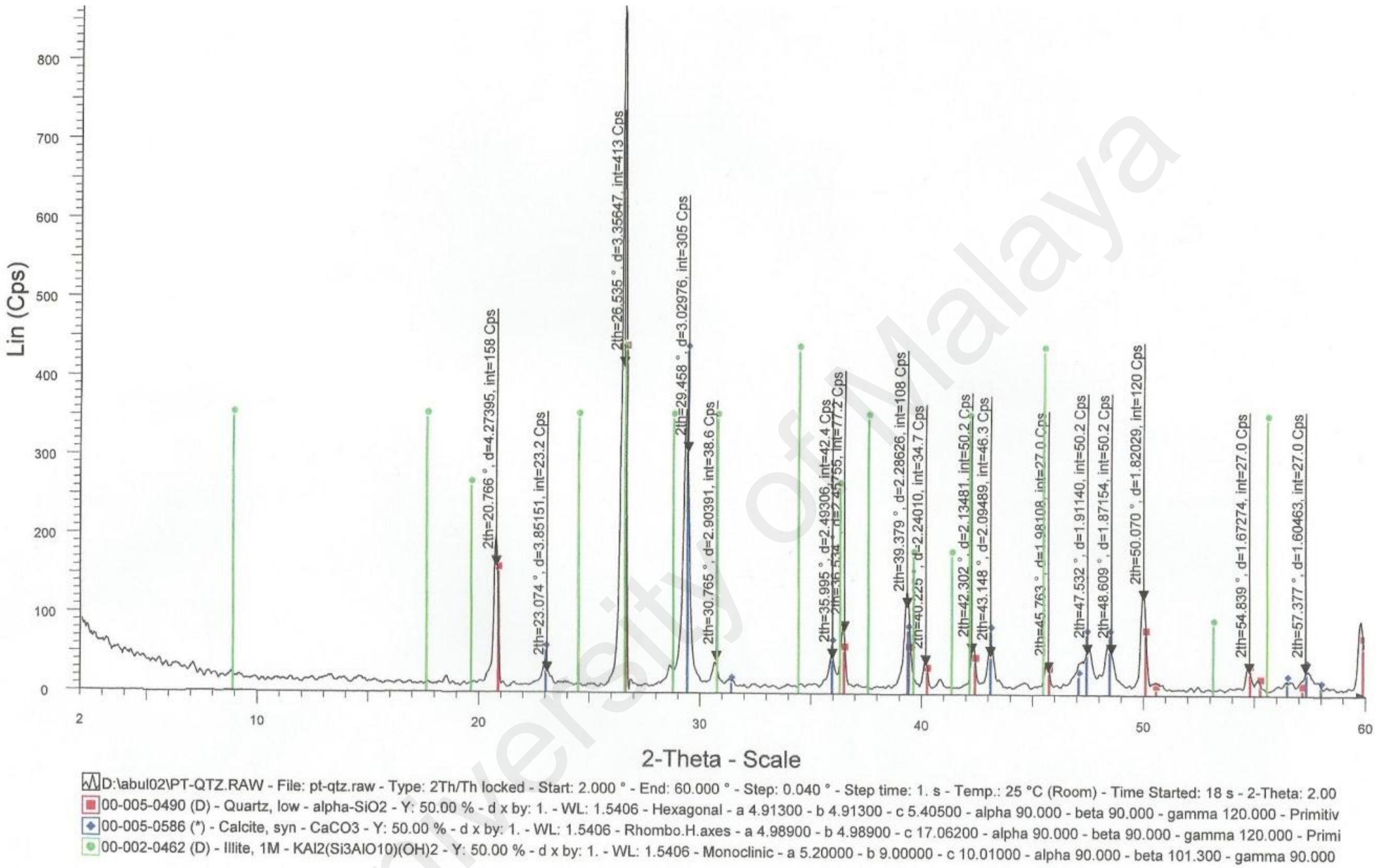

Figure 7.13: XRD analysis of samples along Penjom Thrust hosted vein comprised of quartz, calcite and illite.

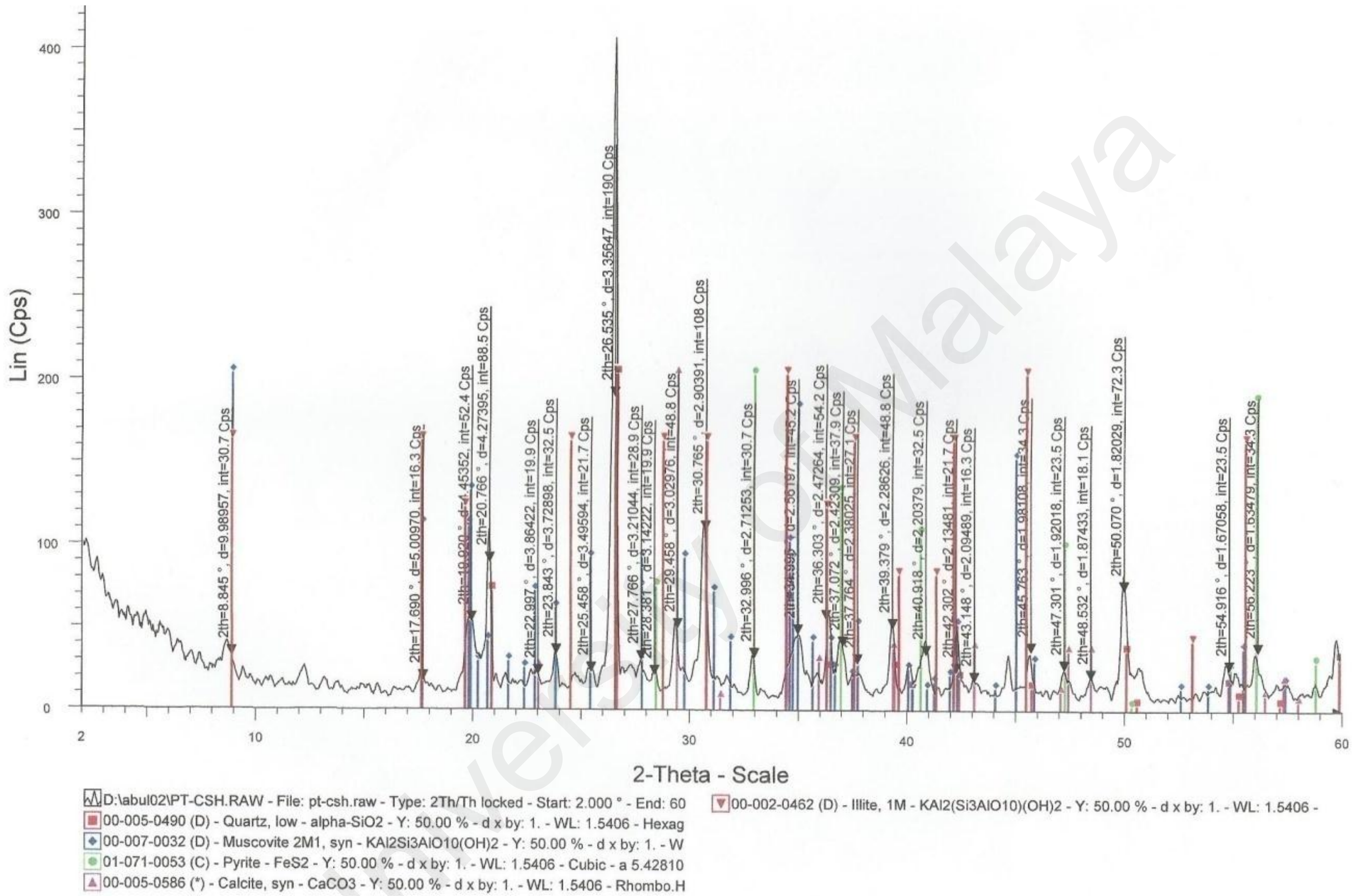

Figure 7.14: XRD analysis of Penjom Thrust wall rock comprised of quartz, muscovite, pyrite and calcite.

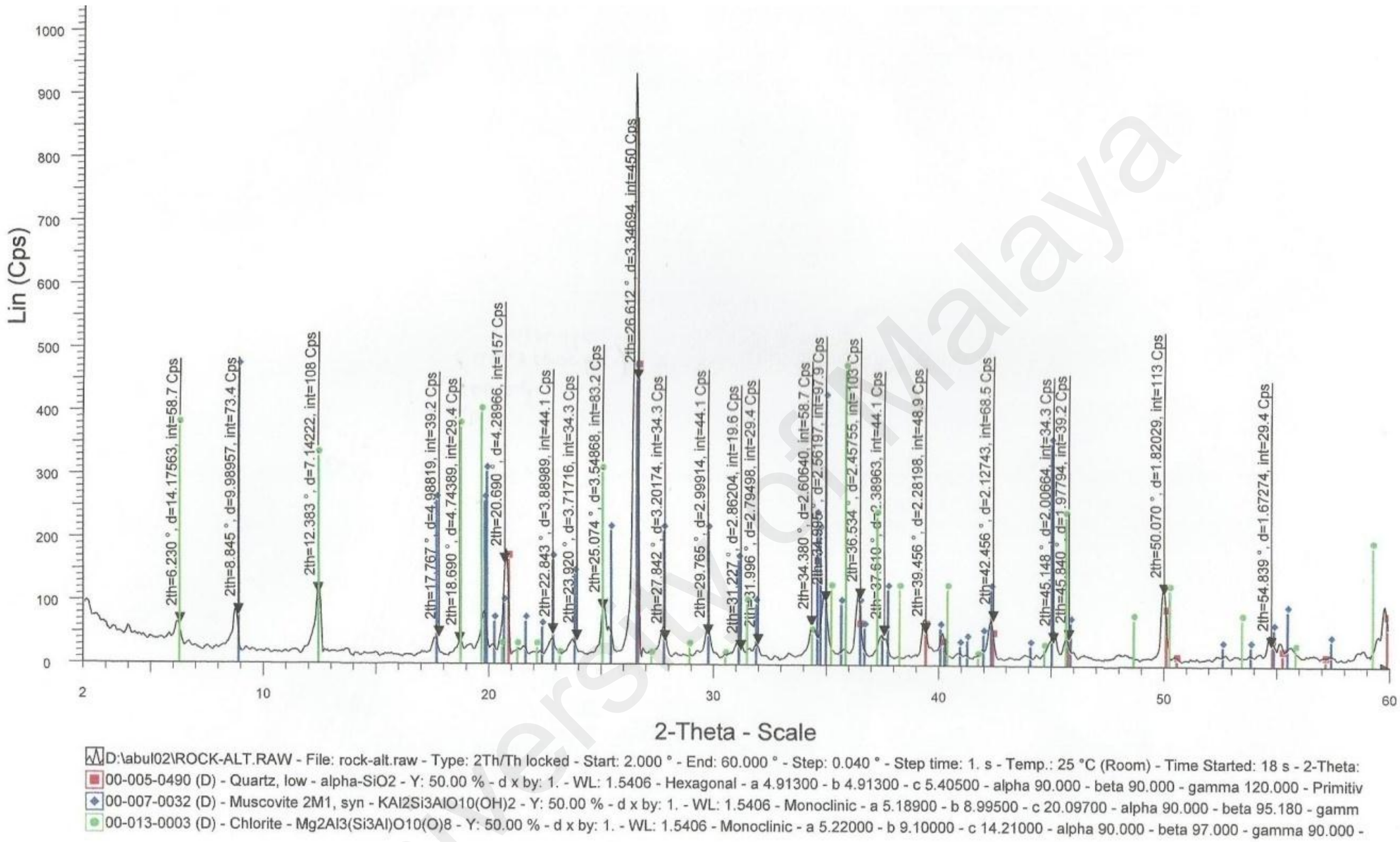

Figure 7.15: XRD analysis of altered wall rock at southern pit extension vein comprised of quartz, muscovite and chlorite.

7.5 Major, REE and trace element analysis

7.5.1 Introduction

All samples (n=15) has been sent to Acme Analytical Laboratories, in Vancouver, Canada for major oxides, REE and trace element analysis. The samples comprised of the hanging wall (2), outside pit area (2), Manik (2) and Kalampong pit (9). The purpose of the analysis is mainly to quantify the content of trace elements to verify the main sulphide minerals at different ore bodies and in the barren zone. This can further support the field observation especially the arsenic and lead. Previous geochemistry analysis has been conducted in significant detail mainly during the early stage of exploration activities (Ariffin and Hewson, 2007; Gunn, 1994). Arsenic is the most significant trace element and correlates well with the gold content.

7.5.2 Methods of study

Sampling has been carried out at main the ore body, mainly veins with wall rock, at the hanging wall and two samples outside the mine area. Some samples were comprised of wall rock. Weights of the samples collected at site are approximately 7 to 10 kg. The samples were crushed and split to 2 kg. These samples were pulverized to 85% passing 75 micron. 250g of the samples were sent to the ACME labs. The samples were analyzed for major oxides by XRF (X-ray fluorescence) and a trace element by ICP-MS. LOI was also determined. Rare earth and refractory elements were determined by ICP mass spectrometry following a Lithium metaborate / tetraborate fusion and nitric acid digestion of a 0.2g sample. Full results of the all elements data are shown in Appendix B. This study discuss As and Pb to explain the paragenesis of the sulphide.

7.5.3 Results

Table 7.6 shows all the result of XRF analysis. Samples location is shown in Figure 7.16. Samples with higher arsenic (As) can be found in carbonaceous dominant host rock either along the Penjom thrust or shear vein (D2) and also along the NNW fault (D3). Samples along the fault (D3) that hosted in brittle host rock have lower As compared to within the carbonaceous host rock. One of the samples from NNW fault has higher As value compared to other D3 samples. The As is dominantly related to the early shear vein that dominantly emplaced within the carbonaceous shale and indicated in Table 7.6.

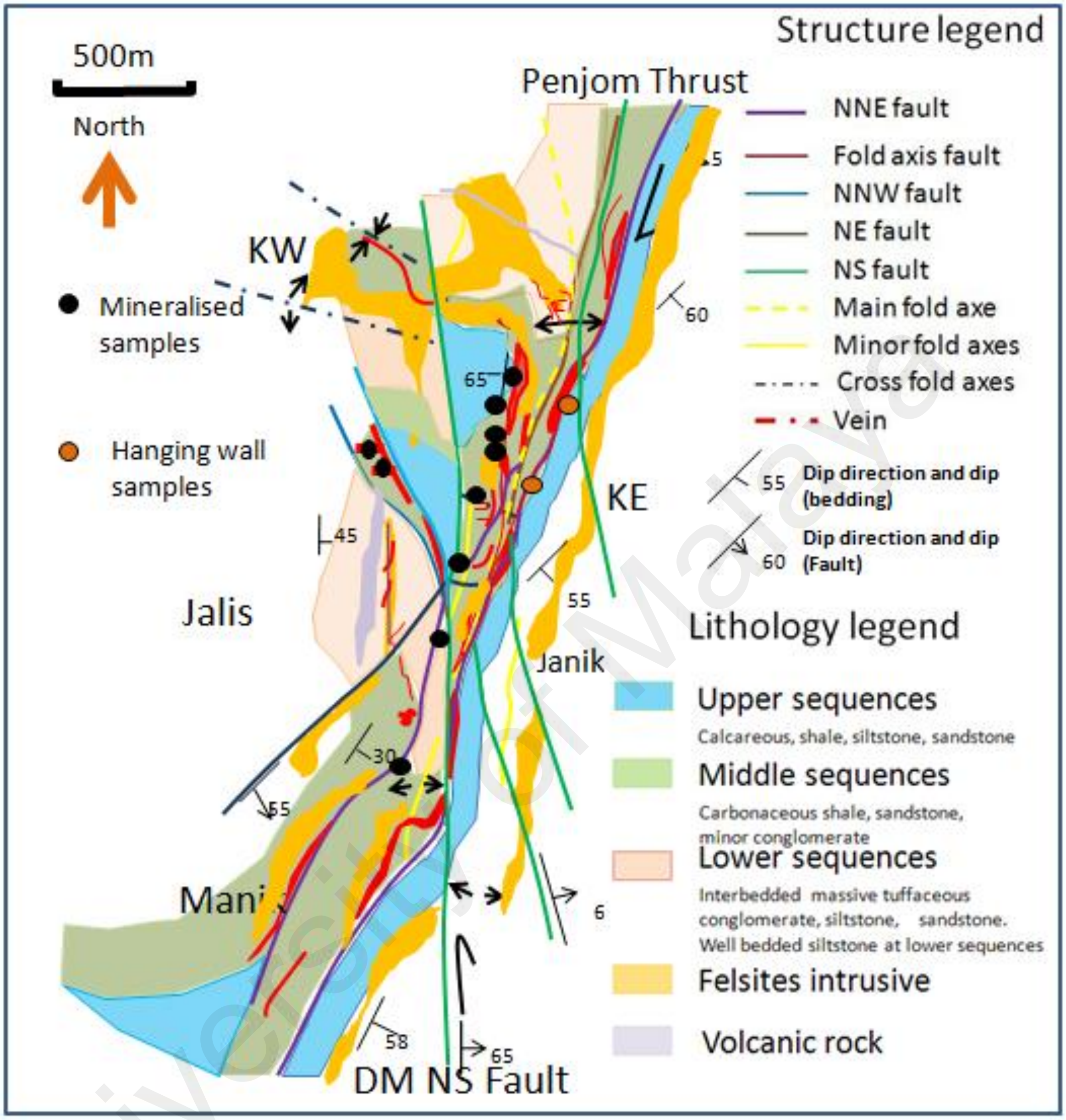

Figure 7.16: Location of samples for XRF analysis. Hanging wall samples are HW-R and HW-NSF

.

Table 7.6: Geochemical results (in ppm) of trace element analyses in three g of rocks. Vein No is referred to Table 6.3. Fe, Mn, Cr, in %: Au in ppb, others in ppm.

Sample ID	MN-1	ESE-1	PT-1	NNW-H	NNW-L	DK-1	Q3W-EX1	NNEDK-JL	NE888	JLIA-SDB	JLIA-SDLC	HW-R	HW-NSF	KLGM	KLB
Fe	6.37	5.45	3.53	7.21	1.98	2.15	2.35	1.84	1.44	4.54	5.47	6.06	4.97	4.41	6.02
Mn	0.2	0.09	0.06	0.09	0.23	0.29	0.07	0.07	0.05	0.09	0.14	0.11	0.08	0.01	0.04
Cr	0.006	0.006	0.001	0.002	0	0	0	0.001	0	0	0.01	0.01	0.003	0.01	0.01
S	0.59	1.73	0.76	1.96	0.87	0.2	0.17	0.39	0.47	0.08	0.25	0.6	0.12	0.32	0.36
Ba	180	244	57	103	91	79	197	233	189	365	289	199	152	304	480
Co	9.2	14.2	5.1	12.7	1	3.8	4.7	1.9	0.7	12.2	13.7	13	7.2	5.2	10.1
Sn	3	4	1	1	15	1	11	8	10	1	2	1	2	3	3
W	7.6	16.1	8.6	3	5.2	2.2	58.6	4.3	3.2	2.2	7.6	6.4	6	1.3	1.4
Mo	0.4	1.5	1.5	1.5	0.3	0.7	0.9	2	1	0.6	0.6	0.5	0.2	3.7	1
Cu	49.7	23.8	27.1	137.9	5.9	2.9	43	28.4	13	39.7	53.3	29.2	4.2	65	35.4
Pb	53.4	115.6	806.6	1374	200	503	109	154.1	158	6.6	4.7	15.1	9.9	70.4	61.8
Zn	25	93	273	1298	6	22	39	26	16	40	36	74	49	44	56
Ag	0.5	0.7	5.2	15.8	3	1.7	1.1	2.1	2.7	0.1	0.1	0.1	0.2	0.1	0.1
Ni	15.3	18.5	4.7	12.4	0.5	3.6	4.4	2	0.6	13.6	12.9	17.1	7.2	14.2	8.8
As	5994	10000	8292	10000	325	3373	52.1	99.6	3546	115	1256	39.9	21.9	37.9	23.5
Au	3.6	18.3	2	12058	4145	2164	1298	8558	661	5.3	115	4.9	7.7	4.8	2
Sb	2.9	7.8	4.3	15.4	0.4	1.7	0.4	0.9	1.3	0.1	0.4	1.2	0.2	3	0.7
Bi	2.3	3.9	14.4	36.7	5.4	2.3	4.4	3.3	5.8	0.8	0.7	0.3	0.2	0.9	0.5
Hg	0.01	0.02	0.04	0.12	0.01	0.01	0.01	0.02	0.01	0.01	0.01	0.02	0.01	0.05	0.09
Se	0.7	0.9	0.5	5.1	0.5	1	0.5	0.5	1.1	0.5	0.5	0.6	0.5	0.5	0.5
Vein No	1+wall rock	2	2+wall rock	6 and 7	7	9	9	9	10	Wall rock	Wall rock	Hanging wall	Hanging wall	Waste	Waste
Rock	Carbonaceous dominance					Felsite dominance				Carbonaceous Siltstone					
Fault	Shear vein			NNW		NNE						NS			
Phase	D2			D3		D3						D4			

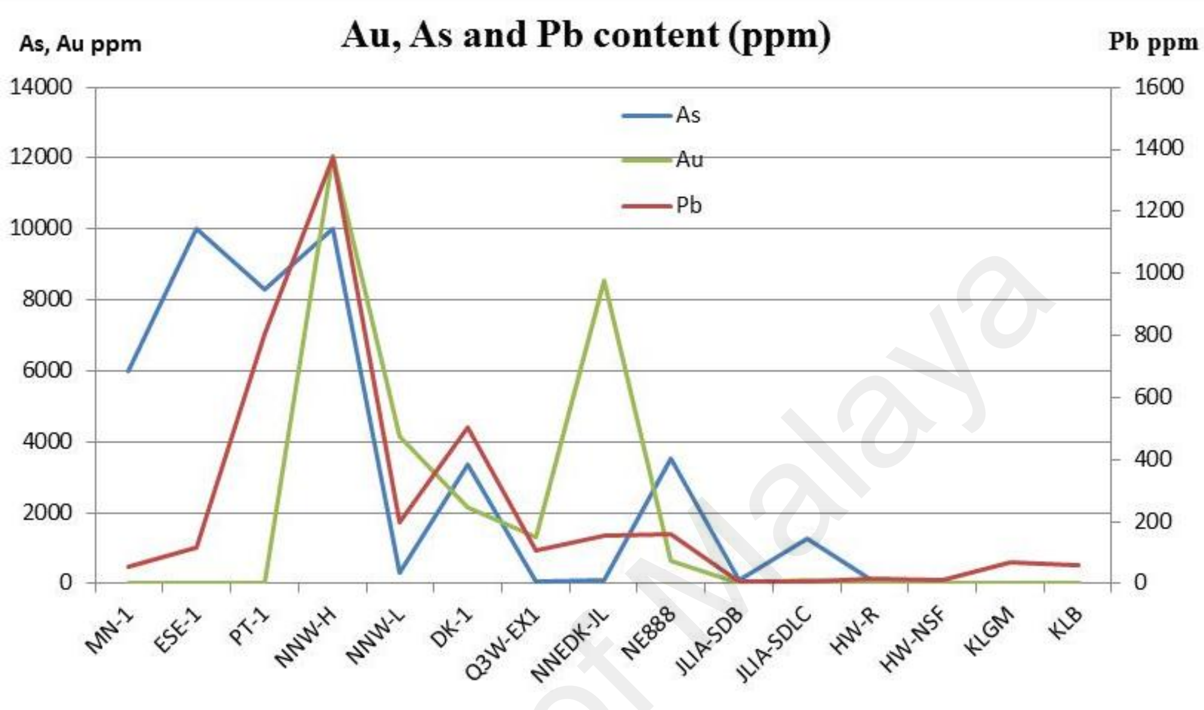

Figure 7.17: Plot of Au, As and Pb in the ore (11 samples, refer to Table 7.6), hanging wall rock (HW-R and HW-NSF) and waste rock outside the mine site (KLGM and KLB).

7.5.4 Discussion

In sulphide paragenesis, As and Pb is important, as this element reflects the occurrence of Arsenides (e.g. arsenopyrite) and galena. Pyrite is dominant at all stages and in all ore zones. The geochemical results of both As and Pb support the field observation that arsenopyrite is relatively abundant within the carbonaceous rich host rock that is associated with the shear veins and less abundant in brittle units and extensional veins. Both As and Pb content are plotted in Figure 7.17. Arsenic content is relatively high in veins associated with the sheared felsite (as in sample NE888). Only samples from NNW fault and PT1 that have high contents of both As and Pb and also corresponded with higher Au grade. This zone is characterized by reactivation of faults along the existing shear veins and thin carbonaceous units (NNW-H samples) and thick carbonaceous phyllite for PT1. Sample NNW-H represents the veins No 6 and 7 as described in Table 6.3. Samples from carbonaceous zone have lower Au (except vein 6 and 7) but higher As even though they are taken from the ore zone. Erratic gold grade may have influence the result of the sampling.

Samples from the hanging wall which represent the higher stratigraphic unit are low in both elements. These samples are not from the mineralized zone. Two samples are from outcrops outside the mine lease comprised of slightly carbonaceous siltstone. Both samples show geochemistry result distinctly different from the mine site except slightly higher Pb.

CHAPTER 8: GALENA GEOCHEMISTRY AND LEAD ISOTOPE

8.0 Introduction

Galena is one of the most common sulphides that accompanying gold mineralization and quartz veining. Galena and gold is hosted only in veins, suggest the same timing and genetic link with the vein emplacement. Galena was analyzed for lead isotope abundances to determine the sources, genesis and age of lead, which is closely associated with gold-sulphide mineralization. Trace element distributions in galena was analyzed to characterize stages of galena formation and to compare with samples from other deposit types. Lead isotopes are useful to investigate the sources of metal or tracer to mineral origin based on the evolution of Pb growth models. Two Pb models were applied here namely, Stacey and Kramers (1975) and Cumming and Richards (1975). The ages of the galena can be constrained from those models although the ages derived from this estimation could be less precise compared to other age dating techniques and need to be properly interpreted.

8.1 Methodology and purpose

Trace element and Pb isotope contents of galena were obtained using Laser Ablation Inductively Coupled Plasma Mass Spectrometry (LA ICP-MS). Several stages of sulphides were classified in the field based on structural control, vein type and textures (refer to Table 6.3, Figure 6.33). Details of vein and sulphide paragenesis are given in chapter 5 and 6. Several representative samples (n=9) of galena-bearing veins belonging to each of the different stages (Table 8.1) were collected for geochemistry and lead isotope analysis. Locations of samples are shown in Figure 8.1. Photograph of the samples as in Figure 8.2.

Geochemistry characterisation of galena can be used to constraint several episodes of structural event that control distribution of the galena.

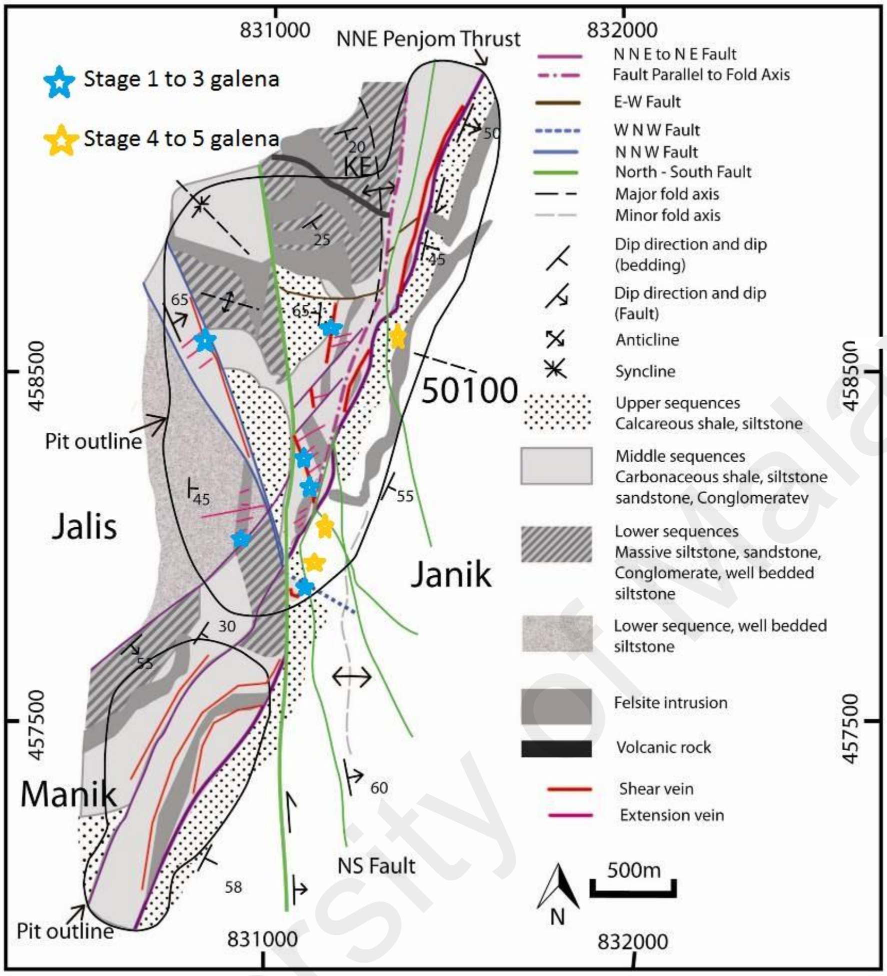

Figure 8.1: Location of galena sample for geochemistry study

Table 8.1: List of galena samples (n=9) from Penjom from several stages.

Host vein	**Stage 1**	**2**	**3**	**4**
Bedding parallel vein	Q2WL			
Bedding parallel vein	ZX3			
Dendritic galena in bedding parallel vein	Q3WA			
Fault related vein		ZNNW		
Fault modified vein (breccia texture)			JL2, JNNE	
Normal fault (hanging wall)				HW-E (H6NS)
Hanging wall				HW-S2
Hanging wall				G1A-HW-S

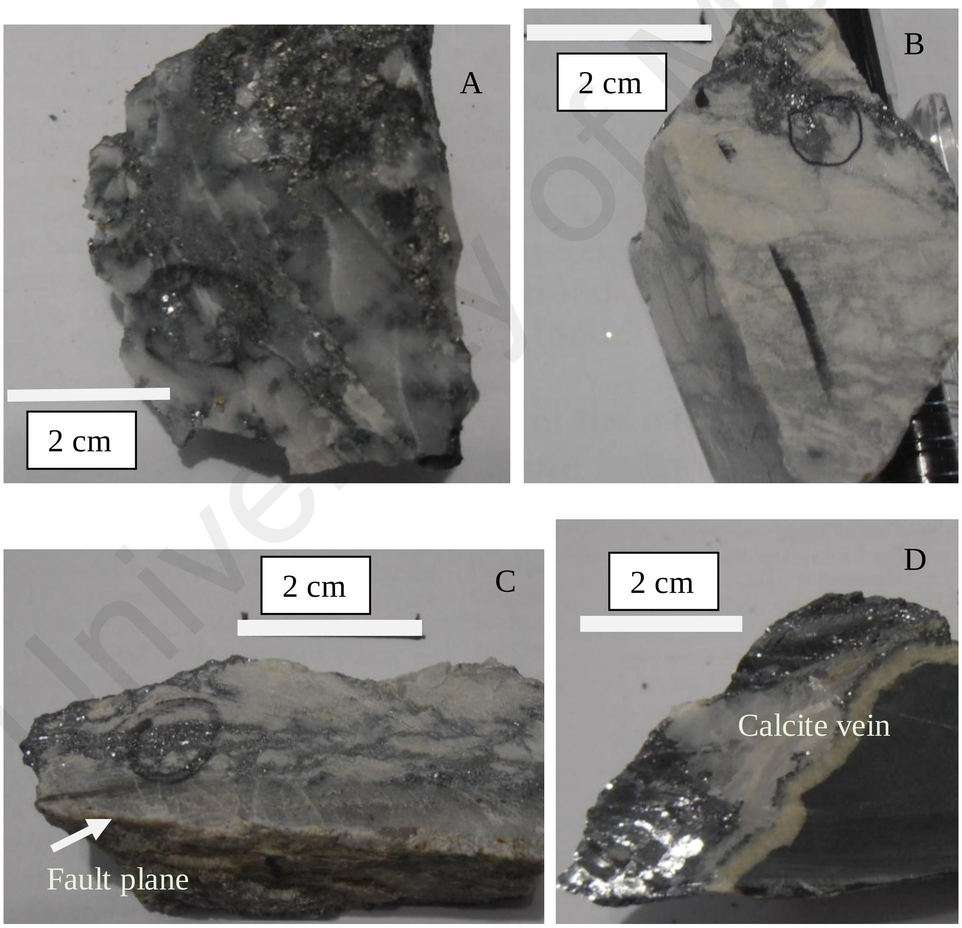

Figure 8.2: Galena samples for the analysis. A. Close up view of sample Q3WA. B. Sample ZNNW, C. JNNE: Galena infilling brecciated calcite along the fault plane, D. Hanging wall galena (HW S2).

8.1.1 Trace elements

Nine galena samples were analysed at the University of Tasmania (as analysed by Dr Sebastien Meffre) on 25 mm polished rock samples using an Agilent 7700 quadrupole ICPMS equipped with a 193 nm excimer laser and the Resonetics S155 laser ablation system. Instrument drift and mass bias correction factors were calculated using the STDGL2b2 standard of Danyushevsky et al. (2011) analysed at the beginning and end of the run and once every 30 minutes throughout the run. Each analysis began with a 30 second blank gas measurement followed by a further 30 seconds of analysis time when the laser was switched on. Galena was sampled on 17 micron spots using the laser at 3 Hz and a density of approximately 1.7 J/cm^2. Data reduction was performed using similar methods to that outlined in Danyushevsky et al. (2011). Counting time on all masses was 0.01s except for Au that was counted for 0.1s to improve precision and lower the detection limit.

Nine samples of galena, representing three structural stages, have been analysed for 13 different trace elements including Cu, Zn, As, Se, Ag, Cd, In, Sn, Sb, Te, Au, Tl and Bi. For each sample, three different spots were analysed. Due to the paucity of trace element analyses of galena in literature, galena from various deposits worldwide were analysed at the same time as the Penjom galena, to understand the significance of the results better. The result for all Penjom and other samples are tabulated in Table 8.2.

8.1.2 Lead isotope

Pb isotopic analyses on galena were carried out on the same instrument and same laser analytical conditions as for the trace elements but on separate spots and using different quadrupole mass spectrometer parameters. The parameters are similar to that outlined in Meffre et al. (2008) and Woodhead et al. (2009). Instrument drift and mass bias correction factors were calculated using the primary Broken Hill galena standard (sample and values from Townsend et al. 1998), taken every 30 min with extra standards at the beginning and end of the run. The results were checked on galena crystals analysed previously by other laboratories (see appendix for results on samples, primary and secondary standards).

The blank gas measurement was shorter than for the trace element analyzed (10s) and the analysis time longer (80s) to get better precision. Fewer elements were analysed more often (2 ms on ^{107}Hg, ^{202}Hg, ^{238}U, ^{232}Th; 5 ms on the ^{206}Pb, ^{207}Pb and ^{208}Pb isotopes; 10 ms for ^{204}Pb) to shorten the quadrupole sweep time and provide better precision on the ratios. A particle filter (see Guillong et al., 2003) was also used to remove larger galena particle and decrease signal noise.

8.2. Results

8.2.1 LA ICP MS: Trace elements

Galena from the mineralized zone is characterised by higher Bi, Te, Se, Cd, Sn and Ag than those from the hanging wall non mineralized zone. Galena samples from the mineralized zone have Bi ranging between 1750 to 11160 ppm, Te from 270 to 860 ppm, Se from 280 to 660 ppm, Cd from 130 to 680 ppm, Sn from 1 to 26 ppm and Ag from 1010 to 5780 ppm. The same trace elements of galena from non-mineralized zones have a Bi range from 0.1 to 240 ppm, Te from 0.3 to 1.0 ppm, Se from 2.0 to 160 ppm, Cd from 40 to 70 ppm, Sn from 0.1 to 0.2 ppm and Ag from 370 to 570 ppm

Overall, all samples show similar value for all trace elements measured except that Cd, Se, Te and Bi, are much lower in hanging wall galena than in other samples (Figure 8.3), indicating different genesis or stages for galena in the hanging wall. This also suggests a different fluid source and timing for the hanging wall galena relative to those from the ores.

Galena crystals with different morphologies from the same vein type (e.g. the anhedral crystal in QW2L (refer to Figure 6.29 Right), dendritic galena in Q3WA (Figure 6.28 Left) and ZX3 (Figure 6.25 Left) along laminated vein show similar trace elements characteristics (Figure 8.4), suggesting that the main controls on chemistry is fluid chemistry rather than growth habit. Different stages of mineralization stages tend to have slightly different trace element composition with stage 1 having much higher Bi and Ag than later stages. Stage 2 is characterised by high Te (Figure 8.5) but all three stages have similar Au (up to 0.28g/t) with a single isolated value of 1.7 ppm possibly a micro inclusion of gold encountered by the laser during analysis.

Trace elements of galena from various deposits worldwide (such as Mt. Isa, Broken Hill, Mt. Murchison, Baia Mare, Tynagh, Sweetwater, and Olympic Dam) have Bi ranging between 0.03 to 150 ppm, Te from 0.5 to 30 ppm, Se from 2 to 40 ppm, Cd from 3 to 140 ppm, Sn from 0.2 to 70 ppm and Ag from 40 to 1760 ppm.

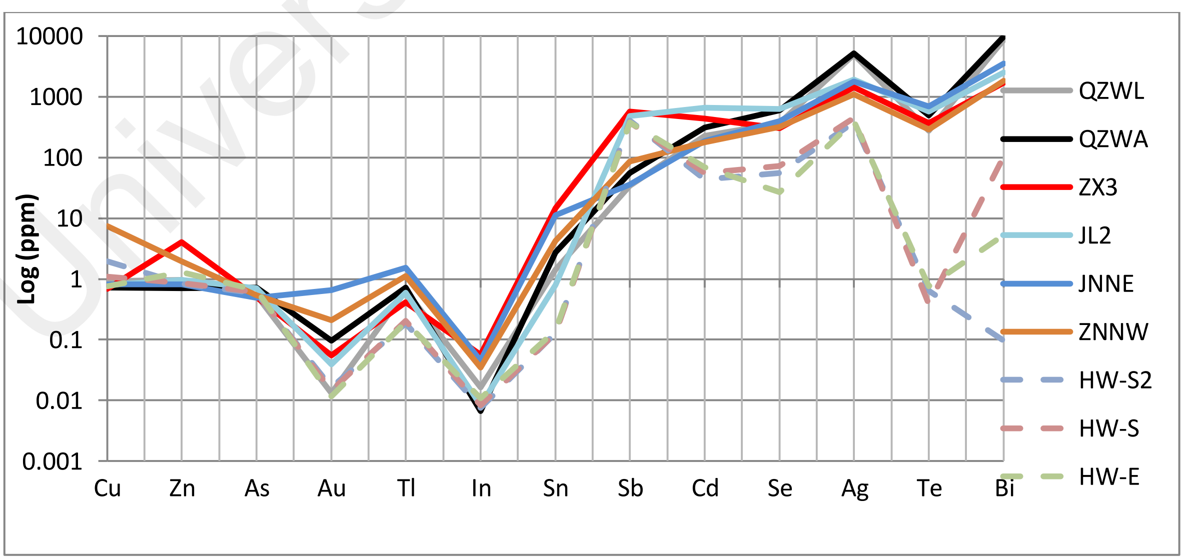

Figure 8.3: Broad correlation of all element in galena (in log scale) except Cd, Se, Ag, Te and Bi, which is very low in hanging wall galena. Refer to Table 8.1 for galena stages

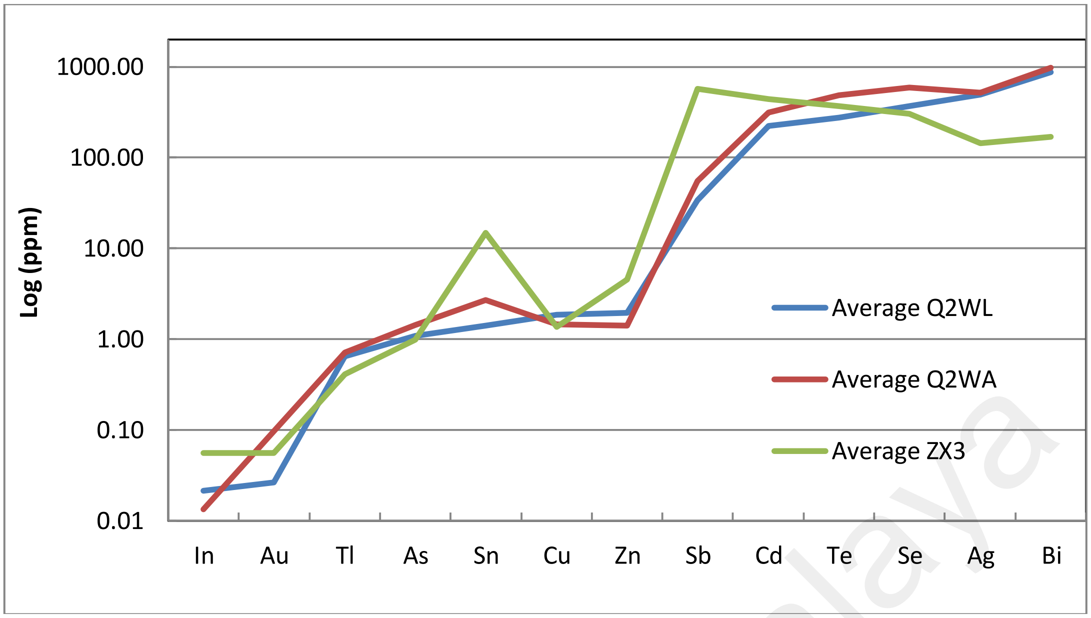

Figure 8.4: Plot of trace element in galena hosted in bedding parallel shear vein (sample Q2WL), dendritic galena (Q2WA) and galena along lamination. All show broad correlation especially the first two samples.

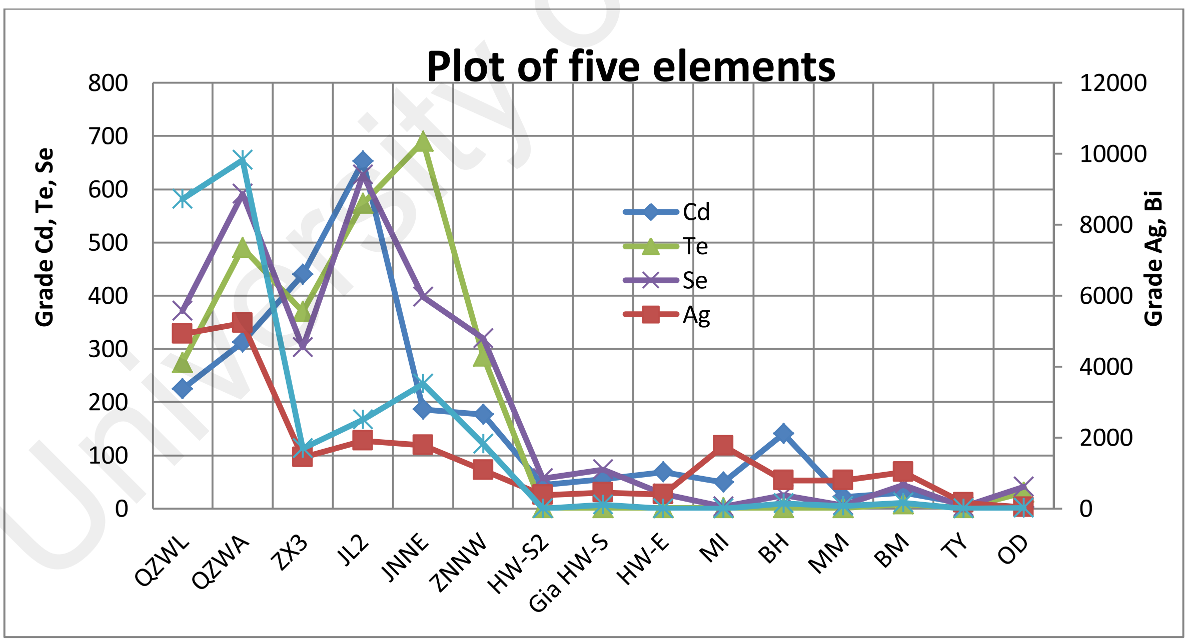

Figure 8.5: Plot of Cd, Te, Se, Ag, Bi of galena in Penjom, Tanah Merah (near Ulu Sokor) and other places (MI-Mount Isa, BH-Broken Hill, MM-Mt Murchison, BM-Baja Mare, TY-Tynagh, OD-Olimpic Dam).

Table 8.2: Results (in ppm) of the trace elements in galena for samples (Q2WL, Q2WA, JL2, ZX3, JNNE, ZNNW, HW-S2, G1a HW-S, HW-E. Three analyses were undertaken for each sample. Other samples are from University of Tasmania collection: MT Isa-Mount Isa, B Hill-Broken Hill, MT M-Mount Murchison, B Mare-Baja Mare, Tynagh, SW-Sweet Water and O Dam-Olympic Dam.

Group 1	Cu	Zn	As	Se	Ag	Cd	In	Sn	Sb	Te	Au	Tl	Bi
Q2WL	1.085	1.270	0.475	325	4815	223	0.01	1.66	38.6	274.75	0.02	0.56	8544.9
Q2WL	0.800	0.745	0.615	396	4959	221	0.02	0.92	28.4	279.37	0.02	0.83	8818.1
Q2WL	0.900	0.900	0.535	391	4974	230	0.02	1.67	35.2	268.18	0.01	0.55	8792.2
Q3WA	0.690	0.965	0.715	578	5779	311	0.01	2.31	47.4	461.93	0.20	0.86	11156.4
Q3WA	0.645	0.650	0.735	604	4941	311	0.01	2.73	57.6	492.19	0.05	0.60	9064.9
Q3WA	0.840	0.510	0.715	593	4944	314	0.01	3.12	61.1	515.78	0.04	0.68	9247.9
ZX3	0.665	10.855	0.485	307	1502	488	0.05	14.89	538.9	361.77	0.09	0.41	1899.2
ZX3	0.705	0.805	0.595	274	1465	449	0.06	14.03	558.8	357.58	0.04	0.38	1688.2
ZX3	0.675	0.540	0.41	326	1363	381	0.05	15.28	609.2	390.26	0.05	0.44	1462.0
JL2	0.785	1.255	0.705	663	1988	683	0.01	0.70	482.7	542.65	0.07	0.68	2548.3
JL2	0.670	0.865	0.595	621	1889	659	0.01	0.86	432.5	540.71	0.03	0.54	2603.3
JL2	0.915	0.755	0.81	599	1827	614	0.01	0.82	514.3	635.46	0.02	0.56	2379.7
JNNE	0.955	0.900	0.57	387	1414	177	0.04	3.88	42.1	693.07	0.07	1.27	2674.3
JNNE	0.740	0.840	0.49	382	1466	186	0.08	26.35	33.9	518.58	1.71	1.92	2875.8
JNNE	0.755	0.720	0.415	424	2445	194	0.02	3.27	31.8	857.15	0.19	1.37	5012.9
ZNNW	18.144	2.229	0.37	316	1095	210	0.06	4.11	131.9	299.82	0.14	0.72	1846.7
ZNNW	0.585	1.135	0.775	305	1019	187	0.04	6.12	94.7	288.24	0.20	1.33	1749.7
ZNNW	3.268	2.435	0.475	336	1136	131	0.01	2.55	27.9	267.87	0.28	1.29	1846.8

Group 2	Cu	Zn	As	Se	Ag	Cd	In	Sn	Sb	Te	Au	Tl	Bi
HW-S2	1.458	0.815	0.595	59	381	45	0.01	0.13	409.3	0.62	0.02	0.16	0.09
HW-S2	1.517	1.015	0.725	57	370	42	0.01	0.14	397.5	0.99	0.01	0.18	0.06
HW-S2	2.915	0.670	0.435	52	379	45	0.00	0.13	415.2	0.31	0.02	0.21	0.15

Gia HW-S	0.725	0.795	0.485	164	571	56	0.01	0.12	390.3	0.43	0.02	0.26	235.79
Gia HW-S	1.927	1.060	0.64	1.88	370	56	0.01	0.12	365.4	0.41	0.01	0.13	3.29
Gia HW-S	0.610	0.725	0.72	52	397	54	0.01	0.15	384.7	0.31	0.02	0.22	73.69
HW-E	0.745	1.213	0.79	22	392	67	0.02	0.13	371.9	0.91	0.01	0.20	1.05
HW-E	0.875	1.685	0.695	20	399	74	0.01	0.16	378.7	1.07	0.01	0.21	6.58
HW-E	0.640	0.940	0.475	38	400	65	0.01	0.14	370.0	0.29	0.02	0.18	8.27
Group 3	Cu	Zn	As	Se	Ag	Cd	In	Sn	Sb	Te	Au	Tl	Bi
MT ISA	0.7	1.03	0.745	2.99	1758	49	0.17	4.32	2045.7	0.68	0.02	23.95	0.36
BROKEN HILL	2.7	0.89	0.43	25	782	141	0.38	70.16	2093.4	0.82	0.03	3.27	138.29
MT MURCHISON	0.6	0.9	0.455	6	784	21	0.02	2.27	723.0	1.43	0.02	0.97	69.72
BAIA MARE	0.6	1.7	0.565	44	1022	30	0.01	0.97	1011.5	8.36	0.02	0.45	151.11
TYNAGH	0.9	31.5	0.73	2.91	166	10	0.00	0.23	178.3	0.53	0.02	1.13	0.09
SWEETWATER	127.7	0.735	190.7	2.23	117	38	3.20	0.15	<0.31	0.81	0.02	0.29	0.03
Olympic Dam	9.8	1.435	0.925	41	41	3	0.02	0.16	<0.33	29.82	0.02	0.27	7.04

The variation in trace elements in galena at Penjom spans the ranges encountered in other ore deposits worldwide. Galena from stages 1, 2 and 3 are similar to those from epithermal (Baia Mare), granite related (Mt Muchison) and Broken Hill type (Broken Hill and Mt Isa) deposits in that they contain a similar range of trace elements (Bi, Tl, Sb, Ag, Au, Cd, Sn). However, ore-stage galenas from Penjom are much higher in Bi, Te and Se (1-2 orders of magnitude) as well Ag (up to one order of magnitude). Galena from Irish style deposits (Tynagh), Missippi Valley type deposits (Sweetwater) and iron oxide copper gold type deposits (Olympic Dam) tend to be low in trace elements, and similar to hanging wall galena from Penjom (with the exception of Sb, which is higher at Penjom).

8.2.2 Pb isotopes

Lead isotope signatures provide another geochemical constraint on mineralisation. The same nine samples analysed for trace elements were also analyzed for lead isotope ratios. Detailed results in Table 8.3 plot in both thorogenic (Figure 8.6) and uranogenic diagrams (Figure 8.7). The dashed lines represent best fit growth curves created using two different Pb models (light grey: Stacey and Kramers 1975; dark grey: Cumming and Richards, 1975). The data can be divided into two main groups.

8.2.2.1 Group 1

All galena samples within this group are from the mineralized zone at the footwall of the Penjom Thrust within clastic sedimentary rock, ranging from carbonaceous shale to tuffaceous sandstone. Galena is hosted within the quartz vein except for the brecciated calcite sample (Stage 3). Lead isotope ratio for Group 1 range from: $^{206}Pb/^{204}Pb$: 18.504-18.594, $^{207}Pb/^{204}Pb$: 15.693-15.756, and $^{208}Pb/^{204}Pb$: 38.864-38.985. Based on the growth curves proposed by Stacey and Kramers (1975), the age of lead at Penjom can be interpreted as 300 Ma, however, based on the model of Cumming and Richards this age decreases to 250 Ma.

8.2.2.2 Group 2

These samples are from the hanging wall of the Penjom Thrust within calcareous shale. The hanging wall galena is hosted within extensional rhombohedra calcite veins near or along the D4-D5 sinistral-normal fault. Lead isotope compositions for group 2 are: $^{206}Pb/^{204}Pb$: 18.691-18.726, $^{207}Pb/^{204}Pb$: 15.736-15.749 and $^{208}Pb/^{204}PB$: 39.093-39.164. Based on the Stacey and Kramers (1975) growth curves, the age of lead at can be interpreted as having formed at 220 Ma however, based on the model of Cumming and Richards (1975) this age decreases to 160 Ma.

Table 8.3: Lead isotope ratio of various stages of galena in Penjom.

Sample	**^{207}Pb/^{206}Pb**	**^{208}Pb/^{206}Pb**	**^{206}Pb/^{204}Pb**	**^{207}Pb/^{204}Pb**	**^{208}Pb/^{204}Pb**
Group 1					
Q2WL	0.848 ± 0.001	2.099 ± 0.002	18.552 ± 0.021	15.737 ± 0.017	38.920 ± 0.037
Q3WA	0.847 ± 0.001	2.103 ± 0.003	18.508 ± 0.018	15.714 ± 0.019	38.925 ± 0.042
JL2	0.849 ± 0.001	2.102 ± 0.003	18.549 ± 0.016	15.756 ± 0.018	38.985 ± 0.039
ZX3	0.847 ± 0.001	2.100 ± 0.002	18.540 ± 0.019	15.721 ± 0.018	38.932 ± 0.04
ZNNW	0.844 ± 0.001	2.092 ± 0.003	18.594 ± 0.018	15.693 ± 0.017	38.864 ± 0.043
JNNE	0.847 ± 0.001	2.101 ± 0.002	18.572 ± 0.016	15.741 ± 0.016	38.969 ± 0.04
Group 2					
HW-S2	0.841 ± 0.001	2.093 ± 0.002	18.691 ± 0.018	15.736 ± 0.017	39.093 ± 0.034
Gia HW-S	0.841 ± 0.001	2.092 ± 0.002	18.721 ± 0.015	15.749 ± 0.013	39.132 ± 0.031
HW-E	0.841 ± 0.001	2.090 ± 0.004	18.726 ± 0.016	15.739 ± 0.015	39.164 ± 0.067

Galena from Group 1 is less radiogenic compared to Group 2 by having less $^{206}Pb/^{204}Pb$, $^{208}Pb/^{204}Pb$ and $^{207}Pb/^{204}$ Pb ratios. In the Pb-Pb isotope ratio diagrams, the data of both groups define two distinct distributions. The $^{207}Pb/^{204}Pb$ vs $^{206}Pb/^{204}$ Pb plot (uranogenic diagram) shows wider distribution within each group compared to the $^{208}Pb/^{204}Pb$ vs $^{206}Pb/^{204}Pb$ plot (thorogenic diagram) which is possibly as a result of larger uncertainty for the measurement of $^{207}Pb/^{204}Pb$ ratio. Both groups plot between the upper crustal growth curves and bulk crustal growth curves or orogen based on Plumbotectonics model of Doe and Zartman (1979).

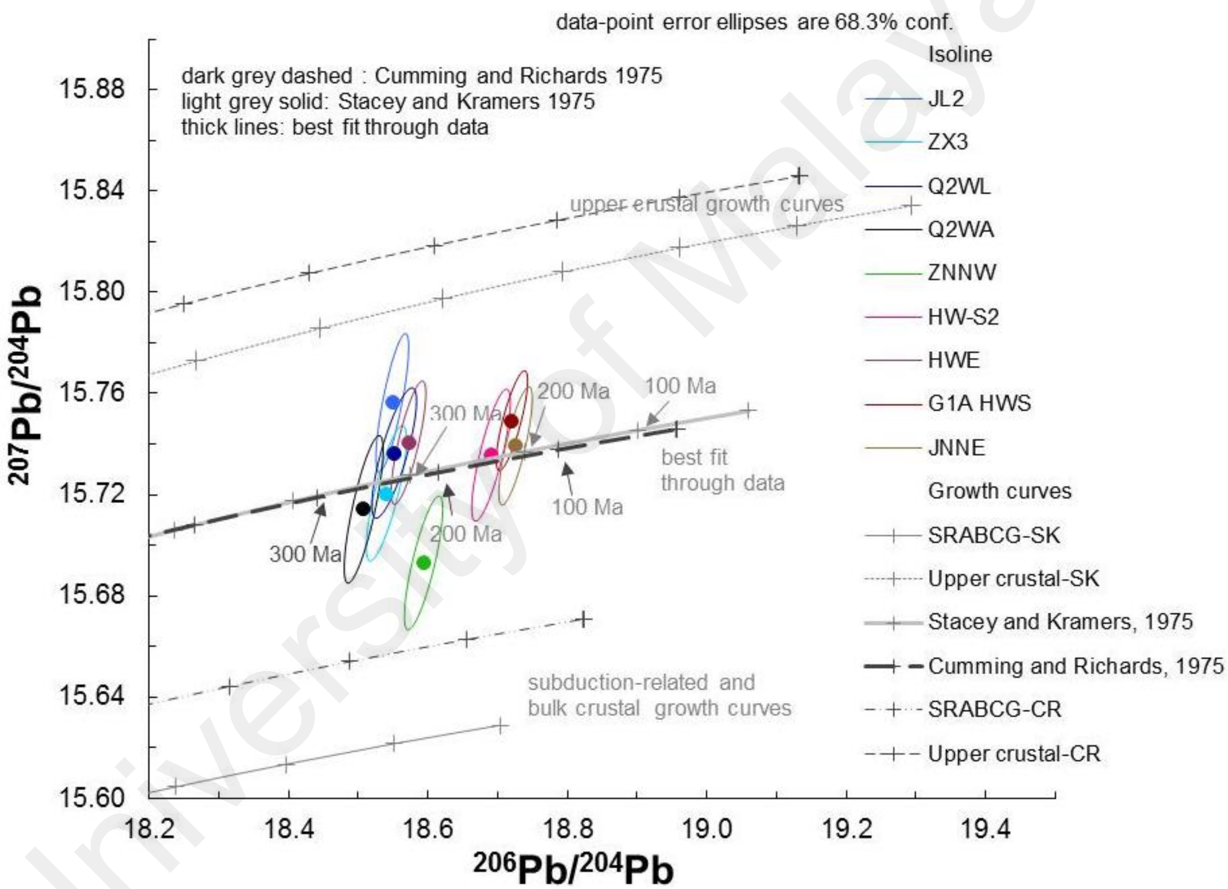

Figure 8.6: Summary plot of lead-isotope ratio $^{206}Pb/^{204}Pb$ vs $^{207}Pb/^{204}Pb$. SRABCG-Subducion-related and bulk crustal growth, SK-Stacey and Kramers (1975), CR- Cumming and Richards (1975)

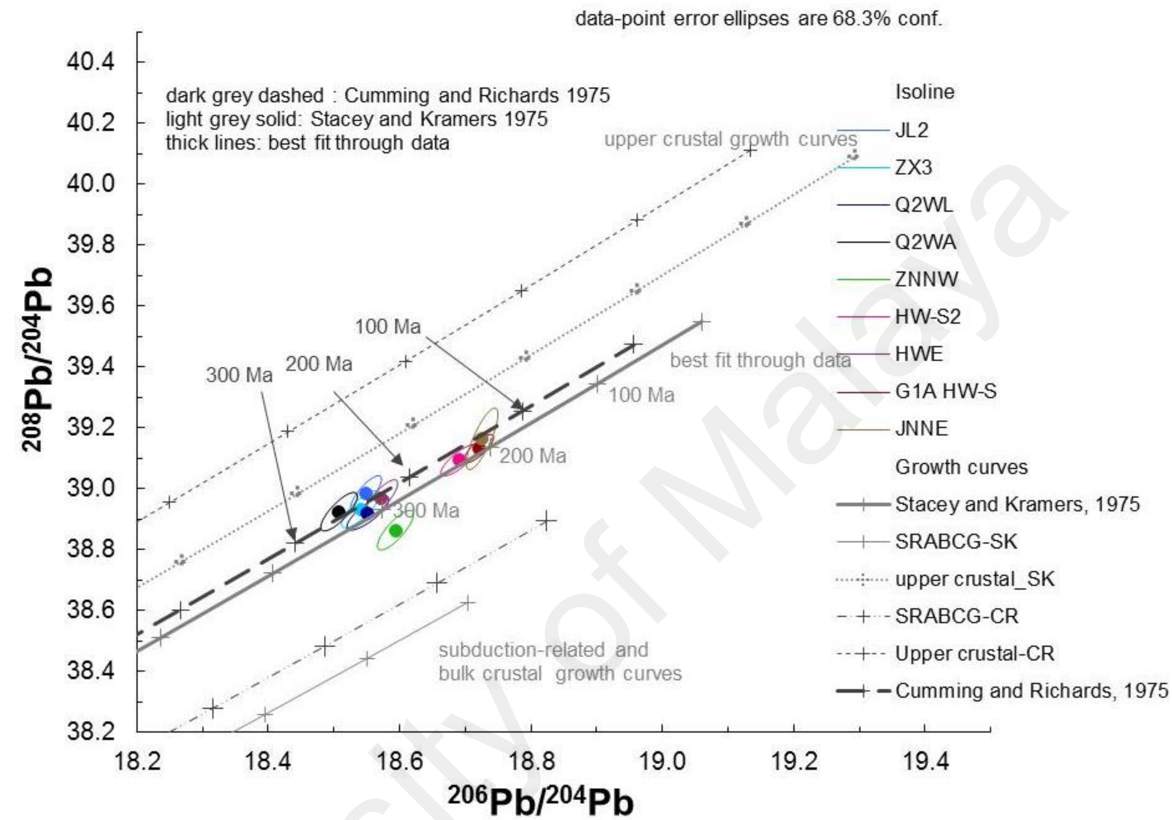

Figure 8.7: Summary plot of lead-isotope ratio $^{206}Pb/^{204}Pb$ vs $^{208}Pb/^{204}Pb$. SRABCG-Subducion-related and bulk crustal growth, SK-Stacey and Kramers (1975), CR- Cumming and Richards (1975)

8.3. Discussion

Detailed geological structural analysis and vein paragenesis are important to the understanding of deformation history and the relationship to gold-sulphide mineralization in the Penjom Gold Mine. This analysis suggests the development of high grade bedding parallel gold-bearing quartz veins, during folding and thrusting, which is during the deposition of stage 1 galena and early gold. Stage 2 sulphide including galena crystallised during faulting but after folding led to the formation of fault-related veins. Stage 3 gold mineralization could be from residual fluid or remobilization during recrystallization of vein at fault margin. However, Stages D4 to D5 faults, which host coarse-grained Stages D4 to D5 galena, is almost certainly not related to the main mineralizing processes and probably much later in origin.

The trace elements geochemistry and Pb isotopes of galena show two main distinct groups and trends. In the galena from mineralisation stages, higher Ag, Te, Se, Cd and Bi were recorded compared to hanging wall galena. Galena in shear veins with two different morphologies (dendritic and anhedral) yielded almost identical results, suggesting that different morphologies can crystallise at the same time and from the same fluids. If the dendritic galena formed as a result of local remobilization of earlier galena it would be unlikely to preserve the same chemistry. Differences in worldwide galena and those from Penjom suggest that trace elements are sensitive to the physical and chemical condition in which they form. This is probably partially as a result of competition for various trace elements between other sulphides which are co-precipitating with the galena as well as a function of fluid chemistry and timing.

Few analyses have been published for trace element analysis of galena in orogenic gold deposits or sediment-hosted vein related deposits due to the lack of galena associated within the ore zone. Galena inclusions in pyrite at sediment-hosted Sukhoi Log have been analysed by Large et al., (2007). The result shows a similar elevated content of Bi (1.9 wt percent), Te (423 ppm) and Ag (1.1 wt percent) interpreted as sourced from sedimentary host rock. This may suggest a similar source of metal for Penjom which is hosted in sedimentary units, especially carbonaceous shale.

The two data clusters in the Pb isotope ratios clearly differentiate between two main episodes of crystallisation. The Pb isotopic ratios are transitional between the bulk crustal growth (or the orogen curve of Doe and Zartman 1979) and an upper crustal growth curve suggesting derivation from arc rocks associated with thick continental crust or a crustal source that includes arc volcanic and old continental sedimentary rocks. The Pb in both groups of galena is from reservoirs with similar U/Pb and Th/Pb ratios but which differ in the amount of radiogenic Pb.

Pb isotopes in SE Asia have recently been reviewed (Meffre, personal communication, 2014) and the growth curve of Cumming and Richards (1975) tends to give more accurate model ages than that of Stacey and Kramers (1975) particularly for samples that plot above the average crustal growth curve. This indicated a Permian or Early Triassic Pb model age for the early Pb and accompanied Au and a Jurassic or Cretaceous for the late stage calcite veins. Interestingly the Pb isotopic composition of the nearby Selinsing Au deposit contrasts markedly with those reported here as they are very radiogenic in composition and plot on an upper crustal growth curve (Meffre, personal communication, 2015; Makoundi et al., 2013; Makoundi 2012).

8.4 Conclusion

The least radiogenic galena (and possibly the oldest) is associated with Au, Te, Se and Bi in contrast to other groups. The higher Te, Se and Bi in the galena from the mineralized group indicated the derivation of fluid and metal from the wall rock, consisting of carbonaceous shale during the migration of hydrothermal fluid. The Permian to Early Triassic Pb model age for Au-bearing galena contrasts with the Jurassic K-Ar age (194-197Ma), previously obtained for the Penjom deposit (Flindell, 2003). However, this age is consistent with the

Late Permian age of the host rocks (Leman et al., 2005). The occurrences of calcite with galena associated with late cross-cutting fault may suggest the timing of that structural event at 160 Ma or middle-late Jurassic. This structural event displaced and deformed the early vein.

CHAPTER 9 DISCUSSION AND CONCLUSIONS

9.0 Introduction

Geological mapping and observation were part of ore mining supervision by the author for the past 17 years of operation. Mapping practice includes pit wall mapping, temporary face mapping, floor mapping and blast surface mapping by using ore mark-out as a reference point. A combination of different types of mapping allowed all aspects of geology from different views to be analyzed and incorporated into an overall understanding. Geological aspects outlined in this study include stratigraphy and host rock, style of veins, gold-sulphides occurrences, folded rock, fault and geochemistry aspect including fluid inclusions and lead isotope.

9.1 Gold deposits classification

Understanding different types of gold deposits classification is critical for regional and local understanding of ore deposits, especially for exploration. Prior to 1999, gold deposit classification has been generally based on depth and temperature of the formation. As such, different types of deposit in contrasting geological settings have not been properly differentiated and actual depth based on micro-thermometry studies not always fix into the definition.

Better understanding of geochemistry, structural control, sources of gold and tectonic settings has led to more refined deposit classifications. For example, the earlier term mesothermal gold deposit has been reclassified into two main categories “orogenic lode” and “intrusion related” gold. Orogenic gold is further subdivided into epizonal, mesozonal and hyipozonal based on temperature and depth of formation. The determining characteristic is the source of the fluid which is commonly metamorphic sources.

Competency contrast is a very common feature of the host rock, and structural deformation often occurs in brittle-ductile zone involving multiple fluctuations of stress. Deposits where in situ sources that are associated with carbonaceous hosted syn-sedimentary or diagenetic pyrite in which gold occurs in solid solution and later remobilised/enriched during metamorphism have been defined as sediment hosted gold deposits.

Another type of deposit is intrusion related located in the environment of orogenic lode gold and hosted in an intrusive, but having relationship to gold more than just being the host rock. The host intrusives are sourced from the same igneous body that provided the heat and metal during the pro-grade metamorphic environment. In other words, the intrusive that hosts the ore bodies has a temporal relationship with mineralizing fluid.

Penjom is classified as orogenic gold, where early pyrite and arsenopyrite dominates over base metal sulphides. A felsite intrusive unit is a very important component of the host rock but only contributes to heat and rheological contrast during structural deformation.

9.2 Summary of structural deformation

At the Penjom deposit, early deformation event can be correlated with the main Late Triassic orogeny along the Bentong–Raub Suture and the formation of Main Range Granite. New ages from the recent U-Pb zircon ion microprobe analysis are entirely Late Triasic, 227-201 Ma (Ng et al., 2015). This event is possibly responsible for the tilted strata at Penjom and the development of strike ridge lineaments. During the late stage of this orogeny or shortly after, Central Belt intrusive such as the Benom Complex were emplaced into Permo-Triassic strata with the injection of many felsic sills and dykes, possibly including those seen in the Penjom area. Confirmation of this requires that the age of the Benom Complex is known. Continuous deformation, regional low-grade metamorphism and early broad folding are classified as D1 deformation. The structural deformation that controls the gold-mineralised vein systems affects the intruded felsic rocks which, in this case, act to provide an important rheological contrast together with carbonaceous host rock. Host rock sequences dominantly strike NNE, similar to the regional strike of the former Padang Tengku Formation (Gunn et al., 1993) which is now included as part of the Gua Musang Formation (Leman, 1995). Rock sequences at the north and south end of the pit are orientated 35°E or NNE parallel to the regional strike. This represents the eastern limb of the broad fold interpreted as formed during the D1 event.

Continuous compressive to transpressive deformation along the Bentong–Raub Suture (Shuib, 2009) which includes the Penjom area resulted in D2 thrusting and folding. In the KE pit, the sequence is folded to an antiform–synform below the Penjom Thrust where the antiform is referred to as the Kalampong anticline and plunges toward the south. Bedding-plane-slip activity and the development of bedding-parallel quartz or shear veins took place during this period of deformation. The western limb of the anticline forms a major ore body where the previously mined ore zone at the upper levels was known as the North–South Jewel Box corridor. The term NS fault used for the cross-cutting fault is a different element from the NS trending ore bodies. Broad cross folds with EW axes affect the limb of the synform, resulting in NNW trending bedding in the southwest and northwest of the Kalampong pit and Manik pit.

Continuous tightening of the Kalampong fold resulted in fold lock-up and development of a fault to accommodate the stress in a D3 deformation event. Dominant NNE trending faults exhibiting reverse, oblique-reverse and dextral sense of movements can be observed displacing the earlier shear veins. Such faults also control significant extensional vein mainly at the contact with the felsic intrusives. A sinistral-reverse sense of movement can further be observed on NNW trending faults which are sub parallel to bedding and carbonaceous shale in the Jalis-west wall corridor; such movements are considered merely as local deformation as they reactivate on the existing D2 shear. These fault movements may in part reactivate the early shear vein by adding more fluid into the structure. Several EW faults offset the ore body and are inferred to be a later stage of the D3 event prior to the change of stress direction before the D4 and D5 events.

Mine scale NS trending D4 (sinistral) and D5 (normal–oblique-normal) faults are easily recognised on the hanging wall of the Penjom Thrust. The faults cross cut and at certain stretch, reactivated along the Penjom Thrust or NNE trending bedding shears. Striations on slickenside surfaces indicate a normal to slightly oblique sense of movement. Fault striations on a NS trending fault on the hanging wall of the Penjom Thrust together with an apparent displacement of a marker bed, indicate that sinistral strike-slip movement may have occurred prior to a normal sense of movement. Recognising this, sinistral movement is inferred as representing a D4 event before relaxation of stress or an extensional period that resulted in normal movement of the same fault; this normal movement is classified as a D5 deformation phase. The D1 to D3 deformations are regarded as having developed during the compressional to transpressional activity, whereas the later D4 deformation marks a change in stress direction with the development of a new NS trending fault. The D4 and D5 events are considered as being developed during the transtensional regime. The final phase of the D5 deformation event may be related to intensive faulting that occurred within the Central Belt and was responsible for basin development and deposition of Cretaceous continental deposits.

9.3 Veins, sulphides and gold

Mineralised veins are related to two main episodes: fold and thrust-related veins mainly comprised of bedding and Penjom Thrust parallel shear veins and associated extension veins developed during the D2 event. In addition, NE to NNE and locally NS trending splays and Penjom-Thrust-parallel reverse faults and dextral strike-slip faults, formed a new episode of extensional veins, mostly at the contacts of intrusives with the sedimentary host rock either as sheeted, stockwork or hydrothermal quartz breccias or as shallow-dipping veins within the intrusive bodies. Style, morphology of veins, lithology of site and reactivation are summarised in Table 5.03.

Pyrite and arsenopyrite are hosted both in the veins and disseminated in altered wall rock. Later sulphides such as galena, sphalerite and chalcopyrite are only found in veins. Pyrite is dominant within the ore zone and in carbonaceous units. Arsenopyrite is dominant in shear veins, hosted in carbonaceous shale and to a lesser extent in fault related veins. Galena shows three modes of occurrence: infilling the interstices between quartz grains, infilling fractures and in a instances, in the hanging wall associated with non-mineralized calcite veins. This represents two different phases of mineralised galena and one of late, barren galena. XRF analysis of different types and phases of ore veins with or without the wall rock indicates the close association of Au with As, Bi, Zn and Pb. D2 veins are higher in As, while As moderate to low in D3 veins. This suggests two stages of As which is during D2 and D3 related vein episodes.

Gold must be introduced in at least two episodes: during the earlier pyrite and arsenopyrite associated with shear vein, and then later during the deposition of galena with pyrite associated with fault related vein. Based on the structural interpretation, D2-D3 event represents ductile and brittle-ductile episodes, and can be correlated with the deposition of gold and sulphides. Gold may have already been deposited during the ductile episode, as indicated by gold inclusions in early arsenopyrite or pyrite, and gold that has been deformed along the graphitic surface in ribbon quartz. Fault events after the fold was locked-up represent the D3 event in which gold was re-introduced together with base metal sulphides and also involved remobilisation of earlier gold. The later D4-D5 event includes transtensional to extensional deformation, and cross cuts and displaces the veins system. A late phase of cubic coarse galena grains associated with barren rhombohedra calcite was introduced during this event. Structural events, vein, mineralogy and sulphide paragenesis is summarized in Table 6.3 and Figure 6.33. The D1 event represents early deformation prior to the main mineralization event of D2-D3 deformation and D4 to D5 mostly reactivated and displaces the ore bodies.

9.4 Geochemistry and wall rock alteration

Geochemistry analysis includes fluid inclusion for thermometry, major and minor analysis of host rock, XRD analysis of CO_3 for vein mineralogy and clay mineral related to wall rock alteration. Galena has been analyzed for the trace elements and Pb isotopes. Major element analyzes of the host rock indicates high alumina content for fine grain material and high silica content for coarse grained rock. This is a typical geochemistry composition for a turbiditic sequence. Bulk sampling across the ore zone shows almost the same trend where carbonaceous rich ore zone is high in alumina and low in silica. Low silica can be attributed to de-silicification during hydrothermal alteration as well as to varying contents of quartz grains and clay in shales. In the south wall, arsenic content only detected in ore zone, and is indication of arsenopyrite as the main mineral accompanying mineralization.

Major element analyzes of carbonate veins indicate that the main carbonate minerals are calcite and minor ankerite. The dominant clay minerals are sericite (fine grain muscovite), chlorite and illite which are typical phyllic alteration assemblages. Alteration sericite related to mineralization in intrusive host rock has been dated and yielded an age of 194Ma (Bogie, 2003) and coincided with the orogenic event in the Triassic-Jurassic involving dextral transpression along the Bentong-Raub Suture (Shuib, 2009) which probably also affected the NNE splay of this structure.

Fluid inclusions with H_2O liquid-vapor phase and CO_2 bearing inclusion have total final homogenization temperatures in a range between 140^{o}C to 200^{o}C and between 250^{o}C to 350^{o}C. Trace element and lead isotopes in galena reveal two chemically distinct types of galena. Galena from the hanging wall has a lower value of Se, Te, Cd and Bi compared to galena from the ore zone, suggesting a possible influence of carbonaceous wall rock. Lead isotope data plotted in thorogenic and uranogenic diagrams plot between upper crustal and bulk crustal growth curves. However, lead from the mineralized zone is less radiogenic compare to hanging wall galena and this gave two population of lead isotope with different age and timing of structural setting. Barren galena-calcite veins show a lead isotope age of 160 Ma (based on Cumming and Richards, 1975) which suggests late, post mineralization fault activity. Geological elements and deformation episodes are summarised in Figure 9.1.

9.5 Implication for regional tectonic setting

The structural evolution and veining episodes at Penjom suggest that a compressional event was followed by a transpressional and later post-vein extensional episodes. These structural events may reflect the deformation affecting the Central Belt. In terms of structural timing of vein episodes, a deformation phase related to vein was started with the D2 deformation of fold and thrust, followed by D3 reverse and dextral strike-slip faults, then sinistral D4 deformation and much later D5 normal faulting. The D2 mineralised veins such as bedding-parallel shear veins, associated discordant E-W extension vein and saddle-reef style are characteristic of the formation under a compressional regime reflecting the regional orogenic event.

Based on the age of sericite as a hydrothermal alteration product (Bogie, 2002, 2004; Flindell, 2003) which is considered here as the age of mineralization, it is proposed that the compressional or transpressional regime that controlled mineralised vein formation at Penjom and possibly other vein-hosted deposits such as at Bukit Koman, Raub and along the Bentong–Raub Suture occurred in Late Triassic-Early Jurassic times. Richardson (1939a) reported that the eastern and western lode channels of Bukit Koman (Raub gold mine) were located along a compression fault and some of the veins were parallel to the bedding (Figure 9.2). The sequences at Bukit Koman have been folded into anticlines and synclines, recumbent towards the northeast or east-northeast. The extensional faults with veins, which are comparable to extensional veins at Penjom, occur more or less simultaneously with a compression fault related vein. Post mineralization oblique faults displace the ore zone in a lateral sense.

The term ‘post-collisional’ is used to describe geological activity after the termination of subduction due to the collision of the Sibumasu terrain and the Eastern Malaya. As a result, the host rock along the Bentong–Raub Suture zone and parallel structures have undergone deformation, providing a conduit and trap for mineralised fluid. Despite the term post-collisional, the timing is considered as the late stage of the orogenic event which is a common characteristic of orogenic gold (Groves et al., 1998; Goldfarb et al., 1998).

The quiet period during the Early to Late Jurassic, without a stratigraphic record, indicates that the Central Belt was already uplifted from the marine environment to form the land mass as a result of the collision between the Sibumasu and Indochina blocks. Faulting during the Late Jurassic responsible for basin development and deposition of continental deposits may be reflected by the series of normal faults at Penjom.

9.6 Conclusion

Through systematic mapping and the right elements of geology studied in Penjom Gold Mine, a comprehensive geological understanding has been developed. A consideration of all aspects of geology including stratigraphy, economic geology and structural geology such as host rock, vein, sulphide, alteration together with fold and fault analysis gives a complete understanding of mineralization events. Two main phases involving vein related episodes and post vein displacement (Endut and Teh, 2010) has been derived.

Mineralization and vein processes dominantly took place during D2 thrusting and folding deformation dominated by ductile-brittle followed by brittle event as the D3 episode that also displaced the earlier veins but also create new veins system. Veins exhibit both structural and textural similarities to many other Orogenic Lode Gold deposits. The relative role of fold and faulting is comparable to other structurally controlled, vein hosted gold deposits as summarised in Table 9.1. Lead isotopes and fluid inclusions also support mobilisation and leaching of metals along the fluid pathways and the metamorphic contribution as indicated by CO_2 inclusions inside the vein systems.

Element	**D1**	**D2**	**D3**	**D4 - D5**
Structural deformation				
Regional fold (D1)	--------			
Local fold and thrust (D2)		--------		
Fault, mainly reverse (D3)			--------	
Fault, mainly normal (D4-D5)				-----------
Vein (mineralised)				
Shear vein		---------		
Extensional vein				
Sheeted vein		---------	----------	
Stockwork		---------	----------	
Hydrothermal breccia		---------	----------	
Brecciated quartz			----------	

Mineralogy				
Quartz (grey)		---------		
Quartz (white)		---------	----------	
Calcite		---------	----------	-----------
Dolomite		----	----	
Texture				
Comb (extensional vein)			----------	
Face control fibers			----------	
Anhedral buck quartz				
In massive shear vein		------------		
In extension vein		------------	-----------	
Laminae (vein septa)		------------		
Stylolite		-----------	-----------	
Planar		-------------		
Irregular/wavy			------------	
Breccia infill			-----------	-------
Breccia aggregate			------------	--------
Ribbon quartz		------------		
Spider veinlet			-----	---------
Micro-texture of vein				
Polygonal grain			-----------	
Undulose extinction		----------		
Suture grain				
Fractured grain			-------------	----------
Sulphide/mineralization				
Free gold		-----------	-----------	
Arsenopyrite		-----------	-----------	
Pyrite	----------	-----------	-----------	
Sphalerite		-----------	-----------	
Chalcopyrite		-----	-----------	
Galena		------	-----------	----------
Wall rock alteration				
Pyritisation	----------	-----------	-----------	
Arsenification		-----------	----	
Pyllic		-----	-----------	

Figure 9.1: Summary of the geological elements studied and a possible correlation with a deformation event

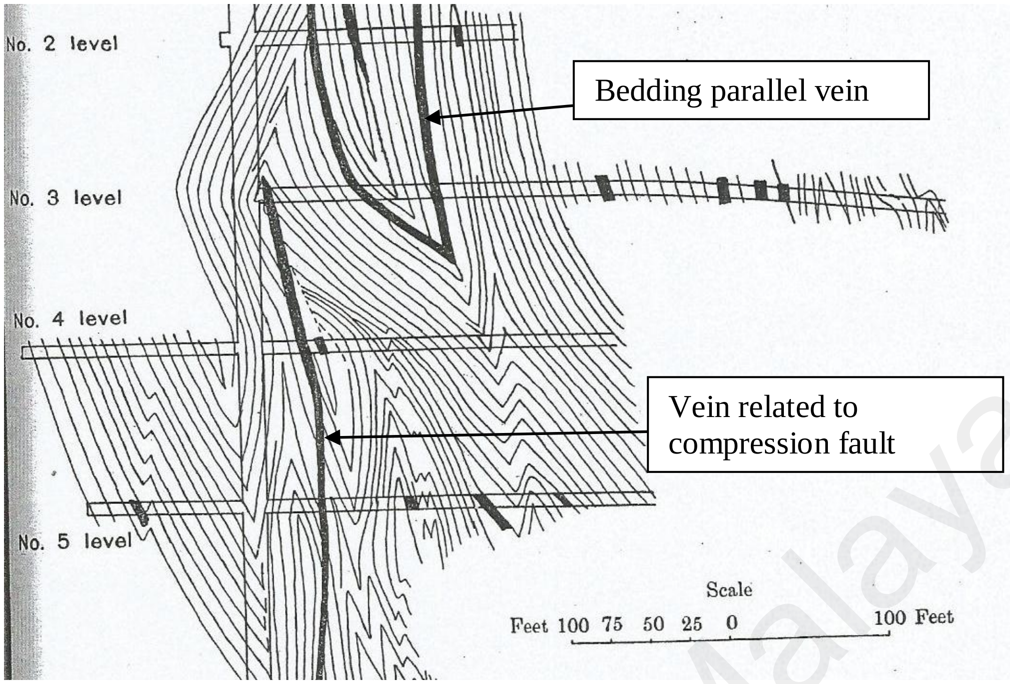

Figure 9.2 Cross section at Bukit Koman (Raub) underground gold mine showing vein parallel to compression fault and bedding

Table 9.1: Tectonic setting, structural episodes and timing of veins formation for several major gold deposits and comparison to Penjom gold deposit.

Mine	Tectonic Environment	Early structure (folding) and veining	Reactivation and veining (faulting)	Post vein faulting
Ashanti Gold Mine, Ghana (Allibone H. A., 2002)	Regional SE directed shortening, reactivation late in the same event	D1-D3, NE-ENE striking fold produced bedding parallel quartz vein. Vein is barren	D5, sinistral fault formed tensional array mineralized quartz vein, geometry controlled by fault	
Magdala gold system, Stawell, Australia	Crustal thickening, closure of the basin, inferred subduction zone	Early ductile produce fold and NW/SW structural trend, produced fold related quartz vein. Vein are barren	Brittle deformation (sinistral reactivation) produced its own geometry quartz vein and mineralized wall rock sulphide	
Bendigo-Ballarat, Australia (Schaubs, P.M., 2002)	Closure of the basin, inferred subduction zone. E-W compression produce chevron fold	Fold produced mineralized bedding parallel quartz, saddle reef and discordant vein.	Reversed fault allowed more mineralized fluid into structural trap such as saddle reef	
Meguma Terrane, Nova Scotia, Canada	NW transpressional produced NE-SW trending fold	Fold produced bedding parallel quartz, saddle reef and discordant mineralized vein.		
Hodgkinson Gold Field, (Davis & Hippert, 1998)	Collisional tectonism	Folded rock and shear at all scale (D2) not related to vein episode	D4 reactivation of shear and fault host to laminated vein and related extensional fractures vein	
Beaufor Gold Deposit, Abitibi Greenstone Belt, Canada (Tremblay A., 2001)	Regional North to NE directed shortening and reactivated late in the same event		Quartz related to the second and third order reversed shear and related fractures	Oblique-reversed and dextral faults, synthetic and antithetic, riedel type.
Penjom gold deposit, Malaysia	Regional compression to transpressional, east to west along Bentong Raub Suture	Fold (D2) and reversed-dextral (D3) fault control bedding parallel quartz and discordant vein respectively.	Reverse/dextral NNE and reverse sinistral for NNW controlled mineralized extensional vein	Extensional faulting mostly displace D2-3 related mineralized quartz vein.

REFERENCES

Abdul Aziz, J. H., 2007. Geochemistry and EPMA characterisation of Gold in the Central Belt Area, Peninsular Malaysia. MSc Thesis University of Malaya, 183p.

Allibone, H. A., 2002, Structural control on gold mineralization at the Ashanti Deposit, Obuasi, Ghana. Society of Economic Geologist Special Publication 9, 2002, p. 65-93.

Alain Tremblay, 2001, Post mineralization faults in the Beaufor Gold Deposit, Abitibi Greenstone Belt, Canada: Geometry,origin and tectonic implication for the Val-d'Or Mining District. Economic Geology. Volume 96. p 509-524.

Ariffin, K. S. (1994). Geology and mineralogy of the Penjom Gold Mineralization prospect Kuala Lipis, Pahang Darul Makmur. Unpublished M.Sc. (Hons) thesis, Department of Geology, University of Malaya.

Ariffin, K.S. and Hewson, N. J., 2007 Gold related sulphide mineralization and ore genesis of the Penjom gold deposit, Pahang, Malaysia. Resource Geology, 57, p. 149-169.

Bierlein F.P., Fuller T., Stuwe K, Arne D.C., Keays R. R., 1998. Wallrock alteration associated with turbidite-hosted gold deposits. Examples from the Palaeozoic Lachlan fold belt in central Victoria, Australia. Ore Geol Rev 13:345–380

Bierlein, P.F., Cartwright, I. and McKnight S., 2001, The role of carbonaceous "Indicator Slate" in the genesis of lode gold mineralization in the Western Lachlan Orogen, Victoria, Southeastern Australia. Economic Geology 96, No 3. p. 432-451.

Blevin, P. L., 2008. Redox and compositional parameters for Interpreting the granitoid metallogeny of Eastern Australia: Implications for Gold-rich Ore Systems. Resources Geology, v54, p. 241-252.

Bogie, I., 2002. Petrology report on 15 samples from Penjom Gold Mine, Malaysia. Report to Specific Resources Sdn. Bhd., p. 1–25 (Unpublished).

Bogie, I., 2004. Petrology report of 27 samples from Penjom Gold Mine, Malaysia. Report to Specific Resources Sdn. Bhd., p. 1-30 (Unpublished).

Bortnikov, N.S., Genkin, A.D., Dobrovol'Skaya, M.G, Muravitskaya, G.N. and Filimonova, A.A., The nature of chalcopyrite inclusions in sphalerite: Exsolution, coprecipitation or 'disease'? Economic Geology 86, p. 1070-1082.

Cline, J. S., Hofstra, A. H., Muntean, J. L., Tosdal, R. M. and Hickey, K. A., 2005. Carlin-Type Gold Deposits in Nevada: Critical Geologic Characteristics and Viable Models. Economic Geology 100th Anniversary Volumepp. p. 451–484.

Cobbing, E.J., Mallick, D.I.J., Pitfield, P.E.J. and Teoh, L.H., 1986. The granites of Southeast Asia. Journal of Geological Society of London, 143, p. 537-550.

Corbett, G.J., and Leach, T.M., 1998, Southwest Pacific rim gold-copper systems: Structure, alteration and mineralisation: Economic Geology, Society of Economic Geologists, Special Publication 6, 238 p.

Corbett G.J., 1997. Comments on the controls to gold mineralization at the Penjom Gold Mine and environs, Malaysia. Report to Specific Resources Sdn. Bhd., 13p (Unpublished.).

Corbett G.J., 1999. Comments on the controls to gold mineralization at the Penjom Gold Mine, Malaysia. Report to Specific Resources Sdn. Bhd., 22 p. (Unpublished.).

Cox S.F., Knackstedt M.A. and Braun J., 2001. Principle of structural control on permeability and fluid flow in hydrothermal systems. In Richards J. P. and Tosdal R.M (Eds) Structural controls on ore genesis, Reviews in Economic Geology, Society of Economic Geology, 14, p. 1-24.

Cox, S.F., Wall, V.J., Etheridge, M.A., and Potter, T.F., 1991, Deformational and metamorphic processes in the formation of mesothermal vein hosted gold deposits- examples from the Lachlan Fold Belt in central Victoria, Australia: Ore Geology Reviews, v. 6, p. 391 – 423.

Cumming, G.L. and Richards, J.R., 1975. Ore lead isotope ratios in a continuously changing earth. Earth and Planetary Science Letters, 28: p. 155-171.

Danyushevsky, L., Robinson, P., Gilbert, S., Norman, M., Large, R., McGoldrick, P., Shelley, M., 2011. Routine quantitative multi-element analysis of sulphide minerals by laser ablation ICP-MS: Standard development and consideration of matrix effects. Geochemistry: Exploration, Environment, Analysis, 11: p. 51-60.

Davis, B. 2005a. Post-workshop report pertaining to the Penjom and North Lanut mining operation. Avocet Mining Plc structural geological workshop. 38p. (unpublished)

Davis, B. 2005b. Avocet Mining Plc, Structural geological training course notes

Davis, B. and Hippertt J.F.M, 1998. Relationships between gold concentration and structure in quartz veins from the Hodgkinson Province, Northeastern Australia. Mineralium Deposita 33: p. 391-405.

Diamond, L.W., 1992. Stability of CO2 clathrate hydrate + CO2 fluid + CO2 vapour + aqueous KCl-NaCl solutions: Experimental determination and application to salinity estimates of fluid inclusions, Geochemica et Cosmochimica Acta Vol 56, p. 273 – 280.

Doe, B.R., Zartman, R.E., 1979. Plumbotectonics I, The Phanerozoic. In: Barnes, H.L. (Ed.), Geochemistry of Hydrothermal Ore Deposits. Wiley Interscience, p. 22–70.

Dowling, K. & Morrison, G., 1989, Application of quartz textures to the classification of gold deposits using north Queensland example. Economic Geology Monograph., 6: p. 342-355.

Fillis, P., 2000. Penjom resource model; Internal Report for Specific Resources Sdn. Bhd. (Unpublished)

Endut, Z., Haznur, R., Mohammed, S., Ismail, S., Prihananto, A., 2014. Geology of the Penjom Gold Deposit, Pahang, Malaysia. Proceeding of Sundaland Resources 2014 MGEI Annual Conference, November 17-18, Palembang, Sumatra, Indonesia. p. 301-308.

Endut, Z., Ng, T. F., Abdul Aziz, J. H., Teh, G. H., 2015a. Structural analysis and vein episode of the Penjom Gold Deposit, Malaysia: Implications for Gold Mineralisation and Tectonic History in the Central Belt of Malaysia, Ore Geology Reviews V. 69, p. 157-173.

Endut, Z., Ng, T. F., Abdul Aziz, J. H., Teh, G. H., 2015b. Style of veins in Penjom Gold Mine, Malaysia–Implications for gold mineralisation and structural episodes. PACRIM Hong Kong, China, 18-20 Mac 2015.

Endut, Z., Ng, T. F., Abdul Aziz, J. H., Teh, G. H., Mohammed, S., 2014. Style, textures and paragenesis of veins in Penjom Gold Mine, Malaysia: Implications on gold mineralization episode. Abstract of GEOSEA 2014 Conference, Yangoon, Myammar

Endut, Z. and Teh, G.H., 2010. Structural control on quartz vein in Penjom Gold Mine with emphasise of Kalampong Pit. Proceedings of the Annual Geological Conference 2010, Geological Society of Malaysia, 11-12 June 2010, Shah Alam.

Endut, Z., Ng, T. F and Teh, G.H., 2012. Some aspect of vein texture, microstructure and implication to gold mineralization episode in Penjom Gold Mine. Proceeding of the Annual Geological Conference 2012, Geological Society of Malaysia, June 2012, Kuching, Sarawak.

Flindell, P., 2003. Avocet mining: Exploration and development across central and Southeast Asia. Australia Institute of Geoscientists (AIG), Mineral Exploration Discussion Group (SMEDG), 10 October, Sydney, Australian Institute of Geoscientists, Perth, 8p.

Fowler, T.J., and Winsor, C.N., 1997. Characteristics and occurrence of bedding-parallel slip surfaces and laminated veins in chevron folds from the Bendigo-Castlemaine goldfields: Implications for flexural-slip folding. Journal of Structural Geology, v. 19, p. 799–815.

Goldfarb, R.J., Phillips, G.N. and Nokleberg, W.J., 1998. Tectonic setting of synorogenic gold deposits of the Pacific Rim. Ore Geology Reviews, 13, p. 185-218.

Groves, D. I., Goldfarb, R. J., Gebre-Mariam, M., Hagemann, S.G. and Robert, F., 1998, Orogenic gold deposits: a proposed classification in the context of their crustal distribution and relationship to other gold deposit types. Ore Geology Reviews, v. 1, p.7-27.

Groves, D.I., Goldfarb, R.J., Robert, F., and Hart, C.J.R., 2003, Gold deposits in metamorphic belts: overview of current understanding, outstanding problems, future research, and significance: Economic Geology, v. 98, p. 1 - 29.

Gunn, A. G., Ab. Halim Hamzah, Paul Ponar Sinjeng, Wan Zawawi Wan Akil, Dzazali Ayub, Chow Chong, 1993. Gold mineralization at Penjom, Kuala Lipis, Pahang, Malaysia: Geological Survey of Malaysia-British Geological Survey Gold sub-programme report 93/1.

Guillong, M., Kuhn, H.R., Gunther, D., 2003. Application of a particle separation device to reduce inductively coupled plasma-enhanced elemental fractionation in laser ablation inductively coupled plasma-mass spectrometry. Spectrochimica Acta - Part B Atomic Spectroscopy, 58: p. 211-220.

Hodgson, C.J., 1989. The structure of shear related, vein type gold deposit: A review. Ore Geology Reviews, 4, p. 231-273.

Kidd, R.P. and Zainuddin, F., 2000. Geology of the Penjom gold deposit, Pahang, Malaysia. Conference Proceeding Asia Pacific Mining & Quarrying 2000, Nov. 16-18, Kuala Lumpur.

Kojima, S. and Sugaki, A. 1987. Phase relations in the Cu_Fe_Zn_S system between 500 ^{o}C and 300^{o}C under hydrothermal conditions, Economic Geology 80, p. 158-171

Large, R.R., Bull, S.W., Maslennikov, V.V., 2011. A carbonaceous sedimentary source rock model for Carlin-type and orogenic gold deposits: Society of Economic Geologists, v. 106, p. 331 - 358.

Large, R.R., Maslennikov, V., Robert, F., Danyushevsky, L.V., Scott, R.J., and Chang, Z., 2007, Multi-stage sedimentary and metamorphic origin of pyrite and gold in the giant Sukhoi log deposit, Lena Goldfield, Russia: Economic Geology and the Bulletin of the Society of Economic Geologists, v. 102, p. 1,233 - 1,267.

Leman, M.S. 1995. The significance of Permian volcanic activity towards faunal development in Padang Tengku area, Pahang. Sains Malaysiana 24(1): p. 17-28.

Leman, M.S, Ramli, N., Mohamed, S. and Molujin, S., 2005. The discovery of Late Permian (early Changshingian) brachiopods from Penjom, Pahang Darul Makmur. Geological Society of Malaysia Bulletin, 48, p. 91-94.

Ludwig, K.R., 2008. User manual for Isoplot 3.70, Berkeley 79.

Lindgren, W., 1933. Mineral Deposits, 4th ed. McGraw Hill, New York and London, 930 p.

Mawer C.K., 1987, Mechanics of formation of gold-bearing quartz veins, Nova Scotia, Canada: Tectonophysics, v. 135, p. 99-119.

Makoundi, C., 2012. Geology, Geochemistry and Metallogenesis of Selected Sediment-hosted gold deposits in the Central Gold Belt, Peninsular Malaysia. Unpublished MSc thesis, University of Tasmania, 212 p.

Makoundi, C., Zaw, K., Large R. R., Meffre, S., Chun, K. L. and Teh, G.H. 2013. Geology, geochemistry and metallogenesis of the Selinsing gold deposit, Central Malaysia. Gondwana Research. doi: 10.1016/j.gr.2013.08.023.

Meffre, S., Large, R. R., Scott, R., Woodhead, J., Chang, Z., Gilbert, S. E., Danyushevsky, L. V., Maslennikov, V., and Hergt, J. M., 2008, Age and pyrite Pb-isotopic composition of the giant Sukhoi Log sediment-hosted gold deposit, Russia: *Geochimica et CosmochimicaActa*, 72: p. 2377-2391.

Meffre, S., Chun, K. L., Zaw, K., Khositanont, S., Salam, A., Manaka, T., Maas, R., Mohd Basori, B. and Makoundi, C., 2015. Lead isotopic evolution of mainland SE Asia: regional tectonic and metallogenic implications. Chemical Geology. (In review)

Metcalfe, I., 2000. The Bentong-Raub suture zone. Journal Asian Earth Sciences, 18, p. 691-712.

Metcalfe, I., 2013. Tectonic evolution of the Malay Peninsula. Journal of Asian Earth Sciences, http://dx.doi.org/10.1016/ j.jseaes.2012.12.011.

McKeag, S.A., Craw, D. and Norris, R.J., 1989, Origin and deposition of a graphitic schist-hosted metamorphogenic Au-W deposit, Macreas, East Otago, New Zealand, Mineralium Deposita 24, p. 124-131.

Morrison, G. 2007. Avocet Mining Plc, Structural, vein textures and gold deposit classification. Training course notes.

Nesbitt, B.E., Murowchick, J.B., Muehlenbachs, K., 1986. Dual origin of lode-gold deposits in the Canadian Cordillera. Geology14, p. 506–509.

Ng, S. W. P, Whitehouse, M. J., Searle, M. P., Robb, L. J., Azman A. Ghani, A. A., Sun-Lin, Oliver G. J. H., Sone M., Gardiner N. J., and Roselee, M. H., 2015. Petrogenesis of Malaysian granitoids in the Southeast Asian tin belt: Part 2. U-Pb zircon geochronology and tectonic model. Geological Society of America Bulletin. doi:10.1130/B31214.1

Nuraiteng Tee Abdullah, 2009. Mesozoic stratigraphy. In:Hutchison C.S. and Tan D.N.K. (eds) Geology of Peninsular Malaysia, University of Malaya and Geological Society of Malaysia, p. 87-129.

Proctor, W.D., 1972, Geology and Mineral Resources Benta area, Pahang. Geological Survey of Malaysia. Map Bulletin 4, 25p.

Purwanto, H. S., 2002. Pemineralan emas dan kawalan struktur di kawasan Penjom, Pahang dan Lubok Mandi, Terengganu, Semenanjung Malaysia, PhD Thesis, Universiti Kebangsaan Malaysia (unpublished).

Ramdhor, P., 1980. The ore minerals and their intergrowth, 2nd edition, Pergamon Press, England

Ramli N., 2004. Geology dan stratigrafi lombong emas Penjom, Pahang, Malaysia. Unpublished BSc. Hons. Thesis, Universiti Kebangsaan Malaysia. p 157.

Ramsay, J. G. and Huber, M. I. (1987) The techniques of modern structural geology. Vol. 2: Fold and Fractures. Academic Press, London.

Ratke A. S. and Scheiner, J., 1970. Studies of Hydrothermal gold deposition (I). Carlin Gold Deposit, Nevada: The Role of Carbonaceous Materials in Gold Deposition, Economic Geology 65. p. 87-102.

Richardson, J.A. 1939a. The Geology and mineral resources of the neighbourhood of Raub, Pahang, Federated Malay States, with and account of the geology of the of the Raub Australian gold mine. Geological Survey Department, Federated Malay States, Memoir 3, 166p.

Richardson, J.A. 1939b. The Geology and mineral resources of the neighbourhood of Chegar Perah and Merapoh, Pahang. Geological Survey Department, Federation of Malaya, Memoir 4 (new series), 162p.

Robb, L., 2008. Introduction to ore forming processes. Second Edition. Blackwell Publishing. UK. p. 373.

Robert, F. and Poulsen, K.H., 2001. Vein formation and deformation in Greenstone Gold Deposit. in Richards J.P. and Tosdal R.M (Eds) Structural controls on ore genesis, Reviews in Economic Geology, Society of Economic Geology, 14, p. 111-155.

Schaubs, P.M., and Wilson, C.J.L, 2002, The relative roles of folding and faulting in controlling gold mineralization along the Deborah anticline, Bendigo, Victoria, Australia: Economic Geology, v. 97, p. 351–370.

Schmitz P. A., Duyvesteyn, S., Johnson W. P., Enloe L.and McMullen, J., 2001. Ammoniacal thiosulfate and sodium cyanide leaching of preg-robbing Goldstrike ore carbonaceous matter, Hydrometallurgy 60. p. 25–40.

Sharp, W. E. 1965. The deposition of hydrothermal quartz and calcite, Economic Geology, v. 60, p. 1635-1644.

Shepherd, T. J., Rankin, A.H., Alderton, D.H.M., 1985. A practical guide to fluid inclusion studies, Blackie, p. 239.

Shuib, M.K., 2009. Structures and deformation. In:Hutchison C.S. and Tan D.N.K. (eds) Geology of Peninsular Malaysia, University of Malaya and Geological Society of Malaysia, p. 87-129.

Sibson R.H., 2001. Seismogenic framework for hydrothermal transport and ore deposition. in Richards J.P. and Tosdal R.M (Eds) Structural controls on ore genesis, Reviews in Economic Geology, Society of Economic Geology, 14, p. 25-50.

Sillitoe, R.H., 2000. Gold-rich porphyry deposits: Descriptive and genetic models and their role in exploration and discovery: Reviews in Economic Geology, v. 13, p. 315–345.

Sony, L.T.C., Sharafuddin Mohamed, Mona Sulaiman, Teh, G.H. & Jasmi Aziz, 2001. Geology, structure, mineralization and geochemistry of the Penjom gold deposit, Pahang, Proceedings of Geological Society of Malaysia Annual Geological Conference, June 2-3 2001, Pangkor Island, p.59-63.

Springer, J.S., 1985, Carbon in Archean rocks of the Abitibi belt (Ontario-Quebec) and its relation to gold distribution: Canadian Journal of Earth Sciences, v. 22, p. 1945–1951.

Stacey, J.S. and Kramers, J.D., 1975. Approximation of terrestrial lead isotope evolution by a two stage model. Earth and Planetary Science Letters 26: p. 207-221.

Stephens J. R., Mair J. L., Oliver N. H.S., Hart C. J.R., Timothy B. 2004. Structural and Mechanical controls on intrusion-related deposits of the Tombstone Gold Belt, Yukon, Canada, with comparisons to other vein-hosted ore-deposit types. Journal of Structural Geology, 26, p. 1025-1041.

Tan, B.K., 1984. The Tectonic framework and evaluation of the Central Belt and its margin, Peninsular Malaysia. Geological Society of Malaysia. Bulletin 17, p. 307 - 322.

Tjia, H.D., Zaiton Harun, 1985. Regional structures of Peninsular Malaysia. Sains Malaysiana 14, p. 95–107.

Townsend, A. T., Yu, Z., McGoldrick, P., and Hutton, J. A., 1998, Precise lead isotope ratios in Australian galena samples by high resolution inductively coupled plasma mass spectrometry: Journal of Analytical Atomic Spectrometry, 13: p. 809-813.

Tretbar, D., Arehart, G.B., and Christensen, J.N., 2000, Dating gold deposition in a Carlin-type gold deposit using Rb/Sr methods on the mineral galkhaite: Geology, v. 28, p. 947–950.

Vearcombe J.R., 1993. Quartz vein morphology and implication for formation depth and classification of Archaean gold-vein deposits, Ore Geology Reviews, Volume 8: p 407-424.

White, N.C, and Hedenquist, J.W., 1995, Epithermal gold deposits: Styles, characteristics and exploration: SEG Newsletter, v. 23, p. 1, 9-13.

William-Jones, A. E., Bowell, R. J., and Migdisov, A. A., 2009. Gold in solution, Elements, Volume 5, p. 281-287.

Windle, S.J., Craw, D., Angus, P.V. (1999) Petrographic and mineralogical factors affecting gold recovery at Macraes Flat, Eastern Otago, New Zeland. Pacrim 1999, Bali Indonesia, October 10-13. p. 149-162.

Woodhead, J., Hergt, J., Meffre, S., Large, R.R., Danyushevsky, L. and Gilbert, S., 2009. In situ Pb-isotope analysis of pyrite by laser ablation (multi-collector and quadrupole) ICPMS. Chemical Geology, 262(3-4): p. 380-390.

Yeap, E.B., 1993. Tin and gold mineralisation in Peninsular Malaysia and their relationships to the tectonic development. Journal of Southeast Asian Earth Sciences, Vol. 8, p. 329-348.

Zaw, K., 2014. Metallogeny of mainland Southeast Asia, Proceeding of Sundaland resources 2014 MGEI Annual Conference, November 17-18, Palembang, Indonesia. p. 27-33.

LIST OF PUBLICATIONS AND PAPERS PRESENTED

PUBLICATION

Endut, Z., Ng, T. F., Abdul Aziz, J. H., Teh, G. H., 2015a. Structural analysis and vein episode of the Penjom Gold Deposit, Malaysia: Implications for Gold Mineralisation and Tectonic History in the Central Belt of Malaysia, Ore Geology Reviews V. 69, p157-173.

Endut, Z., Ng, T. F., Abdul Aziz, J. H, Meffre, S. and Makoundi, C. 2015. Characterization of Galena and Vein Paragenesis in the Penjom Gold Mine, Malaysia: Trace Elements, Lead Isotope Study and Relationship to Gold Mineralization Episodes. Acta Geologica Sinica (English Edition). Vol. 89. No. 6 pp.1801–1840.

PAPERS PRESENTED

Endut, Z., Ng, T. F., Abdul Aziz, J. H., Teh, G. H., 2015b. Style of veins in Penjom Gold Mine, Malaysia–Implications for gold mineralisation and structural episodes. PACRIM Hong Kong, China, 18-20 Mac 2015.

Endut, Z., Ng, T. F., Abdul Aziz, J. H., Teh, G. H., Mohammed, S., 2014. Style, textures and paragenesis of veins in Penjom Gold Mine, Malaysia: Implications on gold mineralization episode. Abstract of GEOSEA 2014 Conference, Yangoon, Myammar

Endut, Z. and Teh, G.H., 2010. Structural control on quartz vein in Penjom Gold Mine with emphasise of Kalampong Pit. Proceedings of the Annual Geological Conference 2010, Geological Society of Malaysia, 11-12 June 2010, Shah Alam.

Endut, Z., Ng, T. F and Teh, G.H., 2012. Some aspect of vein texture, microstructure and implication to gold mineralization episode in Penjom Gold Mine. Proceeding of the Annual Geological Conference 2012, Geological Society of Malaysia, June 2012, Kuching, Sarawak.

Endut, Z., Haznur, R., Mohammed, S., Ismail, S., Prihananto, A., 2014. Geology of the Penjom Gold Deposit, Pahang, Malaysia. Proceeding of Sundaland Resources 2014 MGEI Annual Conference, November 17-18, Palembang, Sumatra, Indonesia.

APPENDIX A – FLUID INCLUSION DATA

SAMPLE	CHIP	TRAIL	FLUID INC	FIRST ICE	LAST ICE/CLATHRATE	T_h CO_2	T_h TOTAL
			No	^oC	MELTING	^oC	^oC
Z3L	1	1	1		3.7	24.2	300
Z3L	2	2	2		-3		200
Z3L	3	4	4		-2		168
Z3L	4	5	5		3.2	24.0	305
Z3L	5	6	6		?		230
Z3L	5	6	7		3.5		220
Z3L	5	6	8		4.7		225
Z3L	5	6	9		?		240
Z3L	6	7	10		3.0		323
Z3L	6	7	11		5		200
Z3L	6	7	12		5		300
Z3L	7	8	13		4.7		256
Z3L	7	8	14		4.7	23.3	285
Z3L	7	8	15		4.7		222
Z3L	7	8	16		CS		147
Z3L	8	9	17		1	24.3	378
Z3L	8	9	18		CS		146
Z3L	8	9	19		-0.6		250
Z3L	8	9	20		CS		250
Z3L	9	10	21		-1.0		349
Z3L	9	10	22		4.0	25.0	280
Z3L	9	10	23		-4.0		228
Z3L	9	10	24		CS		146
Z3L	9	10	25		CS		138
Z3L	10	11	26		-2.0		198
Z3L	10	11	27		-2.0		189
Z3L	10	11	28		-2.0		207
Z1	1	1	29		-6.0		152
Z1	1	1	30		-5.0		148
Z1	1	1	31		-4.0		148
Z1	2	2	32		-3.0		180
Z1	2	2	33		0.5		165
Z1	3	3	34		-5		178
Z1	3	3	35		2		178
Z1	3	3	36		-2		148
Z1	4	4	37		0		195
Z1	4	4	38		-1		185
Z5JLA	1	1	39		-5		150

Z5JLA	1	1	40		-5		177
Z5JLA	1	1	41		-5		207
Z5JLA	1	1	42		-2		278
Z5JLA	1	1	43		-5		197
Z5JLA	1	1	44		-5		183
Z5JLA	3	1	45		-4		215
Z5JLA	3	1	46		-4		140
Z5JLA	3	1	47		-5		170
Z5JLA	3	1	48		-4		180
Z5JLA	4	3	49		4.8	26.8	312
Z5JLA	4	4	50		4.8	26.5	305
Z5JLA	4	5	51		6.7	25.6	322
Z5JLA	4	6	52		5	24.7	307
Z5JLA	4	6	53		5		307
Z5JLA	4	6	54		5		305
Z5JLA	5	7	55		3		150
Z5JLA	5	7	56		0		209
Z5JLA	5	7	57		3		209
Z5JLA	5	7	58		3		275
Z5JLA	6	8	59		4.2		310
Z5JLA	6	8	60		3		190
Z5JLA	6	8	61		-7		200
Z7Q2W	1	1	62		6	24	298
Z7Q2W	1	1	63		4	24	300
Z7Q2W	1	1	64		-3		140
Z7Q2W	1	1	65		CS		202
Z7Q2W	3	1	66		4	25	250
Z7Q2W	3	1	67		3		239
Z7Q2W	3	1	68		4		250
Z7Q2W	3	1	69		4	24.2	250
Z7Q2W	3	1	70		3		250
Z7Q2W	3	1	71		CS		250
Z7Q2W	3	1	72		-3		
Z7Q2W	3	2	73		4.2	24.6	295
Z7Q2W	3	2	74		4.2	24.9	290
Z7Q2W	1	4	75		4	23.3	292
Z7Q2W	1	4	76				292
Z7Q2W	1	4	77		3.2	23.5	292
Z7Q2W	1	4	78		3.2	23.5	290
Z7Q2W	2	5	79		5.9	25.8	320
Z7Q2W	2	6	80		5		255
Z7Q2W	2	6	81		0		258
Z7Q2W	2	6	82		2		250
Z2N	5	7	83		3		315

Z2N	5	8	84		0		280
Z2N	4	9	85		5.6	26	265
Z2N	3	10	86		0		250
Z2N	3	10	87				150
Z2N	3	10	88				148
Z2N	3	10	89				270
Z4EX3	1	1	90		-8		185
Z4EX5	3	3	91		8		300
Z4EX6	4	4	92		6		300
Z2N	2	5	93		4		265
Z2N	1	6	94		4		210
Z2N	1	6	95		-4		165
Z2N	1	6	96		-4		200
Z2N	1	7	97		4		185
Z2N	1	7	98		4		210
Z8F	1	8	99		3		
Z8F	1	9	100		4		284
Z8F	1	10	101		3.5		280
Z8F	2	10	102		0		
Z8F	2	10	103				320
Z8F	4	11	104				220
Z8F	4	11	105				305

Notes:

1) CS – Cannot see
2) 85 data used for the graph only for the data that have both Last Ice/Chlathrate and Total Homogenization Temperatures (T_h TOTAL)

Appendix B: XRF geochemistry data

				Sample	HW-R	HW-NSF	KLGM	KLB	JLIA-SDB	JLIA-SDLC	NNW-H	NNW-L	NE888	NNEDK-JL	DK-1	Q3W-EX1	MN-1	PT-1	ESE-1
Method	Analyte	Unit	MDL	Sample Type	Rock Pulp	Rock Pulp	Rock Pulp	Rock Pulp	Rock Pulp	Rock Pulp	Rock Pulp	Rock Pulp	Rock Pulp	Rock Pulp	Rock Pulp	Rock Pulp	Rock Pulp	Rock Pulp	Rock Pulp
4X	LOI	%	-5.11		9.24	13.76	7.52	9.21	6.81	9.07	6.03	7.52	2.8	3.87	13.1	4.41	11.82	5.83	7.39
4X	SiO2	%	0.1		58.6	57.4	65.1	60.9	62.1	57.7	69.1	65.1	77.9	76.5	62.9	71.4	58.1	80.8	64
4X	Al2O3	%	0.01		12.78	10.02	17.69	18.74	16.23	13.71	5.89	11.04	11.46	11.11	2.8	13.77	8.7	4.32	11.35
4X	Fe2O3	%	0.01		6.06	4.97	4.41	6.02	4.54	5.47	7.21	1.98	1.44	1.84	2.15	2.35	6.37	3.53	5.45
4X	CaO	%	0.01		7.31	8.47	0.04	0.03	3.79	6.31	3.56	8.51	1.88	2.78	15.85	2.2	7.65	2.4	3.32
4X	MgO	%	0.01		2.11	2.82	1.49	1.38	1.6	2.29	1.22	0.26	0.19	0.52	0.58	0.9	2.79	0.92	1.55
4X	Na2O	%	0.01		0.33	0.23	0.07	0.11	0.31	0.53	0.18	2.7	2.25	1.12	0.22	1.8	0.37	0.11	0.39
4X	K2O	%	0.01		2.48	1.29	3.19	3.3	3.47	2.98	0.91	1.86	2.24	2.43	0.41	2.77	1.68	0.65	2.3
4X	MnO	%	0.01		0.11	0.08	<0.01	0.04	0.09	0.14	0.09	0.23	0.05	0.07	0.29	0.07	0.2	0.06	0.09
4X	TiO2	%	0.01		0.43	0.49	0.77	0.74	0.59	0.51	0.2	0.04	0.03	0.16	0.06	0.17	0.29	0.09	0.41
4X	P2O5	%	0.01		0.11	0.08	0.02	0.02	0.12	0.08	0.02	<0.01	<0.01	0.04	0.02	0.03	0.06	0.02	0.08
4X	Cr2O3	%	0.001		0.006	0.003	0.007	0.005	0.004	0.005	0.002	0.002	<0.001	<0.001	<0.001	0.003	0.006	0.001	0.006
4X	Ba	%	0.01		0.03	0.02	0.04	0.05	0.04	0.03	<0.01	<0.01	0.02	0.02	0.01	0.02	0.02	<0.01	0.03
4X	SUM	%	0.01		99.59	99.61	100.34	100.59	99.72	98.82	94.4	99.21	100.25	100.42	98.41	99.85	98.07	98.69	96.36
2A Leco	TOT/C	%	0.02		2.48	3.18	0.98	1.82	1.45	2.03	1.28	1.95	0.41	0.6	3.7	0.61	3.31	2.44	2.14
2A Leco	TOT/S	%	0.02		0.6	0.12	0.32	0.36	0.08	0.25	1.96	0.87	0.47	0.39	0.2	0.17	0.59	0.76	1.73

				Sample	HW-R	HW-NSF	KLGM	KLB	JLIA-SDB	JLIA-SDLC	NNW-H	NNW-L	NE888	NNEDK-JL	DK-1	Q3W-EX1	MN-1	PT-1	ESE-1
Method	Analyte	Unit	MDL	Sample Type	Rock Pulp	Rock Pulp	Rock Pulp	Rock Pulp	Rock Pulp	Rock Pulp	Rock Pulp	Rock Pulp	Rock Pulp	Rock Pulp	Rock Pulp	Rock Pulp	Rock Pulp	Rock Pulp	Rock Pulp
4B	Ba	PPM	1		199	152	304	480	365	289	103	91	189	233	79	197	180	57	244
4B	Be	PPM	1		4	3	2	3	3	3	<1	1	3	90	3	20	1	5	<1
4B	Co	PPM	0.2		13	7.2	5.2	10.1	12.2	13.7	12.7	1	0.7	1.9	3.8	4.7	9.2	5.1	14.2
4B	Cs	PPM	0.1		11.1	8.3	15.9	7.4	13	13.3	7.4	27.8	19.2	18	2.8	30.5	9.3	5.1	14.8
4B	Ga	PPM	0.5		12.9	10	19.4	19.7	16.3	13.5	6	18.9	19.3	16.5	4.1	21.4	11.5	5.6	15.3
4B	Hf	PPM	0.1		3.4	4.4	5.6	5.2	3.4	2.9	1.4	3.7	3.6	3.2	0.4	3.8	2.6	1.1	2.9
4B	Nb	PPM	0.1		5.9	6.6	9.3	7.3	3.9	3.7	2.2	39.3	29.3	17.5	1	24	6.7	2.7	6.2
4B	Rb	PPM	0.1		170.5	72.9	124.2	131.7	196.9	209.9	44.1	241.9	230.8	186.5	25.7	285.1	119.4	44.1	127.8
4B	Sn	PPM	1		1	2	3	3	<1	2	1	15	10	8	1	11	3	1	4
4B	Sr	PPM	0.5		555.1	326.9	16.2	44.2	112.9	131.2	91.8	229.2	117.3	105.7	523	104.3	194.6	63.6	153.9
4B	Ta	PPM	0.1		0.4	0.6	0.9	0.5	0.3	0.2	<0.1	5.3	3.3	1.9	<0.1	2.7	0.3	0.3	0.6
4B	Th	PPM	0.2		6.6	5.9	11.6	11.1	6.9	4.9	2.8	12.7	16.6	11.1	1	16.2	4.4	2.1	6.2
4B	U	PPM	0.1		6.1	1.9	3.1	2.9	4.3	2.3	1	28.9	32.8	20.7	1.1	27	8.9	1.6	3.1
4B	V	PPM	8		93	79	136	142	141	121	48	<8	9	34	27	37	78	37	86
4B	W	PPM	0.5		6.4	6	1.3	1.4	2.2	7.6	3	5.2	3.2	4.3	2.2	58.6	7.6	8.6	16.1
4B	Zr	PPM	0.1		93.9	138.3	181.6	167	131.4	108.2	47.8	41.6	41.8	62.2	19.1	73.2	68	31.4	95.8
4B	Y	PPM	0.1		21.9	19.2	30.7	33.6	28.5	21.8	10.2	26.5	14.8	17.4	66.9	15.5	21.3	13	13.7
4B	La	PPM	0.1		18.2	19.5	38.6	39.1	16.3	13.8	6.5	5.1	2.4	5.2	10.8	9.4	12.1	5.9	13.5
4B	Ce	PPM	0.1		35.1	36.7	71.5	74	37.1	28.9	13	12.8	5.4	11	23.3	19.7	25.5	9.7	27.5
4B	Pr	PPM	0.02		4.27	4.17	8.69	8.67	4.73	3.77	1.62	1.66	0.67	1.35	3.61	2.36	3.08	1.3	3.17
4B	Nd	PPM	0.3		18.5	18.6	36.2	33.8	19	14.6	7	6.3	3.7	6.6	14.8	9.3	14.1	7.8	12.6
4B	Sm	PPM	0.05		4.13	3.15	6.9	7.08	4.15	3.57	1.91	2.7	1.15	1.69	6	2.22	3.34	1.6	2.78
4B	Eu	PPM	0.02		0.91	0.72	1.5	1.71	1.17	0.67	0.78	0.89	0.31	0.41	3.2	0.39	0.82	0.56	0.69
4B	Gd	PPM	0.05		4.29	3.15	6.88	6.67	5.33	4.09	2.12	2.83	1.55	2.14	10.08	2.11	4.1	2.13	2.71
4B	Tb	PPM	0.01		0.59	0.55	1.01	1.03	0.84	0.61	0.31	0.48	0.25	0.36	1.78	0.35	0.58	0.34	0.41
4B	Dy	PPM	0.05		3.87	3.67	6.36	6.14	5.31	3.39	2.29	3.23	1.69	2.38	10.06	2.19	4.24	2.09	2.63

				Sample	HW-R	HW-NSF	KLGM	KLB	JLIA-SDB	JLIA-SDLC	NNW-H	NNW-L	NE888	NNEDK-JL	DK-1	Q3W-EX1	MN-1	PT-1	ESE-1
Method	Analyte	Unit	MDL	Sample Type	Rock Pulp	Rock Pulp	Rock Pulp	Rock Pulp	Rock Pulp	Rock Pulp	Rock Pulp	Rock Pulp	Rock Pulp	Rock Pulp	Rock Pulp	Rock Pulp	Rock Pulp	Rock Pulp	Rock Pulp
4B	Tm	PPM	0.01		0.33	0.31	0.48	0.53	0.46	0.33	0.16	0.35	0.23	0.28	0.74	0.25	0.31	0.18	0.25
4B	Yb	PPM	0.05		2.31	2.11	3.41	3.96	3.38	2.42	1.04	3.25	2.05	2.16	4.48	1.91	2.21	1.17	1.68
4B	Lu	PPM	0.01		0.33	0.34	0.5	0.58	0.45	0.4	0.17	0.61	0.3	0.32	0.56	0.3	0.33	0.18	0.26
1DX	Mo	PPM	0.1		0.5	0.2	3.7	1	0.6	0.6	1.5	0.3	1	2	0.7	0.9	0.4	1.5	1.5
1DX	Cu	PPM	0.1		29.2	4.2	65	35.4	39.7	53.3	137.9	5.9	13	28.4	2.9	43	49.7	27.1	23.8
1DX	Pb	PPM	0.1		15.1	9.9	70.4	61.8	6.6	4.7	1374.1	200.4	158.1	154.1	503.2	109.2	53.4	806.6	115.6
1DX	Zn	PPM	1		74	49	44	56	40	36	1298	6	16	26	22	39	25	273	93
1DX	Ag	PPM	0.1		<0.1	0.2	<0.1	0.1	0.1	0.1	15.8	3	2.7	2.1	1.7	1.1	0.5	5.2	0.7
1DX	Ni	PPM	0.1		17.1	7.2	14.2	8.8	13.6	12.9	12.4	0.5	0.6	2	3.6	4.4	15.3	4.7	18.5
1DX	As	PPM	0.5		39.9	21.9	37.9	23.5	115.2	1256.2	>10000	324.8	3546.7	99.6	3372.9	52.1	5994.7	8292.3	>10000
1DX	Au	PPB	0.5		4.9	7.7	4.8	2	5.3	114.9	12057.7	4145.3	661.2	8558	2164.4	1298.1	3.6	2	18.3
1DX	Cd	PPM	0.1		0.1	0.2	0.4	0.1	0.2	0.1	10.9	0.4	0.3	0.4	0.5	0.7	0.3	4.9	0.7
1DX	Sb	PPM	0.1		1.2	0.2	3	0.7	<0.1	0.4	15.4	0.4	1.3	0.9	1.7	0.4	2.9	4.3	7.8
1DX	Bi	PPM	0.1		0.3	0.2	0.9	0.5	0.8	0.7	36.7	5.4	5.8	3.3	2.3	4.4	2.3	14.4	3.9
1DX	Hg	PPM	0.01		0.02	<0.01	0.05	0.09	<0.01	<0.01	0.12	<0.01	<0.01	0.02	<0.01	0.01	<0.01	0.04	0.02
1DX	Tl	PPM	0.1		<0.1	<0.1	0.1	<0.1	0.1	0.2	<0.1	0.2	0.2	<0.1	<0.1	0.2	<0.1	<0.1	<0.1
1DX	Se	PPM	0.5		0.6	<0.5	<0.5	<0.5	<0.5	<0.5	5.1	0.5	1.1	<0.5	1	<0.5	0.7	<0.5	0.9